Aus dem Institut für Schlaganfall- und Demenzforschung

Institut der Ludwig-Maximilians-Universität München

Verstand: Prof. Dr. Martin Dichgans

Dissertation

zum Erwerb des Doctor of Philosophy (Ph.D.)

an der Medizinischen Fakultät der

Ludwig-Maximilians-Universität zu München

The MIF homolog MIF-2/D-DT in atherosclerosis: Functional role and links to hepatic lipid metabolism

vorgelegt von:

Chunfang Zan

aus:

Datong, China

Jahr:

2022

Mit Genehmigung der Medizinischen Fakultät der
Ludwig-Maximilians-Universität zu München

First evaluator (1. TAC member):   Prof. Dr. Jürgen Bernhagen

Second evaluator (2. TAC member): Prof. Dr. Sabine Steffens

Third evaluator: Priv. Doz. Dr. Ulrich Grabmaier

Fourth evaluator: Prof. Dr. Peter Nelson

Dean: **Prof. Dr. med. Thomas Gudermann**

date of the defense:

27.06.2022

Talent lies fallow without the hard work and persistence.
You need to have an appetite for delayed gratification, some good luck,
to choose a good problem and to be in the right place at the right time.
One of the things that's worked for me is to never follow the pack.

------Prof. Dr. Peter Libby
*Brigham and Women's Hospital, Harvard Medical School*

ABSTRACT

Macrophage migration inhibitory factor (MIF) was identified as one of the first cytokines over half a century ago. In the past 2 decades, MIF has been established as a pivotal player in acute and chronic inflammation, cancer, as well as atherosclerotic cardiovascular diseases. Our laboratory previously investigated the importance of MIF in atherogenesis showing that *Mif*-deficiency leads to atheroprotection in mouse atherogenic models in an *Apoe*$^{-/-}$ or *Ldlr*$^{-/-}$ background. Recently, an increasing body of evidence suggests that D-dopachrome tautomerase (D-DT)/MIF-2, a close MIF homolog, does not always serve as 'just' a backup system of MIF. In fact, some unpublished preliminary work from our laboratory leading up to the topic of this thesis, indicated that MIF-2 exhibits similar or even more pronounced chemotactic activities and leukocyte recruitment properties compared to MIF, while the role of MIF-2 in models of wound healing and adipocyte inflammation turned out to be opposite to that of MIF. Therefore, this PhD thesis aimed at shedding light on the causal role of MIF-2 in atherosclerosis and characterizing the molecular mechanisms driven by MIF-2 and its receptor(s). The *in vivo* phenotype was studied based on a genetic atherosclerotic mouse model (the *Mif-2*$^{-/-}$*Apoe*$^{-/-}$ mouse line), as well as a MIF-2-specific pharmacological blocking approach with a recently discovered selective small molecule inhibitor of MIF-2 (i.e. 4-CPPC) *in vivo*.

After verifying the systemic knockout of *Mif-2* in these mice, by both reverse transcription quantitative polymerase chain reaction (RT-qPCR) and Western blot (WB), mice were subjected to a Western-type 0.21% cholesterol-rich high fat diet (HFD) for 4.5 and 12 weeks to develop the early and advanced atherosclerotic plaques, respectively. Thereafter, atherosclerotic lesion progression was investigated by analyzing the lesion size and components in plaques of both aortic root and the whole aortic arch including three branches, such as lesional macrophage infiltration, necrotic core formation and collagen contents. It turned out that less lesions, reduced vascular inflammation, and attenuated necrotic core formation was observed in *Mif-2*$^{-/-}$*Apoe*$^{-/-}$ mice. Furthermore, the *Mif-2*-deficiency-elicited atherosclerotic phenotype we found was also associated with downregulated circulating inflammatory cytokines/chemokines. For example, the pro-atherogenic cytokines interleukin (IL)-17 as well as interferon (IFN)-γ were decreased in *Mif-2*-deficient mice. Notably, the analysis of the atherosclerotic phenotype combined with body weight analysis directly pointed towards a striking lipid metabolism-related phenotype induced by *Mif-2* deficiency, with detected reduced triglycerides and cholesterol in plasma of *Mif-2*$^{-/-}$*Apoe*$^{-/-}$ mice.

No comparable lipid phenotype was previously observed in *Mif*$^{-/-}$ atherosclerosis models, neither in the *Apoe*$^{-/-}$ nor *Ldlr*$^{-/-}$ background. This suggests that compared to MIF, MIF-2 could distinctively serve as a key regulator in the dynamic process of lipogenesis and lipolysis, which might dominate lipid metabolism associations between hepatosteatosis and atherogenesis. To test this hypothesis and study the mechanism further, we employed the human hepatocyte cell line Huh-7 and evaluated the effects of recombinant MIF-2 and inhibitors of its receptors on the lipogenic process, capitalizing on RT-qPCR, WB, nuclear translocation experiments and lipid uptake assays. It turned out that MIF-2 upregulated the expression of sterol regulatory element binding protein-1 and 2 (SREBP-1, SREBP-2) and their lipogenic downstream targets. Of interest, the analysis of proteolytic activity and lipid uptake results together revealed the involvement of receptors for example CXCR4 and CD74. Consequently, MIF-2 induced-SREBP relevant mechanisms and AMP-activated protein kinase (AMPK) as well as protein kinase B (PKB/AKT) signaling pathways were further studied in this thesis. MIF-2 was found to enhance SREBP activation through inhibiting AMPK phosphorylation whereas promoting AKT phosphorylation. However, there remain disputable points, such as 'the temporal relationship' between cholesterol synthesis and low-density lipoprotein (LDL) clearance, and whether a well-studied negative regulator of LDL receptor (LDLR), proprotein convertase subtilisin-like kexin type 9 (PCSK9) is implicated, which still needs to be explored more deeply. Overall, this thesis could provide a novel clue regarding the underlying molecular and cellular mechanisms how MIF-2 functions in atherosclerosis, with a focus on studying the lesion phenotype, systemic inflammation, and hepatic lipid metabolism in hyperlipidemic mice. Taken together, MIF-2 not only serves as a novel driver of atherosclerosis through promoting atherogenic leukocyte recruitment and vascular inflammation, but also acts as a contributor to hepatic lipid accumulation, which involves CXCR4/CD74-complexes and the AMPK- and AKT-SREBP-mediated signaling pathways.

GRAPHICAL ABSTRACT
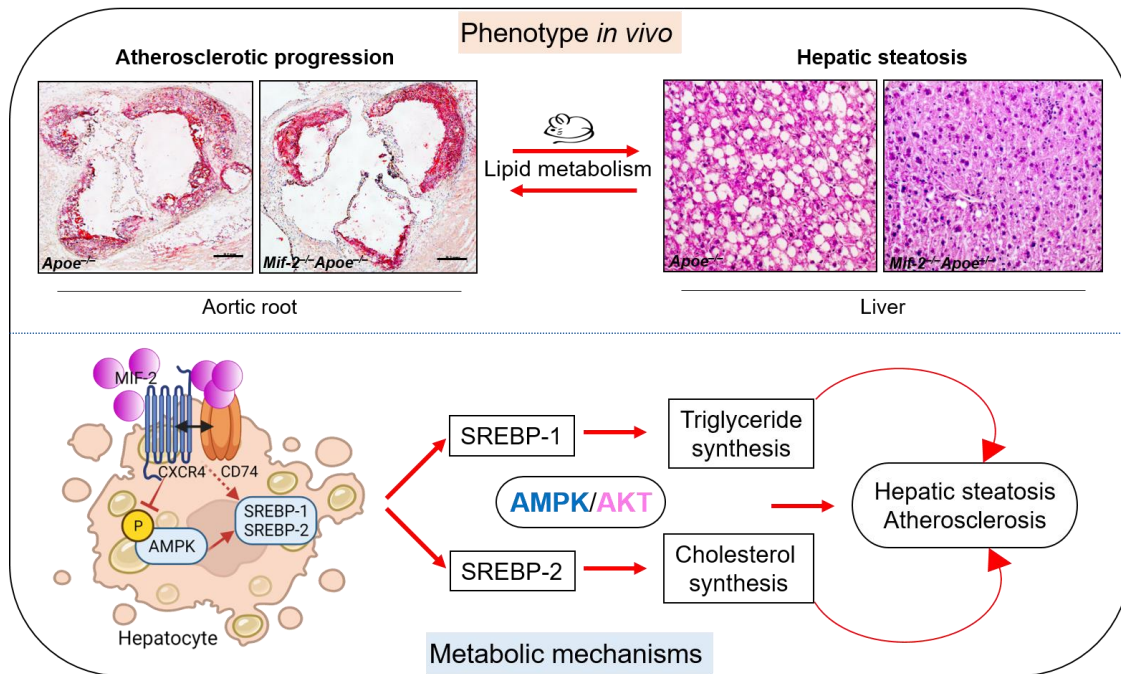
In Brief

This project reveals that *Mif-2* deficiency mitigates plaque progression, accompanied by improved hepatic steatosis in hyperlipidemic mice. These findings together identify MIF-2 as a novel driver of atherosclerosis that unlike its homolog MIF not only promotes atherogenic leukocyte recruitment and vascular inflammation, but also acts as a contributor to hepatic lipid accumulation. The specific mechanism of MIF-2 in hepatocytes involves CXCR4/CD74-complexes and the AMPK- and AKT-SREBP-mediated signaling pathways.

Table of Contents

1. INTRODUCTION

Macrophage migration inhibitory factor (MIF) has been defined as a pleiotropic yet atypical chemokine extensively involved in cardiovascular diseases (CVDs) [1], such as atherosclerosis [2,3], myocardial infarction [4], heart failure [5], and stroke [6,7], etc. MIF has been implicated in an acceleration of atherosclerosis, as demonstrated in both $Apoe^{-/-}$ and $Ldlr^{-/-}$ mouse models [2,3]. As a unique structural homolog to MIF, MIF-2 also termed D-dopachrome tautomerase (D-DT), is a second crucial member of the MIF-protein family, which could exert many overlapping functions as well. Recently, knowledge of MIF-2 and related signaling pathways in inflammation and CVDs are under active investigation. However, the significance of MIF-2 in atherosclerosis and vascular inflammation as well as the mechanisms behind that are still poorly understood, but worth exploring further, based on those similarities and dissimilarities between MIF-2 and MIF.

Overall, MIF-2 was found to bind with Cluster of differentiation 74 (CD74), a high-affinity cell membrane receptor of MIF [8,9], and this subsequently mediates similar cell signaling pathways and effector functions as triggered by MIF [10,11]. On the other hand, both C-X-C chemokine receptor (CXCR) type 2 (CXCR2) and CXCR4, the non-cognate chemokine receptors of MIF, have been suggested to form the receptor complexes with CD74 [2,12,13], providing also potential mechanistic choices for fine-tuning the MIF-2-driven pathways in atherosclerosis. Nevertheless, given the fact that MIF-2 lacks the *pseudo-(E)LR* motif of MIF [12,14], it has been speculated that it may not be able to activate CXCR2, even though systemic studies addressing this possibility have not been conducted. By comparison, unpublished biochemical data of our laboratory and sequence similarities in the N-like loop would at least not contradict the potential that MIF-2 binds to CXCR4. In addition to the induction of a signaling cascade, the binding of MIF-2 to its receptors can provoke its internalization as well [10] due to these unique signaling properties of MIF-2. Hence, what peculiarities MIF-2 possesses when it works with its functional receptors and even the interplay with MIF in the context of atherosclerosis, are well worth investigating further.

The results of my thesis showed that the genetic deletion of *Mif-2* in $Apoe^{-/-}$ mouse model significantly ameliorates advanced atherosclerotic progression, vascular inflammation and hepatic steatosis *in vivo* in both genders, with the highlight of the functional significance of MIF-2 in lipid metabolism. Furthermore, it was revealed that MIF-2 together with the receptor complex CXCR4/CD74 exhibits important functionalities through regulating the AMPK- and

AKT-SREBP-mediated lipogenic pathways. This indirectly explains as well as substantiates the phenotype we found *in vivo*. In summary, on the one hand, MIF-2/D-DT alongside MIF is also characterized as a functional ligand for CXCR4 and CD74 forming a receptor complex, which controls inflammation and atherogenesis based on its similarities with MIF. On the other hand, MIF-2 exerts lipogenic properties during the synthetic process of triglycerides and cholesterol in hepatocytes, which leads to the production of excess circulating lipoproteins and further exacerbates plaque progression. Based on these data, we do believe that MIF-2 behaves as a pivotal player in atherosclerosis as well as hepatic steatosis.

In order to have a systemic understanding of the potential of MIF-2 in lipid metabolism and further obtain some clues from previous findings in different kinds of context, most relevant knowledge about MIF-2, including its discovery and evolutionary origin, structural and functional comparisons with MIF, and published experimental and clinical studies, is summarized in the next chapter.

1.1 Overview of D-DT/MIF-2

1.1.1 The discovery and evolutionary origin of D-DT/MIF-2

Dopachrome tautomerase was a newly discovered protein, partly purified from B16 mouse melanoma tumor in 1990 and thereby firstly named according to its property of catalyzing the discoloration of dopachrome through promoting a tautomeric shift on dopachrome [15]. Even if this enzyme was preferentially associated with melanosomes, it also existed in microsomal as well as cytosolic fractions of cell homogenates. Given its well-known tautomerization ability of converting 2-carboxy-2,3-dihydroindole-5,6-quinone (i.e. D-dopachrome) into 5,6-dihydroxy-indole-2-carboxylic acid (DHICA), putative substrate analogues, stereospecificity and potential inhibitors were further studied since 1991. Consequently, they found that dopachrome tautomerase could be suppressed by carboxylated indoles [16]. Extensive distribution of this protein would prompt the view that it might exert vital functions in regulating melanization in different organisms.

Thenceforward, D-dopachrome tautomerase/D-dopachrome decarboxylase (D-DT/DOPD) was unexpectedly detected when the tautomerization property of L-dopachrome was investigated in cultured melanoma cells, while MIF-2 was used as the control substrate [17]. As a cytoplasmic enzyme with the function of tautomerization, MIF-2 could convert D-

dopachrome into DHICA. Additionally, it was also termed as MIF-2 recently due to the homology to MIF. Odh and co-workers in 1993 showed that MIF-2 was detected in almost all organs examined in their study performed in rats, such as liver, testis, kidney, spleen, brain and heart, which indicates that MIF-2 may have an influence on different physiological and pathological conditions [17]. Moreover, they successfully isolated MIF-2 from rat liver and the gel electrophoresis gave its monomer a molecular weight of about 12 kDa. Later on, human MIF-2 was isolated from human blood cells [18]. Therefore, this protein was just provisionally named D-DT, as it was suspected that D-dopachrome might not be the natural substrate of this protein.

On the way of exploring the real functionality of MIF-2, structural similarities to other enzymes were scrutinized, which were supposed to provide clues for further study. However, MIF-2 was identified to either show no similarities to any of enzymes that catalyze the conversion of L-dopachrome into DHICA in melanin forming, or share rare resemblances to D-amino acid oxidase, which is specific for D-amino acids [19]. Yokoyama and co-workers in 1994 demonstrated that MIF-2 just shared negligible sequence similarity with one of the L-dopachrome tautomerases, such as TRP-1 and TRP-2, through molecular cloning [20]. Afterwards, some researchers found that human MIF-2 displayed 66% identity and 82% homology with rat MIF-2, and furthermore a pronounced homology of rat MIF-2 and MIF was initially addressed by Zhang *et al.* in 1995 during the process of cloning cDNA encoding rat MIF-2 via a homology research in the EST database [21]. They revealed that rat MIF-2 shared 27% identity and 53% homology with rat MIF [21]. In this sense, this homology is of high importance in guiding further investigation of MIF-2, since the functions of MIF in immune responses and inflammatory reactions have been investigated and emphasized during the last 20 years [2,5,12]. In fact, recent cross-kingdom analysis of MIF protein family also included plant MIFs, such as *Arabidopsis thaliana MDL* genes (AtMDLs), with the hint that MIF/MIF-2 with its orthologs in other phylogenetic branches may date back over 800,000,000 years [22]. It suggests a long evolutionary history of MIFs.

Therefore, interests in the structure-function relationship between MIF-2 and MIF have increased, especially with respect to inflammatory considerations. Of note, MIF also displayed an isomerase activity of converting D-dopachrome to DHICA, indicating that its isomerase activity might also be involved in inflammatory and immunological reactions [23], although most researchers currently think that the tautomerase site may indirectly influence

MIF's inflammatory and immunological activities by inducing a conformational change that compromises MIF receptor binding activities. It is accordingly speculated that MIF-2 could act in concert with MIF regarding immunological response, in spite of their different tissue distributions and existing dissimilarities in crystal structures and physicochemical properties [24-26]. Then Kuriyama and co-workers in 1998 identified the complete sequence of mouse MIF-2 gene and relevant properties concerning the structure [27]. In addition, they proposed a durable idea that the comparative study of both MIF and MIF-2 in response to different stimuli for example lipopolysaccharides (LPS) may yield further insights into these two kinds of proteins' pathophysiological functions. Another study from Esumi and co-workers in 1998 compared the structures of MIF and MIF-2 genes, and they found that MIF and MIF-2 were both located on mouse Chromosome (Chr.) 10 and human Chr. 22 [28]. Sugimoto H *et al.* compared the potential active sites, and the surface charge distribution as well as the intersubunit contacts of MIF and MIF-2 in 1999, and concluded that these features would be beneficial to design effective inhibitors to modulate immune-regulatory and hormone-like effects, which might contribute to clinical investigation further [29]. Of interest, the successful isolation and purification of mouse and human MIF-2 protein is of importance for preclinical studies in the next step.

On the other hand, recent several papers demonstrated that the deletion or neutralization of MIF-2 could induce a similar phenotype to that induced by the genetic deletion or immune-neutralization of MIF, yet this effect increased around two-fold more significant in receptor deficient cells [2,30,31], due to the engagement of MIF's cognate receptor CD74. Therefore, better characterization of MIF *versus* MIF-2 dependent responses might be provided by the application of *Mif^{-/-}Mif-2^{-/-}* mouse model in atherosclerosis research, which has been utilized by Vandenbark *et al.* to study multiple sclerosis recently [32].

1.1.2 Acknowledged similarities and differences between MIF-2 and MIF

Since the homology between MIF-2 and MIF was initially reported on in 1995 [21], numerous studies have emerged to clarify their structural similarities and biological relationship. Here, this chapter aims to give a comprehensive summary regarding the similarities and differences between MIF-2 and MIF. Generally, MIF and MIF-2 are small proteins. Their monomers are about 12 kDa, but their active enzymes usually exist as a trimer of 35 kDa. Considering the gross three-dimensional (3D) structure, MIF-2 shares some stereoscopic homology with MIF as well (Figure 1). Each monomer of MIF-2 possesses two βαβ motifs and comparable

trimeric packing by intersubunit β-sheets compared to MIF. In addition, the entire homotrimeric folding of MIF-2 and its subunit topology is nearly the same as that of human MIF. Of special note, MIF-2 does not contain a CALC-motif, which can be found in MIF and is associated with MIF's catalytic thiol-protein oxidoreductase (TPOR) activity [33].
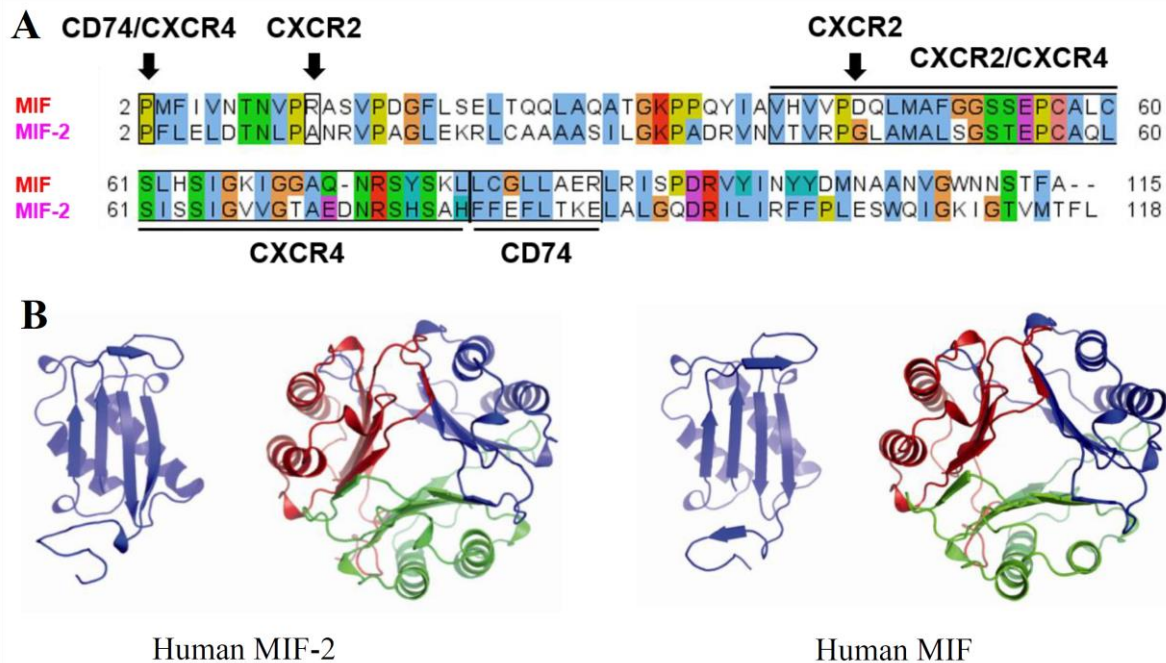
Figure 1: Comparison of the sequence and three-dimensional structures between MIF-2 and MIF. The structures of the human proteins are shown. (A) Amino acid sequences and different receptor binding sites of MIF and MIF-2 were highlighted. (B) Comparison of three-dimensional (3D) structures between MIF-2 and MIF. Left panel of 1B: monomer and trimer of human D-DT/MIF-2, right panel of 1B: monomer and trimer of human MIF. 3D structures were taken from reference [11].

Earlier literatures mainly investigated and compared MIF and MIF-2 among different species such as human, rat and mouse. Hence, there are some accepted similarities between MIF-2 and MIF in various species summarized in Table 1 based on current knowledge. (1) Genome level: both human MIF-2 and MIF are located in the close proximity on Chr. 22 and their mRNA sequences share 50% identity; whereas mouse MIF and MIF-2 genes are located on chromosome 10 and their mRNA sequences share almost 40% identity. Additionally, rat MIF-2 shares 27% identity and 53% homology with rat MIF, and both are located on Chr. 20. (2) Protein level: MIF-2 and MIF proteins present ~27% sequence identity in mice and ~34% in humans. (3) Both MIF-2 and MIF belong to the phenylpyruvate tautomerase family despite of a low level of sequence homology [24]. (4) Similar to MIF, the action of MIF-2 to activate MAP kinase signaling occurs in a CD74-dependent manner.

Table 1: The homology of MIF and MIF-2 among different species

	Human	Rat	Mouse
Chr. location	Chr. 22	Chr. 20	Chr. 10
Genome level	50% identity	27% identity and 53% homology [21]	40% identity
Protein level	33% sequence identity [25]	-	27% sequence identity [27]
Monomeric structure	Each monomer possesses two βαβ motifs		
Trimeric structure	Each trimer has similar trimeric packing		
Functionality	Their actions are dependent on the receptor CD74		

The protein sequence alignments of mouse MIF-2 with human and rat sources suggest that MIF-2 shares highly homologous sequences among various species. Thus, it is conceivable that MIF-2 may serve as a crucial player in the organisms beyond species. Of note, in addition to human and animal MIFs mainly discussed here, the analysis of other organism MIFs such as plant MIFs suggests their ancient origin that goes back 800,000,000 years [22], and further an interesting interplay between plant MIFs and human immune system was revealed by our laboratory recently [34]. Except for these abovementioned similarities between MIF-2 and MIF, we should also pay special attention to these structural differences, which would provide additional support to deeply understand different biological functions of MIF-2 and MIF, as enumerated in Table 2. (1) The expression patterns of MIF-2 and MIF are different in various kinds of tissues. Human and rat MIF-2 expression is largely limited to liver and kidney, whereas MIF expression is ubiquitous. (2) Both MIF and MIF-2 have the same substrate, i.e. D-dopachrome, with regard to their tautomerization activities, but their patterns and products differ. (3) There are some structural differences between MIF-2 and MIF, including cysteine residue number, glycosylation sites, substrate-binding amino acids, active sites and their surrounding area. (4) Binding of MIF to its known receptors, for instance CD74, CXCR4, CXCR2 and CXCR7, always triggers a signaling cascade. In addition to that, binding of MIF-2 to its receptors also leads to its internalization.

Table 2: The structural and functional differences between MIF and MIF-2

	Features	MIF	MIF-2/D-DT
Overall comparisons	Discovery time	~1966 [35,36]	~1993 [17]
	Tissue distribution	MIF is more ubiquitously expressed	Human MIF-2 and rat MIF-2 is largely limited to liver and kidney
Structural differences	Cysteine residue number (Rat) [21]	Two residues are located on position 23 and 56	Three residues are located on position 56, 59 and 80
	Glycosylation sites (Rat) [21,26]	Position 50 and 73	Position 74 and 109
	Active sites and their	MIF protein is positively	MIF-2 is positively charged

	surrounding area	charged in the active site as well as the surrounding area	in the active site, whereas negatively charged in the surrounding area
Tautomerase properties	Tautomerization pattern	Pure tautomerization	With additional decarboxy-lation
	Tautomerized product	5,6-dihydroxyindole-2-carboxylic acid	5,6-dihydroxyindole
	Substrate-binding amino acids	Pro-1, Lys-32, Ile-64, Tyr-95, Asn-97	Pro-1, Lys-32, Ile-64
	Enzymatic efficiency	MIF displays a ~10-times higher efficiency than MIF-2	MIF-2 is 10-fold less active than human MIF protein
Others	Binding receptors	CXCR2, CXCR4, ACKR3, CD74	CD74, ACKR3 (published), and CXCR4 (this thesis)
	Biological activity	Binding of MIF to its receptors always triggers a signaling cascade	Binding of MIF-2 to its receptor(s) may not always induce a signaling cascade, but provoke its internaliza-tion [10]

1.1.3 Preclinical studies: Role of MIF-2 in tumors, inflammation and other diseases

Although there are not enough original studies regarding MIF-2 to date, this chapter still tries to summarize most of relevant literatures here, to have a general overview on current situations of MIF-2 in different disease settings. The majority of researchers has been interested in the roles of MIF-2 in various kinds of cancers, and other a few scientists compared the effects of MIF-2 and MIF on adipose tissue, inflammation, etc., which would be specifically illustrated in the following part.

1.1.3.1 MIF-2 in tumors

Plenty of preclinical studies have shown that MIF-2 is closely associated with several tumors derived from different organs such as lung [37], colon [38], kidney [39], pancreas [40], etc. Coleman and co-workers in 2008 demonstrated that the separate or cooperative effects of MIF-2 and MIF could enhance CXCL8 as well as vascular endothelia growth factor expression levels in A549 lung cell lines, which are recognized as proangiogenic factors in non-small cell lung carcinomas (NSCLC) [37]. In fact, several previous studies already confirmed that MIF was overexpressed in NSCLC tissue and autocrine MIF could promote cell cycle progression in fibroblasts [41,42]. Furthermore, Coleman *et al.* pointed out that the activation of c-Jun N-terminal kinase (JNK), c-Jun phosphorylation as well as activator protein-1 (AP-1) transcription factor, might also contribute to MIF and MIF-2 co-regulation

of CXCL8 transcription [37]. This is the first functional and experimental study *in vitro* to analyze the biological behavior of MIF-2 in the context of pathological conditions, and this kind of positive cooperative effect of MIF with MIF-2 indicates that combination therapy of targeting different MIF family proteins may improve the benefits of currently applied anti-MIF-based strategy.

In addition, some scientists have explored the functional significance of MIF-2 in cyclooxygenase-2 (COX-2) related disorders especially colorectal cancer (CRC) in the past decades [43,44]. Xin and colleagues reported that MIF-2-activated COX-2 transcription was partially reliant on the stabilization and transcriptional regulation of β-catenin, as observed in colorectal adenocarcinoma cell lines [38]. Given the fact that both β-catenin and COX-2 elicited transcriptional processes and act as crucial drivers to accelerate CRC initiation and progression [45,46], it has been suggested that MIF-2 contributes to the pathogenesis of CRC through this pathway. Moreover, they also showed that CD74 expressed at moderately high levels in HT-29 and HCT-16 cells, which endorsed the results from previous study showing upregulated CD74 in a large scale of samples from patients with colorectal adenomas [47], providing a promising candidate regarding the potential binding receptor for MIF-2.

In a similar vein, Pasupuleti and coauthors in 2014 reported that MIF-2 plays a predominant role in clear cell renal cell carcinomas (ccRCCs) via functioning cooperatively with MIF through survival signaling [39]. They found that MIF-2 displayed a similar expression pattern to MIF in ccRCC sections, which was accompanied by a high correlation between MIF and MIF-2. As for the mechanism, MIF-2 acts as a novel hypoxia-inducible gene as well as a target of hypoxia-inducible factor (HIF)-1α and HIF-2α. More importantly, dual inhibition of MIF-2 and MIF can cause a more pronounced phenotype than the single effect, indicating that the current strategy aimed at targeting MIF needs to be expanded to include MIF-2. Guo and coworkers in 2016 studied the significance of MIF-2 in the context of pancreatic ductal adenocarcinoma (PDAC). They utilized PANC-1 cells, and found that knockdown of MIF and MIF-2 attenuated the phosphorylation of AKT and ERK1/2, and upregulated the expression of p53. This was paralleled by inhibition of cell proliferation and invasion and led to the overall inhibition of tumor growth [40]. They also employed a non-selective inhibitor of MIF-2 and MIF, 4-iodo-6-phenylpyrimidine (4-IPP) in PANC-1 cells, and observed that 4-IPP was capable of inhibiting cell proliferation and tumor formation. Therefore, they drew the

conclusion that a combination strategy of targeting both MIF and MIF-2 might provide a benefit for patients with PDAC.

Additionally, given that MIF exerts an essential role in cervical cancer [48,49], several researchers utilized HeLa and SiHa cell lines to verify that the knockdown of MIF-2 and MIF not only inhibited proliferation and migration, as well as invasion of tumor cells, but also constrained the growth of xenograft tumors [50]. Other data from Gavalli and coworkers pointed out that MIF and MIF-2 might have overlapping effects on neuroblastoma (NB) tumorigenesis. They found that the histone deacetylase inhibitor (HDI) vorinostat was capable of reducing MIF and MIF-2 levels significantly in human NB cells *in vitro*. Therefore, MIF-2 and MIF could be regarded as negative prognostic factors for neuroblastoma [51].

In summary, current data from several preclinical studies have consistently displayed the upregulated expression of MIF-2 and MIF in different kinds of human cancers, even if there are less data available for MIF-2 than MIF. Along the same lines in NSCLC, pancreatic and gastric cancer, MIF and MIF-2 have been shown to 'cooperate' in regulating melanoma, hepatocarcinoma, glioma and cervical adenocarcinoma. In the future, more focus should be placed on combined knockdown/inhibition therapies of MIF-2 and MIF to enhance the therapeutic potency.

1.1.3.2 MIF-2 in acute inflammation

Some of the experiments for MIF-2 have been motivated by earlier studies on MIF in a certain disease context. This also holds true for the study of MIF-2 in inflammation. In response to pro-inflammatory stimuli exemplified by LPS, macrophages can produce MIF as well as MIF-2. MIF-2 concentration came to a peak at 16 h after LPS stimulation. However, twenty-fold more MIF than MIF-2 was released by cultured macrophages stimulated with LPS [10]. In addition, Merk and coworkers successfully produced an anti-MIF-2 antibody, which showed a protective effect on mice upon lethal endotoxic shock by lowering the levels of pro-inflammatory cytokines for example interferon (IFN)-γ, interleukin (IL)-1β, tumor necrosis factor (TNF)-α, and IL-12p70. They also demonstrated that MIF-2 could activate signaling through binding to CD74 with a high affinity, and further exerted some pro-inflammatory functions similar to MIF, for instance regulating macrophage random migration and suppressing glucocorticoid-mediated immunoreaction [10]. However, a new study conducted by Tilstam *et al.* in 2021 described that MIF-2 could not contribute to the recruitment of

inflammatory macrophages as triggered by MIF in a sepsis mouse model. This might be attributed to the absence of the *pseudo-(E)LR* motif in MIF-2, which MIF features [52].

More recently, the recruitment of neutrophils has been defined as a new mechanism for the involvement of MIF-2 in inflammation [53]. One study by Winner *et al.* revealed a covalent modification at the N-terminal proline of both MIF-2 and MIF by 4-IPP [54], which finally leads to the production of 6-phenylpyrimidine (6-PP) adduct. Despite their different tautomerase sites, 4-IPP is likely to function with MIF and MIF-2 in a similar pattern. When Rajasekaran *et al.* applied modified MIF-2-6-PP or MIF-6-PP separately; the neutrophil recruitment in lung displayed a moderate reduction by 50% in comparison with the effect induced by Apo proteins. However, the simultaneous administration of MIF-6-PP and MIF-2-6-PP did not show a synergistic effect, as expected. Even so, it was already acknowledged that MIF/MIF-2-mediated intracellular signaling was similarly handled by the binding of extracellular MIF/MIF-2 with CD74 [2,8-10]. To conclude, MIF-2 has a potent property of recruiting neutrophils, which is identical to MIF's CD74-dependent activity overall.

To sum up, taken current applications of MIF inhibitors in inflammatory diseases into account, it will be worthwhile to further explore whether the MIF neutralization strategies should encompass combination approaches against MIF and MIF-2 [55,56].

1.1.3.3 MIF-2 in adipocyte lipid metabolism

Adipokines, secreted by white adipose tissue (WAT) due to its endocrine function, exhibit essential properties in maintaining the homeostasis in the body, and further act as potential biomarkers for early diagnosis of inflammatory, cardiovascular, metabolic or malignant diseases [57]. Since 2012, there are four original research papers about MIF-2 in adipose tissue or adipocytes. One research group from Japan in 2012 identified MIF-2 as a unique adipokine with the function of regulating lipid metabolism [58]. They used recombinant MIF-2 (rMIF-2) protein to stimulate a kind of human preadipocyte cell line, SGBS cells, and found that rMIF-2 could upregulate IL-6 expression and secretion as well as ERK1/2 phosphorylation *in vitro*. Moreover, pretreatment with U0126, an ERK inhibitor, reduced IL-6 expression. Knockdown of CD74 in SGBS cells suppressed rMIF-2-elicited IL-6 upregulation on the mRNA level, which indicates that CD74-ERK signaling pathway participates in the process of rMIF-2 promoting IL-6 expression whereas inhibiting adipogenesis [58]. In the same year, another paper from the same team reported that glucose

intolerance was improved whilst serum free fatty acids were reduced in db/db mice after administration with rMIF-2 [59]. The AMPK pathway is responsible for the energy balance in the body. Specifically, its stimulation increases energy production, while its inhibition induces energy consumption partially through restraining hormone-sensitive lipase (HSL) activity [60,61]. Iwata and coworkers observed that rMIF-2 administration *in vivo* upregulated AMPK phosphorylation-induced HSL expression, whereas downregulated protein kinase A (PKA) phosphorylation-mediated HSL levels [59]. This suggests that both AMPK and PKA pathways are involved in MIF-2-regulated lipid metabolism.

Although MIF-2 was regarded as a homolog of MIF, MIF-2 was reported to show distinct functional properties from MIF in adipose tissue, based on current studies [62-64]. The insulin sensitivity was improved in $Mif^{-/-}$ mice through inducing glucose uptake [62] and inhibiting macrophage infiltration [63], implying that MIF plays a unfavorable role in adipose tissue. In contrast, data from Iwata group reported that MIF-2 had protective effects on adipogenesis and pointed out that AMPK phosphorylation could promote MIF-2 transcription in SGBS adipocytes *in vitro* via modulating mammalian target of rapamycin (mTOR) signaling [64]. Kim and colleagues investigated the potential effects of MIF family proteins including MIF and MIF-2 on white adipose tissue in a murine endotoxemia model and observed an opposite regulation of both MIF family proteins in this context [65]. Of note, *Mif-2* gene deletion induced the transition of adipose tissue macrophages (ATM) towards a pro-inflammatory type, whereas ATMs were found to display an anti-inflammatory type upon *Mif* gene deficiency. Additionally, they observed that LPS stimulation could reduce MIF-2 levels in adipocytes, but did not affect its expression in stromal vascular fraction (SVF), suggesting that adipocytes may be the main cellular source of MIF-2.

Collectively, due to high expression of MIF-2 in liver and adipose tissue, the roles of MIF-2 in metabolic diseases are worth exploring. However, it is currently unclear whether MIF-2 affects physiological functions of adipocytes or hepatocytes and even pathological development. With more studies of $Mif-2^{-/-}$ mouse model and $Mif^{-/-}Mif-2^{-/-}$ mouse model emerging, the role of MIF-2 will be clearer in the near future.

1.1.3.4 MIF-2 in heart, lung and liver diseases

In addition to studies concerning the functional roles of MIF-2 in tumors, inflammation and metabolic diseases, a few studies investigated whether MIF-2 affects the initiation and

progression of liver damage, chronic obstructive pulmonary disease (COPD), ischemic heart injury and heart failure. Qi and coworkers demonstrated that murine cardiomyocytes expressed more MIF-2 after ischemic heart stress [66]. Additionally, they generated conditional cardiomyocyte-specific *Mif-2*-deficient (MIF-2-cKO) mice displaying a damaged response to ischemia-reperfusion, and determined that MIF-2 administration could protect isolated hearts from contractile dysfunction as well as ischemia-reperfusion injury via the AMPK signaling pathway in these mice. This suggests that MIF-2 has protective effects during ischemia heart injury [66]. In comparison, MIF also exerts favorable effects on ischemia-reperfusion and cardiac necrosis by activating AMPK [67,68], but MIF administration would accelerate inflammation and suppress cardiac contractility on the other hand [68,69]. Therefore, it might be preferable to study MIF-2, which hereby could be utilized to prevent limitations or the side effects induced by MIF in ischemic heart diseases.

Recently, Ma and coworkers from Bucala group reported about MIF-2 in the development of heart failure, based on the high expression of MIF-2 in cardiomyocytes. To induce cardiac pressure overload, they performed surgical transverse aortic constriction (TCA) on MIF-2-cKO mice and control mice in parallel. Following this procedure, pronounced cardiac contractile dysfunctions, pulmonary edema and cardiac dilatation were observed in MIF-2-cKO mice [70]. Mechanistically, cardiomyocytes isolated from MIF-2-cKO mice showed impaired contractility, calcium transients, and downregulated sarcoplasmic reticulum calcium ATPase after TCA [70]. Additionally, rMIF-2 showed an anti-fibrotic function through diminishing TGF-β-induced SMAD-2 activation in cardiac fibroblasts, indicating a protective function for MIF-2 in heart failure. To some extent, there are distinct pharmacological functions of MIF and MIF-2 in the heart. In contrast to MIF, MIF-2 was incapable of inhibiting cardiac contractility, which could be because the negative inotropic effect was deficient in the presence of MIF-2 [12,66].

In addition to heart diseases, one recent study from University of Groningen in Netherlands, reported that MIF-2 promoted lung epithelial repair in COPD patients through the interaction with ACKR3/CXCR7 [71]. They observed that MIF-2 enhanced A549 epithelial cell proliferation and thereby conferred protection against apoptosis. Mechanistically, ERK-MAPK and PI3K-AKT signaling pathways participated in this MIF-2-regulated process. This is the first original research to describe the role of MIF-2 in COPD [71], especially highlighting ACKR3 as the second receptor for MIF-2 [71,72]. By contrast, there are quite a

lot of papers studying the functions of MIF in COPD. In general, MIF and its receptor CD74 are necessary to maintain normal alveolar structures and protect against endothelial senescence in COPD mice [73,74]. Apparently, it still requires more evidence to clarify the potential of MIF-2 and its interplay with MIF in COPD.

The last disease to be mentioned here is liver damage. Hiyoshi and coworkers induced experimental liver injury with carbon tetrachloride (CCL4), and they observed that there was a 12-fold upregulation of MIF-2 in damaged liver [75]. Previous researchers demonstrated that MIF-2 levels significantly increased in the damaged liver infected by hepatitis B virus (HBV) or after partial hepatectomy [76,77]. The data obtained in my thesis also revealed a potential association between MIF-2 and hepatic steatosis, the details of which will be described in the result part.

1.1.4 Clinical studies: Plasma/serum MIF-2 levels in human specimens and correlations with disease state

1.1.4.1 MIF-2 in inflammation

Sonesson *et al.* firstly found that MIF-2 was detectable in the skin and also could be associated with inflammation, and its covariation with MIF further supported this finding [78]. A previously published study in 1989 showed that several cytokines were secreted from the skin and released into blood after ultraviolet-B (UVB) radiation [79]. Sonesson and coworkers utilized UVB light to induce a kind of experimental inflammation in 10 healthy subjects of human skin and performed immunohistochemistry to confirm that MIF-2 expression was markedly upregulated after UV irradiation [78]. Merk and coworkers also analyzed the potential association between serum MIF-2 and MIF in patients, who were diagnosed as sepsis or ovarian cancer. They found that circulating MIF-2 significantly increased in patients and it was strongly correlated with the expression of MIF, indicating that both proteins may be affected coordinately under inflammatory conditions [10]. Except for acute inflammation, MIF-2 was also reported to participate in adipose tissue inflammation and acute wound healing [80].

Another study by Kim and coworkers in 2016 investigated the clinical significance of MIF-2 and soluble CD74 (sCD74) in twenty burned patients *versus* twenty controls [81], based on earlier data showing that MIF could be a promising biomarker for patients with burn injury [82]. In this context, they found that MIF-2 and sCD74 levels were obviously elevated in burn

patients, and MIF-2 had a positive correlation with some indexes of burn in early stages such as procalcitonin (PCT) levels. This indicates that MIF-2 has a predictive value in response to burn [81]. Additionally, Pohl *et al.* evaluated several laboratory parameters and mortality for 72 critically ill patients, and showed that there was a higher mortality for these patients with elevated MIF-2 in plasma through Kaplan-Meier analysis, supporting MIF-2 as a marker to assess the prognosis of critically ill patients [83].

1.1.4.2 MIF-2 in autoimmune diseases

This part will mainly summarize several clinical studies of MIF-2 in autoimmune diseases, especially multiple sclerosis (MS). Some studies have displayed that MIF contributes to the regulation of immune response of neural cells such as microglia, which is thereby related to the development of autoimmune diseases in the brain [84-86]. Benedek and colleagues further demonstrated that both MIF and MIF-2 levels went up in male patients with progressive MS compared with female MS patients, and reversely *Mif* or *Mif-2* deficient male mice developed less severe MS signs. These phenotypes together suggest that MIF-2 as well as MIF are gender-specific co-pathogenic contributors to MS progression, and they may behave differently among species [87]. Of note, Vandenbark *et al.* recently applied $Mif^{-/-}$, Mif-$2^{-/-}$ as well as *Mif Mif-2* double deficient mice to discern whether MIF-2 and MIF together would make a greater contribution to disease progression of EAE mice [32]. Surprisingly, a reduction by ~25% in moderate EAE was observed in either *Mif-* or *Mif-2*-deficient mice in comparison with controlsmice, whereas there were no further reductions of EAE severity detected in $Mif^{-/-}Mif$-$2^{-/-}$ mice. Thus, this finding would not support a synergistic manner of MIF-2 and MIF at least in the context of MS. Besides, one recent study from Turkish patients revealed that genetic variant rs755622 polymorphism in MIF promoter was strongly associated with the onset of MS [88]. Given that there are partial common sequences in the promoter shared by MIF-2 and MIF, Han and coworkers in 2018 confirmed that rs755622 could modulate MIF-2 expression of MS subjects in a sex-specific way by utilizing five large-scale expression quantitative trait loci (eQTLs), based on two RNA-sequence datasets of blood and brain [89]. More recently, clinical data from Cavalli group showed that both MIF-2 and MIF were overexpressed in $CD4^+$ T cells from patients diagnosed as clinically isolated syndrome (CIS), which can rapidly develop into clinical defined MS, through a transcriptomic analysis of the expression of MIF and MIF-2 as well as their common receptors in peripheral blood [90].

The other autoimmune disease that MIF-2 contributes to is systemic sclerosis (SS). Several previous studies displayed that circulating MIF levels were obviously elevated in SS patients [91,92]. Vincent and coworkers showed that serum MIF-2 levels were only significantly upregulated in 105 cases of SS patients with low expression of FEV1, and further conversely had a negative correlation with European Scleroderma Trials and Research group (EUSTAR) score, compared with 47 cases of healthy controls. Additionally, a comparative study of MIF and MIF-2 did not show similar expression profiles in SS subjects, indicating functional differences between these two proteins [93]. However, they stressed that serum MIF-2 levels in SS patients did not change significantly in comparison with systemic lupus erythematosus (SLE) patients, implying that upregulated MIF-2 is not associated with specific clinical phenotypes [93]. Even so, aberrant expressions of MIF-2 in these patients would give some indications to relevant research in this field.

1.1.4.3 MIF-2 in other diseases

On the other hand, Roger and coworkers in 2017 delineated circulating MIF and MIF-2 levels in different age groups through a large cohort study, and emphasized the importance of MIF-2 in early life [94]. In their study, MIF-2 level at birth was around 52.0 ng/mL, increased to the highest level of 121.6 ng/mL on postnatal day 4, and decreased to 16.8 ng/mL in healthy adults. Compared with MIF-2, MIF expression also displayed a similar tendency: secretory MIF went up to 82.6 ng/mL at birth, and also reached the peak of 109.5 ng/mL on postnatal day 4, and then reduced to 5.7 ng/mL in healthy adults [94]. During the first few months of life, both MIF and MIF-2 concentrations already decreased to the adult levels. Of special note, MIF-2 levels were strongly correlated with MIF levels in different age groups included in their study. Moreover, Baron-Stefaniak *et al.* measured serum MIF-2 levels in patients after orthotopic liver transplantation (OLT), and they observed that MIF-2 did not affect acute kidney injury after OLT through one-year survival analysis [95]. Until now, most of clinical studies start with plasma or serum MIF-2 measurement. However, some other researchers also measured tissue MIF-2 changes in diseased organs. MIF-2 levels were dramatically elevated in human cervical cancer tissue [50] and neuroblastoma tissue [51], whereas they were significantly decreased in cardiac tissue with advanced heart failure [70].

In summary, since MIF-2 was initially discovered and successfully isolated in 1993, structural characteristics, relevant comparisons with MIF, functional properties and even clinical significance in various disease settings were investigated. Figure 2 gives a brief summary

about current progress based on major studies about MIF-2 in the past three decades. So far, most of researches showed that MIF-2 and MIF expressed in a similar pattern in diseased organs, whereas a few papers revealed that there existed contrary changes in particular diseases due to the potential functional differences between two proteins. Even if there are already a large amount of preclinical as well as clinical studies concerning different specimens, the roles of MIF-2 in various pathological conditions have not been mechanistically clarified yet. For example, elevated MIF-2 levels in the early stage of disease does not really tell us whether MIF-2 exert protective and/or pathogenic effect(s). With the availability of $Mif-2^{-/-}$ mouse model and selective MIF-2 inhibitors, more studies will emerge and clarify these phenotypes as well as relevant mechanisms.
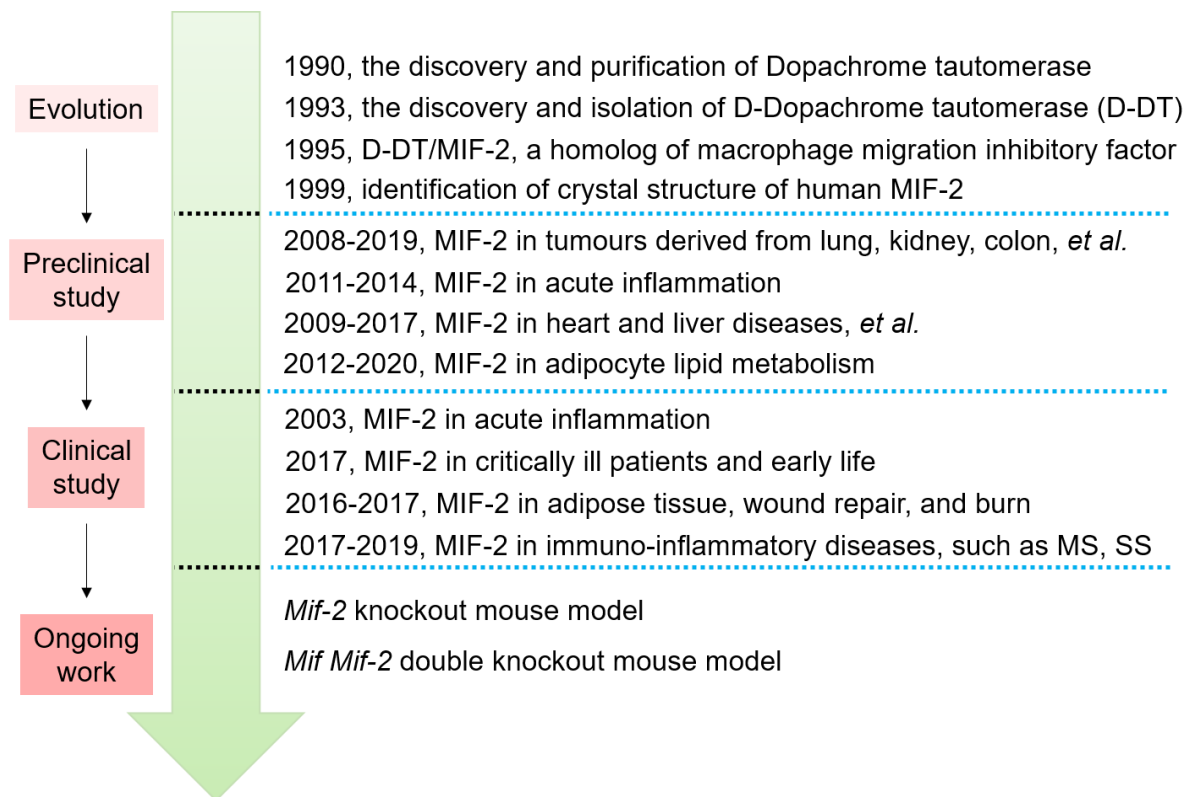

Figure 2: Summary of the discovery, early studies and recent progress of MIF-2. Since MIF-2 was discovered in 1993, numerous clinical and experimental studies emerged, and gradually covered different disease settings. The availability of *Mif Mif-2* double knockout mice in different fields will better decipher the interplay between MIF and MIF-2.

1.2 New insights into associations between atherosclerosis and non-alcoholic fatty liver disease (NAFLD)

1.2.1 Classical chemokines, atypical chemokines and MIF family proteins in atherosclerosis

1.2.1.1 Overview of atherosclerosis (AS): AS is an inflammatory disease

As reported, atherosclerosis remains one of the largest causes of mortality in most industrialized nations, which consequently brings quite high social and economic burdens [96]. In addition, most cardiovascular diseases occur due to underlying atherosclerosis, which acts as a main pathological basis, for example ischemic stroke (IS) and myocardial infarction (MI) [97]. Therefore, it is necessary to study these diseases.

In the mid-19th century, the German pathologist Rudolph Virchow clearly pointed out the role of inflammation in atherosclerosis, whereas with much less knowledge of the mechanism details and relevant signaling pathways [98]. With the development over time, there emerged some predominant theories of atherogenesis mechanisms after heated controversies and discussions. Nevertheless, enormous strides have been made in atherosclerosis research in the past century. Basic and clinical research led by atherosclerosis pioneers such as Peter Libby, Russel Ross, Göran Hansson and others have unraveled the importance of inflammation in cardiovascular disease in general, especially in atherosclerosis. These pioneer researchers were able to follow it from the very earliest of preclinical stages with gels, blots and columns, gradually through pilot clinical studies and even to some large-scale clinical trials that actually showed it is all worthwhile [99-103]. Overall, experimental advances in the past three decades support the causal role of inflammation in all phases of the atherosclerotic process. Clinical studies have shown that this emerging concept that inflammation dominates atherosclerosis could apply to patients directly as well. Of special note, Dr. Peter Libby instigated and led the first large-scale CANTOS trial including 10,061 patients, to principally target at IL-1β with regard to inflammation. This provides the first clinical validation for the role of inflammation in atherosclerosis, independent of lipid-lowering effects [104].

Even though there has been striking progress in this field, this battle against atherosclerosis is not yet won [105]. In spite that some highly effective and preventive measures and substantial LDL lowering therapeutic strategies are commonly applied nowadays, a

considerable residual burden of atherosclerosis persists. Emerging new genetic methods might give a more accurate assessment for the individuals at risk, which is accompanied by a more personalized identification. Of note, these approaches will be available due to application of informatics technologies. More recently, various cell clusters characterizing different cell types and populations directly from atherosclerotic plaques were revealed through single-cell RNA sequencing technique [106], which is promising to provide some novel therapeutic targets beyond some traditional risk factor control measures. Expansion of genetic discovery and predictive work presents an important goal for the future. Furthermore, characterizing different pro-inflammatory chemokines/cytokines as well as identifying unique immune cell subtypes in plaques would contribute to the development of new preventive measures and treatments.

1.2.1.2 Classical chemokines in atherosclerosis

In this complicated process of atherosclerotic initiation and progression, chemokines/cytokines are major drivers of vascular inflammation, mainly through promoting the recruitment of immune cells such as inflammatory leukocytes. In fact, pro-inflammatory chemokines are found to participate in all different stages of atherogenesis. So far, there are around fifty classical chemokines branched into C-, CC-, CXC- and CX3C-type subsets, together with their multiple correspondingly termed receptors, to form this redundant and promiscuous interaction network [107,108]. As for the functionality, these chemokines could influence cell proliferation, apoptosis, gene expression and homeostasis via binding with different receptors on various cell types, such as monocytes, neutrophils, endothelial cells, eosinophils, macrophages, basophils and other cells. This is the reason why chemokines are generally involved in a wide variety of inflammatory diseases. Thereby, the determination of proper targets is essential to exploring real functions of the individual chemokine and/or receptor.

Chemokines belong to cytokine family, trafficking the intricately organized and regulated movements of cells into inflammation sites within the body. More importantly, chemokines are regarded as vigorous activators of different cells due to their functional properties of enhancing the migration of leukocytes [109,110]. In fact, there are several well-studied chemokines involved in the atherogenesis, exemplified by CXCL4/platelet factor 4 (PF4), CXCL12/stromal cell-derived factor 1 (SDF-1), and CXCL1/keratinocyte-derived chemokine (KC) or CCL2/monocyte chemoattractant protein-1 (MCP-1). Among them, the majority of

chemokines exert pro-atherogenic effects, as confirmed by numerous experimental studies. However, other a few chemokines for example CXCL5, CXCL16 and CX3CL1 play a protective role in atherosclerotic progression. Based on current studies, it is very promising to handle with several kinds of pathologies through capitalizing on explicit approaches, either investigating the intracellular mechanisms in chemokine-activated cells or exploring chemokine receptor antagonists. Therefore, Table 3 gives a comprehensive summary about functional roles and specific mechanisms of different classical chemokines in atherosclerosis here.

Table 3: Roles and mechanisms of classical chemokines in atherosclerosis

Classical Chemokines	Mouse models	Roles in atherosclerosis	Mechanisms	Refs.
CCL2/ MCP-1	$Apoe^{-/-}$ mice	Pro-atherogenic	Blockade of CCL2 altered lesion components and downregulated CD40 and ligand levels	[111]
CCL3/ MIP-1α	$Ldlr^{-/-}$ mice	Pro-atherogenic	Leukocyte-secreted CCL3 could traffic neutrophils into plaques	[112]
CCL5/ RANTES	$Apoe^{-/-}$ mice; $Ccr5^{-/-}$ $Apoe^{-/-}$ mice	Pro-atherogenic	YB-1-mediated CCL5 expression contributed to neointimal hyperplasia	[113]
CCL17/ TARC	$Apoe^{-/-}$ mice; $Ccr17^{-/-}$ $Apoe^{-/-}$ mice	Pro-atherogenic	Dendritic cells-derived CCL17 promoted atherosclerosis through regulating Treg homeostasis	[114]
CCL19/ CCL21	$Ldlr^{-/-}$ mice	No effects	CCL19/CCL21 could not change the lesion burden *in vivo*	[115]
CXCL1/ KC	$Apoe^{-/-}$ mice	Pro-atherogenic	Blockade of CXCL1 decreased plaque formation via inhibiting CXCR2-modulated endothelial chemotaxis	[116]
CXCL2/ MIP-2α/ Gro-β/Gro-2	$P2Y_6$ deficient mice	Pro-atherogenic	Plaque sizes were increased with the upregulation of CXCL2 induced by the binding of UDP and $P2Y_6$	[117]
CXCL4/ PF4	$Apoe^{-/-}$ mice	Pro-atherogenic	Deficiency of *Cxcl4* from platelets could attenuate atherosclerotic progression *in vivo* through binding to LDLR and CXCR3	[118]
CXCL5/ ENA-78	$Apoe^{-/-}$ mice	Anti-atherogenic	CXCL5 exerts an atheroprotective effect on macrophages through upregulating ABCA1 levels and promoting cholesterol efflux	[119]
CXCL10/ IP-10/ SCYB10	$Apoe^{-/-}$ mice; $Cxcl10^{-/-}$ $Apoe^{-/-}$ mice	Pro-atherogenic	*Cxcl10* deficient mice displayed less lesions due to the balance of Treg and effector in plaque	[120]
CXCL12/ SDF-1	$Apoe^{-/-}$ mice; $Ldlr^{-/-}$ mice	Pro-atherogenic	CXCL12 exerts multiple atherogenic effects via binding to CXCR4 and CXCR7, related to vascular inflamma-tion, lipid metabolism, angiogenesis	[121-123]

CXCL16/ Bonzon/ STRL33/ TYMSTR	*Apoe*^{−/−} mice; *Cxcl16*^{−/−} *Apoe*^{−/−} mice	Anti-atherogenic	CXCL16-regulated scavenger receptor plays a protective role in atherosclerosis	[124]
CX3CL1/ Fc	*Ldlr*^{−/−} mice	Anti-atherogenic	CX3CL1 could reduce atherosclerosis by inhibiting the adhesion of endothelial cells and monocytes	[125]

1.2.1.3 Atypical chemokines in atherosclerosis

In addition to four types of classical chemokines described in the above part, relevant studies of atypical chemokines (ACKs), also called innate or chemokine-like function (CLF) chemokines, draw a lot of attention in the field of atherosclerosis research as well. ACKs are secreted as small intracellular proteins of ~8-25 kDa, which could also be released as extracellular mediators upon the stimulation of inflammatory factors or stress. Of interest, in comparison with classical chemokines, ACKs still share the gross architectural similarity and display chemotactic properties through binding to receptors, whereas they lack the N-terminal cysteine residue(s) and the classical chemokine-fold [126]. Despite the fact that the structural homology to classical chemokines is at least partially absent in ACKs, various secreted factors (cytokines/chemokines) driven by the interaction of ACKs with classical chemokine receptors (CKRs) or atypical chemokine receptors (ACKRs), carried the load of regulating several inflammatory processes. In fact, ACKs could act as proteinaceous alarmins or damage/danger-associated molecular patterns [127]. More recently, Kapurniotu and co-workers gave a comprehensive summary about well-known ACKs, covering high-mobility group box protein 1 (HMGB1), MIF family proteins, β-defensins, aminoacyl-tRNA synthetases (AaRS) and viral chemokine mimics. Furthermore, they also elucidated multitasking functions of these factors as inflammatory mediators [127]. In this chapter, the roles of HMGB1, β-defensins (HBDs) and thioredoxin (Trx) in atherosclerosis will be emphatically discussed.

As the most famous ACK, HMGB1 is a nuclear protein, mainly released from necrotic cells or secreted by damaged and stressed cells. It could function as a multitasking alarmin in several inflammatory processes. Regarding atherosclerosis, it was initially revealed that HMGB1 showed upregulated expression in smooth muscle cells (SMCs) and lesioned macrophages as well as endothelial cells (ECs) [128-130], which further contributed to the atherosclerotic progression. Besides, HMGB1 induced tissue factor (TF) secretion and hemostatic reactions during the coagulation, thus promoting thrombus formation. This could

also be a possible mechanism how HMGB1 accelerates atherosclerosis [131]. As a late-stage mediator of inflammation, HMGB1 could additionally promote SMCs-derived C-reactive protein (CRP) production, which has been shown to contribute to a pro-atherosclerotic phenotype of advanced human plaques [132]. In addition, Kake *et al.* observed that serum HMGB1 concentrations were negatively correlated with the thrombus formation time in patients, and furthermore they confirmed this kind of relationship in hyperlipidemia-induced micro-minipig model [133].

On the other hand, Kanellakis and coworkers explored the detailed mechanisms based on previous findings that HMGB1 contributed to mice plaque development, in order to offer a propitious therapeutic target against atherogenesis. To this end, they revealed that HMGB1 could promote macrophage migration, regulate pro-inflammatory mediators and recruit different immune cells and SMCs [134]. One experimental study from the Bianchi group mechanistically characterized the heterocomplex formed by HMGB1 and CXCL12, as evidenced through nuclear magnetic and surface plasmon resonance. They next revealed that HMGB1 could recruit inflammatory cells by forming this complex and regulating signaling via CXCR4 [135]. Additionally, the other receptor of HMGB1, the receptor for advanced glycation end product (RAGE), was also confirmed to exert a crucial impact on atherosclerotic progression [136]. Of interest, the activation of the HMGB1-RAGE nexus was mainly related to endothelial dysfunction and vascular inflammation [137]. In turn, Simvastatin administration could ameliorate vascular inflammation and atherosclerotic progression in *Apoe*$^{-/-}$ mice by suppressing the HMGB1-RAGE axis [138]. Moreover, HMGB1 was speculated as a potential downstream target of miR-328 through bioinformatics analysis, and it was implied that miR-328 mitigated endothelial cell injury triggered by oxidized (ox)-LDL mechanistically through targeting HMGB1 in atherosclerosis [139]. In aggregate, HMGB1 plays a pro-atherogenic role in the vascular wall.

Human β-defensins (HBDs), one class of human host defense peptides, have dual functions in innate and adaptive immunity. On the one hand, their original antimicrobial properties are beneficial to combat with microbial invasions through modulating local innate immune response. On the other hand, in addition to T cells, HBDs could exert chemoattractant activities for dendritic cells through its interaction with CCR6 [140], or for monocytes, macrophages and neutrophils via CCR2 [141]. Of note, HBD-2 and HBD-3, in combination with their mouse orthologues including mBD-4 and mBD-14, serve as essential chemotactic

chores, and their behaviors of promoting leucocyte chemotaxis are reliant upon CCR6 and/or CCR2. Subsequently, Li and coworkers in 2016 demonstrated that human β-defensin-3 could attenuate atherosclerotic progression induced by LPS in *Apoe*$^{-/-}$ mice. They further found that HBD-3 dramatically downregulated the expression of IL-6 and TNF-α in serum, and the mRNA and protein levels of ICAM-1, IL-6, and MCP-1 in lesions in the meantime [142]. Mechanistically, HBD-3 inhibited LPS-mediated inflammation though the NF-κB and MAPK signaling, and further suppressed atherosclerotic progression [142,143]. Another study from Korea evaluated the effects of HBD-1 on inflammatory macrophages using fenofibrate and gemfibrozil, which belong to peroxisome proliferator-activated receptor α (PPARα) agonists. They observed that PPARα agonists held down macrophage activation induced by LPS via affecting PPARα, and HBD-1 as well as TLR4 signaling [144]. Additionally, Tiszlavicz *et al.* found that HBD-2 mRNA and protein levels were significantly increased upon *C. pneumoniae* infection, offering potential indications that HBD-2 may be implicated in early immune reactions in this context, and contribute to atherogenesis further [145]. In summary, due to the innate antimicrobial characteristic of HBDs, current studies mainly focus on the functional significance of HBDs in LPS-accelerated atherosclerosis.

In a similar vein, Trx, a ubiquitous small protein of 12 kDa, mainly exists as Trx-1 and Trx-2 in various intracellular components. The well-known function of Trx is to catalyze the reduction of disulfide bonds in target proteins, whereas this reaction could be reversibly counteracted by the action of thioredoxin reductase (TrxR) [146]. In this regard, Trx and TrxR as well as nicotinamide adenine dinucleotide phosphate (NADPH) are together known as the thioredoxin system. Trx system in macrophages was reported to exert important functions in both early and advanced stages of atherosclerosis [147], especially associated with lipid accumulations in macrophages caused by cellular oxidative stress. El Hadri and coauthors have shown that the differentiation of macrophages into anti-inflammatory phenotype induced by Trx-1 could be a possible explanation for its atheroprotective effects. In the meanwhile, Trx-1 was stained to show the colocalization with M2 marker of macrophages but not with M1 marker of macrophages in human plaques [148]. Additionally, some researchers found that Puerarin could inhibit SR-1 and Lox-1 expression and thereby suppress lipid uptake in macrophages via activating Trx-1, which was assumed as a promising target against atherosclerosis [149]. Moreover, NLR family pyrin domain containing 3 (NLRP3) inflammasome was demonstrated to be involved in Trx-1-mediated atherogenesis [150], and this phenotype was observed in macrophages *in vitro* and HFD-fed *Apoe*-deficient mice *in*

vivo. In addition to these effects of Trx on oxidative stress, Trx-1 was also reported to affect reverse cholesterol transport (RCT) *in vivo* and accelerate macrophage cholesterol efflux *in vitro*. Mechanistically, they revealed that Trx-1 stimulated LXRα nuclear translocation and further upregulated the expression of ATP-binding cassette transporter A1 (ABCA1) [151]. Collectively, most of studies suggest that Trx-1 has protective effects on atherosclerosis until now.

Except for HMGB1, HBDs and Trx, MIF family proteins such as MIF and MIF-2 also serve as important ACKs and exert chemokine-like and pro-inflammatory properties in both human and murine atherosclerosis. In hindsight, there is plenty of evidence that MIF could be a pro-atherogenic factor, which will be addressed in the next part.

1.2.1.4 MIF family proteins in atherosclerosis

Among atypical chemokines, MIF family proteins are very interesting candidates with regard to atherogenesis. As we have learned from previous studies, MIF is an upstream modulator of inflammation, and it displays high expression in the inflamed vasculature of various sub-compartments. Of note, MIF, as a multi-functional cytokine in inflammation, features a unique structure and chemokine-like characteristics, which cannot be grouped into any class of classical chemokines. With regard to cardiovascular diseases, it has emerged that MIF acts as an important player in acute and chronic inflammation for example heart failure and atherosclerosis. In atherosclerotic lesions, MIF displayed upregulated expression and functionally promoted atherogenesis by orchestrating the recruitment of leukocytes based on its interactions with CXCR2 and CXCR4 [2,152]. Conversely, a MIF/CD74 axis-elicited cardio-protective effect mediated through an AMPK-dependent intracellular signaling pathway has been found in the ischemic heart [153].

In the context of atherosclerosis, MIF exhibits pro-inflammatory and pro-atherogenic properties overall. In 2002, Burger-Kentischer and coworkers systemically described the immunoreactivities and mRNA expressions of MIF in human plaques at different stages. They emphasized that c-Jun activation domain-binding protein-1 (Jab1), being one potent activator of MIF's actions in blood vessels, could form a functional complex with MIF and further exert critical regulatory functions in plaque evolution, as confirmed by immunohistochemistry and immunoprecipitation [152]. Additionally, MIF levels showed a tight correlation with signs of instability in advanced atherosclerotic lesions from human

carotid endarterectomy (CEA) samples [154]. Moreover, the expression of MIF in angiotensin II-producing mononuclear cells and CD40L positive cells in plaques indicates the causal role of MIF in modulating atherosclerotic plaque stability. Recently, Kontos and coworkers indeed detected highly expressed MIF in unstable and stable CEA plaques in comparison with adjacent healthy tissue [155]. However, MIF mRNA expression did not show any significant changes between stable and unstable plaques, as reflected through quantitative PCR and RNA sequencing. Especially, they designed a novel CXCR4 mimic msR4M-L1, the MIF-specificity of which was proved not only by a competition assay, but also by less staining signals in stable plaques. Of interest, another previously published study indicated that unstable plaques expressed more pronounced CXCL12, an important ligand of CXCR4, compared to stable plaques [123].

In addition to plenty of explorations from human specimens, substantial amounts of evidence for the *in vivo* relevance of MIF in disease progression has been obtained until now. MIF has been broadly implicated in atherogenesis in both *Apoe*$^{-/-}$ and *Ldlr*$^{-/-}$ mouse models, as confirmed by strategies of *Mif* gene knockout or antagonist blocking [2,14,156,157]. In general, the global depletion or short-term inhibition of MIF could attenuate atherosclerotic plaque burdens and lesion progression. As for the cellular contribution, MIF was reported to display different levels of upregulations in various cells such as SMCs, ECs, infiltrated leukocytes and platelets in plaques among several species including humans, mice, and rabbits [152,158-160]. This upregulation of MIF was induced by pro-atherogenic mediators such as ox-LDL after arterial injury, leading to plaque instability finally. Given that MIF acts as a non-cognate CXCR ligand, its pro-atherogenic functions are mainly attributed to its interactions with CXCR4 and CXCR2, respectively [2,12]. Regarding functional activities, MIF promoted the recruitment of atherogenic monocytes and neutrophils, and the arrest of B/T lymphocytes on aortic endothelium [161]. In addition to CXCR4 and CXCR2 addressed above, MIF-triggered atherogenic leukocyte recruitment was also reliant on the MIF-binding protein CD74, which showed the colocalization with CXCR2 and formed the receptor complex eventually [2,162,163]. Similarly, CXCR4/CD74 complex formation has been described in B cell migration driven by MIF [161,163]. Except for CD74, the involvement of CXCR2 and CXCR4 in MIF-mediated immune cell recruitment sheds light on the interplay between ligands and receptors in atherogenesis and vascular remodeling [126]. Specific functions of MIF in atherosclerosis were illustrated in Figure 3, which was modified from one published literature [164].

Considering the pivotal role of MIF in atherogenesis and given the close structural similarity between MIF and its homolog MIF-2, the question arose if MIF-2 would also play a role in atherosclerosis. To this end, our laboratory firstly generated *Mif-2* knockout mouse line under the background of *Apoe*$^{-/-}$, and my PhD project aimed to figure out the significance of MIF-2 in atherogenesis and specific mechanisms behind the phenotype. Recently, 4-CPPC, a novel and reversible inhibitor of 287.23 Da was identified for MIF-2 [165,166], and it has been tested to competitively bind to MIF-2 with a 13-fold selectivity compared to MIF. This would provide us more approaches for MIF-2-related study.
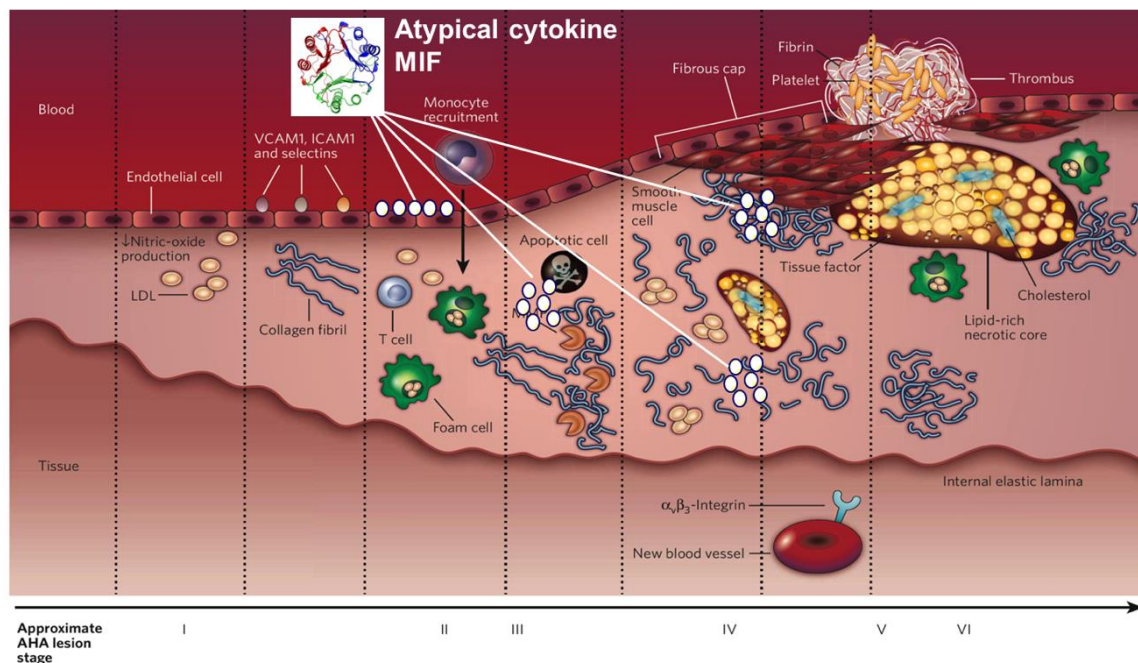
Figure 3: The role of MIF in atherosclerosis development. As an atypical and pro-inflammatory chemokine, MIF contributes to vascular inflammation and atherogenesis through multiple mechanisms. The figure was modified from reference [164].

1.2.2 Chemokines in NAFLD

1.2.2.1 Overview of NAFLD, a class of chronic liver disease

NAFLD, the most prevalent pattern of chronic liver disease, mainly exists in two predominant histological subtypes: non-alcoholic fatty liver and non-alcoholic steatohepatitis (NASH) [167]. Cirrhosis, the late stage of NAFLD, remains a growing cause of mortality in Western nations, ranking 4th in central Europe and 14th worldwide [168]. Abnormal neutral lipid aggradations, chiefly triacylglycerol, in liver are the classical hallmark of NAFLD, especially in the absence of viral infection, excessive alcohol consumption and other external etiologies. There should be a dynamic balance between lipogenesis/lipid uptake and lipid clearance in

the body, whereas its imbalance finally leads to lipoperoxidative cellular stress and hepatic inflammatory injury [169]. The inflammation-fibrosis-cancer axis eventually results in clinical cirrhosis, which leads to death invariably, unless liver transplantation is done. Therefore, taking preventive measures and therapies in time is vitally important to control or prevent the progression of NAFLD to the end stage.

Therefore, a brief overview of well-known risk factors for NAFLD was given here. Without doubt, high fat diet, cigarette smoking and an unhealthy lifestyle have been definitely recognized as independent risk factors for NAFLD progression. A Westernized pattern of diet containing high red meat consumption, high sugar beverages and pastries, and refined grains, has been closely related to the development of NAFLD and metabolic syndrome [170]. Additionally, cigarette smoking seems to be independently related to the onset of NAFLD through one retrospective study including 2029 participants [171], and also associated with insulin resistance [172]. Consistent with these findings, passive smoke exposure is also considered as a strong independent predictor for the metabolic syndrome from a study in the United States [173]. Speaking of the life style, less physical activities and long-term sedentary behavior would aggravate the severity of NAFLD [170]. By contrast, weight loss through a balanced diet or physical exercise could obviously ameliorate NAFLD markers, for example hepatic enzymes [174]. Undoubtedly, ethnic differences [175], gender and age [176] more or less would affect the progression of NAFLD, but these internal factors are unchangeable. Except for their different natural history, metabolic syndrome encompassing hyperlipidemia, and obesity as well as diabetes mellitus is also one type of relatively common risk factors for patients with NAFLD. Furthermore, the rising incidences of NAFLD are consistent with the increasing rates of metabolic syndrome [177]. Moreover, polycystic ovarian syndrome (PCOS) [178] and obstructive sleep apnea (OSA) [179] were confirmed to endanger those patients who developed NAFLD. In summary, there are plenty of recognized risk factors for NAFLD patients. Even if it is difficult to avoid all the potential dangerous sources, it is preferable to minimize their negative effects.

1.2.2.2 Chemokines in NAFLD

Inflammatory injuries virtually exist in all kinds of liver diseases. During the hepatic inflammatory process, chemokines derived from liver resident cells including hepatocytes, biliary epithelial cells, activated stellate cells, and endothelial cells as well as infiltrating immune cells mainly monocytes and leukocytes are pivotal drivers in recruiting relevant immune cells into the injured or diseased sites and inducing corresponding immune reactions in response to specific stimuli [180-183]. Most of important chemokines and involving pathways in liver diseases are summarized in Figure 4. In the context of liver fibrosis, different chemokine-mediated actions based on recruitment of various subsets of immune cells were systemically classified here. In this scheme, CCL1/CCL25, CCL2, CCL3, CCL5, CXCL9, CXCL10, CX3CL1 and CXCL16 exert pro-inflammatory and pro-fibrogenic functions and further promote liver fibrosis progression. In contrast, CX3CL1, CCL2, CCL20 and CXCL9 could serve as anti-fibrogenic factors and be beneficial to the regression of liver fibrosis [180]. However, as we noticed here, CCL2, CXCL9 and CX3CL1 have dual roles in this process regarding different conditions.

Among these chemokines involved in the hepatic pathogenesis, one extensively studied chemokine is CCL2. Remarkably, Kupffer cells could produce high levels of CCL2, which in turn attracted bone marrow-derived CCR2-monocyte to accumulate in liver and thereby enlarged the macrophage pool [184,185]. In this regard, CCL2 could also be released by other cell types, such as hepatocytes [186], hematopoietic stem cells (HSCs) [187], and biliary epithelial cells [188]. In addition to NAFLD, CCL2 was also related to the onset of alcoholic liver disease (ALD). Another large cohort study about ALD patients in 2012 showed that hepatic expression of CCL2 had a close correlation with IL-8 levels and neutrophil infiltration, indicating an important role of CCL2 in ALD pathogenesis [189]. Given that there were still some controversial results about CCL2/CCR2, different genetic mouse models were applied [190,191]. Besides, Wehr and coworkers confirmed the functional roles of CXCL16 and its receptor CXCR6 in regulating chemotaxis and other activities of natural killer T (NKT) cells, by utilizing both human hepatic specimens and murine liver damage models [182]. They found that hepatic NKT cells showed significantly upregulated pro-inflammatory mediator expression for example IFN-γ and IL-4, once liver damage occurred. Additionally, liver-resident macrophages, also termed as 'Kupffer cells', together with infiltrating monocytes were described as main pathogenic factors of hepatic inflammation due to these essential

31

released pro-inflammatory cytokines, which could in turn activate hepatocellular stress, and lipogenesis as well as lipid accumulation [185,192].

In regards of anti-fibrotic chemokines, we mainly talked about CCL20 here. CCL20 mainly targets at γδ T cells and HSCs to play a pro-inflammatory role. Mechanistically, damaged hepatocytes and cholangiocytes strongly secreted CCL20 and further attracted CCR-6-expressing T helper (Th) cells [193] and γδ T cells [194]. Oo and coworkers have demonstrated that Th17 cells recruitment from blood to liver can be enhanced by CXCR3 upon hepatic damage in both mice and humans. And cholangiocyte-released CCL20 directly guided their following positioning near bile ducts [193]. Furthermore, they found that high levels of IL-17 released by Th17 could upregulate CCL20 levels in cholangiocytes. In turn, Th17 cells indeed recruited more IL-17-secreting cells, which formed a positive feedback system to enhance this effect. Hammerich and coworkers initially detected highly expressed CCR6 and CCL20 in patients diagnosed as chronic liver disease, and they observed a similar expression pattern in murine damaged livers [194]. Subsequently, they used $Ccr6^{-/-}$ mouse model to confirm this finding further, and clarified that CCR6-mediated recruitment of γδ T cells into liver could protect against hepatic inflammation and fibrosis through constraining HSCs. Other functional activities of pro-fibrogenic and anti-fibrogenic chemokines were illustrated in Figure 4.
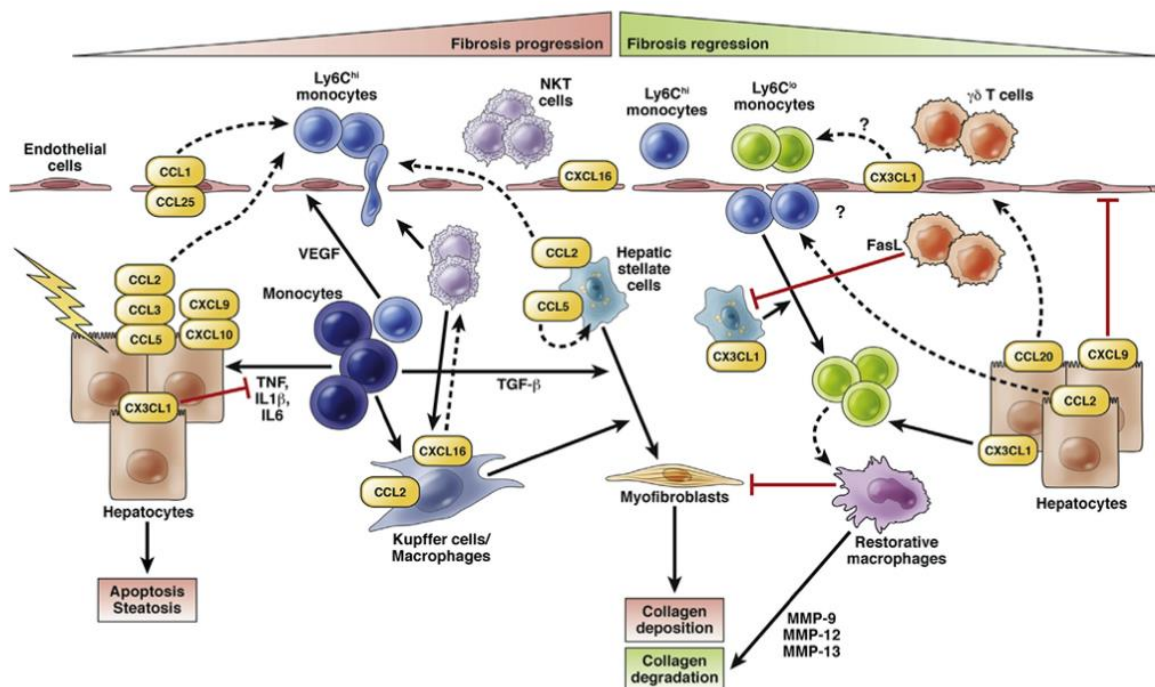

Figure 4: Crucial chemokines and related signaling pathways contribute to the progression and regression of liver fibrosis. Chemokines orchestrate inflammatory reactions through regulating the

recruitment of different immune cell subsets such as monocytes, NK cells and T cell as well as their interactions with liver cells. The scheme was taken from [180].

1.2.3 The interplay of NAFLD and atherosclerosis coupled by inflammation and lipogenesis

Atherosclerosis, characterized by lipid-driven inflammation, is a chronic disease in the artery, which also connects with pathologies of other organs in the body, such as liver, kidney, pancreas, adipose tissue and gut. Among these associations, the lipogenic interplay between atherogenesis and hepatosteatosis has been extensively studied. Following several important hints from our previous data, we checked relevant literatures and found that NAFLD plays an important part in promoting atherosclerotic progression based on numerous clinical data, as shown in Figure 5. In fact, the relationship between NAFLD and CVD seems to be independent of cardio-metabolic risk factors, for example obesity, dyslipidemia, diabetes and hypertension, etc. [195]. Of note, CVDs are currently considered as the leading cause of mortality in patients with NAFLD worldwide through long-term follow-up studies, which especially drew our attention concerning clinical contributions [196-198]. Actually, most relevant evidence about this association came from clinical studies, which will be elucidated and summarized in the following part.

More specifically, NAFLD has been reported to be related to different pathological patterns of atherosclerosis. Mishra and coworkers utilized ultrasonographic scanning to evaluate fatty liver and carotid intima-media thickness (IMT) respectively, and they found that 68.5% NAFLD patients suffered from metabolic syndrome along with high levels of blood pressure, triglycerides and reduced HDL cholesterol *per se* [199]. Especially compared to subjects without NAFLD, NAFLD patients showed significantly greater carotid IMT, which was accompanied by wider plaque prevalence. Therefore, NAFLD was believed to have a close association with the carotid IMT [199]. Of interest, except for carotid IMT, some other studies additionally measured epicardial fat thickness (EFT) and showed that NAFLD patients usually had increased EFT, which could be a possible predictor for arterial stiffness [200,201].

Meanwhile, Ampuero and coworkers performed a meta-analysis including fourteen clinical studies and concluded that NAFLD could multiply the risks of atherosclerosis and coronary artery disease [202]. Furthermore, they proposed that the right management of these patients with NAFLD and atherosclerosis should include improvements in both cardiovascular and hepatic diseases. In addition, there were several interesting studies reporting that NAFLD was

associated with decreased brachial artery flow-mediated vasodilation [203-205], and reduced coronary flow reserve [206]. In a study from 2005, Villanova *et al.* applied brachial artery flow-mediated dilation to evaluate endothelial dysfunction and confirmed the association between liver disease and altered endothelial function [204]. Overall, most literatures associated the index of carotid IMT with NAFLD severity in these patients. Without doubt, this index is very important in clinical practice. The other possible explanation is that this index is easy to measure, and further available in the relevant quantitative analysis especially in outpatients.
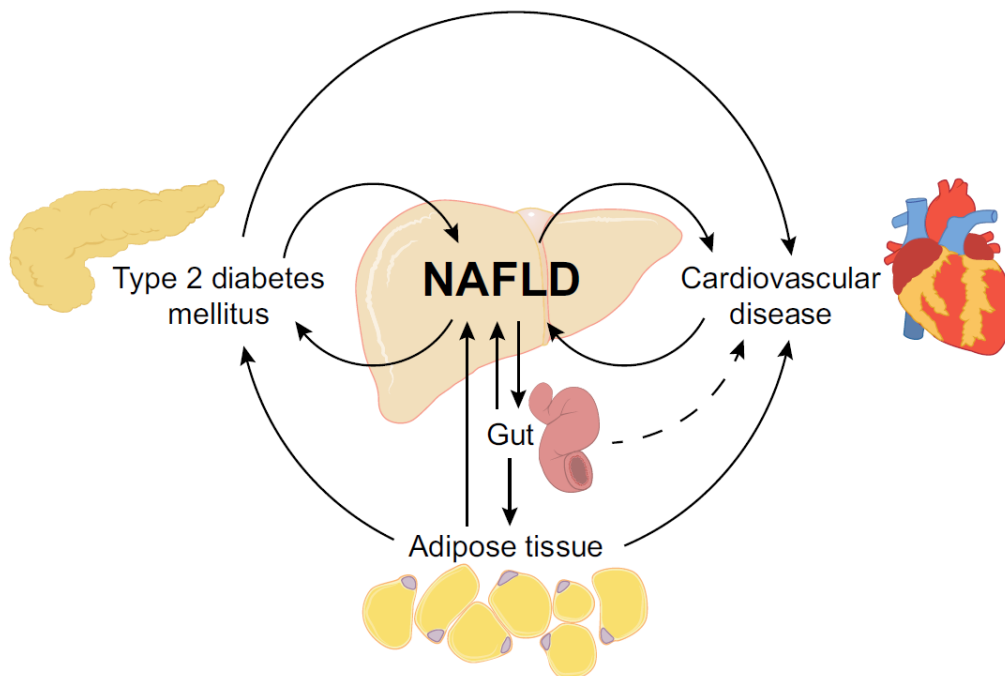

Figure 5: Potential associations among NAFLD, cardiovascular diseases and other metabolic syndrome. As the biggest metabolic organ in the body, liver also interacts with other relevant organs via inflammation- and lipid-dominated signaling pathways. NAFLD can lead to other metabolic syndrome, which in turn can be the cause of NAFLD. The figure was taken from [207].

Mechanistically, the dominant act of liver in lipid and/or glucose metabolism might determine the tight connections between NAFLD and atherosclerotic progression to some extent. Initially, expanded production and secretion of particles such as large triglyceride-laden very low-density lipoprotein (VLDL) is closely linked with progression of NAFLD. Hepatic VLDL particles enter into blood circulation, which are gradually metabolized, and later involved in an exchange proceeding between liver and artery. During this process, cholesteryl ester was removed from the central core of VLDL, and replaced with triacylglycerol. This transformation finally accelerated the production of low-density lipoprotein (LDL) in blood, which possesses a highly atherogenic property and further leads to the formation of plaques

[208]. Specific interaction mechanisms were vividly illustrated in Figure 6. In addition to the involvement of major lipoproteins, some other important pro-inflammatory regulators, vasoactive factors, and thrombogenic molecules together set a stage for CVD progression in these NAFLD patients. As addressed in the above section, these factors can lead to endothelial function disorder and unstable plaque changeover, etc. More importantly, these pathogenic components are also associated with several cardiovascular clinical outcomes, for example stroke, myocardial infarction and cardiovascular death [209], which thereby attract lots of attention from clinicians.
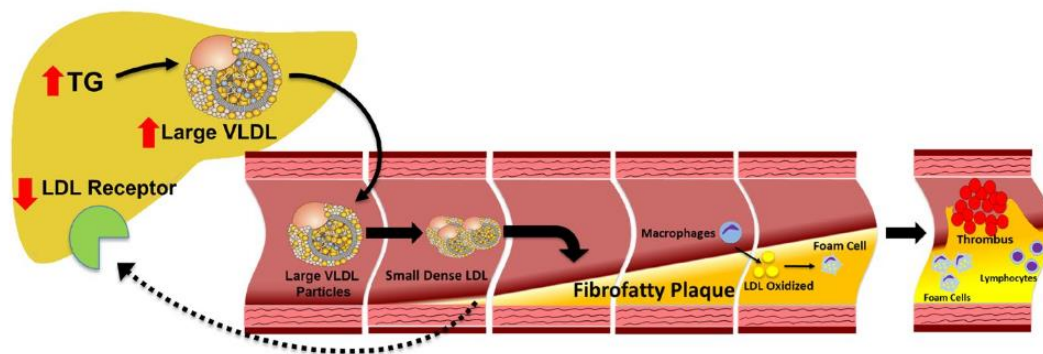

Figure 6: Specific functional mechanisms of how NAFLD promotes atherosclerosis. Excessive production of VLDL was linked with progression of NAFLD. Hepatic VLDL particles entered into blood circulation and metabolized forms were involved in an exchange between liver and artery. This transformation accelerated the production of LDL in blood, which further led to plaque formation. Structures were taken from [210].

In 2015, the PIVENS clinical trial including 222 patients revealed that the treatment of NASH with pioglitazone could significantly ameliorate TG and HDL levels, whereas had no effects on LDL and non-HDL-C levels, which were also regarded as risk factors for cardiovascular events [211]. Therefore, it is hard to draw a conclusion that the improvement of NAFLD could decrease substantial risks of CVD based on the results from this study. In other words, clinical outcomes of CVD patients could be partially improved along with the treatment of NASH, but the remaining lipid risk factors still exist. In addition, lowering TG and HDL levels clinically does not mean the improvement of NASH. The other pilot clinical trial from the United States about clofibrate against NASH showed an obvious TG downregulation, but there was no any hepatic damage recovery through histological analysis [212]. Thus, it is necessary to elucidate this question thoroughly via basic laboratory techniques and figure out the underlying mechanisms linking NAFLD and CVD clearly. Moreover, Siddiqui and coworkers also pointed out the stronger activation of sterol regulatory element binding protein

(SREBP)-1 and more TG synthesis in their phenomenon [208], which gave us some useful clues and more inspirations for further study.

Therefore, this well-known transcription factor (TF), SREBP, can orchestrate lipotoxicity in different organs, which could be a potential linker between NAFLD and atherosclerosis induced by MIF-2. It has been acknowledged that SREBPs participate in the synthesis of triglycerides and cholesterol, and thereby play a pivotal role in lipid metabolism. Furthermore, SREBPs have been extensively studied in various metabolic disorders. In terms of specific mechanisms, there were already some scientific papers displaying that phosphorylation-related regulation of SREBP-1c and -2 by AMPK in the liver, and stressing the role of SREBPs in potential therapeutic implications in hepatic steatosis, insulin resistance and atherosclerosis as well [213,214], which will be comprehensively discussed in the next part.

1.3 SREBPs: pivotal transcription factors linking atherogenesis and hepatosteatosis

1.3.1 SREBPs and downstream targets: structures and functions

SREBPs, a well-known family of transcription factors including two genes (*Srebp-1, Srebp-2*) and three proteins (SREBP-1a, SREBP-1c, SREBP-2), have been reported to exert important functions in regulating endogenous triglyceride and cholesterol synthesis in the past 3 decades [215]. Initially synthesized SREBP precursors are inactive forms, which exist in the endoplasmic reticulum (ER). In general, each precursor, containing around 1,150 amino acids, could be structurally divided into three major domains according to different functions of each part. The most important domain of ~480 amino acids is the functional NH2-terminal domain, including the bHLH-Zip region, which is the main DNA binding site. The connective part is two hydrophobic transmembrane-spanning segments, interrupted by a short 30-amino acid loop and projected into the ER lumen. The third part is the regulatory COOH-terminal domain of ~590 amino acids, performing several essential regulatory functions [216]. To achieve transcriptional activities in nuclei, SREBP precursors (i.e. pSREBPs) have to remove the NH2-terminal domain after twice proteolytic cleavages in hepatocytes and then the cleaved SREBPs (i.e. cSREBPs/nSREBPs) translocate into nuclei [216,217] to upregulate themselves and multiple pivotal downstream targets via binding to sterol response elements (SREs). During this process, any factors affecting phosphorylation, the transport from ER to Golgi or the proteolytic cleavage of SREBPs would finally influence the expression of their

downstream target genes and thereby affect energy states in the organism via the feedback system.

Of interest, it is broadly accepted that SREBPs can directly regulate more than thirty essential downstream targets implicated in both cholesterol and triglyceride synthesis, respectively [217,218]. In general, three isoforms of SREBP have distinctive functions due to different target promoters. SREBP-1 is mainly in charge of the biosynthesis of triglycerides, thus SREBP-1 largely promotes the activation of several genes encoding rate-limiting lipogenic enzymes, exemplified by fatty acid synthase (FASN), stearoyl-CoA desaturase 1 (SCD 1), acetyl-CoA carboxylase 1 (ACC 1), etc. [219,220]. By contrast, the target genes of SREBP-2 are chiefly implicated in cholesterol biosynthesis, encompassing HMG-CoA reductase (HMGCR), LDLR and other rate-limiting cholesterogenic genes [214,221]. Furthermore, different from SREBP-2, the cleavage of SREBP-1c is initially triggered by insulin [222]. Particularly, there are distinct expression patterns between SREBP-1a and SREBP-1c. SREBP-1a displayed more expression in proliferative cells for example tumor cells, whereas SREBP-1c highly expressed in normal cells such as hepatocytes [223]. Here, an important activator of SREBP-1c, liver X receptor (LXR), which contributes to SREBP activation and cholesterol efflux, must be mentioned. Nevertheless, regarding multiple regulatory features and functional characteristics of SREBPs, it would be also very interesting to discover novel modulators of SREBPs from upstream, which might offer vigorous therapeutic targets for metabolic disorders.

Back to 1997, Brown and Goldstein first showed different expression levels of SREBP-2 in contrasting energy-state serum conditions using staining. In addition to 10% fetal bovine serum (FBS), they also cultured human fibroblasts with 10% lipoprotein-deficient serum, and demonstrated that SREBP-2 was mostly detected in cytoplasm when cultured in the whole serum, whereas SREBP-2 expressed more in nuclei if cultured with lipoprotein-deficient serum [224]. Afterwards, more studies revealed that this kind of SREBP-regulated metabolic process exhibits energy-dependent [213,214,225,226]. Overall, SREBPs would be suppressed in the energy-sufficient condition whilst correspondingly activated in the energy-insufficient case, and further participate in the lipid synthesis. In the energy-insufficient state, functional activities of SREBP-1 were partially mediated by mTOR, whereas SREBP-2 regulation belongs to an autonomous feedback loop. Especially, protein synthesis induced by SREBP-1 activation would lead to ER stress, and then adaptive unfolded protein response (UPR) restarts

to keep cellular balance. However, a vicious circle of continuous ER stress along with lengthy UPR results in chronic SREBP-1c activation, and further promotes lipid-mediated hepatosteatosis and cellular inflammation (Figure 7). As a result, chronic hepatic inflammation could also raise the risks of liver fibrosis and hepatic carcinoma [225], which are regarded as the terminal stages of NAFLD.

Indeed, this steatosis-inflammation-fibrosis axis has emerged as an ultimate common pathway for different organ pathologies. Roles of SREBPs in liver and adipose tissue, two important metabolic organs in the body, have been widely studied until now [227,228]. Unlike hepatocytes, upregulation of cleaved SREBP-1c did not induce the transactivation of downstream lipogenic genes in adipocytes [228]. Interestingly, some researchers even found that there was fat redistribution between liver and adipose tissue induced by decreased hepatic SREBP-1 levels in type 2 diabetic rats [229]. Here, this comprehensive scheme aims to illustrate that the activation of SREBPs leads to lipid-driven stress, which in turn contributes to metabolic disorders, exemplified by dyslipidemia, obesity, especially atherosclerosis and hepatosteatosis, etc. These SREBP-triggered pathologies are eventually extended to different organs (Figure 7) [225]. My PhD project mainly focusses on intimate associations mediated by SREBP-inducing lipid phenotypes in NAFLD and atherosclerotic progression.
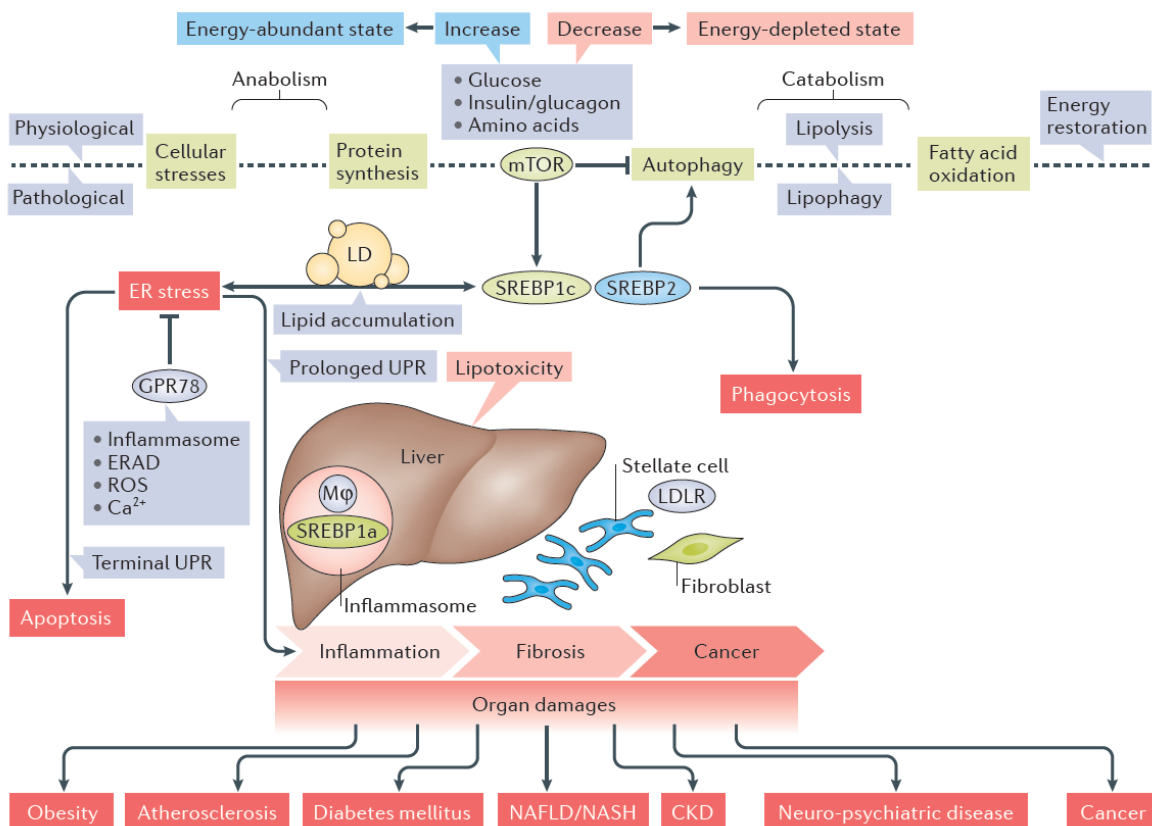
Figure 7: SREBP-mediated lipotoxicity is involved in various metabolic diseases. The scheme illustrates the specific mechanisms of how SREBP-1c and SREBP-2 regulate and/or link different metabolic conditions. SREBP-1c activation was associated with mTOR, whereas SREBP-2 served as a part of autonomous system. The scheme was taken from [225].

1.3.2 Preclinical studies of SREBPs in lipid metabolism

As discussed in the above subchapter, SREBP-modulated metabolic mechanisms have broadly expanded cellular lipogenesis-mediated inflammation to various organ pathologies, such as liver, adipose tissue, brain, pancreatic β cells and kidney. Accordingly, SREBPs and downstream targets have been reported to contribute to relevant diseases such as NAFLD [213,214], alcohol-induced fatty liver disease [230], lipodystrophy [231,232], type 2 diabetes mellitus [233,234], Alzheimer disease [235] and diabetic nephropathy [236]. In 2011, two original research papers from USA and China respectively came out to elucidate the central role of SREBPs in both atherosclerosis and NAFLD connected by lipid metabolism [213,214]. Li and colleagues firstly showed the administration of S17834, a synthetic polyphenol, inhibited plaque formation and hepatic steatosis in high-fat high-sucrose (HFHS) food-fed *Ldlr*-deficient mice *in vivo*. In terms of mechanisms, direct phosphorylation of SREBP-1c and/or interaction of SREBPs with AMPK were important to regulate SREBPs' transcriptional activities [214]. Moreover, this inhibition of SREBPs by AMPK was a SRE-dependent manner via impeding the feed-forward control of *Srebps* and their target genes in hepatocytes. How the AMPK-SREBP works in the context of lipid metabolism was illustrated in Figure 8.
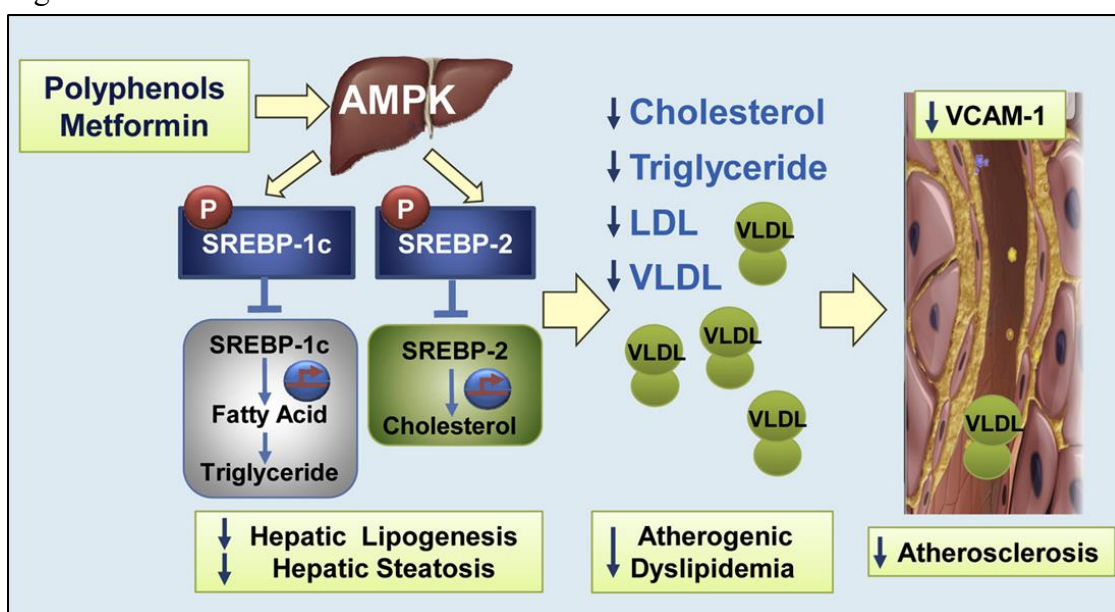

Figure 8: Prospective scheme summarizes detailed mechanisms of how AMPK interacts with SREBPs in hepatocytes and possible therapeutic effects on hepatic steatosis and atherosclerosis.

AMPK activation by polyphenols or metformin suppressed the cleavage and expression of SREBPs, and inhibited triglyceride and cholesterol synthesis. The scheme was taken from [214].

Mechanistically, AMPK can phosphorylate Ser372, which is the residue of SREBP-1c that represses SREBP cleavage and nuclear translocation, and subsequently downregulates the expression of SREBPs and their target genes. As Figure 8 shows, AMPK activation in hepatocytes by metformin or polyphenol could keep the body from atherogenic dyslipidemia, hepatic steatosis and atherosclerosis in $Ldlr^{-/-}$ mice through this pathway. In the same year, Tang and coworkers screened a novel small molecular inhibitor betulin and found that it could inhibit the interaction of SREBPs and SREBP-cleavage activating protein (SCAP), and further keep SREBPs from cleaving and releasing from ER [213]. In their study, betulin treatment attenuated SREBP-2 mRNA expression by ~30% observed in C57BL/6J mice. In the meanwhile, fat/body-weight ratios showed an obvious drop by 35%-40% in betulin-treated mice via metabolic analysis. Moreover, they also applied lovastatin, a kind of HMGCR inhibitor as a positive control *in vivo*, and betulin treatment displayed similar or even better effects on reducing lipid levels in liver as well as adipose tissue, and improving insulin sensitivity compared with lovastatin. However, one limitation in this study was that they mainly focused on the SREBP-SCAP pathway using RNA interference technique, but they did not check the AMPK-SREBP axis.

On the other hand, AKT signaling pathway was also identified as a crucial player in the regulation of SREBPs [237,238]. Porstmann and coworkers demonstrated that SREBP silencing in RPE myrAKT-ER cells could hinder the lipogenic process *in vitro* and suppress the increasing cell size induced by the activation of AKT. Additionally, *in vivo* studies on *Drosophila* showed that flies expressing dSREBP RNAi had smaller body size, lighter body weight and reduced wing area compared to controls [237]. These results indicated that AKT/mTORC1-mediated signaling was involved in SREBP activation and further regulated lipid metabolism. In aggregate, current studies together support the view that AKT phosphorylation enhances the transcriptional activities of SREBPs. There are four kinds of noted possible mechanisms to explain how AKT affects SREBP/SCAP pathway. Firstly, AKT could directly enhance ER-to-Golgi transport of SREBP-2. Du and colleagues showed that stimulation of AKT by IGF-1 enhanced the GFP-SCAP transport from ER to Golgi, in the meanwhile the suppression of AKT by LY294002 disturbed this transport of GFP-SCAP, as evidenced by fluorescence microscopy [239]. Secondly, SREBP-1c could be phosphorylated by AKT, which thereby displayed enhanced transport. One preclinical study from Yellaturu

group demonstrated that insulin promoted AKT-mediated phosphorylation of SREBP-1c, and then accelerated subsequent transport as well as its proteolytic cleavage in rat hepatocytes [240]. Thirdly, AKT could activate mTORC1 through different mechanisms, and further expedited SREBP processing [237,241], which was addressed in the above part as well. Lastly, AKT-mediated phosphorylation negatively regulated a kind of kinase, glycogen synthase kinase-3 (GSK-3), which could promote SREBP-1 proteasomal degradation [218,242]. For sure, more studies are still warranted to clarify some special effectors or targets in AKT-modulated SREBP/SCAP pathway. Overall, the AMPK- and AKT-mediated SREBP-pathways could provide additional insights for promising therapeutic strategies against hepatic steatosis as well as atherosclerosis.

Another question is whether this MIF-2-SREBP-mediated lipogenic process also involves proprotein convertase subtilisin-like kexin type 9 (PCSK9). Because LDLR is one of the most common downstream targets of SREBP-2, while PCSK9 behaves as a recognized negative regulator of LDLR. Some researchers even identified SREBP-2 as an upstream regulator of PCSK9 [243,244]. Akin to SREBPs, originally synthesized PCSK9 exists as a precursor of ~72 kDa, whereas the small prodomain still binds to its mature part when the secretory pathway works [245]. In the functional sense, the first experimental evidence *in vivo* of PCSK9 came from Maxwell and Breslow using a type of adenovirus expressing murine *Pcsk9* in 2004 [246]. They injected this constitutive adenovirus into wild type (WT) mice and *Ldlr*$^{-/-}$ mice respectively, and then found that WT mice overexpressing *Pcsk9* had increasing cholesterol levels in plasma especially LDL cholesterol, due to the absent expression of LDLR at the protein level yet with normal mRNA expression of *Ldlr*. In contrast to WT mice, infected *Ldlr*$^{-/-}$ mice did not show any changes in total cholesterol. Thus, these effects together suggest the behavior that PCSK9 overexpression upregulates LDL cholesterol levels is dependent on LDLR. Moreover, McA-RH7777 rat hepatoma cells transfected with *Pcsk9* *in vitro* showed reduced LDLR protein expression and corresponding less LDL binding, which also substantiates their findings *in vivo* [246]. Of note, there were no relevant *Ldlr* mRNA level changes observed in their study. Therefore, PCSK9 overexpression modulates intracellular LDLR degradation mainly through a post-transcriptional mechanism [246,247]. Yet, a few questionable effects have emerged in preclinical trials of SREBP-targeted therapy. Considering coordinative regulation of PCSK9 and LDLR in lipid metabolism, it definitely will be an alternative choice to bring PCSK9 into the complex therapeutics for atherosclerosis rather than classical SREBP-targeted cholesterol inhibition [248].

Based on the acknowledged therapeutic effects of statins and PCSK9 inhibitors on lowering cholesterol, it is also preferable to think about SREBP-dominated microRNA-based strategy in order to reduce cardiovascular risks further. MiR-33 is regarded as the most well studied miRNA in the lipid metabolism because of its special location within the intron of SREBPs. Horie and colleagues generated $miR\text{-}33^{-/-}Srebp1^{+/-}$ mouse line and showed that the knockout of *mir-33* could aggravate obesity and hepatic steatosis induced by HFD [249], which reveals a novel miR-33-mediated interaction between SREBPs *in vivo*. However, they also pointed out that the phenotype observed in their study was in part different from that in WT mice, which could be attributed to other target genes of miR-33. One year later, the same research group reestablished humanized *miR-33* knock-in mice and emphasized that miR-33 may exert more essential effects on humans than mice regarding the function of lowering HDL cholesterol levels [250]. Because miR-33b locates in SREBP-1 intron in humans and other mammals but not mice, the knock-in technique was utilized in their study to evaluate the significance of miR-33b among different species. In addition to a short-term effect, Karunakaran and partners also applied anti-miR-33 to evaluate the long-term effect via a pharmacological mouse model. After 20-week administration with anti-miR-33, there were no obvious changes in hepatic metabolic parameters, such as body, liver or adipose tissue weight, LDL cholesterol levels, and insulin resistance, etc. [251]. However, there were significant downregulations of several miR-33 target genes, such as *Abca1* and *Ampk*, in the adipose tissue from anti-miR-33-injected mice compared to control mice, indicating that miR-33 is effectively suppressed at this dose [251]. Except for miR-33, there are many other miRNAs, for example miR-182, miR-96, miR-185, miR-29 and miR-122, reported to participate in SREBP-mediated sterol regulation. In conclusion, this brief sketch of SREBP-associated miRNAs shows the complex regulatory pattern orchestrated by a single transcription factor, and more importantly, these miRNAs may give a clearer explanation for controversial or even unknown phenomena.

1.3.3 Clinical trials of SREBPs in lipid metabolism

To date, there are several inhibitors of SREBPs, for instance botulin and fatostatin, which have been well applied in experimental studies to exhibit their inhibitory effects on SREBPs activation and hepatic lipid synthesis and accumulations [213,252]. As for clinical aspects, the most widely used drugs associated with SREBPs regulation are statins, a class of HMGCR inhibitor, which could upregulate SREBP-2 and LDLR levels via the feedback loop of sterol

regulation [253]. Then reduced LDL cholesterol levels in plasma were closely associated with less plaque formation and improved stability in humans. From the very earliest of preclinical stages with gels, blots and columns, through pilot clinical studies and finally to large-scale clinical trials, Lovastatin was the first statin, which was patented in 1979 and approved for patients, to lower cholesterol levels in 1987 [254,255]. Afterwards, simvastatin, the second generation of statin, was confirmed to alleviate risks of heart attacks as well as prolong lifespans of those patients after 5-year treatment through a large-scale clinical trial including 4444 patients in 1994 [256]. Follow-up results showed that simvastatin could effectively downregulate total cholesterol by 25% and LDL cholesterol by 35%, whereas upregulate HDL cholesterol by 8%, with less side effects [256]. Later on, the elucidation of SREBP pathway gave a convincing explanation to the molecular mechanism of feedback regulation of LDLR in statin studies. The largest clinical trial of 20536 patients, which was carried out by Heart Protection Study Collaborative Group, consistently confirmed the beneficial effects of simvastatin, even in subgroups with certain risk factors, such as smoking, hypertension, dyslipidemia, etc. [257].

Even though results from many clinical trials substantiate the dominant role of statins in lowering LDL cholesterol levels, statins still have drawbacks. Except for their positive effects on SREBP-2 and LDLR, long-term treatment with statins upregulates PCSK9 levels. Elevated PCSK9 in turn accelerates LDLR degradation. Sahebkar and colleagues used meta-analysis covering 15 clinical trials to assess how statins affected plasma PCSK9 and LDL cholesterol levels. Statins were found to downregulate LDL cholesterol but upregulate PCSK9 concentrations in plasma [258]. In order to achieve better synergistic clinical outcomes, the treatment with anti-PCSK9 antibodies could downregulate SREBP-2 and LDLR gene expression, which was another successful example involved in sterol regulation in clinical practice [259]. In addition to combinative treatment with statins, the approval of alirocumab and evolocumab in medical use also brought two other advantages. Firstable, humanized anti-PCSK9 antibodies, which are given by parenteral injection, could significantly decrease LDL cholesterol levels, with the reduction of ~39%-62% by alirocumab and ~47%-56% by evolocumab, respectively [259]. Secondly, the application of PCSK9 inhibitors provides an additional opportunity to those patients who are unable to take statins because of statin intolerance. Moreover, one long-term clinical trial published in 2015 also demonstrated that the additional use of evolocumab on the basis of standard therapy, fairly downregulated LDL cholesterol levels and incidences of other cardiovascular events [260]. Therefore, the

favorable clinical application of anti-PCSK9 antibodies stresses the importance of targeting post-translational regulation of LDLR.

In summary, considering clinical importance of SREBP/PCSK9 in lipid metabolism, it is essential to clarify upstream sensors and associated receptors in this lipogenic process. Even though there are still many controversial questions about SREBPs to be answered in the future, steady progress has been made and also brings us some novel strategies to combat atherosclerosis and hepatosteatosis, which calls for more studies. For this reason, my PhD project mainly focusses on MIF-2/CXCR4/CD74-AMPK- and AKT-SREBP-mediated lipogenic processes, and aims to clarify the role of MIF-2 in atherosclerosis and hepatosteatosis as well as specific molecular mechanisms behind this phenotype.

2. MATERIALS AND METHODS

Parts of this materials and methods chapter are also contained in my co-first-author manuscript preprint published on bioRxiv (doi: https://doi.org/10.1101/2021.12.28.474328). All these passages and chapters are marked by a '#' icon.

2.1 Materials[#]

2.1.1 Reagents

2.1.1.1 Key chemicals, proteins, peptides, and medium

Key reagents	Identifier	Supplier
4-(3-Carboxyphenyl)-2,5-pyridinedicarboxylic acid (4-CPPC)	Cat# K00.223.811	Aurora Fine Chemicals
AMD3100 octahydrochloride hydrate	Cat# A5602	Sigma-Aldrich
Low density lipoprotein from human plasma, DiI complex (DiI LDL)	Cat# L3482	Thermo Fisher Scientific
Low density lipoprotein from human plasma (LDL)	Cat# L3486	Thermo Fisher Scientific
Paraformaldehyd (PFA) 4% in PBS	Cat# 1176201000	Morphisto GmbH
TRIzol™ reagent	Cat# 15596018	Thermo Fisher Scientific
CountBright™ absolute counting beads	Cat# C36950	Thermo Fisher Scientific
PolyFect transfection reagent	Cat# 301107	QIAGEN
Recombinant human M-CSF	Cat# 300-25	PeproTech GmbH
RBC lysis buffer (10X)	Cat# 420301	BioLegend
Oil Red O solution 0.5% in propylene glycol	Cat# O1516	Sigma-Aldrich
Ficoll® paque plus	Cat# GE171440-02	GE Healthcare
Albumin fraction V	Cat# 8076.4	Carl Roth
Methanol	Cat# 0082.2	Carl Roth
CozyHi™ prestained protein ladder	Cat# PRL0202	HighQu GmbH
TWEEN® 20 viscous liquid	Cat# P2287	Sigma-Aldrich
Donkey serum	Cat# D9663	Sigma-Aldrich
Goat serum	Cat# ab7481	Abcam
30% acrylamide/bis solution	Cat# 1610156	Bio-Rad Laboratories
Hematoxylin solution, Mayer's	Cat# MHS80	Sigma-Aldrich
Eosin Y solution, aqueous	Cat# HT110232	Sigma-Aldrich
DL-Dithiothreitol ≥98% (HPLC)	Cat# D0632	Sigma-Aldrich
2-Propanol ROTISOLV® ≥99.95 %	Cat# AE73.2	Carl Roth
NuPAGE transfer buffer (20X)	Cat# NP00061	Thermo Fisher Scientific

Xylol Isomergemisch	Cat# 28976.294	VWR International
Recombinant human SDF-1α	Cat# 300-28A	PeproTech GmbH
Water nuclease-free	Cat# 436912C	VWR International
Bouin's solution	Cat# HT10132	Sigma-Aldrich
Sulphuric acid	Cat# KK74.1	Carl Roth
TEMED	Cat# 1610801	Bio-Rad Laboratories
Penicillin-streptomycin (5,000 U/mL)	Cat# 15140-122	Invitrogen
Fetal bovine serum, qualified	Cat# 10091148	Thermo Fisher Scientific
Pierce protease inhibition tablets	Cat# A32963	Thermo Fisher Scientific
Dulbecco's phosphate buffered saline modified, without calcium chloride and magnesium chloride	Cat# D8537	Sigma-Aldrich
Dulbecco's phosphate buffered saline	Cat# D8662	Sigma-Aldrich
RPMI 1640 medium GlutaMax + supplements	Cat# 61870-044	Invitrogen
DMEM/F-12, GlutaMAX™ supplement	Cat# 31331-093	Invitrogen
Fluoromount™ aqueous mounting medium	Cat# F4680	Sigma-Aldrich
Kaiser's glycerol gelatine phenol-free	Cat# 6474.1	Carl Roth
Eukitt® quick-hardening mounting medium	Cat# 25608-33-7	Sigma-Aldrich
Vectashield antifade mounting medium with DAPI	Cat# H-1200	Vector Laboratories

2.1.1.2 Critical commercial assays

Commercial kits	Identifier	Supplier
Proteome profiler mouse cytokine array kit, panel A	Cat# ARY006	R&D systems
First strand cDNA synthesis kit	Cat# K1612	Thermo Fisher Scientific
ORA™ SEE qPCR green ROX L Mix	Cat# QPD0150	HighQu GmbH
Triglyceride colorimetric assay kit	Cat# 10010303	Cayman Chemical
Cholesterol fluorometric assay kit	Cat# 10007640	Cayman Chemical
Trichrome stain (Masson) kit	Cat# HT15-1KT	Sigma-Aldrich
Qiaxcel DNA screening Kit (2400)	Cat# 929004	QIAGEN
RNA/Protein purification plus kit	Cat# 48200	Norgen Biotek Corp.
Pan monocyte isolation kit, human	Cat# 130096537	Miltenyi Biotec
Pierce™ TMB substrate kit	Cat# 34021	Thermo Fisher Scientific
SuperSignal West Femto maximum sensitivity substrate	Cat# 34095	Thermo Fisher Scientific
Weigert's iron hematoxylin set	Cat# 537864	Sigma-Aldrich

SuperSignal West Dura extended duration substrate		Cat# 34076		Thermo Fisher Scientific
QIAfilter plasmid midi kit		Cat# 12245		QIAGEN

2.1.2 Antibodies

2.1.2.1 Primary antibodies

Antigen	Host species	Identifier	Supplier	Application
Anti-mouse CD45 V450	Rat	Cat# 560501	BD Biosciences	Flow cytometry
Anti-mouse CD3 FITC	Human	Cat# 130-119-758	Miltenyi Biotec	Flow cytometry
Anti-mouse CD19 APC/Cy7	Rat	Cat# 115530	BioLegend	Flow cytometry
Anti-mouse CD11c PE	Armenian hamster	Cat# 117308	BioLegend	Flow cytometry
Anti-mouse/human CD11b PE/Cy7	Rat	Cat# 101216	BioLegend	Flow cytometry
Anti-mouse Ly-6C APC	Rat	Cat# 128016	BioLegend	Flow cytometry
Anti-mouse Ly-6G PerCP	Rat	Cat# 127654	BioLegend	Flow cytometry
Anti-human CD74 FITC	Mouse	Cat# 555540	BD Biosciences	Flow cytometry
Anti-human CD184 (CXCR4) APC/Cy7	Mouse	Cat# 306528	BioLegend	Flow cytometry
Anti-SREBP-1 monoclonal antibody	Mouse	Cat# sc-17755	Santa Cruz Biotechnology	WB/IP/IHC /ELISA
Anti-SREBP-2 monoclonal antibody	Mouse	Cat# 557037	BD Biosciences	WB/IP/IHC /ELISA
Anti-FASN monoclonal antibody	Mouse	Cat# sc-55580	Santa Cruz Biotechnology	WB/IP/IHC /ELISA
Anti-LDLR monoclonal antibody	Mouse	Cat# sc-18823	Santa Cruz Biotechnology	WB/IP/IHC /ELISA
Anti-CD68 monoclonal antibody	Rat	Cat# MCA1957 GA	Bio-Rad Laboratories	WB/IP/IHC
Anti-AMPKα monoclonal antibody	Rabbit	Cat# 5832S	Cell Signaling Technology	WB/IP
Anti-phospho-AMPKα monoclonal antibody	Rabbit	Cat# 2535	Cell Signaling Technology	WB/IP

Anti-AKT monoclonal antibody	Rabbit	Cat# 9272S	Cell Signaling Technology	WB/IP
Anti-phospho-AKT monoclonal antibody	Rabbit	Cat# 9271S	Cell Signaling Technology	WB/IP
Anti-ERK monoclonal antibody	Mouse	Cat# sc-514302	Santa Cruz Biotechnology	WB/IP
Anti-phospho-ERK monoclonal antibody	Mouse	Cat# sc-7383	Santa Cruz Biotechnology	WB/IP/IHC /ELISA
Anti-β-Actin monoclonal antibody	Mouse	Cat# sc-47778	Santa Cruz Biotechnology	WB/IP/IHC /ELISA
Anti-CXCR4 polyclonal antibody	Rabbit	Cat# PA3-305	Invitrogen	WB/IHC/IF
Anti-CD74 monoclonal antibody	Mouse	Cat# sc-6262	Santa Cruz Biotechnology	WB/IP/IHC /ELISA
Anti-MIF monoclonal antibody	Mouse	Cat# MAB289	R&D Systems	ELISA
Anti-MIF biotinylated antibody	Goat	Cat# BAF289	R&D Systems	ELISA
Anti-MIF-2 polyclonal antibody	Rabbit	Not applicable	Bucala lab (Yale University)	WB/ELISA/ IF

2.1.2.2 Secondary antibodies

Antigen	Host species	Identifier	Supplier	Application
Alexa Fluor 647-conjugated donkey anti-rat IgG (H+L)	Donkey	Cat# 712-606-153	Jackson Immuno-Research	IF
Alexa Fluor 488-conjugated goat anti-mouse IgG (H+L)	Goat	Cat# A-11001	Invitrogen	IF
Alexa Fluor 555-conjugated goat anti-rabbit IgG (H+L)	Goat	Cat# A-21429	Invitrogen	IF
Goat anti-mouse HRP-conju-gated secondary antibody	Goat	Cat# ab6789	Abcam	WB
Goat anti-rabbit HRP-conju-gated secondary antibody	Goat	Cat# NA934V	GE Healthcare	WB

2.1.3 Quantitative PCR primers

2.1.3.1 Human primer sequences

Gene symbol	Forward primer (5'→ 3')	Reverse primer (5'→ 3')
SREBP-1	ACGGCAGCCCCTGTAACGACC	TGCCAAGATGGTTCCGCCACTC

	ACTGTGA	ACCAGG
SREBP-2	AGCTGGTCTGTGAAG	CGCAATGGGGTCAGC
FASN	GAAACTGCAGGAGCTGTC	CACGGAGTTGAGGCGCAT
LDLR	GTGTCACAGCGGCG	CGCACTCTTTGATG
PCSK9	AGGGGAGGACATCATTGGTG	CAGGTTGGGGGTCAGTACC
CD36	AGTCACTGCGACATGATTAATGGT	CTGCAATACCTGGCTTTTCTCA
GLUT1	CAGCAGCCCTAAGGATCTCTCA	CCGGCTCGGCTGACATC
GLUT4	GCTACCTCTACATCATCCAGAATCTC	CCAGAA ACATCGGCCCA
HMGCR	CTTGTGTGTCCTTGGTATTAGAGCTT	GCTGAGCTGCCAAATTGGA
MIF	AGAACCGCTCCTACAGCAAGCT	GGAGTTGTTCCAGCCCACATTG
MIF-2	CCCTGACCCAGAAACGACTG	GCAAATTCGTGTCCAGCTCC
CD74	GATGACCAGCGCGACCTATC	GTGACTGTCAGTTTGTCCAGC
CXCR4	TGACGGACAAGTACAGGCTGC	CCAGAAGGGAAGCGTGATGA
β-Actin	AGAGCTACGAGCTGCCTGAC	CGTGGATGCCACAGGACT

2.1.3.2 Murine primer sequences

Gene symbol	Forward primer (5'→ 3')	Reverse primer (5'→ 3')
SREBP-1	GGCAAAGGAGGCACTACAG	AGATAGCAGGATGCCAACAG
SREBP-2	CCAAAGAAGGAGAGAGGCGG	CGCCAGACTTGTGCATCTTG
FASN	CTGAAGAGCCTGGAAGATCG	GTCACACACCTGGGAGAGGT
LDLR	ACCTGCCGACCTGATGAATTC	GCAGTCATGTTCACGGTCACA
PCSK9	TGCAAAATCAAGGAGCATGGG	CAGGGAGCACATTGCATCC
CD36	GATGACGTGGCAAAGAACAG	CAGTGAAGGCTCAAAGATGG
GLUT1	TCAACACGGCCTTCACTG	CACGATGCTCAGATAGGACATC
GLUT4	GTAACTTCATTGTCGGCATGG	AGCTGAGATCTGGTCAAACG
HMGCR	CTTTCAGAAACGAACTGTAGCTCAC	CTAGTGGAAGATTGGACATGAT
MIF	ACAGCATCGGCAAGATCG	AGGCCACACAGCAGCTTAC
MIF-2	CCAGCTTCTTCAAGTTCCTCA	GGGAAGAAGCGGATAACGAT
CD74	CCCCATTTCTGACCCATTAGT	TGTCCAGCCTAGGTTAAGGGT
CXCR4	TGGAACCGATCAGTGTGAGT	GGGCAGGAAGATCCTATTGA
β-Actin	GGAGGGGGTTGAGGTGTT	GTGTGCACTTTTATTGGTCTCAA

2.1.4 Equipment

Equipment	Manufacturer	Identifier
BD FACSVerse™ flow cytometer	BD Biosciences	Cat# 651155
Mini gel tank	Invitrogen	Cat# A25977

Mini blot module	Invitrogen	Cat# B1000
Power supply EV3020	Carl Roth	Cat# EV3020
Odyssey Fc imaging system	LI-COR Biosciences	Cat# OFC-0976
Heraeus™ Megafuge™ 16R centrifuge	Thermo Fisher Scientific	Cat# 75004270
EnSpire multimode plate reader	Perkin Elmer LAS	Cat# 23001395
NanoDrop one microvolume UV-Vis spectrophotometer	Thermo Fisher Scientific	Cat# AZY1602185
Biometra TRIO 48 touch thermocycler	Analytik jena	Cat# 2070723
Horizontal gel electrophoresis system	Life Technologies	Cat# 41060
Centrifuge 5424 R	Eppendorf	Cat# 5404000210
Vortex shaker, VV3	VWR International	Cat# 444-0007
Thermal shake lite	VWR International	Cat# 460-0249P
Leica DMi8 fluorescent microscope	Leica Microsystems	Cat# S/N 425074
Confocal microscope	Carl Zeiss	Cat# LSM 880
Leica TCS SP8 DIVE multiphoton microscope	Leica Microsystems	Cat# Leica TCS SP8
Biosafety cabinet	Kojair Tech Oy	Blue series
Heracell ™ VIOS 160i CO_2 incubator	Thermo Fisher Scientific	Cat# 51030285
TC20™ automated cell counter	Bio-Rad Laboratories	Cat# 1450102
Zeiss Axio imager M2	Carl Zeiss	Cat# M2
Cryotome Leica CM1950 platform	Leica Microsystems	Cat# Leica CM1950
Leica dissection microscope	Leica Microsystems	Cat# Leica M125C
Embedding machine STP 120	Leica Microsystems	Cat# STP-120
Rotor-gene Q	QIAGEN	Cat# R0915111
Tissue lyser LT	QIAGEN	Cat# 23.1001/07538

2.1.5 Software

GraphPad Prism 8 software (Version 8.4.3)

Rotor-Gene 6000 series 1.7 software (Version 2.3.1)

BD FACS Diva software (Version 1.0.6.5230)

FlowJo V10 software (Version 17.0.2.0)

Image Studio™ software (Version 5.2.5)

ImageJ software/Fiji software (Version 64-bit Java 1.8.0_172)

Leica application suite X (Version 3.0.15878.1)

Carl Zeiss ZEN 2010 (Version 2.3.64.0)

BioRender (BioRender.com)

2.2 Main methods

2.2.1 Murine experimental techniques *in vivo*[#]

2.2.1.1 Atherosclerotic mouse models and treatment

All *in vivo* experiments in this thesis were approved by the Animal Care and Use Committee of the local authorities, and performed in accordance with the animal protection representative at the Center for Stroke and Dementia Research (CSD), Munich, Germany. Hyperlipidemic *Apoe*$^{-/-}$ mice with C57BL/6 background were originally obtained from Charles River Laboratories, and generally backcrossed at the CSD when the experiment was planned. Additionally, there were no methods of statistics utilized to predetermine the sample size. However, G power analysis was applied to different mouse cohorts to verify that the number of mice is enough in this study.

Genetic mouse model: *Mif-2*$^{-/-}$*Apoe*$^{-/-}$ mouse line was firstly generated and housed at the CSD. Genetically deficient mouse experiments were performed on eight-week-old female and male *Mif-2*$^{-/-}$*Apoe*$^{-/-}$ mice and *Apoe*$^{-/-}$ mice in parallel. The distribution of these mice was not random and the researcher in this study was not blinded during experiments and outcome assessment.

Pharmacological mouse model induced by 4-CPPC: 8-week-old male *Apoe*$^{-/-}$ mice were separated into two groups at random, with 11 mice in each group. The experimental group was intraperitoneally (i.p.) administrated with 50 µg 4-CPPC solubilized in 400 µL physiological saline (i.e. 0.9% NaCl) per mouse every two days for 4.5 weeks (in total 14 times), and the other group (control group) was injected with 400 µL 0.9% NaCl solution at the same time intervals. The 4-CPPC injection did not show any toxicity and other side effects on mice in this study.

These mice were housed under a 12-hour light/dark cycle with *ad libitum* access to water and food. At the age of eight weeks, mice are challenged with a Western-type food including 0.21% cholesterol (Ref. E15721-347; ssniff Spezialdiäten GmbH, Soest, Germany) for 4.5 weeks or 12 weeks. Early-to-intermediate atherosclerotic lesion develops in this mouse model [261]. At the endpoint of these planned experiments, mice were subject to isoflurane and midazolam/medetomidine/fentanyl (MMF) administration until deeply anesthetized, body and liver weight was measured, blood was collected through cardiac puncture and intended

for routine blood cell counts and lipoprotein analysis further. After blood samples were obtained, mice were transcardially perfused with saline, half of hearts including the aortic root and proximal aortas were isolated, trimmed and sectioned for plaque morphometry and quantitative measurements. Other organs such as spleen, liver and adipose tissue were isolated and stored in -80°C for future use.

2.2.1.2 RNA extraction and gene expression analysis by RT-qPCR

Half of heart tissue was collected, fresh-frozen on powered dry ice and then transferred to 40 μm cell strainer (Corning, NY, USA), and the other half of heart was used to analyze plaques. This part of tissue for mRNA isolation was cut into small pieces and ground thoroughly using a pipette tip. Genomic DNA was removed from lysate, and total RNA was purified through wash and elusion using the RNA/Protein Purification Plus kit, in keeping with the constructor's instructions. The concentrations of RNA samples were measured by Nanodrop spectrophotometer and 1000 ng RNA was prepared for reverse transcription. cDNA was subsequently synthesized using First strand cDNA synthesis kit and then diluted in a 1:5 ratio using nuclease-free water. Afterwards, real-time quantitative PCR process was carried out by employing 2x SensiMix PLUS SYBR No-ROX kit in a Rotor-Gene 6000 machine. Specific mouse *Mif-2* primer pair was indicated here: forward: 5'-CCAGCTTCTTCAAGTTCCTCA-3'; reverse: 5'-GGGAAGAAGCGGATAACGAT-3' (Eurofins BioPharma Product Testing Munich, Planegg, Germany). All raw data were obtained from the Rotor-Gene 6000 series 1.7 software (QIAGEN), and relative mRNA levels were calculated by using the $\Delta\Delta C_t$ method with *β-actin* as the housekeeping gene. The same RNA isolation and quantification procedures were applied to murine liver tissue as well.

2.2.1.3 Blood leukocyte counts by flow cytometry, triglyceride and cholesterol level measurement, and lipoprotein analysis

Fresh mouse whole blood was collected by 30 G needles into EDTA tubes, placed at room temperature (RT) for 10 min before keeping on the ice, and blood cells and plasma were separated by centrifugation at the speed of 300 g for 12 min at 4°C. To estimate percentages of different types of white blood cells (WBC), RBC lysis buffer at RT was used to lyse red blood cells (RBC) for 3 min, and filtered phosphate-buffered saline (PBS) dissolving 0.5% BSA (i.e. FACS buffer) was utilized to wash and suspend WBC pellets. Then, an antibody cocktail panel (1:100) encompassing V450-conjugated anti-CD45, FITC-conjugated anti-

CD3, APC-Cy7-conjugated anti-CD19, PE-Cy7-conjugated anti-CD11b, PE-conjugated anti-CD11c, APC-conjugated anti-Ly6C and PerCP-conjugated anti-Ly6G, was applied to stain leukocyte subsets. After 45 min of antibody incubation and three times of washing, these stained cells were sorted in a FACSVerse™ flow cytometer, compensations and special gating strategies were set using isotype controls and fluorescence minus one (FMO) antibody combinations. These raw data were obtained by FACSiva software, and analysis was carried out via FlowJo software (Treestar).

The concentrations of total triglyceride and total cholesterol in plasma from different mouse cohorts were enzymatically determined capitalizing on triglyceride colorimetric assay kit (1:2) and cholesterol fluorometric assay kit (1:2000) following the manufacturer's guidance, respectively. Especially, proper dilution ratios of plasma are critical factors taken into account in both two assays.

As for the visualization of lipoprotein profiles, plasma samples were subjected to FPLC using Superose 6 column (GE Healthcare) for gel filtration. Different lipoprotein fractions were separated and collected according to their retention (flow-through) times as follows: VLDL between 40 and 50 min, LDL between 50 and 70 min, and HDL between 70 and 90 min. Separated lipoproteins were evaluated and results were presented as Optical Density (OD) 492 measurements by a plate reader with a 492 nm filter.

2.2.1.4 Plaque size and component analysis (ORO, HE, CD68 and Masson staining)

To analyze plaque sizes and components for different mouse cohorts, samples were prepared and staining was performed. In brief, the heart tissues were embedded in Tissue-Tek optimum cutting temperature (O.C.T.) compound and directly fresh-frozen on dry ice for sectioning in the next step. After the block was trimmed, serial eight-μm thick frozen sections were arranged for Oil Red O (ORO), hematoxylin and eosin (HE) staining, and subsequent quantification of other plaque components, such as immune cells, collagen and necrotic core. The lipid content in aortic root was stained with 0.5% ORO solution in propylene glycol at 37°C for 45 min and nuclei were lightly stained with hematoxylin at RT for 1 min. The lesion area was alternatively stained with hematoxylin for 10 min and eosin for 30 sec. The macrophage content in plaques of the aortic root was visualized by a rat anti-CD68 antibody (1:100) in combination with a Cy5-conjugated secondary antibody (1:300). In the meanwhile, nuclei were stained with DAPI. Previously isolated and trimmed aortic arch was fixed in 1%

paraformaldehyde (PFA) overnight and transferred into PBS on the day before dehydration. After immersed completely, samples were embedded in paraffin. Molded blocks can be stored at RT or for direct section. Four-µm paraffin sections including three main branches were cut and HE-stained for plaque measurement. In addition, collagen and necrotic core were stained in consonance with the manufacturer's procedures of trichrome stain (Masson) kit. Nuclei stains black, cytoplasm and muscle fibers stain red, whereas collagen displays blue coloration. Images were acquired with a Leica DMi8 fluorescence microscope, and signals were quantified using computer-assisted image analysis software (ImageJ).

2.2.1.5 Mouse cytokine array analysis

Differently expressed cytokines or chemokines were detected in plasma from $Mif\text{-}2^{-/-}Apoe^{-/-}$ mice and $Apoe^{-/-}$ mice using proteome profiler through mouse cytokine array panel A following the standard protocol. Commercial membranes were blocked at RT in the blocking buffer provided by this kit for 1 h. At the same time, samples were constituted by mouse plasma in a 1:10 dilution of array buffer, mixed with a detection antibody cocktail (1:100), and incubated at RT for 1 h. Then pre-blocked membranes were covered with reconstituted samples at 4°C overnight. The second day, membranes were rinsed followed by 30 min of incubation with the diluted streptavidin-horseradish peroxidase (HRP) (1:2000) solution, and then visualized with chemi-reagent mix and developed by an Odyssey® Fc imager for 2 min, 10 min and 1 h, respectively. All measurements in this assay were conducted in duplicates. The mean pixel density of the pair of duplicate spots was quantified by ImageJ and is represented as the level of corresponding cytokine.

2.2.1.6 Hepatic immunochemistry

ORO staining and HE staining for OCT-embedded mouse liver tissue were carried out using 8 µm thick frozen sections and 4 µm paraffin sections. After placed at RT for 30 min, frozen sections were immersed in propylene glycol for 2 min and stained with pre-warmed ORO solution for 10 min. Following the staining procedure, tissues were differentiated in 85% propylene glycol for 1 min, and then counterstained using modified Mayer's hematoxylin and mounted using an aqueous mounting medium. Given the fact that lipids are dissolved by organic solvents during the sample preparation, ORO staining is not appropriate to perform on paraffin sections. In addition, hepatic HE staining procedures on either paraffin or frozen sections are same as the general HE staining procedures described above in 2.2.1.4.

2.2.1.7 Hepatic SREBP protein analysis by immunoblotting

40 mg liver tissue was collected from each mouse and lysed in 150 µL 1x RIPA lysis buffer added with protease inhibitor (each tablet was dissolved in 50 mL RIPA buffer). Samples were disrupted at the speed of 30-50 Hz for 2 min to release protein, and the concentrations were measured by bicinchoninic acid (BCA) assay. 200 µg protein was calculated, diluted to a volume of 100 µL by 1x RIPA buffer, and added with 100 µL 2x LDS sample buffer. Proteins were denatured at 95°C for 10 min, and stored at -20°C for future use. For immunoblot analysis, 10 µL protein/lane (around 10 µg protein) was loaded onto 11% SDS-PAGE gel with 15 wells, electrophoresis was carried out, and proteins were electro-transfer to PVDF membrane. After blocked with 5% BSA-TBST, membranes were incubated with primary antibodies diluted in 3% BSA-TBST. Antibodies used were targeted against mouse SREBP-1 (E-4) (1:500) and mouse SREBP-2 (1:1000). After overnight incubation with primary antibodies, the membranes were rinsed in 1x TBST for three times and incubated with goat anti-mouse HRP-linked secondary antibody (1:10,000). Following thorough washing, the immunoblot was eventually visualized by an Odyssey® Fc imager.

2.2.2 Functional methods *in vitro*

2.2.2.1 Cell lines and cell culture[#]

Human hepatocellular carcinoma cell line (Huh)-7 cells were epithelial-like and cultured in DMEM-GlutaMAX supplemented with 10% FCS and 1% penicillin/streptomycin (P/S), and cells were subcultivated for 2-3 times every week with a 1:3-1:5 split ratio.

Human embryonic kidney (HEK)-293 cells were purchased from German Collection of Microorganisms and Cell Cultures GmbH (DSMZ, Braunschweig, Germany). They were kept in DMEM-GlutaMAX supplemented with 10% FCS and 1% P/S, and split in a ratio of 1:3-1:5 generally.

Primary human monocytes and differentiated macrophages were maintained in full growth medium (RPMI 1640 medium with 10% FCS, 1% P/S, 2 mM L-glutamine and 1% non-essential amino acids (NEAA)). Additionally, detailed isolation procedures of monocytes were described in the following part.

2.2.2.2 Purification and differentiation of peripheral blood monocytes[#]

Peripheral blood mononuclear cells (PBMCs) were isolated as illustrated in the previous study [2]. In brief, peripheral blood was obtained from healthy volunteers and gently mixed with the equal volume of pre-warmed PBS, and the layer of PBMCs were separated by density gradient centrifugation (i.e. at 2000 rpm for 30 min with deceleration of 0) using Ficoll-Paque Plus density gradient media. After centrifugation, cells in the interphase were carefully sucked out using a plastic pipette, and RBCs were lysed using 1x RBC lysis buffer subsequently. The pellet of PBMCs was washed with pre-warmed PBS, then resuspended in full RPMI 1640 medium, and maintained at 37°C in a humidified atmosphere of 5% CO_2. Human Pan Monocyte Isolation Kit was then used to purify primary human monocytes from PBMCs based on negative depletion, in accordance with the producer's instructions. Flow cytometry was applied to assess the purity of isolated monocytes by using an anti-CD14 antibody. All the isolation procedures were approved by the local ethics committee of the LMU Munich University and all experiments were carried out in line with the guidelines of the LMU Munich University. These purified monocytes are intended for Transwell migration assay and 3D chemotaxis assay (data not shown). Macrophage colony-stimulating factor (M-CSF) was additionally used to accelerate the differentiation of monocytes into macrophages. After monocytes were purified, they were seeded in full growth medium with 100 ng/mL M-CSF, and the half of medium was regularly replaced every two days until they were differentiated into macrophages after about 7 days. These differentiated macrophages were subjected to DiI-LDL uptake assay.

2.2.2.3 Transwell migration assay in primary monocytes[#]

The transwell migration ability of primary human monocytes was assessed using the Boyden chamber as reported previously [161]. Briefly, monocytes were isolated from PBMCs using magnetic beads and subsequently maintained in full RPMI 1640 medium overnight. The second day, 600 µL/well of different treatments was prepared and loaded in 24-well plate. Transwell culture inserts (i.e. 5 µm filters) were then transferred into the wells containing 4 nM MIF-2 with or without different concentrations of 4-CPPC, and together placed at the incubator for 30 min. In the upper chamber, 1x 10^6 cells in a total of 100 µL suspension were loaded. The inhibitory effect on MIF-2-mediated cell migration was assessed by prior incubation of inhibitors with MIF-2 at 37°C for 45 min. For chemotaxis, these chambers were kept at 37°C incubator for 4 h. Afterwards, inserts were cleaned by ethanol and PBS for reuse,

while migrated cells were washed by 500 µL PBS, collected and counted by flow cytometer utilizing CountBright™ Absolute Counting Beads.

2.2.2.4 DiI-LDL uptake assay in primary macrophages[#]

The uptake assay of DiI complex-labeled low density lipoprotein (DiI-LDL) in primary human monocyte-derived macrophages was performed following the well-established procedures, as formerly illustrated [262]. In short, macrophages were kept in the full RPMI 1640 medium at 37°C, and then changed to MEM medium containing 0.2% BSA for 2-4 h to get starvation. Later, cells were pre-incubated with inhibitors (10 µM AMD3100, 4-IPP and 4-CPPC) for 30 min along with 1 µg/mL MIF-2 overnight. The second day, cells were cultured in the same medium added with 1% 2-Hydroxypropyl-β-cyclodextrin (HPCD) at 37°C for 45 min. After rinsed with PBS for three times, macrophages were first maintained in 25 µg/mL DiI-LDL solution at 4°C for 30 min (i.e. the binding process), and subsequently removed to 37°C for 20 min (i.e. the uptake process). Treated macrophages were washed with PBS, fixed with 4% PFA, permeabilized with 0.1% Triton X in PBS, and finally stained with DAPI (1:100,000). Representative images were acquired with a Leica DMi8 fluorescence microscope and the uptake effect was characterized as the index of relative corrected total cell fluorescence (CTCF) via ImageJ.

2.2.2.5 Huh-7 stimulation, *Srebp* and target gene detection by RT-qPCR[#]

4×10^5 Huh-7 cells were seeded in the 12-well plate on the day before starting the experiment and then starved with DMEM medium containing 2% FCS overnight. On the third day, Huh-7 cells were stimulated with different concentrations of MIF-2 protein (0 nM, 4 nM, 8 nM, 16 nM, 32 nM, 48 nM) for 24 h. Supernatant was discarded, monocellular layers were lysed by TRIzol™ reagent, and total RNA was isolated following the standard protocol. The concentrations of RNA samples were measured by Nanodrop spectrophotometer and 1000 ng RNA was prepared for reverse transcription. cDNA was subsequently synthesized using First trand cDNA synthesis kit and then diluted in a 1:5 ratio. Afterwards, real-time quantitative PCR process was carried out by employing specific human *β-Actin, Fasn, Psck9, Cd36, Glut1, Glut4, Srebp-1, Srebp-2, Ldlr, Hmgcr, Lxra, Cxcr4 and Cd74* primer pairs (Eurofins BioPharma Product Testing Munich, Planegg, Germany) and 2x SensiMix PLUS SYBR No-ROX Kit in a Rotor-Gene 6000 machine. All the primer sequences were attached in the section 2.1.3. All the raw data were obtained from the Rotor-Gene 6000 series 1.7 software

(QIAGEN), and relative mRNA levels were calculated by using the $\Delta\Delta$Ct method with *β-actin* as the housekeeping gene.

2.2.2.6 Analysis of SREBPs and signaling pathways in Huh-7 cells by immunoblotting[#]

1×10^5 Huh-7 cells were seeded in 24-well plate on the day before starting the experiment and then starved with 2% FCS DMEM medium overnight. On the third day, Huh-7 cells were stimulated with different concentrations of MIF-2 (0 nM, 4 nM, 8 nM, 16 nM, 32 nM, 48 nM) or in the presence IgG control, AMD3100 and LN-2, dissolved in 2% FCS DMEM medium for 24 h, in terms of SREBPs detection. Huh-7 cells were washed with pre-warmed PBS, and lysed in 100 µL 1x LDS lysis buffer with dithiothreitol (DTT). Proteins were collected and denatured at 95°C for 10 min, and stored at -20°C for use. 20 µL protein per lane was loaded onto 7.5% SDS-PAGE and immunoblot analysis were carried out using primary antibodies diluted in 3% BSA-TBS-T. Antibodies used were targeted at mouse anti-SREBP-1 (E-4) (1:500), mouse anti-SREBP-2 (1:1000), mouse anti-FASN (A-5) (1:500) and mouse anti-LDLR (C7) (1:500). After incubation, these membranes were rinsed in 1x TBS + 0.1% Tween and incubated with a goat anti-mouse HRP-conjugated secondary antibody (1:10,000).

As for signaling pathway analysis, Huh-7 cells were starved with DMEM medium containing 0.05% FCS overnight, stimulated with different concentrations of MIF-2 in 0.05% FCS DMEM medium for 30 min, and other experimental settings were the same as described above. After treatment, cells were lysed and subjected to 11% SDS-PAGE gel, for Western blotting. AMPK activation was revealed with rabbit antibodies against phosphorylated AMPK (1:1000) and total AMPKα (1:1000) as well as β-Actin detected for standardization. Similarly, AKT phosphorylation was detected with rabbit antibodies against phosphorylated AKT (1:1000) and total AKT (1:1000), and ERK phosphorylation was revealed with mouse antibodies against phosphorylated ERK (1:500) and total ERK (1:500). Goat anti-rabbit HRP-conjugated secondary antibody (1:10,000) was used for visualization and protein bands were developed as chemiluminescence using an Odyssey® Fc imager. Quantifications were made by ImageJ.

2.2.2.7 Detection of SREBP-2 nuclear translocation in Huh-7 cells by immuno-fluorescence staining[#]

1×10^4 Huh-7 cells were seeded in 24-well plate on the day before starting the experiment and then starved with DMEM medium including 2% FCS overnight. On the third day, Huh-7

cells were stimulated with two concentrations of MIF-2 (8 nM and 16 nM) in 2% FCS DMEM medium for 24 h. After stimulation, Huh-7 cells were fixed with 4% PFA and permeabilized with 0.02% Triton X-100 in PBS. Cells were washed with PBS, blocked with 1% BSA and 5% goat serum in PBS and then incubated with mouse anti-SREBP-2 (1:300) at 4°C overnight. Cells were washed with PBS for three times and incubated with goat anti-mouse Alexa Fluor 488 (1:500) at RT for 1 h. After three times of washing, the cover glasses were incubated with Vectashield Antifade Mounting medium with DAPI, placed in the slides, and fixed using the nail polish. Then images displaying nuclear SREBP-2 expression were acquired using a Leica DMi8 microscope.

2.2.2.8 Analysis of CXCR4 and CD74 receptor expression in Huh-7 cells by immunostaining and flow cytometry[#]

Cell fluorescence staining procedures were specifically described in 2.2.2.7. After blocking, hepatocytes were incubated with mouse anti-CD74 (1:100) and rabbit anti-CXCR4 (1:100) overnight. The second day, cells were washed with PBS for three times and incubated with goat anti-mouse Alexa Fluor 488 (1:200) and goat anti-rabbit Alexa Fluor 555 (1:200) at RT for 1 h. After three times of washing, the cover glasses were incubated with Vectashield Antifade Mounting medium with DAPI, placed in the slides, and fixed using the nail polish. Then images displaying CXCR4/CD74 receptor expression were acquired using a Zeiss confocal microscope.

To analyze the surface expression of receptors in hepatocytes, 1×10^6 Huh-7 cells were collected and stained with FITC-conjugated anti-CD74 and APC-Cy7-conjugated anti-CXCR4 for 45 min. After three times of washing by FACS buffer, these stained cells were sorted in a FACSVerse™ flow cytometer, compensations and special gating strategies were set using isotype controls and fluorescence minus one (FMO) antibody combinations. Raw data were obtained by FACSiva software, and analysis was carried out via FlowJo software.

2.2.2.9 Native LDL uptake assay in Huh-7 cells by ORO staining[#]

1×10^4 Huh-7 cells were seeded in 24-well plate on the day before starting the experiment and then starved with 2% FCS DMEM medium overnight. On the third day, Huh-7 cells were stimulated with 8 nM MIF-2 with or without IgG, AMD3100 and LN-2, dissolved in 2% FCS DMEM medium for 24 h. After treatment, hepatocytes were subsequently incubated with 10 µg/mL human plasma LDL at 37°C for 4 h, followed by 3 times of washing in PBS. Later

on, cells were fixed in 4% PFA and subsequently stained with ORO solution for 5 min. Stained cells were then washed and counterstained with DAPI (1:10,000) and then mounted on a glass slide. Images showing positive uptake LDL signals under different treatments were captured using a Leica DMi8 microscope.

2.2.2.10 FLIM-FRET analysis including transformation and transfection

The interest DNA (i.e. YFP-CD74 and CFP-CXCR4) was transformed into competent *E. coli* cells (i.e. DH5α cells) using heat shock at 42°C for 60 sec. Recovered competent cells were plated and incubated at 37°C overnight. Then bacterial cells were harvested and plasmid DNA of YFP-CD74 and CFP-CXCR4 was purified through the QIAfilter Plasmid Midi Kit, and the DNA concentrations were determined by the absorbance at 260 nm via UV spectrophotometry. On the day before transfection, HEK-293 cells were split and suspended in 100 mm dish meanwhile. When the confluence of HEK cells was up to 70%-90%, a total of 8 μg DNA was introduced into HEK-293 cells using polyfectamine transfection reagent following the producer's protocol. The receptor complex CXCR4/CD74 in HEK-293 cell transfectants with/without MIF or MIF-2 stimulation was visualized by multi-photon laser scanning microscopy (MPLSM), and the histograms of FRET-efficiency and FRET-binding were acquired by applying fluorescence lifetime imaging microscope-fluorescence resonance energy transfer (FLIM-FRET) methodology. After stimulation of MIF (8 nM) and MIF-2 (4 nM), the life time decay of the donor (CFP-CXCR4) arguing for the CXCR4/CD74 complex formation was measured by FLIM-FRET analysis *ex vivo*.

2.2.3 Statistical analysis

Statistical analysis was performed capitalizing on GraphPad Prism version 8 software. Data are represented as means ± standard deviation (SD) from more than three independent experiments. After testing for normality, data were analyzed by Student's t-test, Mann-Whitney test, one-way ANOVA with multiple comparison test or Kruskal-Wallis test as appropriate. $P < 0.05$ were considered statistically significant. In this thesis, statistically significant differences are indicated by asterisks: * $P < 0.05$; ** $P < 0.01$; *** $P < 0.001$; **** $P < 0.0001$.

3. RESULTS

3.1 Genetic knockout and pharmacological targeting of MIF-2 attenuate early and advanced atheroprogression *in vivo*

3.1.1 Genetic knockout of *Mif-2* attenuates atherogenesis in an early model of atherosclerosis in female *Apoe⁻/⁻* mice

In order to assess the role of MIF-2 in early atherosclerotic progression, we applied a well-established *in vivo* mouse model, in which *Apoe* knockout mice are fed a short-term HFD for 4 to 5 weeks to develop early-stage plaques in the aortic root and aortic arch. To start this project, we generated a genetic *Mif-2* and *Apoe* double knockout mouse line using the crossbreeding strategy outlined in Figure 9A at the animal facility of the Institute for Stroke and Dementia (ISD). To obtain homozygous *Mif-2⁻/⁻Apoe⁻/⁻* mice, RT-qPCR analysis of mouse heart tissue along with Western blot (WB) and immunofluorescence staining employing mouse liver tissue was performed to verify the complete global knockout of *Mif-2* in these mice at both mRNA and protein level (Figures 9B-9D). These results together indicated that the *Mif-2⁻/⁻Apoe⁻/⁻* mouse line was successfully generated in our laboratory.
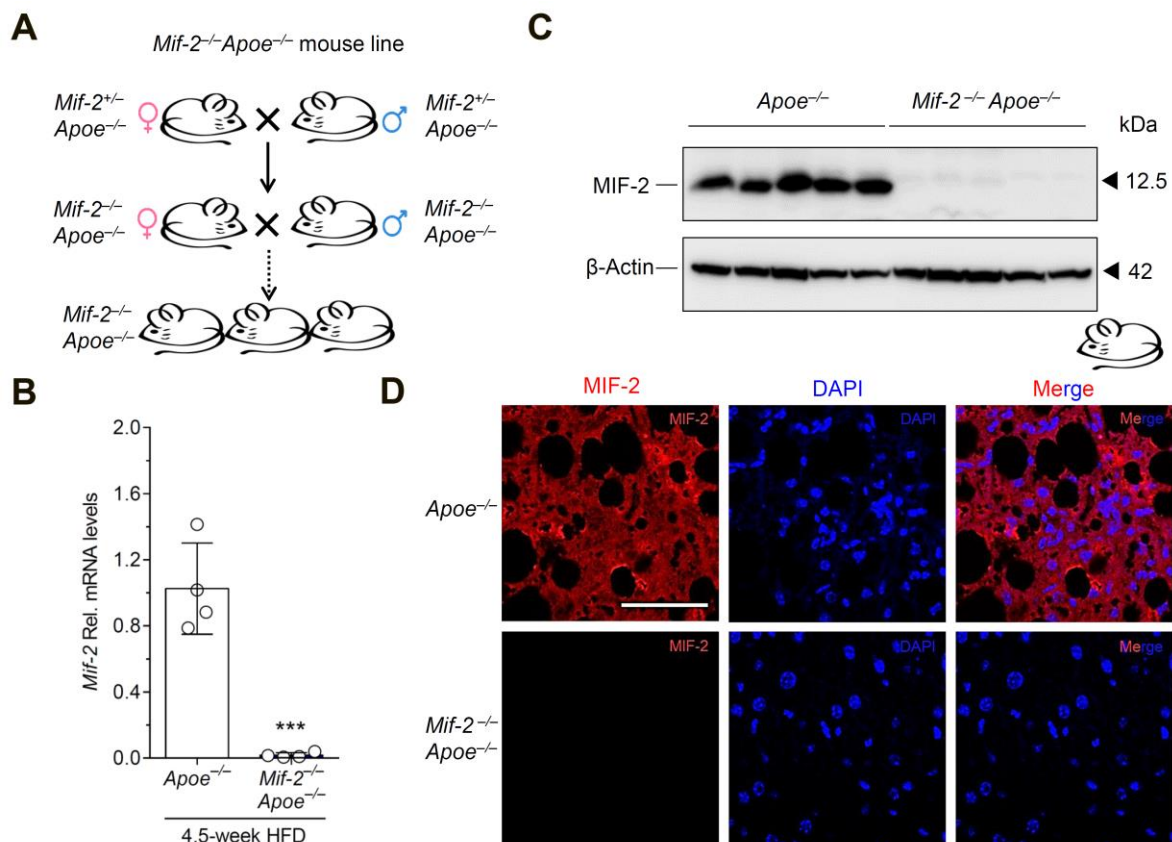
Figure 9: The breeding strategy and genotype results of *Mif-2$^{-/-}$Apoe$^{-/-}$* mouse line. (A) Scheme of the crossbreeding strategy to generate *Mif-2$^{-/-}$Apoe$^{-/-}$* mouse line. All genetic mouse experiments were performed in *Apoe$^{-/-}$* and *Mif-2$^{-/-}$Apoe$^{-/-}$* mice. (B) The complete deficiency of *Mif-2* on gene level was checked on heart tissue by RT-qPCR from the above two groups of female mice. n = 4 for each group. (C) The complete deficiency of *Mif-2* on protein level was analyzed on liver tissue by WB from the above two groups of female mice. n = 5 for each group. (D) Fluorescence staining was performed on liver tissue from the above two groups of female mice. Scale bar, 50 μm. This figure is part of a preprint manuscript version published on bioRxiv (doi: https://doi.org/10.1101/2021.12. 28.474328).

In general, eight-week-old female *Apoe*-deficient mice as well as *Mif-2*-deficient atherogenic mice were subjected to a Western-type cholesterol-rich (0.21%) high-fat diet (HFD) for 4.5 weeks (Figure 10A) to develop early-stage lesions. After 4.5-week HFD exposure, both groups of mice were sacrificed and organs were harvested for following experiments. Body weight was regularly measured, circulating triglyceride and cholesterol levels were determined by commercial kits, and blood immune cell percentages counted using flow cytometry (Supplemental Table 1). Analysis of atherosclerotic lesions was confined to frozen sections of the aortic root as well as sections of the aortic arch embedded in paraffin. Oil Red O (ORO) staining demonstrated fatty streak lesions in the aortic root, as observed in atherogenic *Apoe$^{-/-}$* mice, suggesting early development of atherosclerotic plaques (Figure 10B). There was markedly less plaque formation in the aortic root as well as arch from *Mif-2*-deficient atherogenic mice in comparison to control *Apoe$^{-/-}$* mice (Figures 10B and 10E), indicating that *Mif-2* deficiency is protective in early stage atherogenesis. This result was surprising as *Mif*-deficient *Apoe$^{-/-}$* mice exhibit a protective phenotype only in the abdominal aorta as well as brachiocephalic artery, but not in aortic root and arch. In addition, quantification results of HE-stained plaques underscored the robustness of this phenotype upon *Mif-2* deletion (Figure 10C). The lesion area in aortic root showed a ~50% reduction after *Mif-2* deletion, as confirmed via both ORO and HE staining. Of note, protection from lesion progression in *Mif-2*-deficient atherogenic mice was accompanied by dramatically diminished lesional macrophages in comparison with control mice, as determined by anti-CD68 staining (Figure 10D), indicating a role in vascular inflammation.
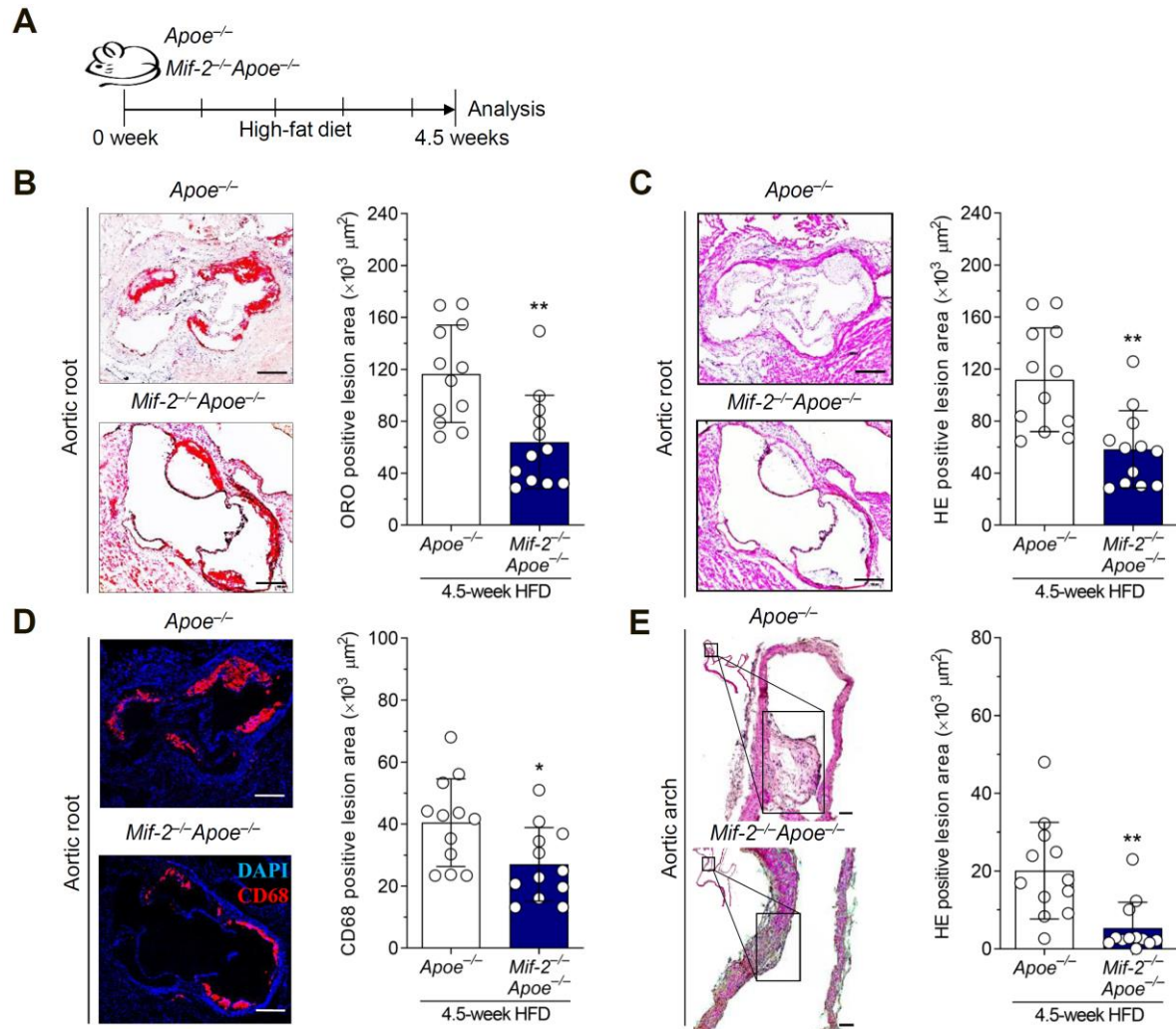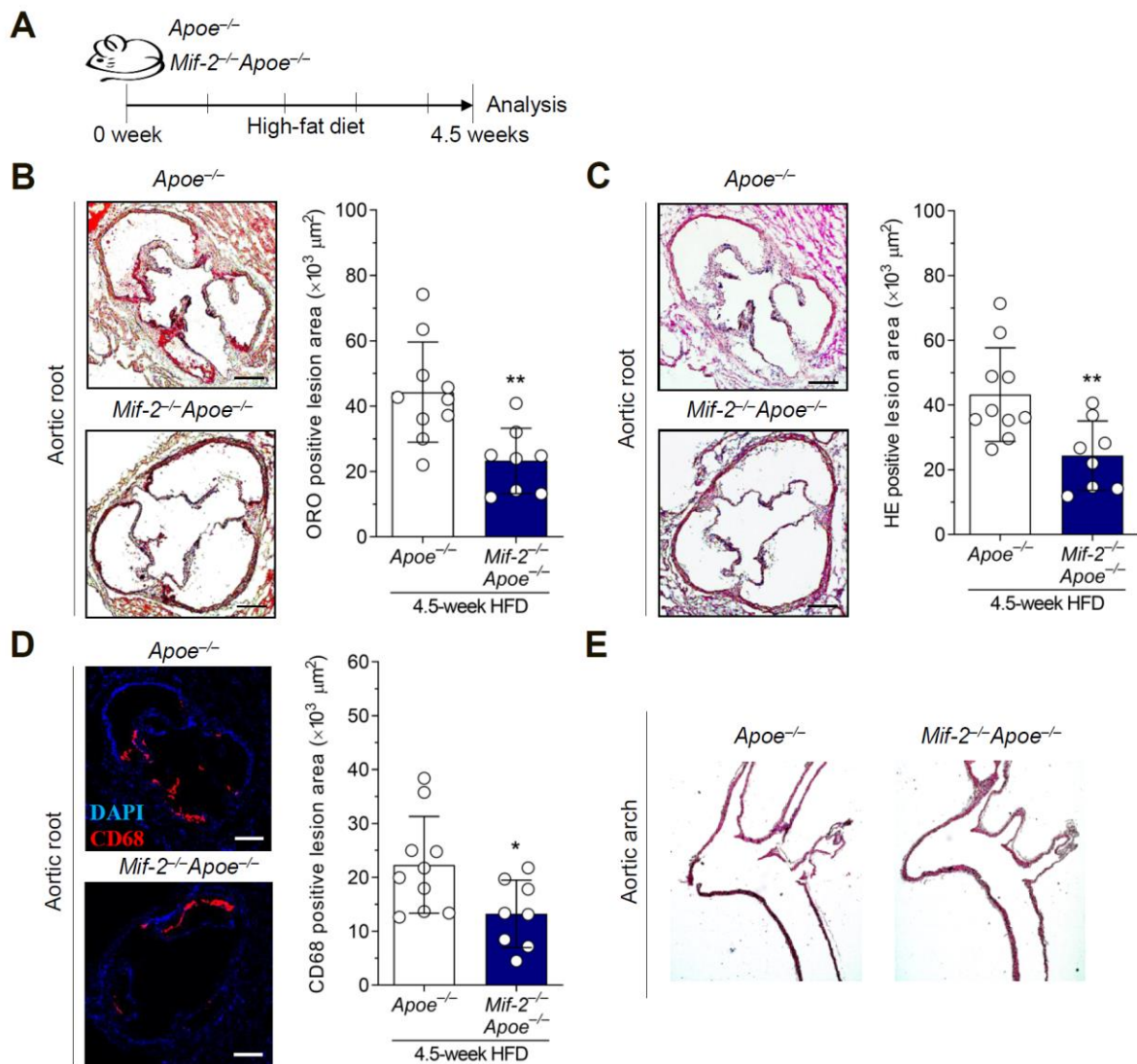
Figure 10: Genetic deletion of *Mif-2* mitigates atherogenesis in an early model of atherosclerosis in female *Apoe*$^{-/-}$ mice. All genetic mouse experiments were performed in *Apoe*$^{-/-}$ and *Mif-2*$^{-/-}$*Apoe*$^{-/-}$ mice. (A) Scheme of describing that the above two groups of female mice were exposed to 4.5-week HFD to develop early atherosclerosis. (B) Representative ORO-stained images of aortic roots in frozen sections from the above two groups of female mice and corresponding quantification results. (C) Representative HE-stained images of aortic roots in frozen sections from the above two groups of female mice and corresponding quantification results. (D) Representative anti-CD68-stained images (CD68, red; DAPI, blue) from the above two groups of female mice and quantification results of macrophage area. (E) Representative HE-stained images of aortic arch in paraffin sections from the above two groups of female mice and quantification results. n = 12 for each group; each mouse is represented as one data point; scale bar, 250 μm. This figure is part of a preprint manuscript version published on bioRxiv (doi: https://doi.org/10.1101/2021.12.28.474328).

Subsequently, a cytokine/chemokine array was performed using mouse plasma from the same experiment, in order to determine inflammatory cytokine levels in the circulatory system between the two groups. This proteome profiler array measures 40 cytokines/chemokines. Confirming the lesional CD68+ macrophage staining data, there was a marked reduction of several circulating inflammatory cytokines in *Mif-2*-deficient atherogenic mice in comparison with *Apoe*-deficient mice (Figure 11A). In addition to decreased IL-2 and IL-17, significant

reductions in IFN-γ and IL-16 (Figures 11A and 11B), CXCL13/BLC as well as IL-1α (Figures 11A and 11C) were detected in *Mif-2*-deficient atherogenic mice, with trends for IL-27, CCL2 and CXCL12, implying that *Mif-2* knockout leads to a broad downregulation of the inflammatory response associated with atherogenesis. Additionally, the inflammatory cytokine levels were just briefly evaluated here, and this project did not study them further regarding the special cytokines/chemokines.
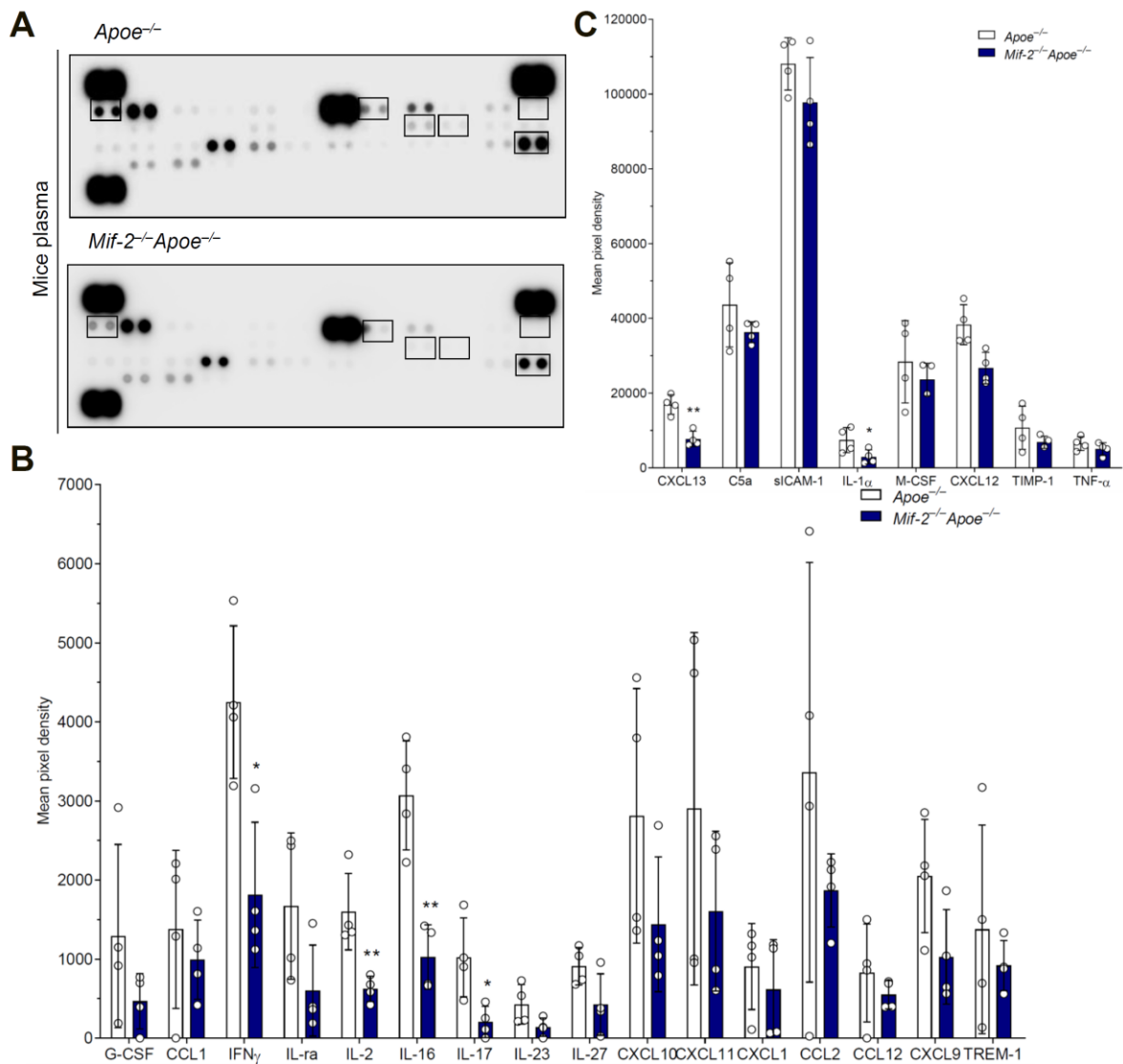
Figure 11: *Mif-2* deletion is associated with decreased inflammatory cytokine expression in *Apoe*-deficient mice. (A-C) The cytokine array using mouse plasma from both *Apoe*$^{-/-}$ and *Mif-2*-deficient atherogenic *Apoe*$^{-/-}$ mice fed 4.5-week HFD was performed to detect forty cytokines/chemokines. (A) Representative dot blots from four times of independent experiments. (B, C) Quantification results to select key inflammatory cytokines involved in atherogenesis. (B) Relatively low expressed chemokines/cytokines: *Mif-2*$^{-/-}$*Apoe*$^{-/-}$ mice displayed significantly reduced circulating IFN-γ, IL-2, IL-16 and IL-17. (C) Relatively high expressed chemokines/cytokines: *Mif-2*$^{-/-}$*Apoe*$^{-/-}$ mice displayed significantly downregulated CXCL12 and CXCL13. All the measurements were performed in duplicate; n = 4 for each group. This figure is part of a preprint manuscript version published on bioRxiv (doi: https://doi.org/10.1101/2021.12.28.474328).

3.1.2 Genetic knockout of *Mif-2* attenuates atherogenesis in an early model of atherosclerosis in male *Apoe⁻/⁻* mice

In addition to female mice, early atherosclerotic progression was also studied in male mice under the same experimental settings (Figure 12A). Compared with female mice, male mice usually developed less pronounced lesions in the aortic root. ORO and HE staining for plaque size assessment and CD68 staining for lesional macrophage area evaluation (Figures 12B-D) in aortic root as well as HE staining in aortic arch (Figure 12E) were performed as before in female mice, and plaques and lesional macrophages were found to be decreased in *Mif-2*-deficient atherogenic mice compared with controls.

Figure 12: Genetic deletion of *Mif-2* attenuates atherogenesis in an early model of atherosclerosis in male *Apoe*-deficient mice. All genetic mouse experiments were performed in *Apoe⁻/⁻* and *Mif-2⁻/⁻ Apoe⁻/⁻* mice. (A) Scheme of describing that the above two groups of male mice were exposed to 4.5-week HFD to develop early atherosclerosis. (B) Representative ORO-stained images of aortic roots in frozen sections from the above two groups of male mice and corresponding quantification results. (C)

Representative HE-stained images of aortic roots in frozen sections from the above two group male mice and corresponding quantification results. (D) Representative anti-CD68-stained images (CD68, red; DAPI, blue) from the above two groups of male mice and quantification results of macrophage area. (E) Representative HE-stained images of aortic arch in paraffin sections from the above two groups of male mice. n = 8-10 for each group; each mouse is represented as one data point; scale bar, 250 μm. This figure is part of a preprint manuscript version published on bioRxiv (doi: https://doi.org/10.1101/2021.12.28.474328).

It is worth noting that sex differences of plaque progression in mice are contrary to those features in humans. Humans usually develop more pronounced plaques in men, whereas mice always grow larger lesions in females with less weight in general. This tendency is associated with characteristics of the circulation in mice, as exemplified by extremely high heart rates. Of note, not all male mice in this cohort develop visible plaques in the aortic tree, as detected by HE staining (Figure 12E). Therefore, it is impracticable to quantify total plaque area in the aortic arch of male mice. To conclude, the above data indicate that genetic deletion of *Mif-2* attenuates early-stage plaque formation in mice of both genders.

3.1.3 Pharmacological blockade of MIF-2 by the selective inhibitor 4-CPPC attenuates early atherosclerosis in male atherogenic *Apoe$^{-/-}$* mice

Next the inhibitory or therapeutic capacity of 4-(3-carboxyphenyl)-2,5-pyridinedicarboxylic acid (4-CPPC) on vascular lesions in *Apoe$^{-/-}$* mice was determined. 4-CPPC was recently developed as the first small molecular inhibitor, showing a 13-fold higher selectivity for MIF-2 compared to MIF. Given that there has been no functional data about 4-CPPC in atherogenic disease models yet, we first tested whether 4-CPPC has an inhibitory impact on MIF-2 atherogenic effects on monocytes or macrophages *in vitro*. A Transwell migration assay using primary human monocytes and a DiI-labeled native LDL uptake assay utilizing human monocyte-derived macrophages were applied to evaluate the functionality of 4-CPPC in the context of atherosclerosis. These results provided some fundamental data and useful indications for the subsequent *in vivo* experiment.

As shown in Figure 13A, MIF-2 at a concentration of 4 nM significantly promoted the chemotaxis of monocytes compared with the control. Different concentrations of 4-CPPC could inhibit the effect induced by MIF-2, and 20 nM of 4-CPPC showed the strongest inhibitory ability. After confirming the effects of MIF-2 and 4-CPPC on monocytes, a native LDL uptake assay in human macrophages was additionally performed. These macrophages treated with MIF-2 displayed upregulated LDL uptake, and 4-CPPC inhibited LDL uptake

induced by MIF-2 (Figure 13B). In addition to 4-CPPC, this assay utilized a CXCR4 antagonist AMD3100 and an MIF inhibitor 4-IPP as well. Quantification results demonstrated that AMD3100 (10 µM) and 4-IPP (10 µM) could considerably diminish LDL uptake induced by MIF-2, and 4-CPPC showed a similar inhibitory property to AMD3100 and 4-IPP.
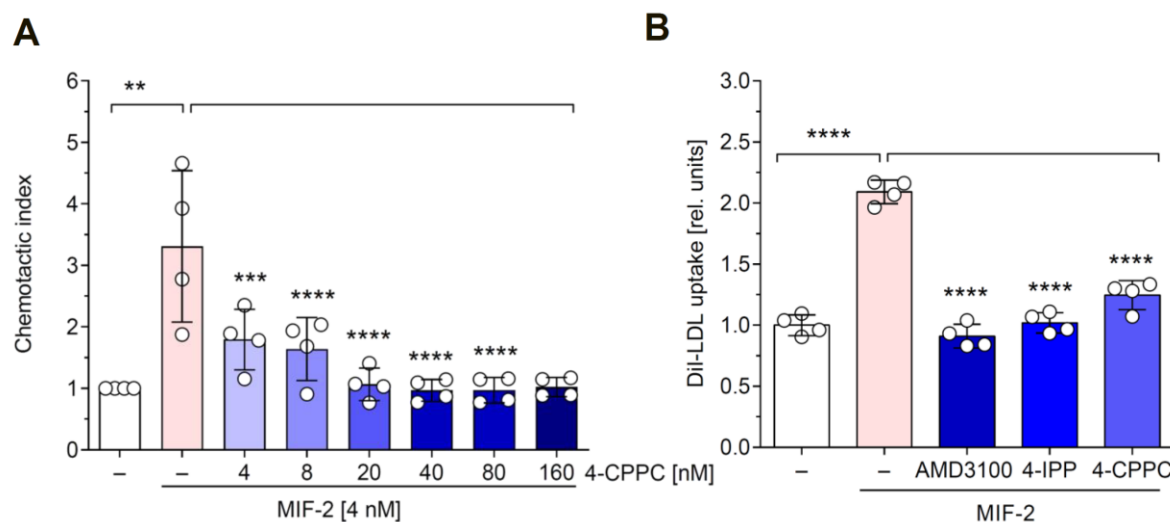

Figure 13: MIF-2 promotes primary monocyte migration and macrophage LDL uptake *in vitro*, and 4-CPPC inhibits this effect. (A) Transwell migration assay performed on primary human monocytes showed that recombinant MIF-2 significantly enhanced the chemotaxis of monocytes and that 20 nM 4-CPPC could counteract the effect induced by MIF-2. n = 4 biological replicates. (B) Native LDL uptake assay performed on human macrophages displayed a similar picture. MIF-2 promoted LDL uptake *in vitro* and 4-CPPC had an inhibitory property, comparable to that of AMD3100 and 4-IPP. n = 4 biological replicates. This figure is part of a preprint manuscript version published on bioRxiv (doi: https://doi.org/10.1101/2021.12.28.474328).

After verifying the functionality of MIF-2 and 4-CPPC *in vitro*, an *in vivo* experiment using 4-CPPC was then performed. Atherogenic *Apoe*-deficient mice were exposed to 4.5-week HFD and in parallel administrated with 4-CPPC (50 µg/mouse, 3×/week) or vehicle treatment (Figure 14A). After 4.5-week HFD along with treatment, the mice were then sacrificed, and the lesion size and macrophage content were analyzed. Notably, 4-CPPC-injected atherogenic mice showed significantly decreased lesions, i.e. by ~60%, in the aortic root compared to controls, as demonstrated by both ORO- and HE-stained images (Figures 14B and 14C). Moreover, it is well acknowledged that macrophages are not only major components of early-stage plaques, but also responsible for regulation of inflammatory process and reverse cholesterol transport (RCT). Consistently, the 4-CPPC-injected group was found to show a striking decrease of lesional macrophages, as visualized by anti-CD68 staining (Figure 14D) as well. However, atherosclerotic plaques in the aortic arch could be hardly detected and further quantified here, because male mice develop less lesions as outlined above (Figure 14E). In addition, no significant impact of 4-CPPC treatment on body weight and blood

leukocyte counts were detected in this study within the observed 4.5-week time frame. Taken together, these results not only confirmed the phenotype observed in the genetic mouse model previously, but also suggested the therapeutic potency of 4-CPPC in early stage atherogenesis.
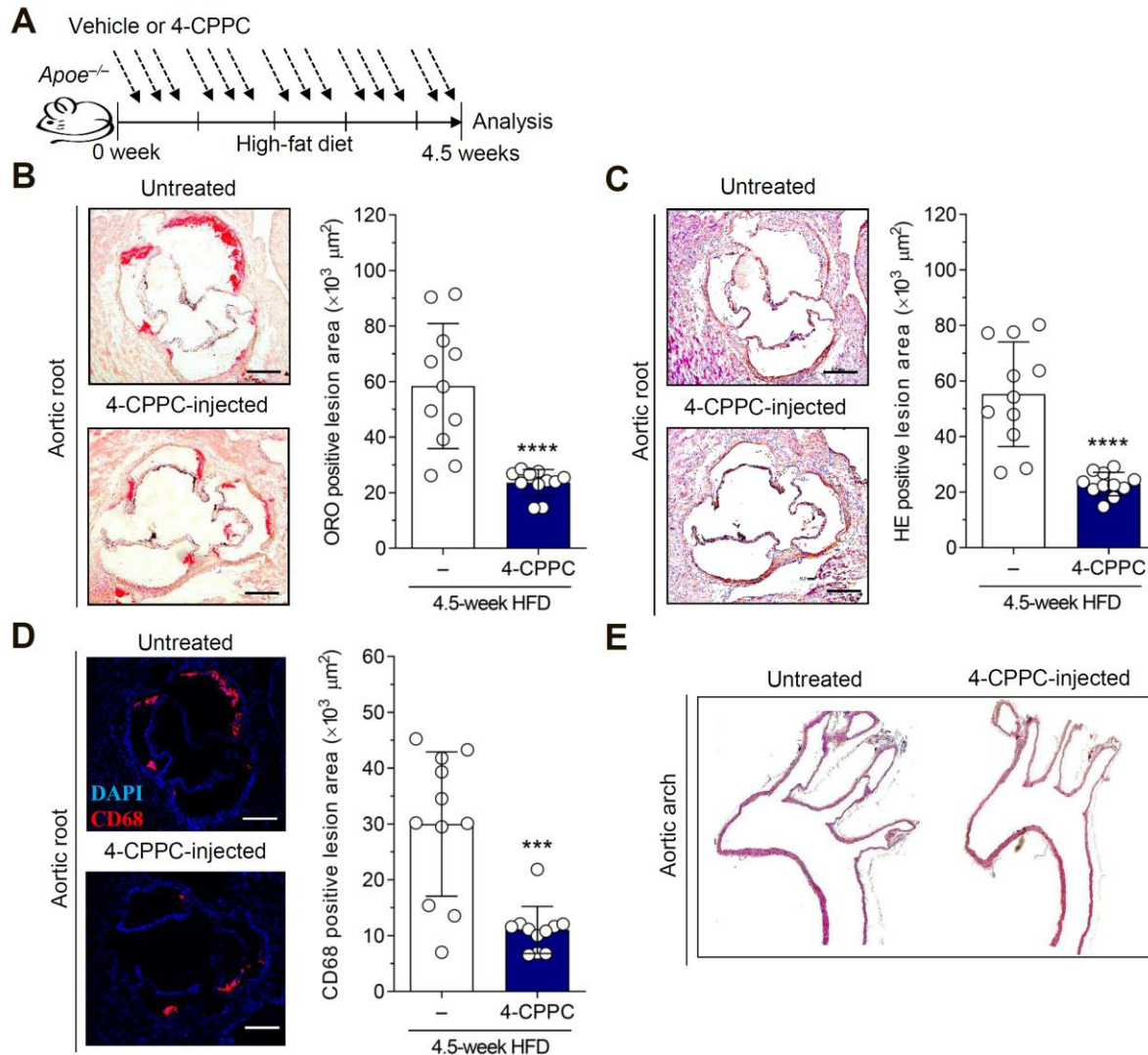

Figure 14: Pharmacological blockade of MIF-2 by the selective inhibitor 4-CPPC attenuates early atherosclerosis in male atherogenic *Apoe*$^{-/-}$ mice. (A) Scheme of describing *in vivo*-injection regimen for 4-CPPC in atherogenic *Apoe*$^{-/-}$ mice during the 4.5-week HFD period. (B) Representative ORO-stained images of aortic roots in frozen sections from 4-CPPC- *versus* vehicle-treated mice and corresponding quantification results. (C) Representative HE staining images of aortic roots in frozen sections from 4-CPPC- *versus* vehicle-treated mice and corresponding quantification results. (D) Representative anti-CD68-stained images (CD68, red; DAPI, blue) from 4-CPPC- *versus* vehicle-treated mice and quantification results of macrophage area. (E) Representative HE-stained images of aortic arch in paraffin sections from 4-CPPC- *versus* vehicle-treated mice. n = 11 for each group; each mouse is represented as one data point; scale bar, 250 μm. This figure is part of a preprint manuscript version published on bioRxiv (doi: https://doi.org/10.1101/2021.12.28.474328).
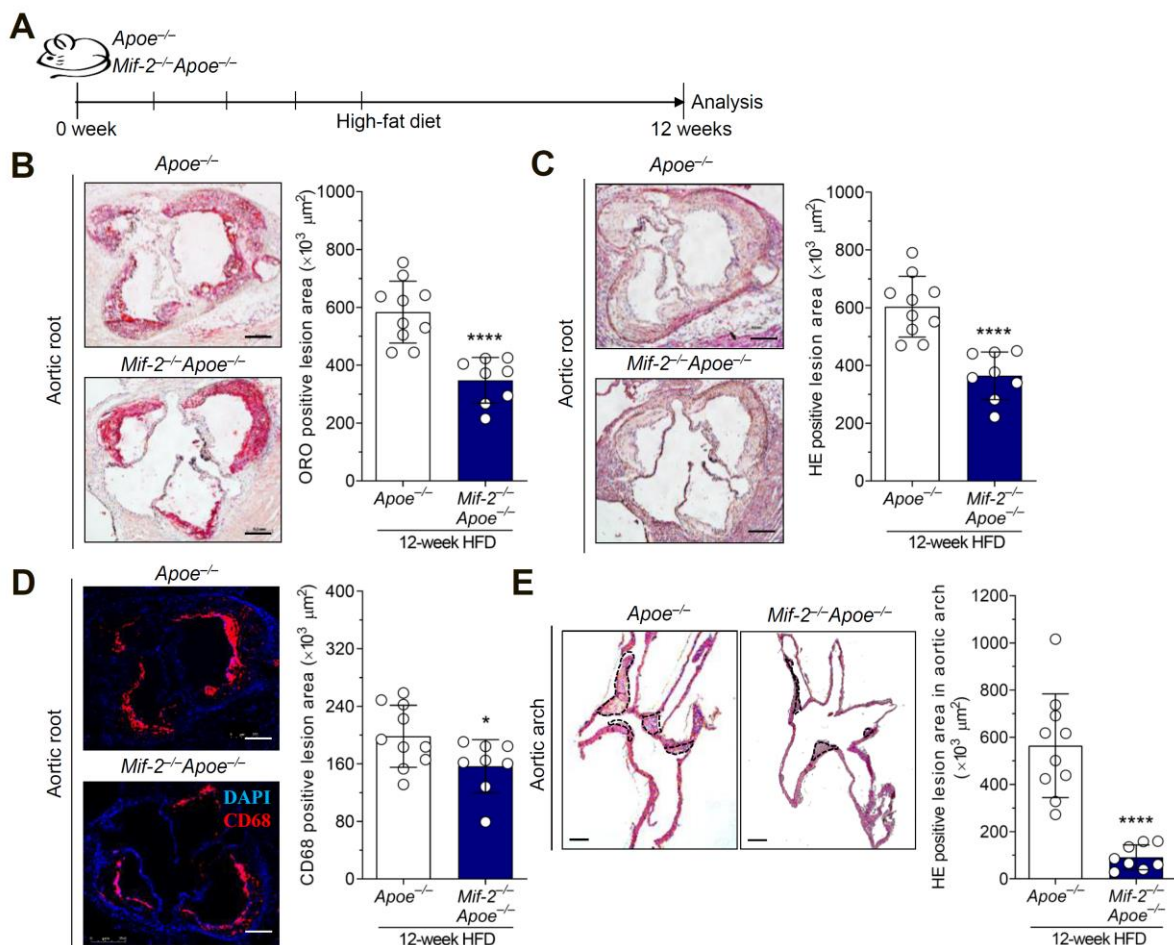
3.1.4 Genetic knockout of *Mif-2* attenuates atherogenesis in an advanced model of atherosclerosis in female *Apoe*⁻/⁻ mice

In light of previous data showing pro-atherogenic properties of MIF-2 *in vivo* and *in vitro*, we next tested the significance of MIF-2 in a model of advanced atherosclerosis. This condition would also better physiologically mimic plaque progression in human beings according to the mouse-to-human age map. Female *Apoe*-deficient mice and *Mif-2*-deficient atherogenic mice were exposed to 12 weeks of HFD to develop advanced plaques (Figure 15A). Compared to the early stage model which previous chapter presented, *Apoe*-deficient mice developed ~3 fold more plaques in the aortic root after 12-week HFD (Figure 15B), which was in accord with atherosclerotic development in a prior study [263]. Even so, *Mif-2*-deficient atherogenic mice were found to show a significant reduction of measurable plaques by ~40% in the aortic root (Figures 15B and 15C) and by ~80% in the aortic arch (Figure 15E) compared to controls, as showed in ORO- and HE-stained images. The CD68 positive macrophage content only decreased slightly (Figure 15D). In fact, the differences of macrophage contents from early stage to advanced stage became smaller (Figures 10D and 15D). Collectively, these data are suggestive of a detrimental impact of MIF-2 on advanced atherosclerosis.

Figure 15: Genetic knockout of *Mif-2* attenuates atherogenesis in an advanced model of atherosclerosis in female *Apoe*$^{-/-}$ mice. All genetic mouse experiments were performed in *Apoe*$^{-/-}$ and *Mif-2*$^{-/-}$*Apoe*$^{-/-}$ mice. (A) Scheme of describing that the above two group female mice were exposed to 12-week HFD to develop advanced atherosclerosis. (B) Representative ORO-stained images of aortic roots in frozen sections from the above two group female mice and corresponding quantification results. (C) Representative HE-stained images of aortic roots in frozen sections from the above two group female mice and corresponding quantification results. (D) Representative anti-CD68-stained images (CD68, red; DAPI, blue) from the above two group female mice and quantification results of macrophage area. (E) Representative HE-stained images of aortic arch in paraffin sections from the above two groups of female mice and quantification results. n = 8-10 for each group; each mouse is represented as one data point; scale bar, 250 μm. This figure is part of a preprint manuscript version published on bioRxiv (doi: https://doi.org/10.1101/2021.12.28.474328).

Of note, *Mif-2*-deficient mice generally developed a bigger necrotic core, as showed by Masson staining (Figure 16B). In contrast, *Mif-2* deficiency did not affect collagen content in plaques (Figure 16A). Combined with Figure 15, some cells displayed a positive DAPI signal, whilst CD68 negativity was noticed.
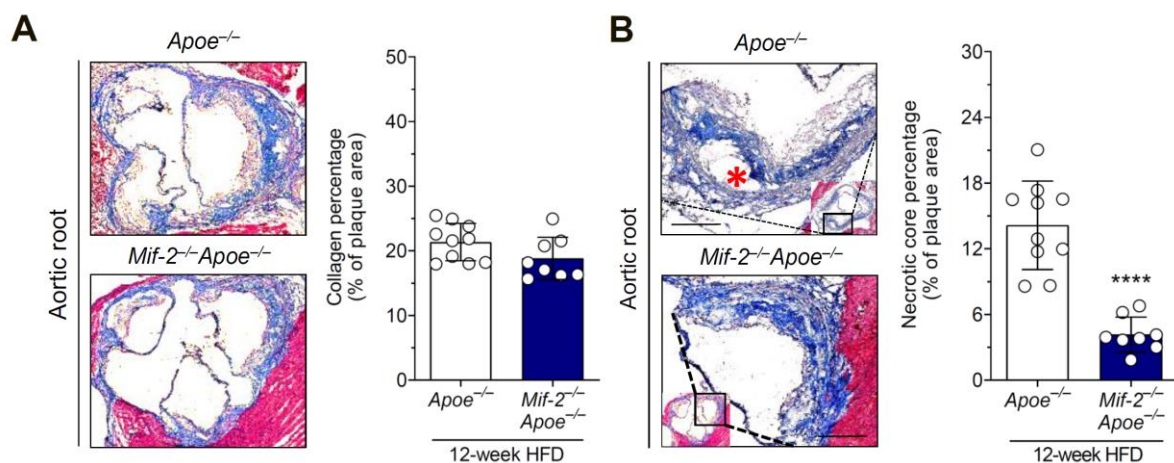
Figure 16: *Mif-2* gene deletion mitigates necrotic core formation. (A) Representative Masson-stained images and quantification results of collagen content from female *Apoe*-deficient mice and *Mif-2*-deficient atherogenic mice after 12-week HFD. (B) Representative structure of a necrotic core indicated by the red star and quantification results of lesional necrotic core percentages. n = 8-10 for each group; each mouse is represented as one data point; scale bar, 250 μm. This figure is part of a preprint manuscript version published on bioRxiv (doi: https://doi.org/10.1101/2021.12.28.474328).

In summary, this chapter applied a genetic as well as a pharmacological mouse model under both short- and long-term HFD to study MIF-2's pro-atherogenic property *in vivo*. We found that *Mif-2* deficiency attenuated plaque formation and lesional macrophage content, as shown by ORO, HE and CD68 staining. These *in vivo* results obtained from two types of mouse models together indicated that MIF-2 exerted a detrimental property in early and advanced atherosclerosis and there were no gender differences.

3.2 Genetic knockout of *Mif-2* in atherogenic mice ameliorates hepatic steatosis and lowers plasma lipids

3.2.1 *Mif-2*-deficient atherogenic *Apoe*^{−/−} mice display a reduction in body weight and liver size

After establishing a role of MIF-2 in early and advanced plaque formation, we further explored the mechanisms behind this phenotype. We noticed that attenuated lesion formation induced by *Mif-2* deficiency was not only accompanied by diminished inflammation but also by a profound reduction in hepatic lipid accumulation and steatosis. The latter was a surprising observation, because *Mif*^{−/−}*Apoe*^{−/−} mice did not show a hepatic phenotype. In line with this observation, *Mif-2*-deficient atherogenic mice exhibited reduced circulating triglyceride as well as cholesterol levels and a drop in body and liver weight, together pointing towards a pronounced hepatic lipid metabolism phenotype of *Mif-2* knockout mice.

Of note, female *Mif-2*-deficient atherogenic mice exposed to 12-week HFD had smaller body size and less body weight compared with *Apoe*^{−/−} mice (Figures 17A and 17B). Consistently, it was noticed that *Mif-2*-deficient atherogenic mice had smaller liver size and less liver weight compared to *Apoe*^{−/−} mice in most cases (Figures 17C and 17D).
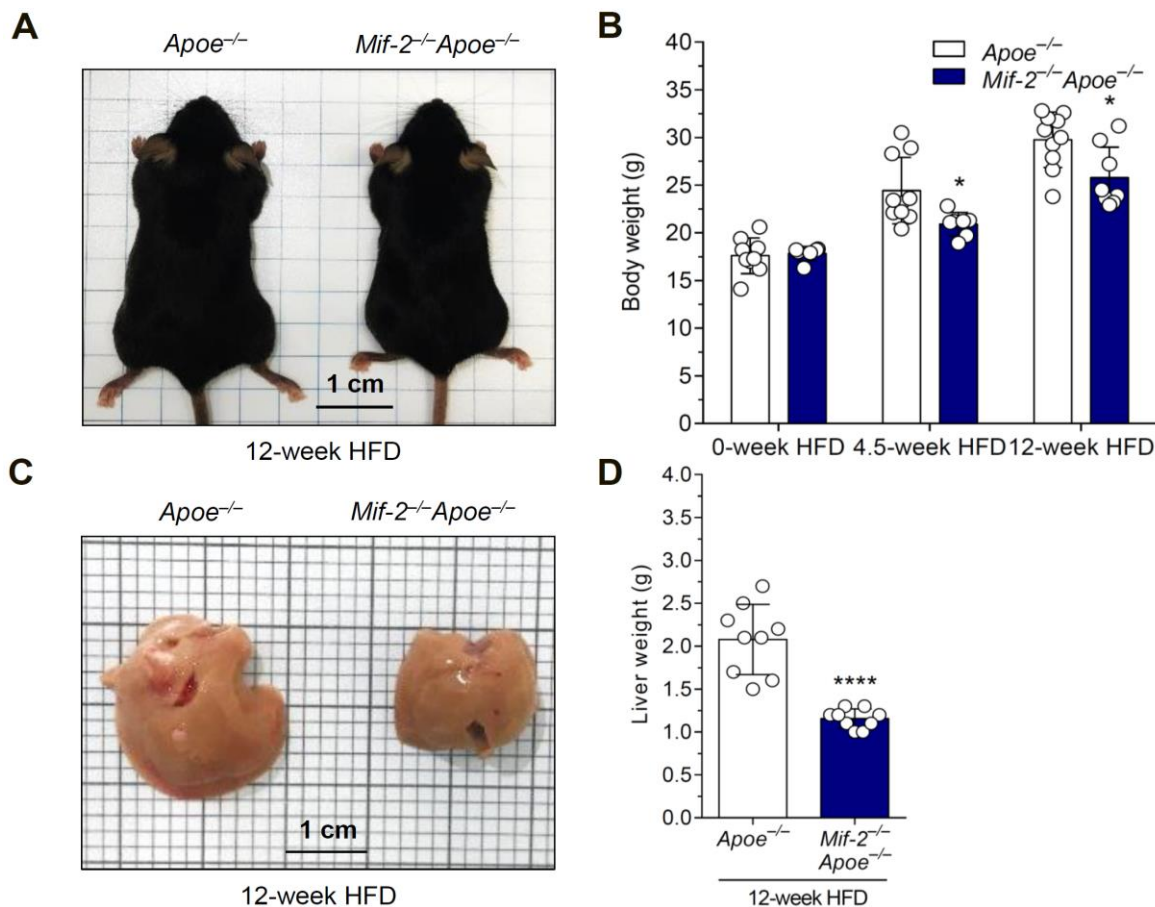
Figure 17: *Mif-2*-**deficient atherogenic** *Apoe*$^{-/-}$ **mice exhibit a drop in body weight and liver size compared with control mice.** (A, C) Gross morphology of mouse body and liver was acquired from indicated female *Apoe*-deficient mice and *Mif-2*-deficient atherogenic mice exposed to HFD for 12 weeks. (B, D) Quantification results of body and liver weight data from the same cohorts. n = 5-12 for each group; each mouse is represented as one data point. This figure is part of a preprint manuscript version published on bioRxiv (doi: https://doi.org/10.1101/2021.12.28.474328).

In addition, it was apparent that mouse livers from other mice cohorts, such as female mice under 12-week chow diet (Figure 18A) and male mice under 12-week HFD (Figure 18C), showed a similar phenotype that *Mif-2*-deficient atherogenic *Apoe*$^{-/-}$ mice had smaller livers compared with control *Apoe*$^{-/-}$ mice. Overall, livers from *Apoe*$^{-/-}$ mice were bigger than livers from *Mif-2*$^{-/-}$*Apoe*$^{-/-}$ mice under the same experimental setting (Figures 18A-18C), and this phenotype may be independent of diet.
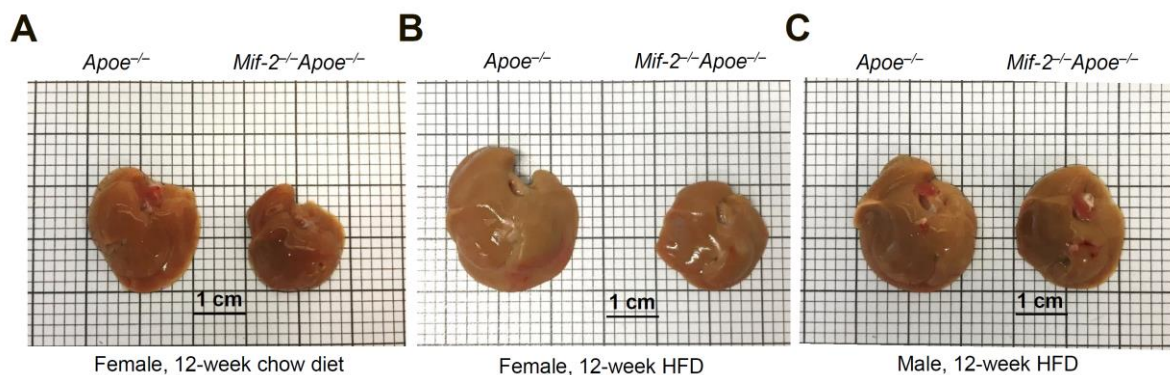
Figure 18: *Mif-2*-**deficient** *Apoe*$^{-/-}$ **mice have smaller livers compared with control mice in both genders.** (A-C) Representative liver images were acquired from randomly selected *Apoe*-deficient and *Mif-2*-deficient atherogenic mice under the same experiment setting. (A) Female mice exposed to 12-week chow diet. (B) Female mice exposed to 12-week HFD. (C) Male mice exposed to 12-week HFD. Scale bar, 1 cm. This figure is part of a preprint manuscript version published on bioRxiv (doi: https://doi.org/10.1101/2021.12.28.474328).

In fact, the proportion of liver in mice commonly falls in the 3-5% range of body weight (around 2-3 g), even if this index varies with different species and strains. We also collected liver weight data from male mice on a 12-week HFD. Livers from *Apoe*-deficient mice were bigger as well as heavier than those from *Mif-2*-deficient atherogenic mice for both females and males (Figures 17D and 19A), which was in accordance with the observed changes in body weight in both genders (Figures 17B and 19B).

We next collected systematic weight data from mice at different time points during diet. There was a continuous increase in body weight among different HFD points of 0, 4.5 and 12 weeks (Figure 19C). Additionally, a similar phenotype to female mice was also observed in male cohorts using the same feeding strategy (Figure 19B), indicating there were no gender

differences in body weight reduction upon *Mif-2* deletion. Intriguingly, there was no or less significant differences in body weight before the exposure to HFD. Gradually, body weight of *Mif-2$^{-/-}$Apoe$^{-/-}$* mice increased slower than *Apoe$^{-/-}$* mice (Figure 19C). Together, *Mif-2$^{-/-}$Apoe$^{-/-}$* mice had evident body weight loss on either chow diet or HFD, suggesting this phenotype could be independent of the HFD (Figure 19C).
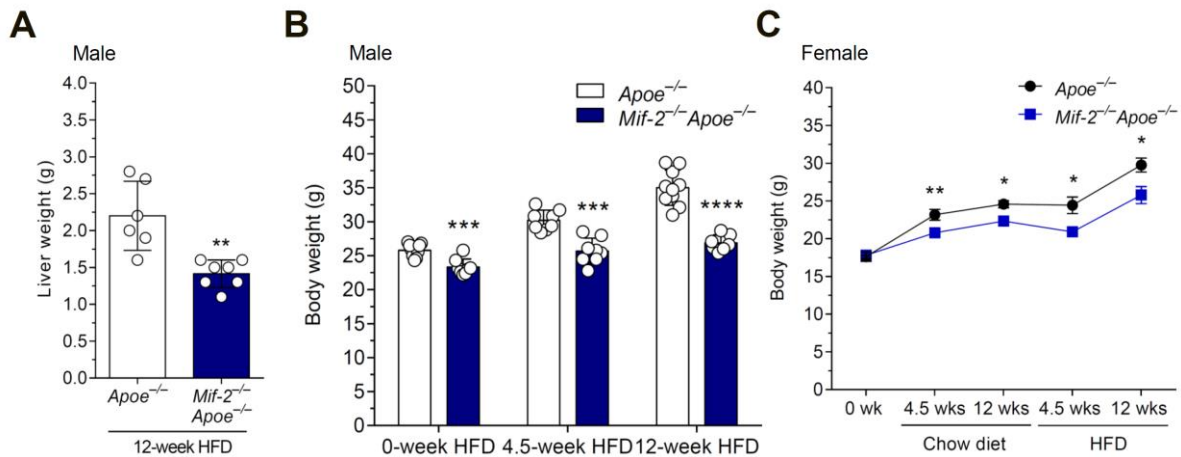

Figure 19: Male *Mif-2*-deficient atherogenic mice show a significant drop in body and liver weight compared with control mice. (A) Male *Mif-2*-deficient atherogenic mice exposed to 12-week HFD showed a significant drop in liver weight compared with control mice. (B) Male *Mif-2*-deficient atherogenic mice exposed to both 4.5-week and 12-week HFD showed a reduction in body weight compared with controls. (C) The weight progression curve displayed that body weight of female *Apoe*-deficient and *Mif-2*-deficient atherogenic mice gradually increased with a longer period of standard chow diet and HFD, but body weight of *Mif-2$^{-/-}$Apoe$^{-/-}$* mice increased slower than that of *Apoe$^{-/-}$* mice. n = 5-12 for each group; each mouse is represented as one data point. This figure is part of a preprint manuscript version published on bioRxiv (doi: https://doi.org/10.1101/2021.12.28.474328).

3.2.2 *Mif-2* deletion in atherogenic mice downregulates plasma triglycerides and cholesterol

In line with these findings of decreased necrotic core formation and weight loss in *Mif-2$^{-/-}$Apoe$^{-/-}$* mice, circulating triglyceride as well as cholesterol levels were significantly reduced by ~10%-25% in *Mif-2*-deficient atherogenic mice. This phenotype was observed in both mouse cohorts, which were exposed to either 4.5- or 12-week HFD respectively (Figures 20A and 20B), indicating a possible link between MIF-2 expression and lipid levels. These data together supported that the atheroprotective effect of *Mif-2* deficiency was associated with diminished circulating lipoproteins.
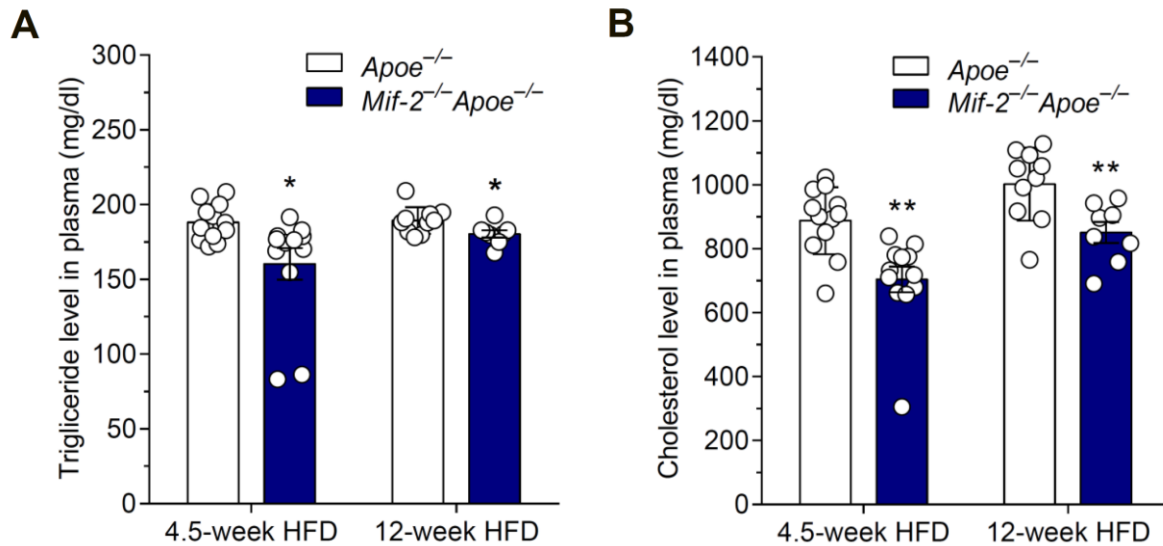
Figure 20: *Mif-2* **deletion downregulates plasma triglycerides and cholesterol in both early and advanced models of atherosclerosis in female** *Apoe⁻/⁻* **mice.** Total triglyceride and total cholesterol levels in plasma from *Apoe⁻/⁻* mice and *Mif-2*-deficient atherogenic mice under either 4.5- or 12-week HFD were measured by commercial triglyceride and cholesterol assay kit. (A, B) *Mif-2*-deficient atherogenic mice showed a significant reduction in both triglycerides and cholesterol compared to control mice. (A) Plasma triglyceride levels. (B) Plasma cholesterol levels. n = 8-12 for each group; each mouse is represented as one data point. This figure is part of a preprint manuscript version published on bioRxiv (doi: https://doi.org/10.1101/2021.12.28.474328).

Given that triglycerides and cholesterol were significantly downregulated in *Mif-2* deficient atherogenic mice in our study, we next asked how the lipoprotein profile was affected. Then the lipoprotein fractions such as high-density lipoprotein (HDL), low-density lipoprotein (LDL) and very-low-density lipoprotein (VLDL) were analyzed by HPLC chromatography. We noted striking reductions in the LDL as well as VLDL fractions in *Mif-2*-deficient atherogenic mice under either 4.5- or 12-week HFD compared with control mice, whereas HDL levels did not change (Figures 21A and 21B). In addition, there was a slight increase in VLDL and LDL levels of mice under 12-week HFD compared with mice under 4.5-week HFD, suggesting more circulating atherogenic lipoproteins along with a longer period of HFD. Of note, the lipoprotein levels measured in this experiment were apparently in accordance with the common mouse lipoprotein profile, with VLDL and LDL being the predominant lipoproteins in plasma of atherogenic mice, a profile that is different from that seen for the lipoprotein profile in humans, with LDL and HDL representing the major classes of lipoproteins.
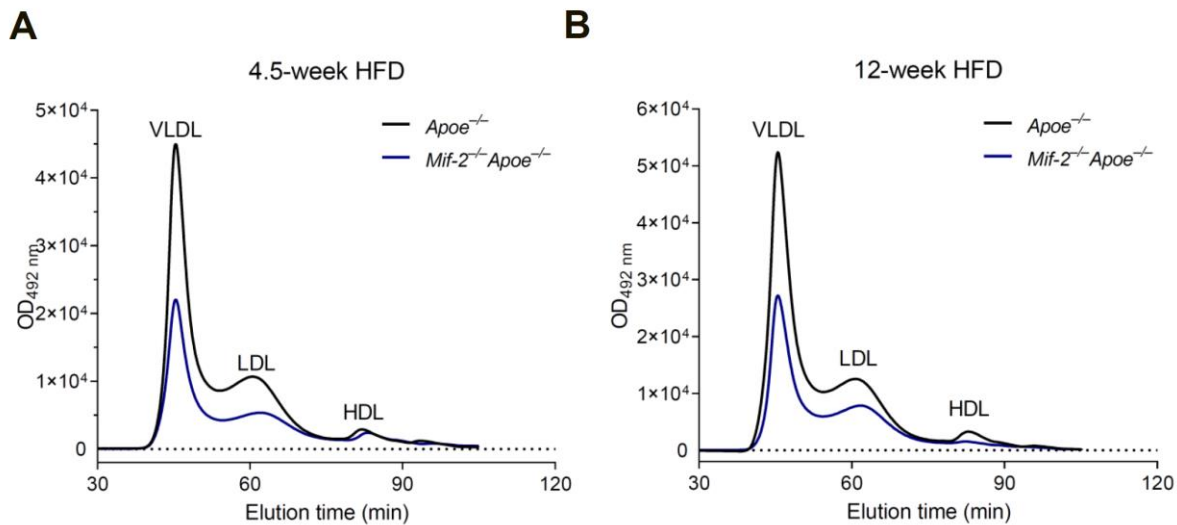
Figure 21: *Mif-2* **deletion is associated with downregulated VLDL and LDL levels in both early and advanced models of atherosclerosis in female** *Apoe*$^{-/-}$ **mice.** (A, B) Representative HPLC chromatograms of lipoprotein fractions in plasma from female *Apoe*-deficient and *Mif-2*-deficient atherogenic mice. (A) The above two group female mice under 4.5-week HFD. (B) The above two group female mice under 12-week HFD. Representative chromatograms shown are from one of three different mice in each cohort. This figure is part of a preprint manuscript version published on bioRxiv (doi: https://doi.org/10.1101/2021.12.28.474328).

Consistent with the body and liver weight data, comparisons of lipids and lipoprotein fractions in early and advanced atherogenic models indicate that the lipogenic property of MIF-2 also contributes to early atherosclerosis in addition to its involvement in advanced atherogenesis, revealing a potential regulatory function in lipid homeostasis. Of note, MIF-2 exerts an essential impact on the regulation of triglycerides as well as cholesterol, as confirmed by the above findings that *Mif-2*$^{-/-}$*Apoe*$^{-/-}$ mice had downregulated triglycerides and cholesterol as well as lipoproteins compared with control mice.

3.2.3 *Mif-2* deletion attenuates hepatosteatosis in *Apoe*-deficient atherogenic mice

Based on the differences of triglycerides and cholesterol between *Mif-2*$^{-/-}$*Apoe*$^{-/-}$ mice and *Apoe*$^{-/-}$ mice, we further focused on studying the role of MIF-2 in lipid metabolism. To this end, the liver was a prime organ to focus on. We analyzed the lipid content on liver frozen and paraffin sections, which was visualized by HE-stained (Figures 22 and 23) as well as ORO-stained images, respectively (Figure 24). Because HE staining and ORO staining are two basic methods equally applied to visualize lipids in liver tissues, both techniques were applied here in order to determine potential lipid deposit changes in mouse livers between the two groups.

Under normal physiological conditions, lipids accumulate to some extent in the wild type (WT) liver. Lipid accumulation is markedly enhanced upon HFD [264]. Accordingly, there was evident hepatosteatosis in livers from both *Mif-2*$^{-/-}$*Apoe*$^{-/-}$ mice and *Apoe*$^{-/-}$ mice in comparison with WT mice. Of note, representative HE-stained images of frozen liver sections from *Apoe*-deficient mice and *Mif-2*-deficient atherogenic mice showed that *Mif-2* deletion led to attenuated hepatic lipid accumulation (Figure 22). Also, detailed inspection of the images from hepatic tissue specimens, we could recognize some classical steatosis structures on these liver sections, such as microvesicular steatosis that is indicated in Figure 22 by dotted line arrow, and macrovesicular steatosis that is labeled by bold arrow. Besides, we could observe some clusters of immune cells in *Apoe*-deficient mice, indicated by circles (Figure 22).
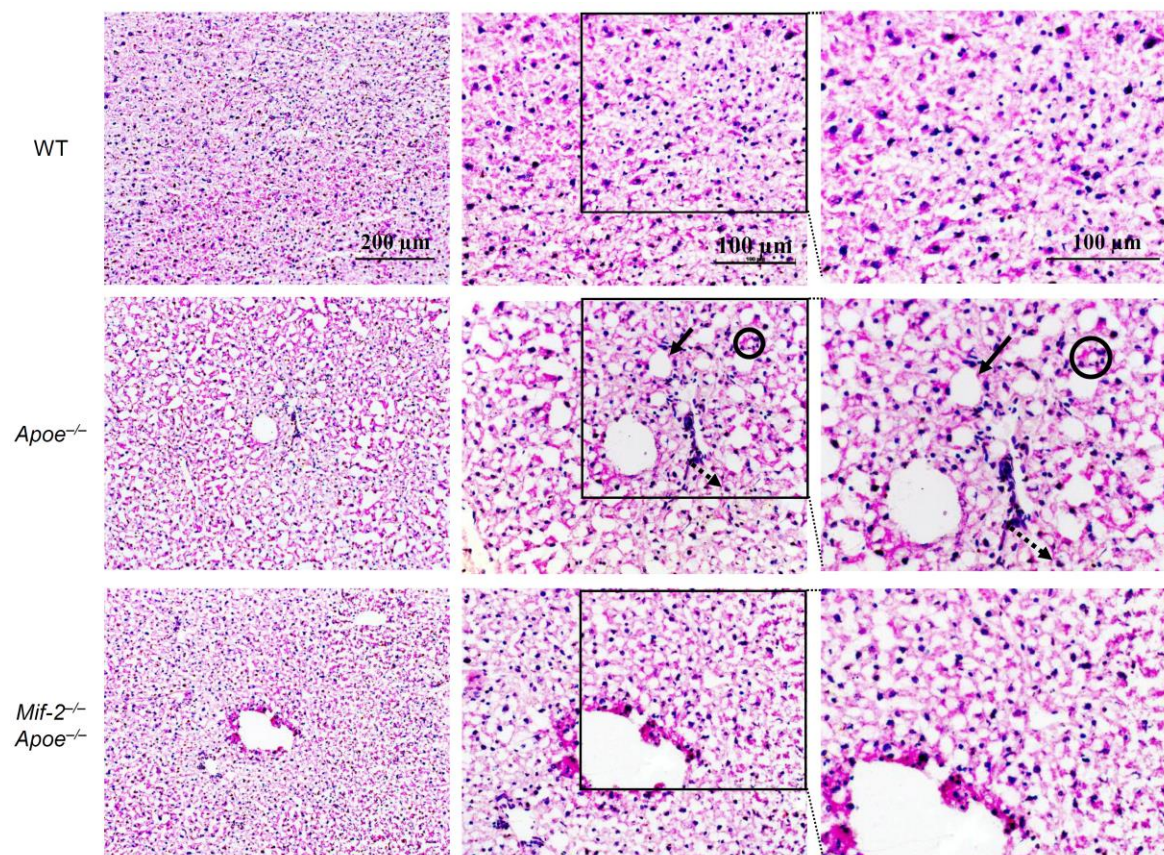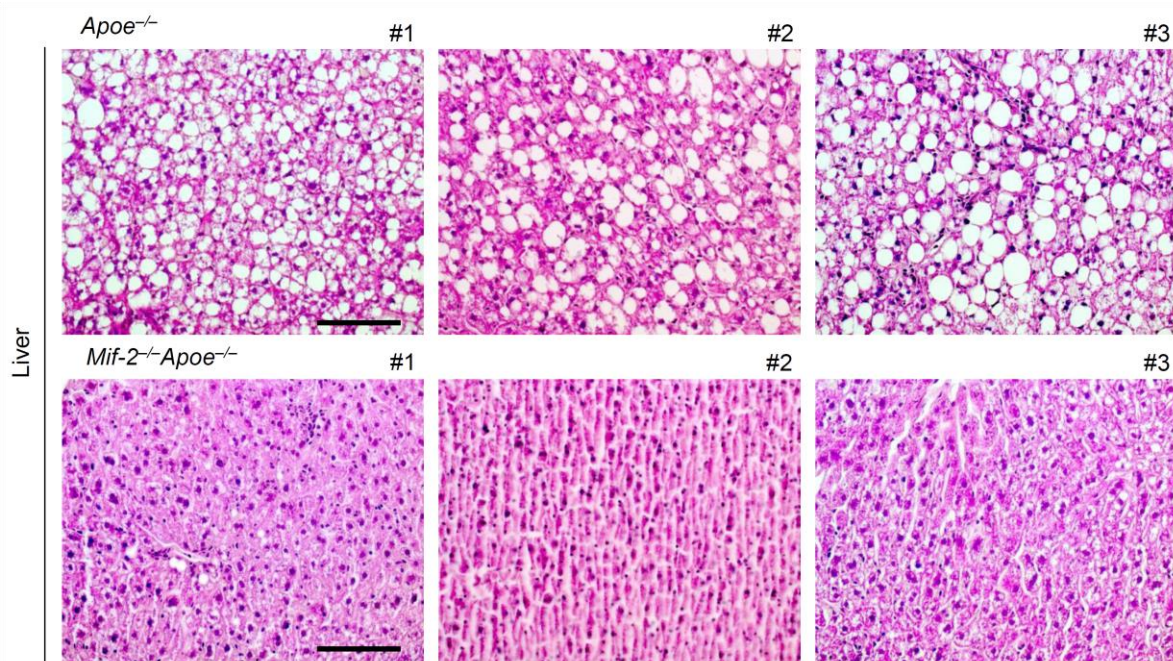

Figure 22: *Mif-2*-deficient atherogenic mice show less hepatic lipid content compared with *Apoe*-deficient mice, as investigated by HE staining on frozen sections. Livers from *Apoe*-deficient mice and *Mif-2*-deficient atherogenic mice under 12-week HFD as well as age-matched WT mice on chow diet were sectioned and stained. Representative HE-stained images of frozen liver sections from *Mif-2*-deficient atherogenic mice showed attenuated lipid accumulation in comparison with *Apoe*-deficient mice. Several typical steatosis structures could be observed, exemplified by macrovesicular steatosis (large lipid droplets are present in cells) indicated by bold arrow, microvesicular steatosis (small lipid droplets are present in cells) indicated by dotted line arrow, and clusters of immune cells indicated by

circle. This figure is part of a preprint manuscript version published on bioRxiv (doi: https://doi.org/10.1101/2021.12.28.474328).

Specifically, $Apoe^{-/-}$ mice undergoing 12-week HFD usually had uniformly fatty livers and hepatomegaly according to histological characteristics, as evidenced by HE-stained paraffin sections (Figure 23). Representative views from paraffin sections gave us additional insight into the morphology of fatty hepatocytes and the pronounced phenotype. Importantly, *Mif-2* deficiency surprisingly counteracted these pathological changes in the same liver area from different mice, suggesting a causal role of MIF-2 in regulating hepatic lipogenesis and implicating MIF-2 as a novel linker between atherogenesis and hepatosteatosis.

Figure 23: ***Mif*-2-deficient atherogenic mice show less hepatic lipid content compared with *Apoe*-deficient mice, as investigated by HE staining on paraffin sections.** The same parts of livers from female *Apoe*-deficient mice and *Mif-2*-deficient atherogenic mice under 12-week HFD above were sectioned and stained. Representative HE-stained images from *Mif-2*-deficient atherogenic mice displayed attenuated hepatic lipid content in comparison with *Apoe*-deficient mice. Representative images shown are from three different mice randomly selected from each cohort. Scale bar, 200 μm. This figure is part of a preprint manuscript version published on bioRxiv (doi: https://doi.org/10.1101/ 2021.12.28.474328).

These lipogenesis differences between *Mif-2*-deficient atherogenic mice and control *Apoe*-deficient mice were quite clear even by eye, as demonstrated in Figures 22 and 23. Because the lipid distribution in the liver section was relatively even, this phenotype was very robust. In the next step, ORO staining, the other method to display lipid accumulation, was performed using serial frozen liver sections to verify this phenotype further (Figure 24).
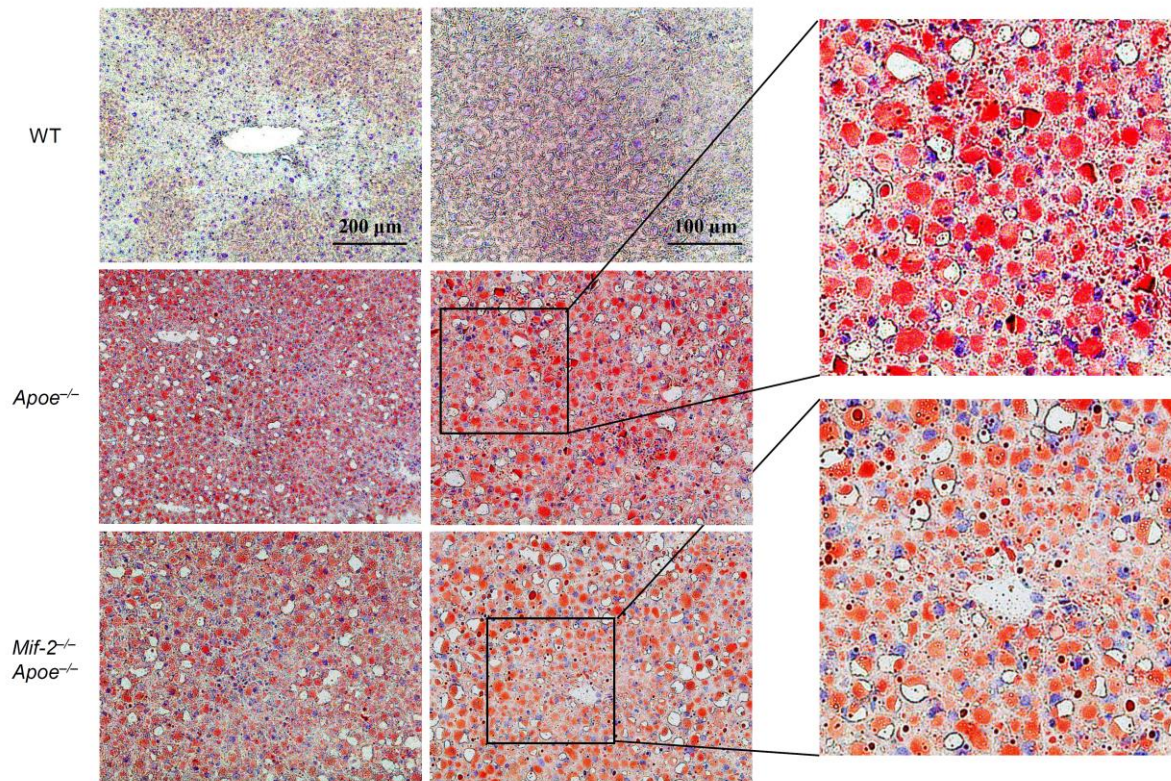
Figure 24: *Mif-2*-**deficient atherogenic mice show less hepatic lipid content compared with** *Apoe*-**deficient mice, as investigated by ORO staining on frozen sections.** Livers from *Apoe*-deficient mice and *Mif-2*-deficient atherogenic mice under 12-week HFD were sectioned and ORO-stained. *Mif-2*-deficient atherogenic mice displayed attenuated lipid content in comparison with *Apoe*-deficient mice. Enlarged images showed more lipids in *Apoe*$^{-/-}$ mice. This figure is part of a preprint manuscript version published on bioRxiv (doi: https://doi.org/10.1101/2021.12.28.474328).

3.3 MIF-2 stimulates lipogenesis through activating SREBPs and its lipogenic targets via regulating AMPK as well as AKT phosphorylation in human hepatocytes *in vitro*

After the association between hepatosteatosis and atherogenesis in *Mif-2*-deficient atherogenic mice and control *Apoe*-deficient mice was confirmed, lipid metabolism related research definitely is the following direction of this project. Mechanistically, the dominant act of liver in lipid and/or glucose metabolism determines the tight connections between non-alcoholic fatty liver and atherosclerotic progression to some extent [210]. Then whether lipid metabolism related genes were involved in this regulatory process was further asked. To test the hypothesis that MIF-2-mediated lipogenic effects on *Apoe*$^{-/-}$ mice might be due to the control of downstream lipogenic genes in mouse livers, we utilized the hepatocyte cell line Huh-7, which is derived from a human hepatic carcinoma, to screen for differentially expressed genes by real-time qPCR after 24 h MIF-2 stimulation. Based on numerous

background information and relevant knowledge from literatures, the following lipogenic genes were initially included in this study: *Srebp-1*, *Fasn*, *Psck9*, *Glut1*, *Glut4*, *Hmgcr*, *Srebp-2*, *Ldlr* and *Cd36*. Additionally, potential receptors of MIF-2, for example *Cxcr4* and *Cd74* were included.

3.3.1 Stimulation of Huh-7 hepatocytes with MIF-2 upregulates the expression of SREBPs and their downstream targets on both mRNA and protein level

To test the hypothesis, the Huh-7 human hepatocytes were primarily applied to figure out the specific molecular mechanism how MIF-2 regulates lipogenesis through the SREBP pathway. Recombinant MIF-2 was used to stimulate Huh-7 cells and RT-qPCR was performed to check and further select some relative genes involved in the lipogenesis process. Interestingly, the mRNA levels of hepatic *Srebp-1* and *Srebp-2* as well as their corresponding key targets *Fasn* and *Ldlr* were significantly upregulated after incubation with MIF-2 for 24 h, as showed by the quantitative results in Figure 25, with three to six repeats of independent experiments.
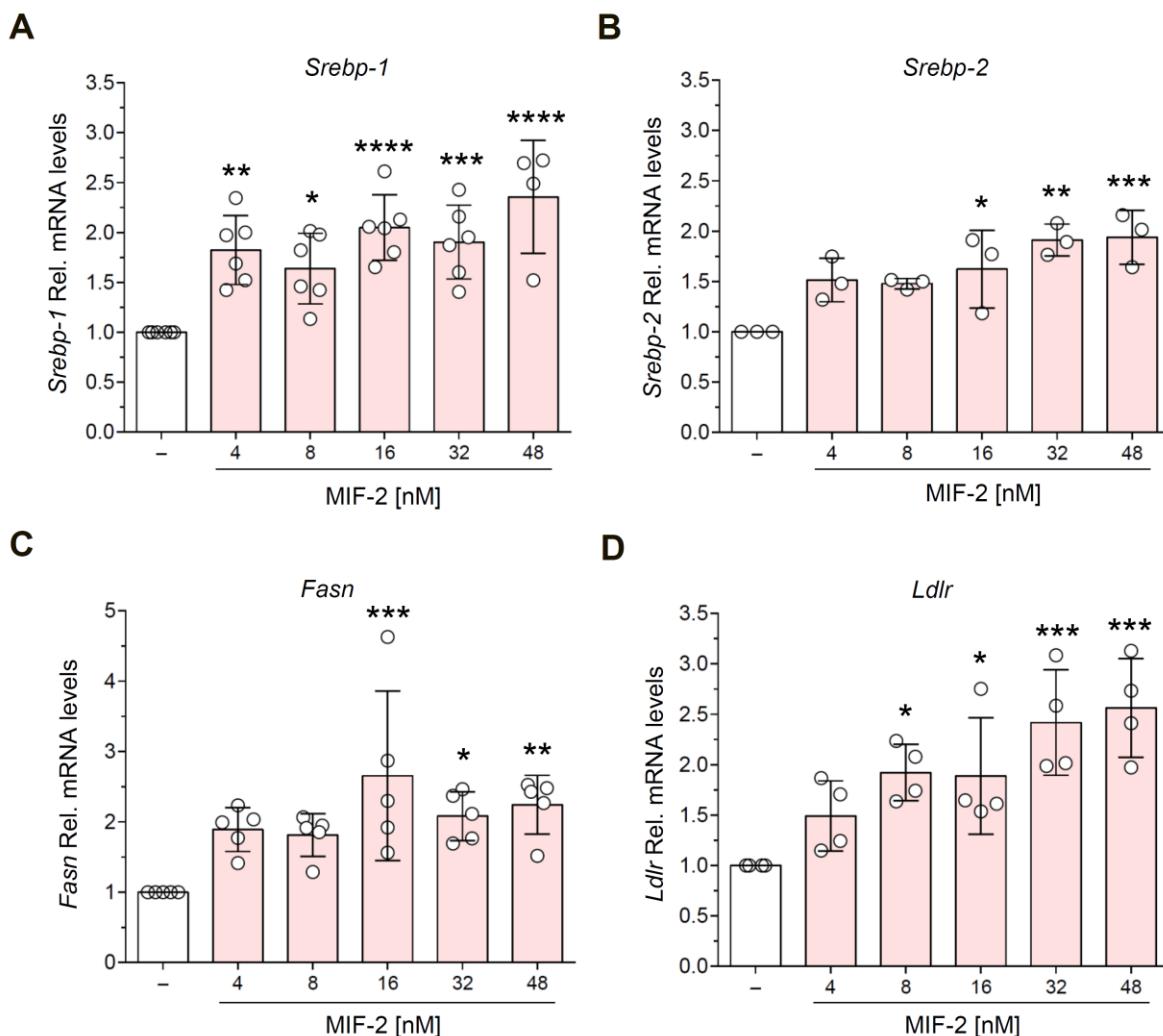
Figure 25: *Srebps* and their target genes are upregulated in Huh-7 cells after MIF-2 stimulation. After starvation, recombinant MIF-2 was used to stimulate Huh-7 cells for 24 h. Subsequently, mRNA was isolated, synthesized into cDNA and RT-qPCR was performed. (A, C) *Srebp-1* and its main target *Fasn* were significantly increased with stimulation of MIF-2. (B, D) *Srebp-*and its main target *Ldlr* levels were upregulated after incubation with MIF-2. n = 3-6 biological replicates. This figure is part of a preprint manuscript version published on bioRxiv (doi: https://doi.org/10.1101/2021.12.28. 474328).

Furthermore, it was checked whether MIF-2 affected SREBP-1 as well as SREBP-2 proteolytic cleavage, as reflected by expression levels of the precursor form of SREBP (the ~125 kDa pSREBP) and active nuclear form (the ~65 kDa nSREBP) via Western blot. We measured cleaved SREBP-1 proteins at two time points: 6 h and 24 h. With regard to pSREBP-1 expression, there were clear and equal protein bands. Additionally, it was noticed that there was an obvious upregulation of nuclear SREBP-1 after 24 h stimulation with MIF-2, whereas there was little nSREBP-1 detected after 6 h incubation (Figure 26). It implied that the expression of nSREBP-1 promoted by recombinant MIF-2 could be visualized after 24 h stimulation but not 6 h. Therefore, 24 h incubation was chosen to be the stimulation time point in the following experiments.
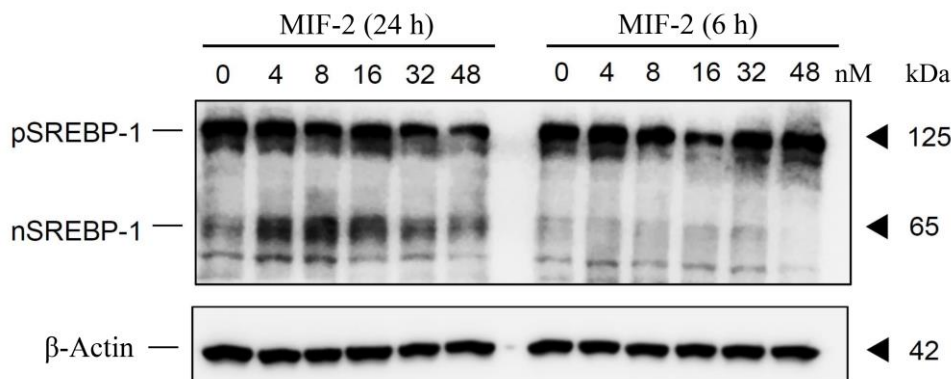
Figure 26: Activated nSREBP-1 is dose-dependently upregulated in Huh-7 hepatocytes after 24 h incubation with recombinant MIF-2. After starvation with medium containing reduced FCS overnight, recombinant MIF-2 protein was used to stimulate Huh-7 hepatocytes for 24 h or 6 h, respectively. Different samples were collected and protein expression was detected by WB. SREBP-1 precursor was obviously cleaved to produce nSREBP-1 after 24 h MIF-2 stimulation. nSREBP, nuclear SREBP representing the activated processed form of SREBP. Representative images shown are from one of three independent experiments.

Here, nSREBP-1 and FASN protein levels displayed a ~2-fold increase when MIF-2 was applied at 8~16 nM (Figures 27A-27C), which was quite consistent with their changes on the mRNA level (Figures 25A and 25C). In combination with RT-qPCR data (Figures 25A and 25C), these results revealed the involvement of MIF-2 in triglyceride synthesis.
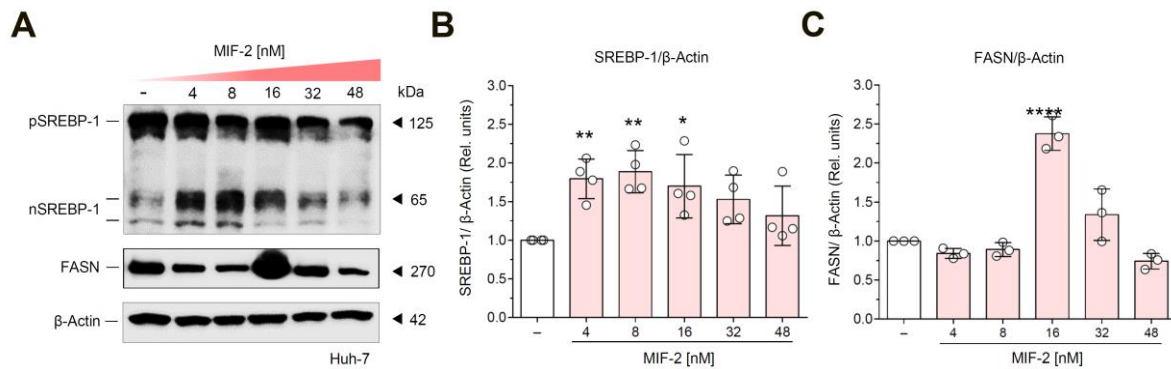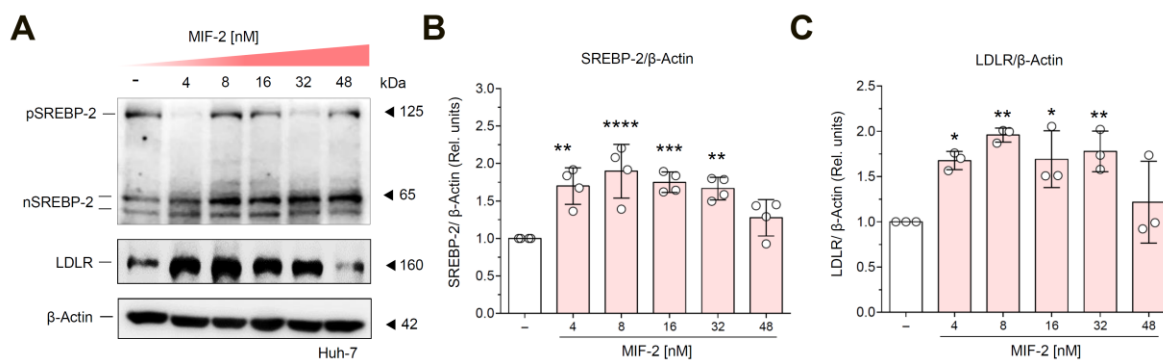
80

Figure 27: Recombinant MIF-2 promotes the expression of nSREBP-1 and its main lipogenic target FASN. (A) The expression of pSREBP-1, nSREBP-1, FASN and β-Actin was visualized by representative blots. (B, C) Quantitative results showed nSREBP-1 and FASN were upregulated after MIF-2 stimulation for 24 h, and their levels came to a peak when MIF-2 was applied at 8~16 nM. n = 3-4 biological replicates. This figure is part of a preprint manuscript version published on bioRxiv (doi: https://doi.org/10.1101/2021.12.28.474328).

In line with these changes of nSREBP-1 and FASN in Huh-7 cells stimulated with MIF-2, it was observed that there was also a significant increase of nSREBP-2 and LDLR, as detected in the same samples (Figures 28A-28C). Similarly, nSREBP-2 and LDLR protein levels showed a ~2-fold increase when MIF-2 was applied at ~8 nM. In combination with RT-qPCR data (Figures 25B and 25D), these results indicated the involvement of MIF-2 in cholesterol synthesis, in addition to its impact on hepatic triglyceride synthesis.

Figure 28: Recombinant MIF-2 enhances the expression of SREBP-2 and its main lipogenic target LDLR. (A) The expression of pSREBP-2, nSREBP-2, LDLR and β-Actin was visualized by representative blots. (B, C) Quantitative results showed that nSREBP-2 and LDLR displayed a dose upregulation after MIF-2 stimulation, and the expression of SREBP-2 and LDLR came to a peak when MIF-2 was ~8 nM. n = 3-4 biological replicates. This figure is part of a preprint manuscript version published on bioRxiv (doi: https://doi.org/10.1101/2021.12.28.474328).

As mentioned before, we primarily focused on genes related to lipid metabolism, with evident upregulations observed for *Srebp-1*, *Srebp-2*, *Fasn* and *Ldlr* upon MIF-2 stimulation (Figure 25). Additional genes of potential relevance such as *Glut1*, *Glut4* and *Cd36* did not change (Figures 29A-29C) upon MIF-2 stimulation, at least as analyzed by mRNA analysis. Similarly,

the gene expression of potential receptors of MIF-2, i.e. *Cxcr4* and *Cd74* were not altered in hepatocytes with different treatments of MIF-2 (Figures 29D and 29E), indicating the possibility of receptor involvement.
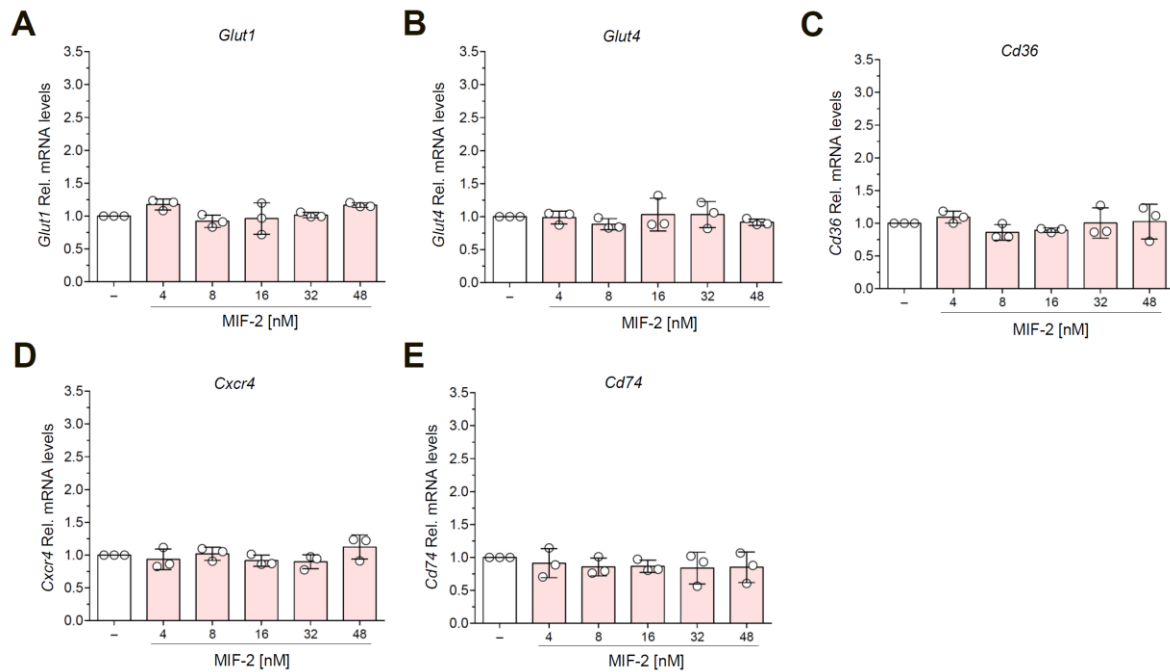

Figure 29: The expression of other relevant genes is not altered by recombinant MIF-2 in Huh-7 hepatocytes. (A-C) MIF-2 did not induce any changes in several lipid related genes on gene level, for example *Glut1* and *Glut4* as well as *Cd36*. (D, E) MIF-2 did not alter the mRNA levels of potential receptors of MIF-2, *Cxcr4* and *Cd74*. n = 3 biological replicates each. This figure is part of a preprint manuscript version published on bioRxiv (doi: https://doi.org/10.1101/2021.12.28.474328).

3.3.2 Stimulation with MIF-2 enhances the nuclear translocation of SREBP-2 in Huh-7 hepatocytes

Since subcellular localization of SREBPs determines their functional activities, the effects of MIF-2 on translocation behavior of SREBP-2 in hepatocytes were further evaluated via immunofluorescence microscopy. According to the above results from RT-qPCR and WB, two different concentrations of recombinant MIF-2 were applied for this experiment, i.e. 8 nM and 16 nM. Huh-7 human hepatocytes were similarly cultured with recombinant MIF-2 or vehicle for 24 h, and SREBP-2 expression was visualized by fluorescent staining. Visible fluorescent signals for SREBP-2 were mostly located in both the ER/Golgi and the nucleus of untreated cells. In line with elevated nSREBP-2 mRNA and protein levels, hepatocytes stimulated with MIF-2 demonstrated more positive SREBP-2 signals in nuclei than cytoplasm compared to untreated cells (Figure 30), indicating that MIF-2 promotes SREBP-2's nuclear translocation.
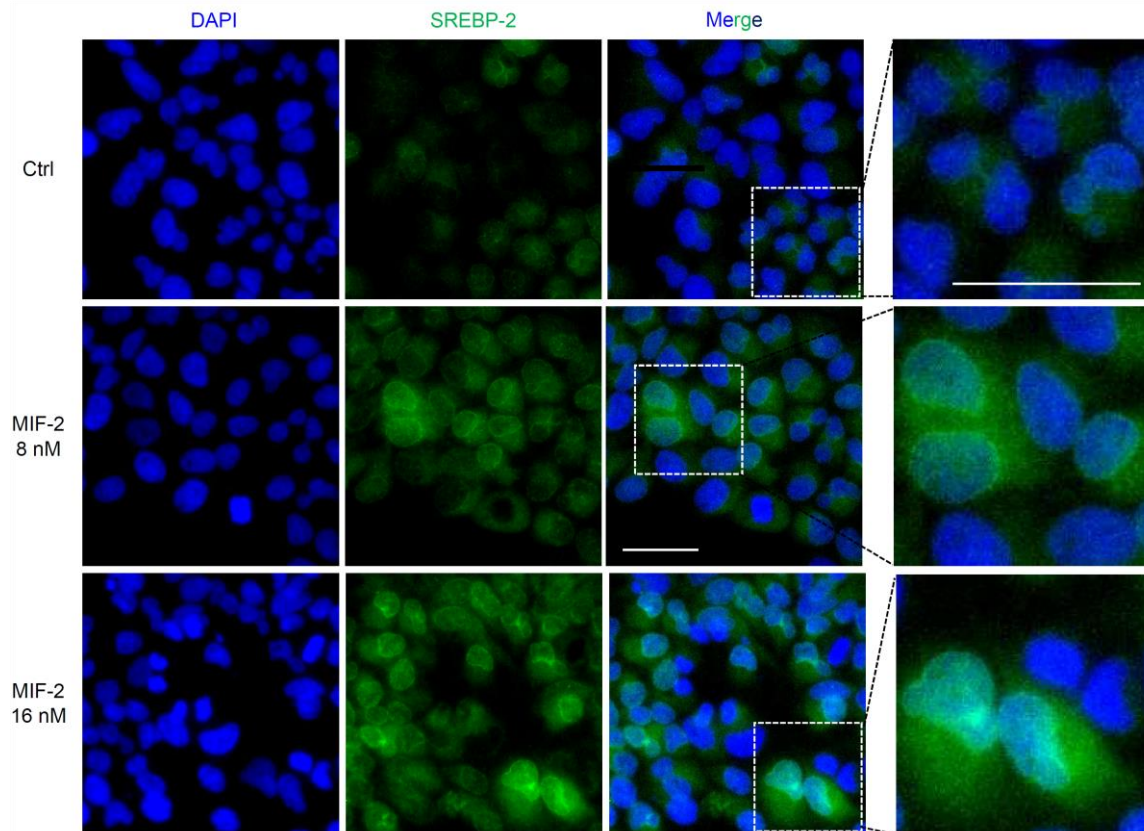
Figure 30: Recombinant MIF-2 promotes the nuclear translocation of SREBP-2 in Huh-7 cells. Compared to control, hepatocytes stimulated with 8 nM and 16 nM of MIF-2 displayed strong nuclear SREBP-2 signals (SREBP-2: green; DAPI: blue). Enlarged images showed cleaved SREBP-2 in the nucleus. Scale bar, 40 µm. This figure is part of a preprint manuscript version published on bioRxiv (doi: https://doi.org/10.1101/2021.12.28.474328).

It is well known that the translocation from ER/Golgi to nucleus is an important and necessary step for SREBP-2 to exert transcriptional functions, as shown in previous studies [214]. Therefore, this data gives a plausible explanation of how MIF-2 regulates SREBPs' activities in the context of lipid metabolism. Alongside this notion, LDL uptake assay using hepatocytes was applied later to check for an effect of MIF-2 on the functionality of LDLR (see chapter 3.4.2), which functions as a key downstream target of SREBP-2. To conclude, recombinant MIF-2 promoted SREBP-2 nuclear translocation in Huh-7 cells *in vitro* and induced transcriptional regulation mediated by SREBP-2.

3.3.3 *Mif-2*-deficient mice shows a downregulation of activated SREBPs in hepatic tissue

As shown in the above chapter 3.3.1, activated nSREBPs in huh-7 human hepatocytes were dramatically upregulated after MIF-2 stimulation. To confirm this finding and address the *in vivo* relevance, we focused on SREBPs and detected their expression in mouse liver from two

mouse cohorts on 12-week HFD (five mice each group). There was a significant decrease of nSREBP-1 and nSREBP-2 in *Mif-2*-deficient atherogenic mice compared to *Apoe*-deficient mice (Figure 31), indicating this phenotype is likely to hold true *in vivo*. This finding further confirmed the hypothesis in this study that *Mif-2* deficiency might suppress SREBP cleavage and nuclear translocation, and then repress triglyceride and cholesterol synthesis in the liver.
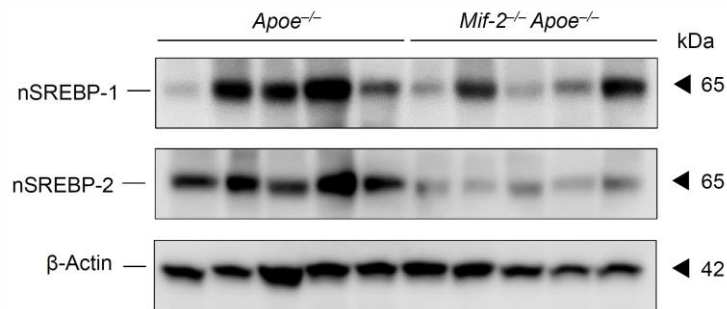

Figure 31: Activated nSREBP-1 and nSREBP-2 are decreased in *Mif-2*-deficient atherogenic *Apoe*$^{-/-}$ mice. Hepatic nSREBP-1 and nSREBP-2 were downregulated in *Mif-2*-deficient atherogenic mice in comparison with *Apoe*-deficient mice. n = 5 for each group. This figure is part of a preprint manuscript version published on bioRxiv (doi: https://doi.org/10.1101/2021.12.28.474328).

3.3.4 Stimulation of Huh-7 hepatocytes with MIF-2 reduces AMPK and enhances PI3K/AKT and MAPK/ERK signaling

As a cellular energy sensor as well as a master switch, AMPK exerts an essential impact on the control of lipid metabolism, which better explains some complex regulatory processes. It is worth noting that the suppression of hepatic SREBP functions in regulating hepatosteatosis and atherogenesis was found to be dependent on the AMPK signaling pathway [214]. Whether MIF-2 affects the AMPK pathway was examined in this thesis. As shown in Figures 32A and 32B, MIF-2 dose-dependently inhibited AMPK phosphorylation with a ~20% reduction in the pAMPK/AMPK ratio observed, when MIF-2 was applied at ~16 nM.
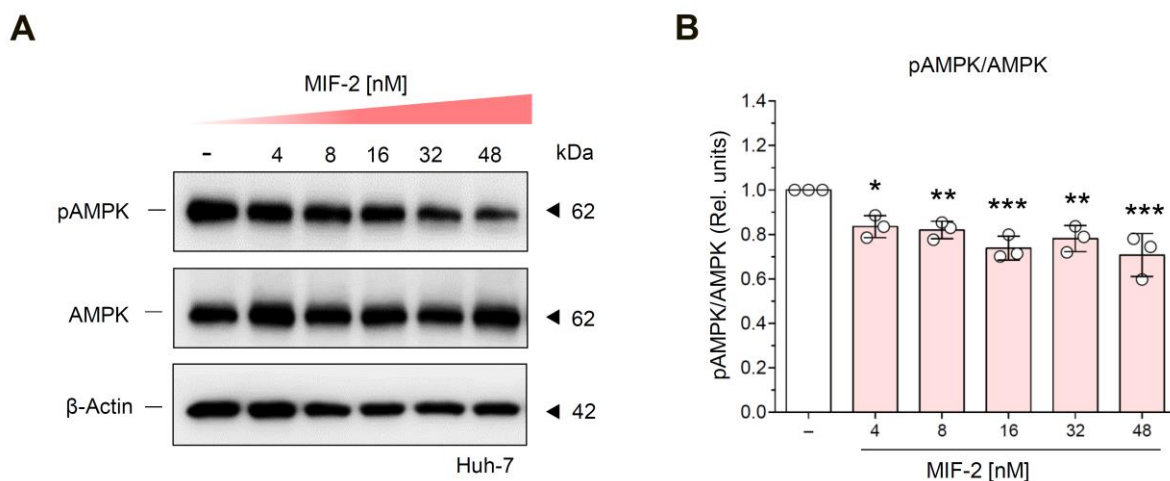
Figure 32: Recombinant MIF-2 inhibits AMPK phosphorylation in Huh-7 cells. MIF-2 repressed AMPK phosphorylation in a dose dependent manner, and phosphorylated AMPK decreased to the lowest level when MIF-2 was ~16 nM. Quantification results were presented as the ratio of phopho-AMPK to total AMPK. n = 3 biological replicates each. This figure is part of a preprint manuscript version published on bioRxiv (doi: https://doi.org/10.1101/2021.12.28.474328).

Besides, the AKT-SREBP nexus has been identified as another predominant cell signaling to be involved in lipid metabolism through activating SREBPs [225]. Notably, pAKT levels were upregulated by stimulation with MIF-2, and came to a peak of ~75% increase when MIF-2 was applied at ~16 nM (Figures 33A, 33B). Additionally, the MAPK/ERK pathway was checked. The results showed that recombinant MIF-2 also promoted the phosphorylation of ERK in Huh-7 hepatocytes (Figures 33C, 33D). Even though an upregulation of the MAPK/ERK pathway was detected here, AMPK and AKT are likely the major signaling pathways involved in MIF-2-SREBP-mediated processes based on current literatures.
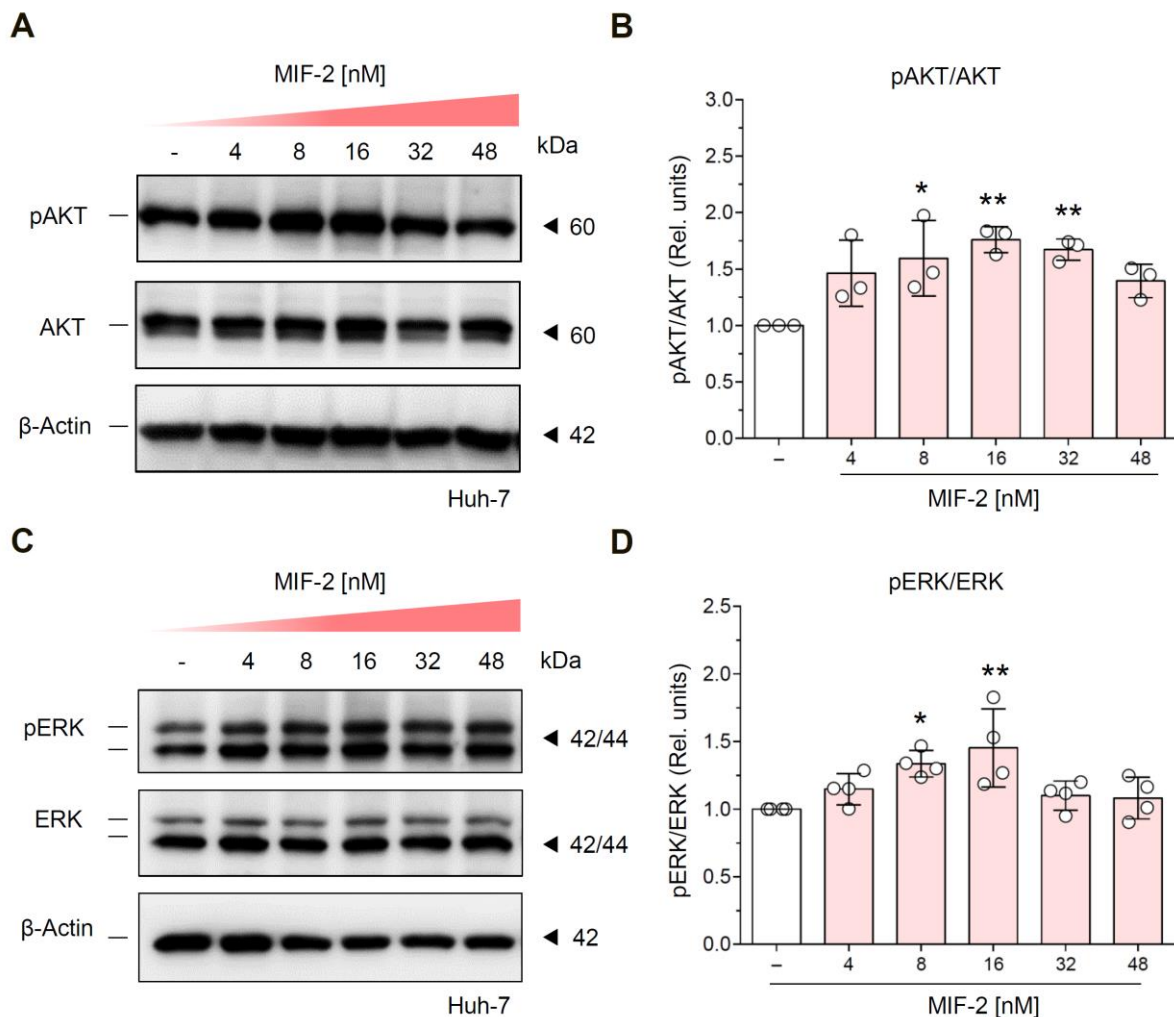

Figure 33: Recombinant MIF-2 promotes AKT and ERK phosphorylation in Huh-7 cells. (A-D) Recombinant MIF-2 upregulated AKT and ERK phosphorylation in a dose-dependent manner, and phosphorylated AKT and ERK increased to the highest levels when MIF-2 was ~16 nM. (A, B) Detection and quantification of phosphorylated AKT after MIF-2 stimulation. (C, D) Detection and

quantification of phosphorylated ERK after MIF-2 stimulation. Quantification results are presented as the ratio of phopho-AKT to total AKT and phopho-ERK to total ERK, respectively. n = 3-4 biological replicates.

Taken together, these results reveal an engagement of MIF-2 in critical cellular signaling pathways in human hepatocytes that control cell metabolism. This finding together with the previous *in vitro* data on SREBPs in hepatocytes suggest that MIF-2 may enhance SREBP proteolytic cleavage and nuclear translocation in an AMPK- and/or AKT-dependent manner.

3.4 CXCR4 and CD74 mediate MIF-2-elicited proteolytic processing of SREBPs and evidence for a role of receptor complex formation

3.4.1 CXCR4 and CD74 colocalize in Huh-7 hepatocytes and participate in MIF-2-elicited activation of SREBPs and their lipogenic target genes

After validating the effects of MIF-2 on SREBPs by Huh-7 human hepatocytes as well as atherogenic mice, we next wished to further explore the underlying mechanisms and a potential participation of its receptors CXCR4 and CD74. To investigate the involvement of CXCR4/CD74 in MIF-2-mediated processes, it was first necessary to confirm the expression of CXCR4 and CD74 in human hepatocytes. The expression was analyzed by immuno-fluorescence staining and confocal laser-scanning microscopy (CLSM) in Huh-7 hepatocyte cultures and specific mouse anti-CD74 and rabbit anti-CXCR4 antibodies. Confocal images showed that both CXCR4 and CD74 are expressed and that they are substantially colocalized in Huh-7 cells (Figure 34).
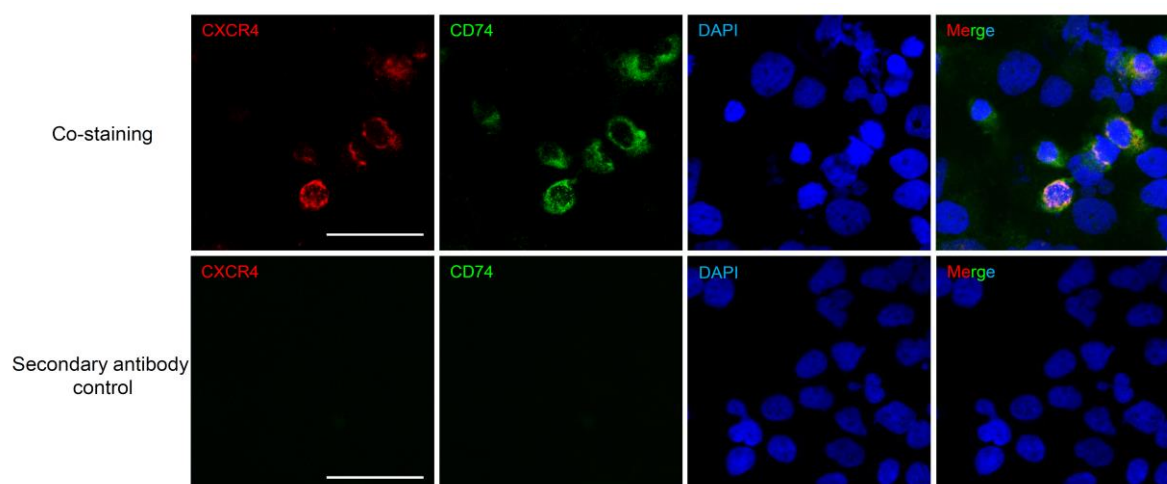

Figure 34: CXCR4 and CD74 receptors display colocalization in Huh-7 hepatocytes. Rabbit anti-CXCR4 and/or mouse anti-CD74 were utilized to stain unstimulated Huh-7 hepatocytes, and the colocalization was displayed by confocal microscopy. Upper panel: stained hepatocytes; lower panel:

secondary antibody control. Scale bar, 50 µm. Representative pictures shown are from one of three independent experiments. This figure is part of a preprint manuscript version published on bioRxiv (doi: https://doi.org/10.1101/2021.12.28.474328).

In addition to immunofluorescence staining, flow cytometry, another common method, was applied to analyze the expression of CXCR4 as well as CD74 on hepatocyte surface. Analysis showed that CXCR4 and CD74 were detected on cell surface of Huh-7 human hepatocytes. Of note, CXCR4 showed a more pronounced expression pattern than CD74 (Figure 35).
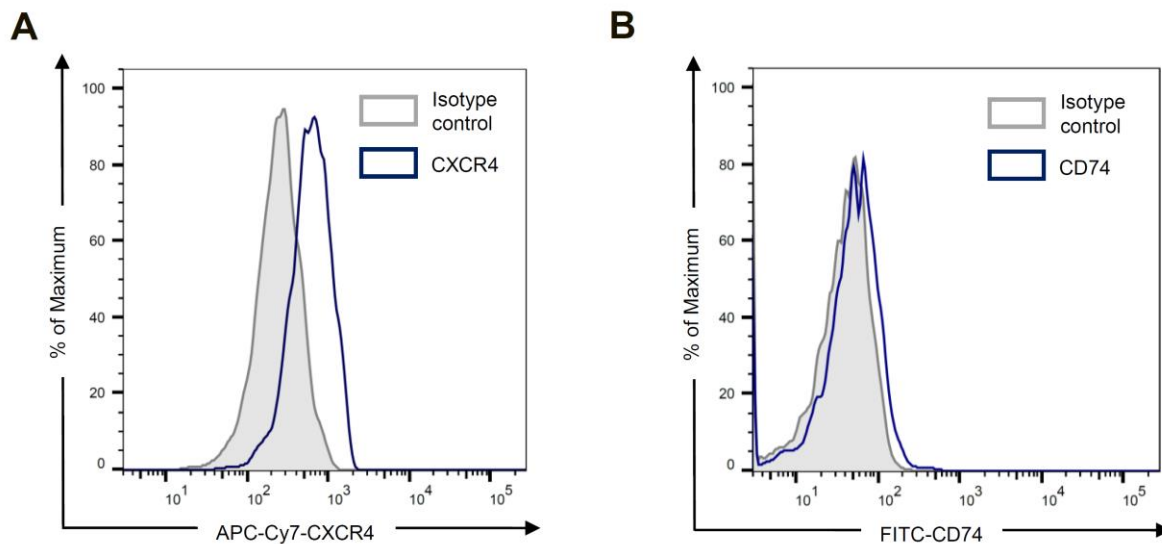
Figure 35: CXCR4 and CD74 are expressed on cell surface of Huh-7 hepatocytes. Rabbit anti-CXCR4 as well as mouse anti-CD74 were utilized to stain unstimulated Huh-7 human hepatocytes, and their expression was displayed by flow cytometry. Histograms depict relative receptor expression of specifically labeled cells (dark blue) and isotype control cells (light grey). Representative histograms shown are from one of three independent experiments. This figure is part of a preprint manuscript version published on bioRxiv (doi: https://doi.org/10.1101/2021.12.28.474328).

Based on strong expression and colocalization of CXCR4 and CD74 in hepatocytes, functional experiments were performed next in order to figure out the potential interaction of MIF-2 and its receptors and their roles in MIF-2-triggered SREBP activation. To test this hypothesis, we utilized an anti-CD74 antibody LN-2 as well as a small molecule CXCR4 inhibitor AMD3100 to block effects through the MIF-2/CD74 or MIF-2/CXCR4 axis in the SREBP activation pathway. As shown in Figures 36A and 36B, the combinative use of LN-2 and AMD3100 fully abrogated the proteolytic cleavage of SREBPs as well as the expression levels of their main downstream targets FASN and LDLR induced by MIF-2. The neutralization of CD74 alone seemed to exert a more pronounced inhibitory effects than the blockade of the CXCR4 axis alone, highlighting the significance of CD74 in MIF-2-mediated SREBP proteolytic processing. Together with the findings from Figures 27 and 28, these results suggested that MIF-2 promoted the generation of nSREBP-1, nSREBP-2, FASN, and

LDLR through both CXCR4 and CD74. Importantly, in conjunction with data performed by others in our laboratory (data not shown), these results also identified CXCR4 as a novel receptor of MIF-2, in addition to CD74.
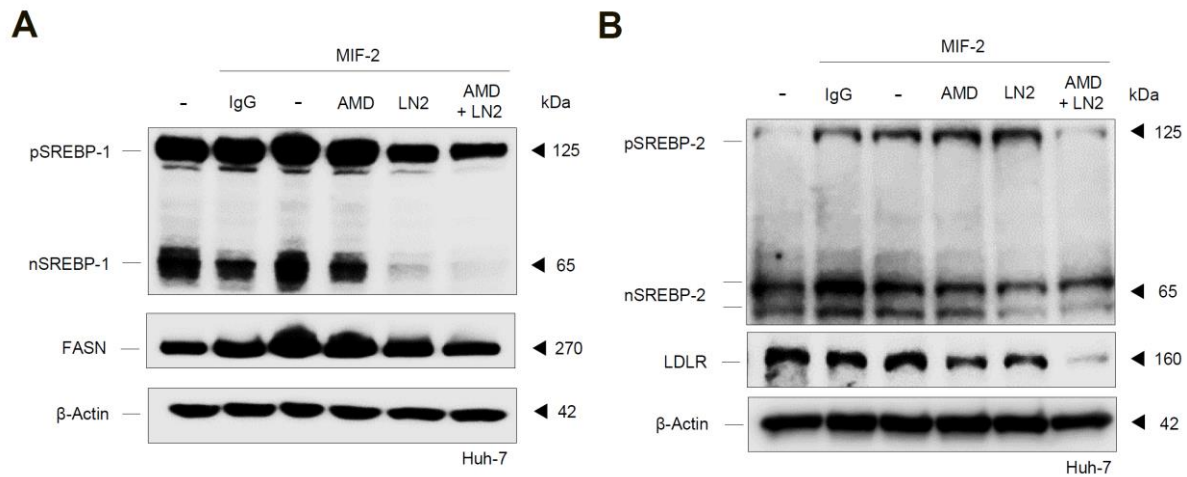

Figure 36: LN-2 antibody and/or AMD3100 inhibitor suppresses SREBP upregulation induced by MIF-2. Hepatocytes stimulated with MIF-2 showed increased expression of nSREBP-1, FASN, nSREBP-2 and LDLR. In addition, LN-2 seemed to exert stronger function than AMD3100. Blocking with both AMD3100 and LN-2 displayed the strongest inhibitory effect. (A) The expression of pSREBP-1 and nSREBP-1 as well as FASN was visualized by representative blots. (B) The expression of pSREBP-2 and nSREBP-2 as well as LDLR was visualized by representative blots. Representative blots shown are from one of two independent experiments. This figure is part of a preprint manuscript version published on bioRxiv (doi: https://doi.org/10.1101/2021.12.28.474328).

3.4.2 Both CD74 and CXCR4 participate in MIF-2-elicited native LDL uptake in Huh-7 hepatocytes

LDL uptake is an important function of the SREBP-2 pathway in hepatocytes associated with regulation of lipid homeostasis. To further determine the functional consequences of interactions of MIF-2 with the above mentioned CD74 and/or CXCR4 in hepatocytes, a native LDL uptake assay was designed and performed in Huh-7 human hepatocytes and lipid uptake was visualized by ORO staining. Huh-7 cells were exposed to IgG control or MIF-2 with or without inhibitors, and then incubated with LDL particles. Acquired images showed that hepatocytes following MIF-2 stimulation took in more native LDL compared with untreated cells (Figure 37). This suggested that MIF-2 increased LDLR expression in hepatocytes to lead to more LDL uptake. Of note, LN-2 and AMD3100 strongly blocked the effect induced by MIF-2, as indicated by ORO staining of hepatocytes treated with AMD3100 and LN-2, together with MIF-2, had less native LDL uptake (Figure 37) compared with the MIF-2-alone treated group. This implies that CXCR4 and CD74 may be involved in MIF-2-mediated LDL

uptake in hepatocytes. Of interest, the LDL uptake assay was previously carried out in human macrophages (Figure 13B) in this project, and CXCR4 was found to be involved in that process as well. This suggests that MIF-2 exerts similar enhanced effects on native LDL uptake of both hepatocytes and macrophages, with CXCR4 and/or CD74 being involved.
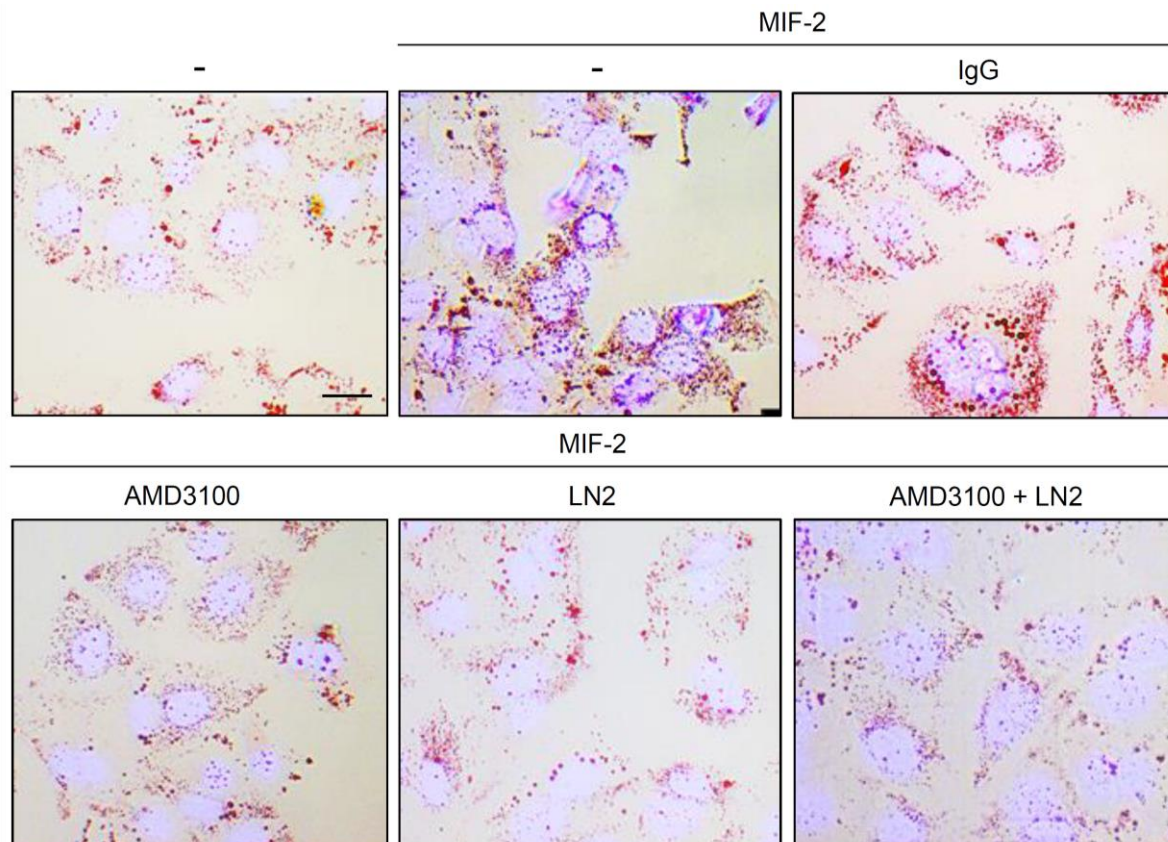

Figure 37: Recombinant MIF-2 enhances LDL uptake in Huh-7 human hepatocytes. Huh-7 human hepatocytes with stimulation of 16 nM MIF-2 showed increased native LDL uptake. 10 μg/mL AMD3100 and/or 10 μg/mL LN-2 reversed these effects induced by MIF-2. Scale bar, 25 μm. Representative images shown are from one of three independent experiments. This figure is part of a preprint manuscript version published on bioRxiv (doi: https://doi.org/10.1101/2021.12.28.474328).

To conclude, these observations declare that CXCR4 and/or CD74 are essential to the process of LDL uptake through promoting MIF-2-mediated proteolytic processing of SREBP-2 in hepatocytes.

3.4.3 FLIM-FRET microscopy suggests CXCR4/CD74 heterodimer formation and its ligand-mediated enhancement by MIF-2

We next took advantage of a well-developed method, FLIM-FRET to visualize the formation of potential receptor complexes between CXCR4 and CD74, using an *in vitro* HEK293 cell model. FLIM-FRET methodology was applied using HEK-293 cells transfected with both CFP-tagged CXCR4 as a FRET donor and YFP-CD74 as the FRET acceptor, and the

fluorescence lifetime of the donor was read-out by multiphoton laser-scanning microscopy (MPM) (Figure 38). CFP together with YFP is a well-established FRET pair in cell biological applications. Robust co-localization of CFP-CXCR4 and YFP-CD74 in fixed cells was revealed by the FLIM-FRET measurements (Figure 38A). Additionally, the excitation of CFP-CXCR4 had a close association with a high FRET efficiency (Figure 38B) and an effective FRET binding (Figure 38C), confirming robust interactions between both receptors.
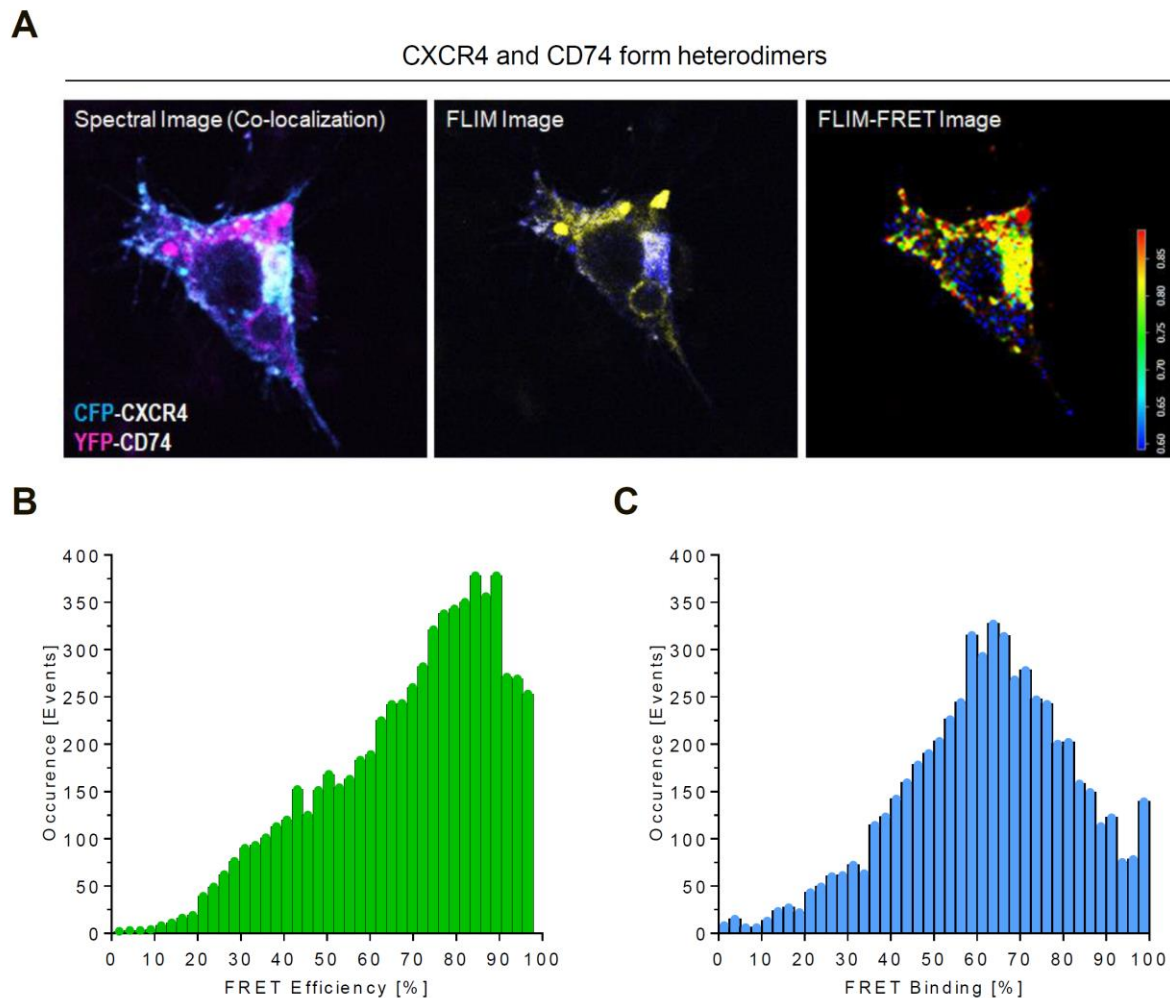
Figure 38: FLIM-FRET methodology shows the formation of a receptor complex between CXCR4 and CD74. HEK-293 cells were transfected with CFP-tagged CXCR4 as a donor and YFP-CD74 as the acceptor, and this interaction was measured by MPM. (A) Evident co-localization of CXCR4 and CD74 in fixed cells was displayed. (B, C) The excitation of CFP-CXCR4 was associated with a high FRET efficiency and an effective FRET binding. This experiment was performed together with and under the supervision of Dr. Omar El Bounkari.

After the visualization of CXCR4/CD74 receptor complex on the HEK293 cell surface, we next asked whether CXCR4/CD74 complex formation was dependent on or could be enhanced by MIF-2 stimulation. To answer this question, we compared the fluorescence lifetime of the donor CFP-CXCR4 within an interval of 1 min under MIF or MIF-2

stimulation, utilizing a time-correlated single photon counting (TCSPC) system, which technically provides a higher sensitivity and a better accuracy to multi-exponential decay analysis. Co-localization signals consistent with heterodimer formation were seen in living cells after MIF-2 stimulation (Figure 39A). Apparently, MIF and MIF-2 stimulation was associated with a reduced lifetime, arguing for an enhancement of complex formation between CXCR4 and CD74 (Figures 39B and 39C). Of interest, a more significant reduction was observed when recombinant MIF-2 was applied in comparison with that elicited by MIF, indicating that MIF-2 has a stronger ability to enhance the complex assembly between CXCR4 and CD74 than MIF.
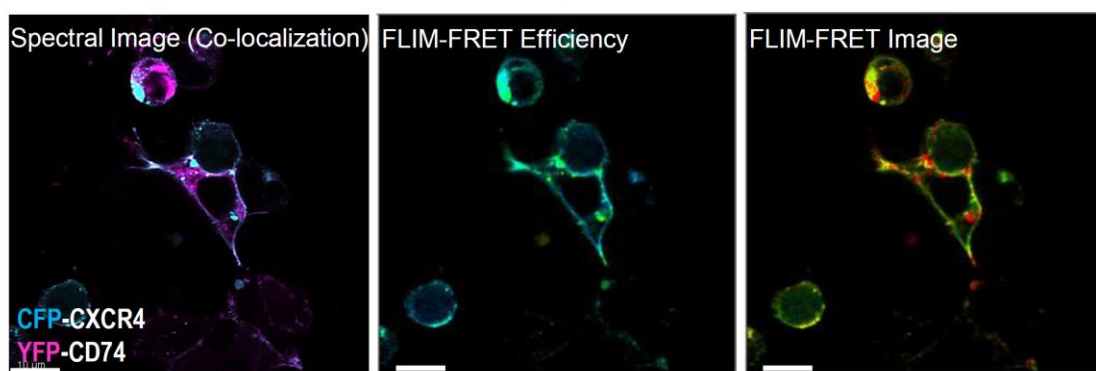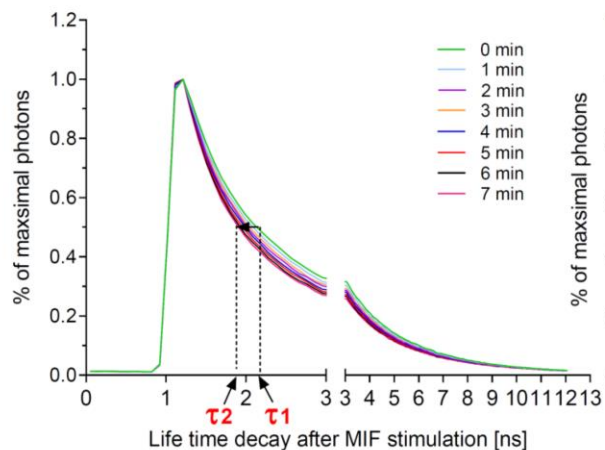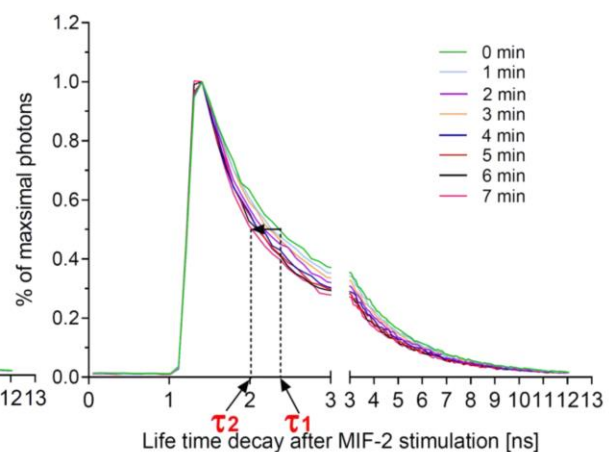

Figure 39: Multi-exponential decay analysis indicates that MIF-2 enhances complex assembly of CXCR4 and CD74 and that this stimulatory effect is stronger than that induced by MIF. (A) Co-localization signals of CXCR4/CD74 complexes were showed in living cells after MIF-2 stimulation. (B, C) Both MIF and MIF-2 were associated with a reduced lifetime arguing for an enhancement of complex formation between CXCR4 and CD74. MIF-2 had a stronger effect than MIF. This experiment was performed together with and under the supervision of Dr. Omar El Bounkari.

Collectively, these results provided evidence that a receptor complex functionally forms between CXCR4 and CD74 and that complex formation is potently elicited by MIF-2. In conjunction with our functional data as described above, it may be concluded that receptor complex formation might also occur on hepatocytes and might participate in the molecular mechanisms of MIF-2 in hepatosteatosis.

4. DISCUSSION

In this thesis, the pro-atherogenic role of the MIF-2, the homolog of MIF, is firstly identified based on experimental evidence achieved from *in vivo* atherogenic mouse model as well as *in vitro* cell line. The *in vivo* studies showed that genetic knockout as well as pharmacological inhibition of MIF-2 not only mitigates early and advanced atherosclerotic progression, but also attenuates hepatic steatosis. Furthermore, the *in vitro* studies revealed that in addition to the pro-inflammatory effect on macrophages, recombinant MIF-2 also enhances lipogenesis through activating SREBP signaling pathway in Huh-7 hepatocytes, which mechanistically explained how MIF-2 promotes atherogenesis and hepatosteatosis. In brief, MIF-2 serves as a pathogenic linker between atherosclerosis and hepatic steatosis, by not only exacerbating inflammation but also affecting lipogenesis. To have a deeper understanding of the potential value of MIF-2 in atherosclerosis, its homolog MIF in this context will be referred and discussed. Additionally, two important functional properties of MIF-2 observed in this study, pro-inflammatory and pro-lipogenic activities, will be also emphatically addressed. Next specific molecular mechanisms, mainly involving the AMPK-SREBP pathway and CXCR4/CD74 receptor complexes, will be discussed. Lastly, several limitations in our study and potential follow-up experiments will be outlined, which aims to provide some interesting research directions for the future.

4.1 The significance of MIF-2 in atheroprogression and relevant comparisons with MIF

When studying the specific property of MIF-2 in atheroprogression, the significance of the MIF-2 homolog MIF in the context of cardiovascular diseases needs to be considered. MIF, as a pro-inflammatory atypical chemokine, has been identified as a causal factor in atherosclerotic vascular diseases, showing upregulated expression in human plaques [152] and a correlation with the disease severity in these patients with coronary artery disease [1,265]. Experimental evidence from different mouse models including $Apoe^{-/-}$ and $Ldlr^{-/-}$ mice showed that MIF accelerates atherogenic progression as well as affects plaque stability [2,157,266]. A recent study from our laboratory revealed that *Mif* deficiency induced an atheroprotective phenotype that was not only related to T-cell and monocyte recruitment, but also associated with complex B-cell regulation [3]. Of interest, there was a reduced circulating B cell population along with a developmental deficiency of decreased splenic B cells and

elevated myeloid immature and premature B cells observed in *Mif*-deficient atherogenic *Apoe*$^{-/-}$ mice [3]. Mechanistically, this phenotype was closely associated with downregulation of B-cell-activating factor receptor (BAFF-R) in immature B cells, which was accompanied by diminished differentiation-driving transcription factors, suggesting that this inhibitory effect is mainly targeted at immature B cells. A study recently performed in *Apoe*$^{-/-}$ mice using msR4M-L1, a novel CXCR4-derived peptide-based inhibitor of MIF [155], confirmed the important place of the MIF/CXCR4 interaction in atheroprogression that had been suggested earlier [2], at the same time distinguishing the MIF-blocking effects from those potentially co-addressing the MIF/CD74 or CXCL12/CXCR4 pathways [155].

In contrast, no studies referring to the significance of MIF-2 in the context of atherosclerosis are available and to my knowledge, so far this thesis provides the first systematic study to address this question. Genetic as well as pharmacological mouse models were utilized to clarify how MIF-2 affects and regulates atherosclerosis. MIF-2 was found to be pro-atherogenic, but the precise phenotype differed substantially from that of MIF in a number of characteristics. While for MIF, Schmitz *et al.* demonstrated that *Mif*$^{-/-}$*Apoe*$^{-/-}$ mice developed less plaques only in abdominal aorta and brachiocephalic artery (BCA), but not in the aortic root or arch in comparison with *Apoe*$^{-/-}$ mice [3], *Mif-2*$^{-/-}$*Apoe*$^{-/-}$ mice as examined in this thesis had fewer plaques all across the aortic bed.

In addition to the site-specific effect of MIF but not MIF-2, potential differences caused by various model applications will be addressed as well. Considering different physiological characteristics and pathological features between humans and mice, the *Apoe*$^{-/-}$ mouse model can be applied in preclinical studies of atherosclerosis, which was also used in our study. However, particular attention needs to be given to the diversity. Mice generally develop plaques from the aortic sinus to the aortic arch while not in the coronary artery, which is quite different from humans, and probably due to the rapid heartbeats (~500-700 beats/min) in mice [267]. In consideration of murine diversity, researchers now always examine more than the aortic root and also expand the experimental endpoints to several time points of HFD, giving insights into how genetic modifications and/or inhibitor applications affect atherosclerosis in different stages and whether there exists the potential site-specificity. In addition, it is not suitable to study unstable plaque features in WT mice, which is of great significance for clinical outcomes of patients. However, Dr. Karlheinz Peter's group developed a novel mouse model by applying a tandem stenosis to *Apoe*$^{-/-}$ mice upon HFD, representing plaque

94

instability features that are only in humans [268], which provides a new choice. Except for the conservative concept of plaque rupture, some researchers put more attention to superficial plaque erosion, giving a new mechanism for acute coronary syndrome [269]. Even so, the mouse is still regarded as the most preferred model in the atherosclerosis research. The aortic root and aortic arch with lesser curvature are the most frequently analyzed atheroprone regions during lesion development. Of note, the region-specific effect of *Mif* deficiency was only seen in *Apoe*^{−/−} mice but not *Ldlr*^{−/−} mice [2,3], which could be due to the rapid plaque progression in *Apoe*^{−/−} mice compared with *Ldlr*^{−/−} mice, amplifying this site-specific impact somehow.

In line with the site-specific effect induced by MIF, there were some other studies reporting this kind of vascular site-dependent impact, as exemplified by platelet endothelial cell adhesion molecule-1 (PECAM-1/CD31) deficiency-, CX3CL1 knockout- and a non-activatable IKKα kinase-related phonotype [270-272]. More specifically, Teupser and coworkers found that the deficiency of *Cx3cl1/fractalkine*, an important adhesion molecule, attenuated plaque formation in the BCA but not the aortic root based on the detected fractalkine-background interaction [270]. Interestingly, *fractalkine* deficiency did not affect plaque area in the aortic root, whereas remarkably reduced lesions in the BCA by 85% in female and male mice. They did not perform any further mechanistic experiments, although they speculated that different expression of fractalkine under different flow conditions and/or its potential interactions with other regulatory genes could be a reason why CX3CL1-regulated site-dependent phenotypes occur. Similarly, Goel and colleagues demonstrated that PECAM-1 exerted the totally opposite functions at different vascular sites in *Ldlr*^{−/−} mice, with atheroprotective effects in the aortic sinus and several other positions, whereas pro-atherosclerotic effects were observed at the inner curvature of arch [271]. Possible explanations would be that the detrimental effect of PECAM-1 was attributed to its mechano-stimulatory functions, while the beneficial side of PECAM-1 was dependent on its expression on endothelial cells and bone marrow-derived cells. One recent study from Tilstam and coworkers revealed that IKKα kinase regulated atherogenesis in a site-specific manner. Higher IKKα protein expression in the aortic root and elevated IKKα phosphorylation could be associated with this vascular site-specific effect of IKKα on atherosclerosis in aortic root *versus* aortic arch/BCA [272]. In this thesis, MIF-2 did not show a site-specific phenotype in atherogenic mice, which behaves differently from MIF. Interestingly, *Mif* deficiency-induced region-specific effect was only observed in *Apoe*^{−/−} but not *Ldlr*^{−/−} mice [2,3], as mentioned

above. However, the specific mechanism of site-specificity upon *Mif* deletion still needs more scrutiny.

In addition to these differences in atheroprone sites, MIF and MIF-2 are involved in at least partially different regulatory mechanisms when exerting their pro-atherogenic properties. It has been acknowledged that immune reactions in atheroma and inflammatory mediators contribute to atheroscleroprogression [273]. Indeed, both MIF- and MIF-2-mediated atherogenesis was related to inflammatory regulation. Some *in vitro* functional data about MIF-2 generated by my colleagues showed that MIF-2 has a strong potency in promoting chemotactic migration and monocyte adhesion [274]. Of note, murine splenic B lymphocytes displayed a more pronounced effect towards MIF-2 in comparison to MIF [274]. In addition, genetic *Mif-2* deficiency and MIF blockade by msR4M-L1 seemingly showed at least partially different inflammatory cytokine/chemokine changes in atherogenic $Apoe^{-/-}$, as revealed by a cytokine array [155,274]. Reductions in $Mif\text{-}2^{-/-}Apoe^{-/-}$ mice were seen for IFNγ, IL-2, IL-16, IL-17, CXCL12 as well as CXCL13, whereas downregulations in mice treated with msR4M-L1 were observed for TNF-α, IL-1α, IL-16 and CXCL13, suggesting that different types of cytokines may be involved in inflammatory regulation of MIF and MIF-2 in different mouse models [155,274]. Additionally, genetic *Mif* deletion or neutralization of MIF *in vivo* was generally accompanied with decreased immune cells in the intima and downregulated inflammatory cytokine levels in blood [2,3,157,159]. In a hypercholesterolemic mouse model of wire-induced vascular injury, blockade of MIF with a monoclonal antibody reduced the infiltration of neointimal monocytes and foam cell formation. But increased SMCs and collagen content reversely led to a shift of plaque to a more stable type [159]. Two years later, another study revealed that neutralization of MIF not only results in a significant reduction of intimal macrophages, but also leads to a noticeable downregulation of circulating inflammatory cytokines for example IL-6 as well as aortic mediators such as ICAM-1, indicating a causal role of MIF in promoting atherosclerosis through modulating intimal inflammation [157]. In a similar vein, *Mif-2*-deficient atherogenic $Apoe^{-/-}$ mice in our study also showed a downregulation of inflammatory cytokines/chemokines, exemplified by IL-2, IFNγ, IL-16, CXCL12, and IL-17, as well as CXCL13, as addressed above.

Of note, Bernhagen *et al.* in 2007 identified CXCR4 and CXCR2 as functional receptors of MIF, interacting with MIF to regulate inflammatory cell recruitment and atherogenesis [2]. Specifically, MIF elicited monocyte- and T cell-arrest and chemotaxis via binding with its

cognate ligands CXCR2 and CXCR4, which was Gαi- and integrin-dependent as well. In addition, monocyte arrest triggered by MIF in atherosclerotic arteries was associated with the receptor complex formation of CXCR2 and CD74. As mentioned above, the study from our laboratory in 2018 submitted a new association between B-cell response and MIF in atherogenesis. They pointed out that *Mif* deficiency was against atherosclerosis through improving the hypersensitivity of B cells and inducing protective B-cell responses. Taken together, these studies demonstrate that MIF promotes atherogenesis though multiple regulatory mechanisms of various immune cells with the involvement of immune reactions. In contrast, there are no studies to report the role of MIF-2 in atherosclerosis until now. Interestingly, the data of this thesis indicated that *Mif-2* deficiency downregulated the general inflammatory levels in the whole body through affecting immune cells and cytokine levels. On the one hand, macrophage content significantly decreased in *Mif-2$^{-/-}$Apoe$^{-/-}$* mice in early and advanced stages in comparison with control mice. On the other hand, several inflammatory cytokines for example IL-2, IFN-γ, and IL-16 as well as IL-17 remarkably reduced in *Mif-2$^{-/-}$Apoe$^{-/-}$* mice, and most of them were associated with T-cell regulation. Collectively, these data reveal that both MIF and MIF-2 participate in regulating inflammatory processes in the context of atherosclerosis, yet through targeting different immune cells, interacting with particular receptors and involving various signaling pathways. In fact, these points are in line with my thesis topic and provide insights for the future study. Overall, consistent with the effects of MIF, *Mif-2* deficiency mitigates vascular inflammation through downregulating inflammatory cytokine/chemokine levels and reducing macrophage content. This process involves two common receptors (CXCR4, CD74) of MIF and several pathways (MAPK, AKT). However, the inflammatory regulation of MIF and MIF-2 may be associated with different types of cytokines, as described above. Receptors and signaling pathways of MIF-2 involved in this context also need to be explored further.

Except for inflammatory regulation, MIF family proteins are additionally implicated in hepatic lipid metabolism, indicating the potential connection with atherosclerosis, primarily as a lipid storage disease. Increasing evidence *in vivo* suggests that *Mif* deficiency accelerates adipogenesis and hepatic lipogenesis [275-277]. Predominantly, Gligorovska and coworkers found *Mif* knockout impaired insulin sensitivity, which was independent of the diet. *Mif$^{-/-}$* mice fed with an energy-rich fructose diet displayed more energy intake, increased visceral adiposity as well as enlarged adipocytes, as mechanistically associated with the activation of glucocorticoid receptor (GR)-regulated lipogenic genes, such as PPARG and SREBP-1c [275].

Later on, the same group showed that $Mif^{-/-}$ mice fed a fructose diet for 9 weeks had dramatic lipid accumulation in the liver, similarly through enhanced inflammation and activation of GR signaling pathway [276]. In a similar vein, Heinrichs *et al.* revealed the hepatoprotective effect of MIF on both Hepa 1-6 cells and primary hepatocytes, which was associated with the AMPK pathway [277]. These findings together identified a protective role of MIF in hepatic steatosis and lipid metabolism. Inversely, the results of this thesis surprisingly indicated that MIF-2 promotes lipogenesis via activating the maturation of SREBPs. Of note, *Mif-2*-deficient atherogenic mice showed less steatosis in hepatic tissue and a reduction in liver weight, plasma triglycerides and cholesterol. Mechanistically, MIF-2 enhanced the synthesis of triglyceride and cholesterol through the AMPK-SREBP signaling. Combined with these findings in my thesis, it is very interesting to think about the roles of MIF family proteins in lipid metabolism. It may be speculated that MIF and MIF-2 are antagonists regarding their functions in lipid metabolism, and maintain the homeostatic balance in the organic body in normal conditions, which would give a plausible explanation for current data.

To sum up, MIF and MIF-2 display similar pro-atherogenic properties based on published data and the findings of this thesis. However, they behave at least partially differently, affecting particular vascular sites and functioning in special molecular mechanisms. *Mif* deficiency mainly decreased plaque formation in BCA, while *Mif-2* knockout largely exacerbated atherosclerotic lesion area in aortic root in addition to arch. Considering major pathological processes, both MIF and MIF-2 are involved in inflammatory regulation and lipid homeostasis, whereas they possess evidently distinct functions to modulate lipogenesis. MIF seems to reduce lipogenesis, whilst MIF-2 is likely to promote lipogenesis. If the responsibilities of MIF and MIF-2 in lipid metabolism are further elucidated and confirmed, it would be very promising to target MIFs. Of note, 4-CPPC, a selective inhibitor of MIF-2, was used in our study recently, showing a therapeutic capacity in atherogenic $Apoe^{-/-}$ mice. Therefore, the application of MIF-2 inhibitors will for sure provide more approaches to clarify the significance of MIF-2 in atherosclerosis as well as hepatosteatosis, and even offer encouraging therapeutic strategies in the future.

4.2 MIF-2-triggered inflammation and lipogenesis orchestrate athero-sclerosis and hepatosteatosis

As discussed in the previous chapter, MIF and MIF-2 are both involved in the regulation of inflammation and lipogenesis based on reported literatures and our data. Additionally, considering the observation in my thesis that *Mif-2*-deficient mice showed reduced plaques as well as less hepatic steatosis meantime, it is intelligible to speculate that MIF-2 acts as a pathogenic linker between atherosclerosis and hepatosteatosis by affecting both inflammatory and lipogenic processes. Therefore, this chapter will discuss the potential association between atherosclerosis and hepatosteatosis, summarize some relevant targets already reported, and highlight the role of MIF-2 in this context.

In fact, it has been acknowledged that the tight connections between atherosclerosis and hepatosteatosis encompass mechanisms of lipid metabolism and inflammation. Regarding the pronounced effects of MIF-2 on plaque formation and fatty liver, the roles and probable linkers inducing or regulating inflammation and lipogenesis in these two disease settings need to be also considered here, especially the significance and potential therapeutic value of MIF-2 in this relationship.

The potential association will be discussed, which starts with the significance of inflammation and lipids in atherosclerosis. Atherosclerosis is a main underlying cause for cardiovascular diseases, mainly driven by inflammation and lipid disorders. At the cellular level, foam cell formation could be a functional mediator, and macrophages and hepatocytes are involved in the interactions. In fact, hepatocytes can coordinate with macrophages in the regulation of lipid metabolism [278]. For example, Schuster *et al.* reported liver X receptors (LXRs) as one important type of factors linking potential communications between foam cells and hepatocytes [279]. At the molecular level, NF-κB in macrophages, SREBPs in hepatocytes and other factors such as miR-33 participate in this regulatory process. Volzke and coworkers in 2005 firstly revealed an independent association between carotid atherosclerotic plaques and hepatic steatosis through a clinical cross-sectional study including 4222 patients. Additionally, it has been speculated that this relationship might be attributed to metabolic changes induced by non-alcoholic fatty liver disease. This means that atherosclerosis may be considered as a pathological cause of hepatosteatosis in this intercommunication. Further insights into how these two pathological conditions affected each other are provided by studies that applied inhibitors or antagonists in mouse or rat models, for example urantide, 5-

HT synthesis inhibitor, flavone, salusin-α, etc., the detailed mechanisms of which will be discussed subsequently [280-283].

Salusin-α, a peptide from prosalusin, could improve atherosclerosis and hepatic steatosis in $Ldlr^{-/-}$ mice after 12-week HFD though several beneficial effects, including amelioration of hyperlipidemia, anti-inflammatory regulation of some mediators for example TNF-α and IL-6, regulation of some lipid metabolism genes such as *Fasn* and *acetyl coenzyme A carboxylase-α* (ACC) in the liver, and anti-oxidative effect in both liver and aorta [280].

Another *in vivo* study in $Apoe^{-/-}$ mice after 16-week HFD showed that flavone, a kind of metabolite from plants, on the one hand inhibited atherosclerotic lesions by reducing monocyte adhesion, downregulating inflammatory cytokine levels, ameliorating lipid dysfunction, and suppressing miR-33 and NF-κB pathways. On the other hand, flavone improved hepatic steatosis mainly through reducing lipid metabolism related genes expression. This in turn affects atherosclerosis, indicating that lipid disorders and inflammation are the main mechanisms leading to the acceleration of both pathological conditions [281]. In addition, the synthesis and degradation of 5-HT are also responsible for lipid-induced hepatic steatosis as well as atherosclerosis. Mechanistically, both the 5-HT2AR antagonist and the 5-HT synthesis inhibitor could suppress macrophage infiltration, foam cell formation and improve dyslipidemia and insulin resistance as well as hepatic steatosis partially through the NF-κB pathway [283]. Moreover, the protective effects of urantide, an urotensin-II receptor (UT-II-R) antagonist, on atheosclerosis and hepatosteatosis were mainly regulated via the MAPK pathway. The injection of urantide not only improved clinical conditions of atherosclerosis and hepatosteatosis, but also reduced the binding of GPR14 to UII, and further decreased ERK and JNK activation [282]. In brief, there are quite a lot of studies investigating the inhibitory effects of various interventions on atherosclerosis and hepatic steatosis, and most of studies show a close association with inflammatory regulation and lipoprotein homeostasis, specifically covering the MAPK, AMPK, NF-κB signaling pathways, etc. Besides, a few studies mentioned other regulatory mechanisms, such as anti-autophagy dysfunction, anti-oxidative effects and anti-ER stress (Table 4). Among these specific mechanisms, the AMPK-SREBP-mediated lipogenic process is an extensively investigated target, which is also the major pathogenic mechanism investigated in this thesis and will be broadly discussed in the next chapter. Even though not all the details are addressed here, main messages of some representative preclinical studies are summarized in Table 4.

Table 4: Preclinical studies of different targets affecting atherosclerosis and hepatosteatosis

Interventions	Model	Diet	Main mechanisms	Ref.
Salusin-α	$Ldlr^{-/-}$ mice	12-week HFD	Anti-inflammation (IL-6, TNF-α), anti-lipid dysfunction, anti-oxidative stress	[280]
Flavone	$Apoe^{-/-}$ mice	16-week HFD	Anti-inflammation (NF-κB), anti-lipid dysfunction	[281]
5-HT2AR antagonist, 5-HT synthesis inhibitor	$Apoe^{-/-}$ mice	16-week HFD	Anti-inflammation (NF-κB), anti-lipid dysfunction	[283]
Urantide	Rat	6-week HFD	Anti-inflammation (MAPK/ERK/JNK pathway)	[282]
Liver-selective γ-secretase	WT mice $Apoe^{-/-}$ mice	16-week HFD/chow diet	Anti-dyslipidemia (LDLR cleavage and degradation)	[284]
Trehalose	$Apoe^{-/-}$ mice	16-week HFD/chow diet	Anti-autophagy dysfunction	[285]
Viola mandshurica	$Apoe^{-/-}$ mice	16-week HFD/chow diet	Anti-lipid dysfunction (AMPK-SREBP), anti-inflammation	[286]
Apple polyphenol	$Apoe^{-/-}$ mice	12-week HFD	Anti-inflammation (ROS/MAPK/NF-κB pathway)	[287]
Alda-1	$Apoe^{-/-}$ mice	16-week chow diet	Anti-mitochondrial dysfunction (ALDH2)	[288]
Polyphenol S17834	$Ldlr^{-/-}$ mice	16-week chow or HFHS diet	Anti-dyslipidemia (AMPK-SREBP pathway)	[214]
Valproate	$Apoe^{-/-}$ mice	16-week chow diet	Anti-inflammation, anti-lipid dysfunction (ER stress, GSK-3)	[289]
Deficiency of Atg7 in T cells	Mice with rA-AV2/8-D377 -Y-mPCSK9	22-week HFD	Anti-inflammation (IFNγ, IL-17, T cells, NK cells), anti-lipid dysfunction	[290]
Mast cell deficiency	$Apoe^{-/-}$ mice	12- and 24-week HFD	Anti-inflammation (IL-6, IL-10), anti-dyslipidemia	[291]
GSK 3α deficiency	$Ldlr^{-/-}$ mice	10-week chow diet or HFD	Anti-ER stress	[292]

The data of my thesis suggest that *Mif-2* deficiency attenuates atherosclerosis and hepatosteatosis at the same time based on experimental evidence obtained from *Apoe*$^{-/-}$ mouse model. Mechanistically, *Mif-2*$^{-/-}$*Apoe*$^{-/-}$ mice displayed less inflammation characterized by reduced cytokine secretion and decreased plaque macrophage counts, as well as less lipid accumulation in the liver regulated by the AMPK-SREBP-signaling pathway. SREBPs are pivotal regulators in this process, controlling triglyceride and cholesterol synthesis, and maintaining the balance of lipogenesis and lipolysis. On the other hand, SREBP-modulated lipogenesis also aggravates cellular stress, which further exacerbates the inflammatory status. Therefore, inflammation and lipid metabolism actually function as interactive parts, through promoting their effects on each other to some extent.

In addition to liver, the biggest metabolic organ in the body, is the white adipose tissue. It is well acknowledged that SREBPs strongly contribute to metabolic remodeling especially in white adipose tissue [293]. It would be very interesting to investigate how metabolic organs liver and adipose tissue interact or function congenially to modulate the dynamic balance of lipids. Apparently, MIF-2 is a good candidate in this context due to its high expression in adipose tissue and involvement in SREBP regulation, which is worth to explore further in the future.

4.3 AMPK-regulated SREBP activity and lipogenesis

AMPK, a vital energy sensor as well as a master switch, exerts pivotal functional properties to regulate lipid and/or glucose metabolism, and is broadly applied in therapeutics in relevant metabolic disorders, for example metformin/phenformin in diabetes. Once AMPK signaling pathway is activated, there is a concomitant upregulation in glucose and fatty acid uptake and oxidation, and a reduction in triglyceride and cholesterol biosynthesis. As a result, the activation of AMPK suppresses energy-consuming biosynthetic pathways, for example glucose and fatty acid synthesis [294]. Here, the phosphorylated regulation of AMPK in lipid metabolism is a prime focus. Earlier studies from Indiana in 1973 demonstrated that the activities of ACC as well as HMGCR, essential regulators in cholesterol and fatty acid biosynthesis, were strongly associated with phosphorylation and dephosphorylation of AMPK [295,296]. Partially purified ACC was activated by magnesium ions while inactivated by ATP in a temperature- and time-dependent manner [295]. Similarly, with the pre-incubation of cAMP, HMGCR activity was abated in some hepatic systems, whilst it could be at least partially restored in inactivated microsomes [296]. Additionally, these genes encoding HMGCR, ACC, FASN, and other lipid metabolism-related genes, are together targeted by one transcription factor, i.e. SREBP, which was studied in my thesis.

In fact, the process that AMPK downregulates SREBPs, both SREBP-1 and SREBP-2, to suppress lipogenesis serves as an acknowledged mechanism of AMPK involved in lipid metabolism. Negative regulation of SREBP-1c by AMPK was systemically revealed by Li and colleagues in 2011 [214]. They used S17834, a synthetic polyphenol, to verify the interaction between AMPK and SREBP-1c, and showed that AMPK can directly phosphorylate SREBP-1c to regulate its transcriptional activities in hepatocytes. Specifically, AMPK phosphorylates Ser372, which is the residue of SREBP-1c, represses the cleavage as well as nuclear translocation of SREBPs, and subsequently downregulates the expression of

SREBPs and their downstream targets. Of interest, S17834 attenuated atherosclerosis and hepatic steatosis in high fat/high sucrose (HFHS) food-fed $Ldlr^{-/-}$ mice *in vivo*. Considering therapeutics, AMPK activation in hepatocytes by metformin or polyphenol could keep the body from atherogenic dyslipidemia, hepatic steatosis and atherosclerosis in $Ldlr^{-/-}$ mice through this pathway. In addition to polyphenol, there have emerged some other studies including inhibitors, antagonists or Chinese herbs, to block the AMPK pathway as well as target SREBPs. As mentioned in the above part, *viola mandshurica* ameliorated atherosclerosis and hepatosteatosis mainly through downregulating SREBP-1c and FASN expression under the activation of the AMPK signaling pathway [286]. Of note, suppression of SREBP-1c and FASN modulated by AMPK was also confirmed in the liver of atherosclerotic mice treated with *viola mandshurica*, giving evidence for its validity *in vivo*.

Moreover, sauchinone, as an antioxidant to activate AMPK, was used to investigate its therapeutic effect on SREBP-1c-modulated lipogenesis and AMPK-related molecular mechanisms. Mechanistically, sauchinone treatment not only prevented hepatic injury induced by oxidative stress directly, but also suppressed LXRα-mediated SREBP-1c expression and further inhibited SREBP-1c-dependent hepatosteatosis [297]. Besides, betulinic acid (BA) was another candidate in the inhibition of AMPK-SREBP-mediated lipogenic process. They used both insulin-resistant HepG2 cells and ICR mice to verify the phenotype that BA reduced lipid accumulation, and that BA suppressed lipogenesis via the AMPK-mTOR-SREBP-1 pathway [298]. Interestingly, Nammi and Roufogalis found that a small amount of ethanol diminished hepatic SCAP and SREBP-1 levels, as observed in rats, whereas there were no food-intake differences among these groups. Specially, light to moderate ethanol was able to upregulate the expression of phosphorylated AMPK-α in the liver, suggesting the involvement of the AMPK-SREBP pathway [299]. Additionally, there are emerging quite a lot of relevant studies talking about other factors or substances involved in the AMPK-SREBP signaling pathway [300-303], such as α-lipoic acid, 5-aminoimidazole-4-carboxyamide ribonucleoside (AICAR), curcumin, phenylpropanoid glycosides, isoquercetin, etc., which are summarized in Table 5. Together, these studies suggest that the AMPK-SREBP pathway is of great importance in regulating lipogenesis in the liver and that it may be advisable to develop therapies targeted at this pathway for patients with NAFLD and other metabolic disorders.

Table 5: Summary of preclinical studies focusing on negative regulation of SREBPs by AMPK in lipogenesis

Interventions	Model	Diet	Main mechanisms	Ref.
S17834	*Ldlr*^{−/−} mice	16-week chow or HFHS diet	AMPK directly phosphorylated SREBP-1c and suppressed SREBPs cleavage	[214]
Viola mandshurica	*Apoe*^{−/−} mice	16-week chow diet or HFD	AMPK inhibited *de novo* lipogenesis by suppressing SREBP-1c and FASN	[286]
Sauchinone	C57BL/6 mice	11-week chow diet or HFD	Sauchinone activated AMPK and further repressed LXRα-elicited SREBP-1	[297]
Curcumin	Diabetic rats	8-week chow diet	Curcumin activated AMPK and inhibited SREBP-1c in the kidney	[300]
Betulinic acid (BA)	ICR mice	3-week RD or HFD	BA inhibited SREBP-1 through the AMPK-mTOR-SREBP pathway	[298]
Light-to-moderate ethanol	Sprague-Dawley (SD) rats	3-week standard pellet diet	Low consumption of ethanol activated AMPK and downregulated SREBP-1 and SCAP in the liver	[299]
Alpha-lipoic acid	C57BL/6 mice	24-week chow diet or HFD	Alpha-lipoic acid reduced SREBP-1 expression via SIRT1/LKB1/AMPK axis	[301]
AICAR	*Tshr*^{−/−} mice	5~7-week diet (thyroid powder)	AICAR activated AMPK through TSH/SREBP-2/HMGCR pathway.	[302]
Antrodia cinnamomea	C57BL/6 mice	10-week chow diet or HFD	Antrodia cinnamomea activated AMPK and suppressed SREBPs, FASN, HMGCR, etc.	[303]
Phenylpropanoid glycosides	Hamsters	4-week chow diet or HFD	Phenylpropanoid glycosides reduced lipid via AMPK-SREBP-1c pathway	[304]
Scutellaria baicalensis	KK-A[y] Mice C57BL/6 mice SD rats	8-week chow diet	*Scutellaria baicalensis* suppressed free fatty acid-induced lipotoxicity via regulating AMPK-SREBP	[305]
Mangiferin	KK-A[y] Mice C57BL/6 mice SD rats	4-week chow diet	Mangiferin improved hepatosteatosis by SIRT-1-AMPK-SREBP-1c signaling	[306]
Kanglexin	SD rats	5-week HFD	Kanglexin attenuated lipid accumulation via AMPK/SREBP-2/PCSK/LDLR axis	[244]
Chlorella pyrenoidosa	SD rats	8-week chow diet or HFD	*Chlorella pyrenoidosa* improved hyperlipidemia by AMPK-HMGCR/SREBP-1c signaling	[307]
Dibutyl phthalate (DPB)	SD rats	6-week chow diet or HFD	DPB affected lipid metabolism based on PPARα/SREBP-1c/FAS/GPAT/AMPK pathway	[308]

As shown in Table 5, there were slightly different mechanisms when referring to particular inhibitors or targets. Most of these preclinical studies focus on the AMPK-SREBP pathway and some well-investigated downstream target genes of SREBP-1 and SREBP-2 such as FASN, HMGCR, ACC, and LDLR, etc. In addition, several other researchers also pointed out the involvement of SCAP-1 and mTOR. Another interesting point is that the lipogenic process induced by the AMPK-SREBP pathway occurs not only in the liver, but also in the kidney,

which is associated with obesity-related kidney disease [226]. Curcumin, another type of polyphenol, has been studied in the type 1 diabetic rat model and showed its inhibitory property to induce renal lipogenesis through activating AMPK phosphorylation and repressing SREBP-1c expression in the kidney [300]. Reversely, nifedipine, a calcium channel blocker has been found to accelerate renal lipogenesis through suppressing pAMPK activity and inducing SREBPs and target genes expression *in vitro* [226]. In this project, *Mif-2* deficiency activated AMPK phosphorylation and downregulated SREBPs and downstream target gene expression, further to suppress the lipogenic process induced by HFD. As a result, *Mif-2* knockout mice with *Apoe*$^{-/-}$ background displayed less plaque formation and attenuated hepatosteatosis. Furthermore, *in vitro* experiments in hepatocytes mimic and confirm the findings *in vivo*. Collectively, these preclinical studies might provide some auspicious hints or suggest potential strategies to prevent or combat lipogenesis in the liver and kidney.

4.4 CXCR4 and CD74 complex formation and involvement in MIF-2-SREBP-modulated lipogenesis

Both CXCR4 and CD74 are well characterized as functional receptors for MIF during MIF-induced leukocyte migration [2], and afterwards this receptor complex formation was firstly observed and confirmed to be involved in MIF-specific signaling pathway in 2009 [163]. Schwartz *et al.* showed fused CXCR4 and CD74 colocalization in HEK-293 cells as well as endogenous complex formation in monocytes. More interestingly, this receptor complex also participated in AKT phosphorylation in T cells induced by MIF, but not in the case of CXCL12, which could be the specific difference between MIF's and CXCL12's actions [163]. Furthermore, Lue *et al.* revealed that MIF-activated JNK pathway in fibroblasts and T cells, not only implicated its upstream kinases for example PI3K and SRC, but also relied on the existence of the CD74 and CXCR4 complex [309]. It is noteworthy that the clathrin/dynamin-dependent endocytosis pathway has been identified as the major track for MIF internalization, and this type of MIF-related endosomal signaling mechanism is dependent on the heteromeric receptor complex of CXCR4 and CD74 [310]. In addition to monocytes, T cells and fibroblasts, the cooperative involvement of CXCR4 and CD74 was also verified in the functional migration assay of primary splenic B cells elicited by MIF through the Zeta-chain-associated protein kinase 70 (ZAP-70) pathway [161]. Blockade of CXCR4 or CD74 *in vitro* completely abolished chemotactic effects of splenic B cells induced by MIF, indicating the cooperative engagement of both receptors. Moreover, a recent study in cardiac myofibroblasts

demonstrated that soluble CD74 suppressed MIF-elicited survival pathway through the CXCR4/AKT axis [311]. Additionally, a previous study demonstrated the expression of CXCR4 and CD74 in Hepa 1-6 cells and primary mouse hepatocytes, as confirmed by Western blot analysis [31,312]. In the same study, flow cytometry only showed the surface expression of CD74, whereas no visible fluorescence intensity for CXCR4, which was at least partially inconsistent with our results that high fluorescence intensity was observed for CXCR4 and low fluorescence intensity was seen for CD74. This can be attributed to the diversity of different cells. Taken together, these findings imply both the colocalized expression and functional formation of the CXCR4 and CD74 complex in different cells, encompassing T and B cells, monocytes, hepatocytes and fibroblasts.

However, all of these findings mentioned in the above part were associated with the functionality of MIF, and there are no related publications regarding MIF-2 yet. This thesis for the first time identified CXCR4 as a novel receptor of MIF-2 in addition to CD74, and further displayed the engagement of CXCR4/CD74 receptor complex in MIF-2-SREBP-mediated lipogenic process. First of all, our laboratory had some *in vitro* data of MIF-2 released in bioRxiv recently, showing that blockade of CXCR4 inhibited MIF-2-elicited chemotaxis of B cells, T cells and monocytes [274]. Secondly, *in vitro* data from this thesis demonstrated that neutralization of CXCR4/CD74 diminished MIF-2-mediated lipogenic effect. Intriguingly, the combinative use of LN-2 and AMD3100 fully abrogated the proteolytic cleavage of SREBPs, which further diminished the expression of their corresponding targets induced by MIF-2 respectively, as shown via Western blot analysis. Of note, the neutralization of CD74 alone seems exert more pronounced inhibitory effects than the blockade of CXCR4 in this study, emphasizing the significance of CD74 in MIF-2-mediated SREBP processing. Thirdly, hepatocytes treated with AMD3100 and LN-2, together with MIF-2, demonstrated less native LDL uptake compared with the MIF-2-stimulated group, implying that CXCR4 and CD74 might be involved in MIF-2-mediated LDL uptake in hepatocytes. Accordingly, these observations together suggest that CXCR4/CD74 complex formation and/or synergistic signaling contributes to MIF-2-facilitated activation of SREBPs in Huh-7 cells.

As discussed in the above part, CXCR4/CD74 complexes may participate in a MIF- and MIF-2-elicited functional process. Next potential differences as to how MIF and MIF-2 may interact with these receptors were studied. It was necessary to compare the binding

efficiencies of ligand-receptor affected by MIF and MIF-2 stimulation. To answer this question, a powerful technique, FLIM-FRET *in vitro/in situ* was utilized to demonstrate the formation of this receptor complex CXCR4/CD74 with or without stimulation in this study. One of the advantages of FRET is that small donor-acceptor distance changes are easy to detect in this assay. Based on this property, FLIM-FRET assay is also applied to catch subtle shifts in the complex conformation in addition to detect the entire complex disassembly [313]. In combination with equilibrium time-resolved FRET, the information can be further enhanced, which is acquired from mean FRET efficiency kinetics [314]. Given the fact that CFP and YFP are popular FRET pairs in biological applications, CFP-tagged CXCR4 was used as a donor and YFP-CD74 as an acceptor here. A clear and robust co-localization of CFP-CXCR4 and YFP-CD74 was observed in fixed as well as living cells using FLIM-FRET. In line with this finding, the excitation of CFP-CXCR4 was closely associated with a high FRET efficiency and an effective FRET binding, implying there exists a higher likelihood of this interaction between both receptors. Moreover, the distance between two adjacent molecules was around 0.6 to 2.4 nm when excitation energy exchanged, which was in accord with reported values ranging from 2 to 10 nm [315]. To decipher whether CXCR4/CD74 heterodimer formation relied on the existence of MIF-2 and its functional differences with MIF, the fluorescence lifetime of the donor CFP-CXCR4 within an interval of 1 min under MIF or MIF-2 stimulation was compared. The above results were achieved by utilizing a time-correlated single photon counting (TCSPC) system, giving multi-exponential decay analysis a higher sensitivity and a better accuracy. Both MIF and MIF-2 enhanced CXCR4 and CD74 complex formation, as shown by a reduced lifetime. However, of interest, the lifetime was found to show a more pronounced decrease when MIF-2 was present, suggesting that MIF-2 may have a stronger ability to promote the complex assembly of CXCR4 and CD74 than MIF. In aggregate, this study is the first to define a novel heterodimer formation of CXCR4/CD74 by FLIM-FRET and demonstrate a greater potential of interaction with MIF-2 compared to MIF.

4.5 Limitations and potential follow-up studies of this project

This study has several limitations and further experimental evidence needs to be obtained to substantiate some of the notions and conclusions. To this end, some mechanistic follow-up experiments are already ongoing. Several seemingly controversial questions are under consideration and require more evidence to support.

4.5.1 Atherosclerotic mouse model used

One limitation is that so far only $Apoe^{-/-}$ mouse model has been used in this study. Especially, the metabolic phenotype should be further explored in another mouse model, such as $Ldlr^{-/-}$ mouse model or the PCSK9-adenoassociated virus (AAV) mouse model, which is able to develop plaques under HFD within 3 months with normal ApoE and LDLR levels [316]. $Ldlr$ knockout mice are somewhat preferred in the field of metabolism research [317]. Compared to $Ldlr^{-/-}$ mice, atherosclerosis-prone $Apoe^{-/-}$ mice exhibit higher circulating cholesterol levels as well as develop more plaques in the aortic root and arch with larger necrotic cores after 3-month HFD along with more chondrocytes and bone formation, and more smooth muscle cells and matrix [318]. Mechanistically, $Apoe^{-/-}$ mice generally have a poor property of clearing lipoproteins. As a result, circulating lipoproteins were abnormally elevated, which leads to atheroscleroprogression eventually. Even though the functions of ApoE and LDLR are partially different, they are essential players and responsible for clearing extra circulating lipoproteins. In fact, the biggest difference is that ApoE functions as a ligand for all LDLR family members, and is not limited to LDLR. In addition, synthesized ApoE exerts an anti-atherogenic effect on macrophages, which is not affected by plasma cholesterol levels. As a consequence, cholesterol-rich VLDL as well as intermediate-density lipoprotein aggregates in blood of atherogenic $Apoe^{-/-}$ mice, by contrast, LDL mainly accumulates in $Ldlr^{-/-}$ mice. Regarding previous metabolic studies, actually most of researchers utilized $Apoe^{-/-}$ mice, as shown and summarized in Table 4. This was consistent with the mouse model used in our project. Additionally, in collaboration with the laboratory of Prof. Christian Schulz (Department of Cardiology, LMU University Hospital), we are currently performing bone marrow transplantation (BMT) experiments, in which BM from $Mif-2^{-/-}$ mice *versus* WT mice is adoptively transferred into $Ldlr^{-/-}$ recipient mice on HFD, to ask or verify the effects of $Mif-2$ deficiency on bone marrow-derived monocytes and macrophages and clarify the significance of a vascular *versus* systemic source of MIF-2 for the observed metabolic phenotype.

Therefore, the phenotype in our study should be verified in a second mouse model, for example using $Ldlr^{-/-}$ mice in combination with the MIF-2-specific pharmacological inhibitor 4-CPPC or using $Mif\text{-}2^{-/-}$ mice in conjunction with an induction of atherosclerosis and hyperlipidemia by the PCSK9-AAV approach. Of interest, the latter could help to enunciate the metabolic mechanisms further. As described above, BMT mouse model additionally tells whether this phenotype involves a hematopoietic effect. Consequently, the confirmation of this phenotype in multiple mouse models in the future would be beneficial to deeply understand the significance of MIF-2 in lipid metabolism.

4.5.2 SREBP-2 autoloop regulation: LDLR *versus* PCSK9

An interesting question is whether PCSK9 is also involved in MIF-2-mediated functional processes. In this project, there were no significant changes of *Pcsk9* observed in the mRNA level, so we did not go further and checked PCSK9 protein levels. However, some other researchers proposed that altered PSCK9 functions could be due to the post-transcriptional modifications [319]. In other words, PCSK9 could exert functions through protein level changes that would not be apparent on mRNA expression level. In normal conditions, there exists a certain kind of dynamic balance between cholesterol synthesis, LDL release and LDL clearance to maintain the homeostasis. In this project, MIF-2 was found to enhance cholesterol synthesis based on my current data. Through endogenous pathway, VLDL and more pro-atherogenic LDL were produced afterwards. Extra LDL particles were released into plasma to form more plaques in arteries. Nevertheless, due to self-protection mechanism or the feedback regulation, LDLR expression would be also upregulated to remove extra LDL from plasma. Here, one reason why PCSK9 engrosses our attention is that SREBP-2 behaves as an upstream regulator of LDLR, whereas PCSK9 acts as a negative regulator of LDLR. Some researchers even pointed out that SREBP-2 could transcriptionally activate PCSK9 as well as LDLR simultaneously [245]. PCSK9 functions as a 'brake' to inhibit the cholesterol uptake through its degradation of LDLR. Not surprisingly, combined targeting of SREBPs and PCSK9 would achieve an improved outcome. Nevertheless, how LDLR and PCSK9 affect or restrain each other, and whether MIF-2 influences this interaction will be an intriguing direction, which can be definitely followed in the future.

4.5.3 Complementary effects or restriction of MIF and MIF-2 in lipid metabolism

Even if MIF-2 shares high homology with MIF, how MIF and MIF-2 function in different disease settings seems not always similar. Positive cooperative effects of MIF with MIF-2 indicate that a better outcome might be achieved through a combination approach in some disease settings, as exemplified by consistent functionalities of MIF-2 and MIF in NSCLC [37]. Similarly, both MIF and MIF-2 exert a pro-atherogenic impact based on the results of my thesis in combination with previous publications [2,3,14]. By contrast, MIF and MIF-2 were found to show opposite properties in the context of adipose tissue inflammation and wound healing [65], as well as in discoid lupus erythematosus (DLE) [320]. Concerning lipogenesis, there are controversial views about the roles of MIF and MIF-2 [59,64,275,276]. Recently, accumulating evidence *in vivo* suggested that *Mif* deficiency exacerbated adipogenesis and hepatic lipogenesis capitalizing on $Mif^{-/-}$ mice fed an energy-rich fructose diet [275,276]. This phenotype is likely to hold true *in vitro*, as shown by Heinrichs *et al.* in 2014 [277]. Interestingly, our study revealed that *Mif-2* deficiency attenuated hepatic steatosis via inhibiting the maturation of SREBPs. Combined with our findings in this project, it is very interesting to think about the roles of MIF family proteins in lipid metabolism. MIF and MIF-2 might be antagonists for each other regarding their functions in lipid metabolism, and maintain the balance in the organic body in normal conditions, which would give a better explanation for my current data. Therefore, it would be attractive to generate a *Mif Mif-2* double knockout (DKO) mouse line and explore whether the joint knockout of MIF and MIF-2 could produce synergistic or complementary effects overall. Collectively, targeting MIF protein family, thoroughly evaluating the comprehensive mechanisms and even focusing on the internal interactions and/or differences would be beneficial to understand the contributions of MIF family proteins to different disease settings, which definitely warrants more evidence to confirm.

4.5.4 Potential impact of MIF-2 on SREBPs in adipose tissue

In addition to liver, the biggest metabolic organ in the body, the adipose tissue is the second organ to focus on. The main function of WAT is to store energy and being a backup of BAT. Additionally, it has the endocrine function to secrete different types of adipokines. Whereas BAT mainly exert thermogenic property to keep body temperature. Fujii and coworkers demonstrated that SREBP-1c promoted mitochondrial biogenesis and enhanced metabolic remodeling within WAT under caloric restriction (CR) conditions [232]. In addition, the

involvement of MIF-2 in adipocyte lipid metabolism has been reported by several research groups [58,59,64,65,80], as discussed in chapter 1.1.3.3. Even though current literatures argue a controversial role of MIF-2 in adipose tissue, it is still an interesting topic to follow in the future. Investigating the metabolic role of MIF-2 in adipose tissue and connecting SREBPs targets to MIF-2-mediated lipid regulation are beneficial to produce more anti-obesity approaches.

5. SUMMARY AND OUTLOOK

5.1 English summary

This thesis sheds light on a novel and important property of MIF-2 in atherosclerosis and hepatic steatosis linked by lipid metabolism, and unravels the underlying molecular and cellular mechanisms, with a focus on studying the systemic and hepatic cholesterol metabolism in atherosclerotic mice. Integrated evaluation on plaque progression through genetic as well as pharmacological mouse models revealed that the pro-atherogenic and pro-inflammatory properties of MIF-2 in early and advanced stages of atherosclerosis was intriguingly accompanied by a tight association with hepatic lipid accumulation. Reduced triglyceride and cholesterol levels in the plasma of $Mif\text{-}2^{-/-}Apoe^{-/-}$ mice along with consistent decreased body and liver weight pointed towards a conspicuous phenotype displaying that $Mif\text{-}2$ deficiency improved lipid metabolism. However, there was no similar phenotype previously observed in any kind of Mif deficiency atherosclerotic models. This implies that MIF-2 behaves at least partially differently from MIF in the context of hepatosteatosis and atherogenesis.

Indeed, inflammation and lipids are essential to the pathophysiology of atherosclerosis and hepatic steatosis, which in turn is of clinical significance to define the association between these two diseases. Preliminary explorations gave me some clues to target SREBPs and plenty of *in vitro* experiments were performed to test and further clarify my original hypothesis. Here, SREBPs were employed to decipher and validate the role of MIF-2 in lipid metabolism, and further connect the phenotypes in the artery and liver. AMPK, as a master switch for energy, is responsible for the balance of lipogenesis and lipolysis, and determines the energy homeostasis. The hepatocyte cell line Huh-7 was used to analyze the impact of MIF-2 on the lipogenic process, and the data demonstrated that the interaction of MIF-2 with CXCR4/CD74 complexes inhibited AMPK phosphorylation, enhanced SREBP cleavage and expression, upregulated their target gene expression, and herein promoted lipogenesis. Of note, an $Apoe^{-/-}$ mouse model was utilized in this study, whilst additional evidence will have to be obtained by confirmation in other mouse models, such as $Ldlr^{-/-}$ or PCSK9-AAV mice. Collectively, this project demonstrated MIF-2 has a pro-atherogenic role, as well as a pronounced property to promote lipid accumulation in liver, particularly with new insights into the specific mechanism related to the AMPK- and AKT-SREBP-mediated signaling pathways and CXCR4/CD74 receptor complexes.

5.2 Zusammenfassung

Dieses Projekt beleuchtet eine neuartige und wichtige Rolle von MIF-2 in der Atherosklerose und hepatischer Steatose, verbunden mit Prozessen des Lipidstoffwechsels. Zusätzlich werden die zugrundeliegenden molekularen und zellulären Mechanismen, mit einem Fokus auf die Analyse systemischer Entzündung und hepatischer Cholesterinwerte, im atherosklerotischen Mausmodell aufgeklärt. Eine umfassende Analyse der Plaqueprogression mittels genetischer und pharmakologischer Mausmodelle zeigte die entzündungsfördernden Eigenschaften von MIF-2, begleitet von hepatischer Lipidakkumulation, in frühen und fortgeschrittenen Stadien der Atherosklerose. Reduzierte Triglycerid- und Cholesterinwerte im Plasma von $Mif\text{-}2^{-/-}Apoe^{-/-}$ Mäusen, in Übereinstimmung mit vermindertem Körper- und Lebergewicht, deuten auf einen auffälligen Phänotyp mit einem durch die $Mif\text{-}2$ Gendefizienz bedingten, gesteigerten Lipidstoffwechsel hin. Ein ähnlicher Phänotyp wurde allerdings bisher in keinem anderen Mausmodell unter Mif Gendefizienz nachgewiesen. Dies deutet darauf hin, dass sich MIF-2 verglichen mit MIF im Kontext der hepatischen Steatose und Entwicklung von Atherosklerose zumindest teilweise unterschiedlich verhält.

Tatsächlich sind entzündliche Prozesse und Lipide essentiell für die Pathophysiologie der Atherosklerose und hepatischen Steatose, was hinsichtlich der Assoziation der beiden Erkrankungen auch klinisch bedeutsam ist. Vorläufige Untersuchungen haben Hinweise auf die Beteiligung von SREBPs geliefert und eine Vielzahl von *in vitro* Experimenten wurde zur Aufklärung und weiteren Bestätigung meiner ursprünglichen Hypothese durchgeführt. In diesem Rahmen dienten SREBPs dazu, die Rolle von MIF-2 im Lipidstoffwechsel zu erklären und zu validieren, sowie die arteriellen und hepatischen Erscheinungsbilder weiter miteinander zu verknüpfen. AMPK, ein Hauptregulator im Energiestoffwechsel, ist verantwortlich für das Gelichgewicht zwischen Lipogenese und Lipolyse, und bestimmt die Energiehomöostase. Die humane Hepatozyten-Zelllinie Huh-7 wurde verwendet, um die Rolle von MIF-2 in lipogenen Prozessen *in vitro* zu bestimmen. Derzeitige Ergebnisse lassen darauf schließen, dass die Interaktion von MIF-2 mit CXCR4/CD74 zur Inhibition der AMPK Phosphorylierung, verstärkter SREBP-Spaltung und zur erhöhten Expression von Zielgenen führt, was wiederum die Lipogenese fördert. Hervorzuheben ist, dass das $Apoe^{-/-}$ Mausmodell in meinem Projekt verwendet wurde, wobei ein verlässlicher Nachweis durch Bestätigung in anderen Mausmodellen, einschließlich $Ldlr^{-/-}$ oder PCSK9-AAV Mäusen zukünftig noch erfolgen muss. Insgesamt wurde im Rahmen dieses Projektes die pro-atherogene Rolle von MIF-2 und die Eigenschaften zur Förderung der Lipidakkumulation in

der Leber erarbeitet. Dabei wurden neue Einblicke in spezifische Mechanismen mit Bezug zu MIF-2-CXCR4/CD74-AMPK- und AKT-SREBP-vermittelten Signalwegen identifiziert.

6. SUPPLEMENTAL TABLES

This supplemental table is contained in my co-first-author manuscript preprint published on bioRxiv (doi: https://doi.org/10.1101/2021.12.28.474328).

Supplemental Table 1: Blood cell count, body weight and serum lipid levels from female *Apoe$^{-/-}$* mice *Mif-2$^{-/-}$Apoe$^{-/-}$* mice under 4.5-week and 12-week HFD.

Female, 4.5-week HFD	*Apoe$^{-/-}$*	*Mif-2$^{-/-}$Apoe$^{-/-}$*	*P* value
Serum lipid levels			
Triglyceride (mg/dL)	188.135 ± 12.244	160.297 ± 36.357	0.0197
Cholesterol (mg/dL)	887.799 ± 104.492	703.902 ± 138.302	0.0013
Blood cell percentages (%)			
Lymphocytes (%)	59.107 ± 1.929	63.339 ± 2.334	0.0313
T-lymphocytes (%)	17.713 ± 4.350	26.363 ± 5.052	0.0409
B-lymphocytes (%)	41.387 ± 5.159	36.943 ± 4.546	0.2437
Neutrophils (%)	22.283 ± 4.952	24.212 ± 4.296	0.5777
Monocytes (%)	3.711 ± 1.131	1.493 ± 0.519	0.0118
Body weight			
Weight (g)	24.420 ± 3.487	20.886 ± 1.254	0.0222
Female, 12-week HFD	*Apoe$^{-/-}$*	*Mif-2$^{-/-}$Apoe$^{-/-}$*	*P* value
Serum lipid levels			
Triglyceride (mg/dL)	189.344 ± 8.910	180.375 ± 7.116	0.0343
Cholesterol (mg/dL)	1002.305 ± 113.935	850.557 ± 92.842	0.0077
Blood cell percentages (%)			
Lymphocytes (%)	69.461 ± 8.879	73.228 ± 7.893	0.3618
T-lymphocytes (%)	24.519 ± 10.904	25.970 ± 3.704	0.7248
B-lymphocytes (%)	44.765 ± 5.474	47.168 ± 6.488	0.4061
Neutrophils (%)	13.189 ± 6.990	17.682 ± 6.487	0.1811
Monocytes (%)	3.482 ± 2.347	2.627 ± 0.700	0.3368
Body weight			
Weight (g)	29.750 ± 2.914	25.775 ± 3.199	0.0140

Table legend. Data are presented as means ± SD. *P* values were calculated by Student's t-test. Leukocytes were identified as CD45$^+$; T lymphocytes as CD45$^+$CD3$^+$; B lymphocytes as CD45$^+$CD19$^+$; neutrophils as CD45$^+$CD11b$^+$Ly6G$^+$; monocytes as CD45$^+$CD11b$^+$Ly6C$^+$.

7. REFERENCES

1.   Zernecke A, Bernhagen J, Weber C. Macrophage migration inhibitory factor in cardiovascular disease. Circulation. 2008;117(12):1594-1602.
2.   Bernhagen J, Krohn R, Lue H, Gregory JL, Zernecke A, Koenen RR, Dewor M, Georgiev I, Schober A, Leng L, Kooistra T, Fingerle-Rowson G, Ghezzi P, Kleemann R, R McColl S, Bucala R, J Hickey M, Weber C. MIF is a noncognate ligand of CXC chemokine receptors in inflammatory and atherogenic cell recruitment. Nat Med. 2007;13(5):587-596.
3.   Schmitz C, Noels H, Bounkari OE, Straussfeld E, Megens RT, Sternkopf M, Alampour-Rajabi S, Krammer C, Tilstam PV, Gerdes N, Bürger C, Kapurniotu A, Bucala R, Jankowski J, Weber C, Bernhagen J. Mif-deficiency favors an atheroprotective autoantibody phenotype in atherosclerosis. FASEB J. 2018;32(8):4428-4443.
4.   Voss S, Krüger S, Scherschel K, Warnke S, Schwarzl M, Schrage B, Girdauskas E, Meyer C, Blankenberg S, Westermann D, Lindner D. Macrophage migration inhibitory factor (MIF) expression increases during myocardial infarction and supports pro-inflammatory signaling in cardiac fibroblasts. Biomolecules. 2019;9(2):38.
5.   Luedike P, Alatzides G, Papathanasiou M, Heisler M, Pohl J, Lehmann N, Rassaf T. Circulating macrophage migration inhibitory factor (MIF) in patients with heart failure. Cytokine. 2018;110:104-109.
6.   Wang Y, An R, Umanah GK, Park H, Nambiar K, Eacker SM, Kim B, Bao L, Harraz MM, Chang C, Chen R, Wang JE, Kam T-I, Jeong JS, Xie Z, Neifert S, Qian J, Andrabi SA, Blackshaw S, Zhu H, Song H, Ming G-L, Dawson VL. A nuclease that mediates cell death induced by DNA damage and poly (ADP-ribose) polymerase-1. Science. 2016;354(6308).
7.   Inácio AR, Ruscher K, Leng L, Bucala R, Deierborg T. Macrophage migration inhibitory factor promotes cell death and aggravates neurologic deficits after experimental stroke. J Cereb Blood Flow Metab. 2011;31(4):1093-1106.
8.   Leng L, Metz CN, Fang Y, Xu J, Donnelly S, Baugh J, Delohery T, Chen Y, Mitchell RA, Bucala R. MIF signal transduction initiated by binding to CD74. J Exp Med. 2003;197(11):1467-1476.
9.   Shi X, Leng L, Wang T, Wang W, Du X, Li J, McDonald C, Chen Z, Murphy JW, Lolis E, Noble P, Knudson W, Bucala R. CD44 is the signaling component of the macrophage migration inhibitory factor-CD74 receptor complex. Immunity. 2006;25(4):595-606.
10.   Merk M, Zierow S, Leng L, Das R, Du X, Schulte W, Fan J, Lue H, Chen Y, Xiong H, Chagnon F, Bernhagen J, Lolis E, Mor G, Lesur O, Bucala R. The D-dopachrome tautomerase (DDT) gene product is a cytokine and functional homolog of macrophage migration inhibitory factor (MIF). Proc Natl Acad Sci U S A. 2011;108(34):E577-E585.
11.   Merk M, Mitchell RA, Endres S, Bucala R. D-dopachrome tautomerase (D-DT or MIF-2): doubling the MIF cytokine family. Cytokine. 2012;59(1):10-17.
12.   Weber C, Kraemer S, Drechsler M, Lue H, Koenen RR, Kapurniotu A, Zernecke A, Bernhagen J. Structural determinants of MIF functions in CXCR2-mediated inflammatory and atherogenic leukocyte recruitment. Proc Natl Acad Sci U S A. 2008;105(42):16278-16283.
13.   Tilstam PV, Qi D, Leng L, Young L, Bucala R. MIF family cytokines in cardiovascular

diseases and prospects for precision-based therapeutics. Expert Opin Ther Targets. 2017;21(7):671-683.

14. Sinitski D, Kontos C, Krammer C, Asare Y, Kapurniotu A, Bernhagen J. Macrophage migration inhibitory factor (MIF)-based therapeutic concepts in atherosclerosis and inflammation. Thromb Haemost. 2019;119(04):553-566.

15. Aroca P, Garcia-Borron JC, Solano F, Lozano JA. Regulation of mammalian melanogenesis I: partial purification and characterization of a dopachrome converting factor: dopachrome tautomerase. Biochim Biophys Acta Gen Subj. 1990;1035(3):266-275.

16. Aroca P, Martinez-Liarte JH, Solano F, García-Borrón JC, Lozano JA. The action of glycosylases on dopachrome (2-carboxy-2, 3-dihydroindole-5, 6-quinone) tautomerase. Biochem J. 1992;284(1):109-113.

17. Odh G, Hindemith A, Rosengren A-M, Rosengren E, Rorsman H. Isolation of a new tautomerase monitored by the conversion of D-dopachrome to 5, 6-dihydroxyindole. Biochem Biophys Res Commun. 1993;197(2):619-624.

18. Björk P, Åman P, Hindemith A, Odh G, Jacobsson L, Rosengren E, Rorsman H. A new enzyme activity in human blood cells and isolation of the responsible protein (d-dopachrome tautomerase) from erythrocytes. Eur J Haematol. 1996;57(3):254-256.

19. Ryuichi K, Yosihiro Y. D-Amino-acid oxidase and its physiological function. Int J Biochem. 1992;24(4):519-524.

20. Yokoyama K, Yasumoto K-i, Suzuki H, Shibahara S. Cloning of the human DOPAchrome tautomerase/tyrosinase-related protein 2 gene and identification of two regulatory regions required for its pigment cell-specific expression. J Biol Chem. 1994;269(43):27080-27087.

21. Zhang M, Åman P, Grubb A, Panagopoulos I, Hindemith A, Rosengren E, Rorsman H. Cloning and sequencing of a cDNA encoding rat d-dopachrome tautomerase. FEBS Lett. 1995;373(3):203-206.

22. Michelet C, Danchin EG, Jaouannet M, Bernhagen J, Panstruga R, Kogel K-H, Keller H, Coustau C. Cross-kingdom analysis of diversity, evolutionary history, and site selection within the eukaryotic macrophage migration inhibitory factor superfamily. Genes. 2019;10(10):740.

23. Rosengren E, Bucala R, Åman P, Jacobsson L, Odh G, Metz CN, Rorsman H. The immunoregulatory mediator macrophage migration inhibitory factor (MIF) catalyzes a tautomerization reaction. Mol Med. 1996;2(1):143-149.

24. Rosengren E, Thelin S, Åman P, Hansson C, Jacobsson L, Rorsman H. The protein catalysing the conversion of D-dopachrome to 5, 6-dihydroxyindole is a phenylpyruvate tautomerase (EC 5.3. 2.1). Melanoma Res. 1997;7(6):517-518.

25. Sugimoto H, Taniguchi M, Nakagawa A, Tanaka I, Suzuki M, Nishihira J. Crystallization and Preliminary X-Ray Analysis of Humand-Dopachrome Tautomerase. J Struct Biol. 1997;120(1):105-108.

26. Yoshida H, Nishihira J, Suzuki M, Hikichi K. NMR characterization of physicochemical properties of rat D-dopachrome tautomerase. IUBMB Life. 1997;42(5):891-899.

27. Kuriyama T, Fujinaga M, Koda T, Nishihira J. Cloning of the mouse gene for D-dopachrome tautomerase. Biochim Biophys Acta. 1998;1388(2):506-512.

28. Esumi N, Budarf M, Ciccarelli L, Sellinger B, Kozak CA, Wistow G. Conserved gene structure and genomic linkage for D-dopachrome tautomerase (DDT) and MIF. Mamm Genome. 1998;9(9):753-757.

29. Sugimoto H, Taniguchi M, Nakagawa A, Tanaka I, Suzuki M, Nishihira J. Crystal structure of human D-dopachrome tautomerase, a homologue of macrophage

migration inhibitory factor, at 1.54 Å resolution. Biochemistry. 1999;38(11):3268-3279.

30.   Meyer-Siegler KL, Iczkowski KA, Leng L, Bucala R, Vera PL. Inhibition of macrophage migration inhibitory factor or its receptor (CD74) attenuates growth and invasion of DU-145 prostate cancer cells. J Immunol. 2006;177(12):8730-8739.

31.   Heinrichs D, Knauel M, Offermanns C, Berres M-L, Nellen A, Leng L, Schmitz P, Bucala R, Trautwein C, Weber C, Bernhagen J, Wasmuth HE. Macrophage migration inhibitory factor (MIF) exerts antifibrotic effects in experimental liver fibrosis via CD74. Proc Natl Acad Sci U S A. 2011;108(42):17444-17449.

32.   Vandenbark AA, Meza-Romero R, Wiedrick J, Gerstner G, Headrick A, Kent G, Seifert H, Benedek G, Bucala R, Offner H. Brief report: Enhanced DRα1-mMOG-35-55 treatment of severe EAE in MIF-1-deficient male mice. Cell Immunol. 2021:104439.

33.   Kleemann R, Kapurniotu A, Frank RW, Gessner A, Mischke R, Flieger O, Jüttner S, Brunner H, Bernhagen J. Disulfide analysis reveals a role for macrophage migration inhibitory factor (MIF) as thiol-protein oxidoreductase. J Mol Biol. 1998;280(1):85-102.

34.   Sinitski D, Gruner K, Brandhofer M, Kontos C, Winkler P, Reinstädler A, Bourilhon P, Xiao Z, Cool R, Kapurniotu A, Dekker FJ, Panstruga R, Bernhagen J. Cross-kingdom mimicry of the receptor signaling and leukocyte recruitment activity of a human cytokine by its plant orthologs. J Biol Chem. 2020;295(3):850-867.

35.   Bloom BR, Bennett B. Mechanism of a reaction in vitro associated with delayed-type hypersensitivity. Science. 1966;153(3731):80-82.

36.   David JR. Delayed hypersensitivity in vitro: its mediation by cell-free substances formed by lymphoid cell-antigen interaction. Proc Natl Acad Sci U S A. 1966;56(1):72.

37.   Coleman AM, Rendon BE, Zhao M, Qian MW, Bucala R, Xin D, Mitchell RA. Cooperative regulation of non-small cell lung carcinoma angiogenic potential by macrophage migration inhibitory factor and its homolog, D-dopachrome tautomerase. J Immunol. 2008 Aug 15;181(4):2330-7.

38.   Xin D, Rendon BE, Zhao M, Winner M, McGhee Coleman A, Mitchell RA. The MIF homologue D-dopachrome tautomerase promotes COX-2 expression through beta-catenin-dependent and -independent mechanisms. Mol Cancer Res. 2010 Dec;8(12):1601-9.

39.   Pasupuleti V, Du W, Gupta Y, Yeh IJ, Montano M, Magi-Galuzzi C, Welford SM. Dysregulated D-dopachrome tautomerase, a hypoxia-inducible factor-dependent gene, cooperates with macrophage migration inhibitory factor in renal tumorigenesis. J Biol Chem. 2014 Feb 7;289(6):3713-23.

40.   Guo D, Guo J, Yao J, Jiang K, Hu J, Wang B, Liu H, Lin L, Sun W, Jiang X. D-dopachrome tautomerase is over-expressed in pancreatic ductal adenocarcinoma and acts cooperatively with macrophage migration inhibitory factor to promote cancer growth. Int J Cancer. 2016 Nov 1;139(9):2056-67.

41.   Rendon BE, Roger T, Teneng I, Zhao M, Al-Abed Y, Calandra T, Mitchell RA. Regulation of human lung adenocarcinoma cell migration and invasion by macrophage migration inhibitory factor. J Biol Chem. 2007;282(41):29910-29918.

42.   White ES, Flaherty KR, Carskadon S, Brant A, Iannettoni MD, Yee J, Orringer MB, Arenberg DA. Macrophage migration inhibitory factor and CXC chemokine expression in non-small cell lung cancer: role in angiogenesis and prognosis. Clin Cancer Res. 2003;9(2):853-860.

43.   Mitchell RA, Liao H, Chesney J, Fingerle-Rowson G, Baugh J, David J, Bucala R.

Macrophage migration inhibitory factor (MIF) sustains macrophage proinflammatory function by inhibiting p53: regulatory role in the innate immune response. Proc Natl Acad Sci U S A. 2002;99(1):345-350.

44. Carli C, Metz CN, Al-Abed Y, Naccache PH, Akoum A. Up-regulation of cyclooxygenase-2 expression and prostaglandin E2 production in human endometriotic cells by macrophage migration inhibitory factor: involvement of novel kinase signaling pathways. Endocrinology. 2009;150(7):3128-3137.

45. Mann B, Gelos M, Siedow A, Hanski M, Gratchev A, Ilyas M, Bodmer W, Moyer M, Riecken E, Buhr H, Hanski C. Target genes of β-catenin–T cell-factor/lymphoid-enhancer-factor signaling in human colorectal carcinomas. Proc Natl Acad Sci U S A. 1999;96(4):1603-1608.

46. Araki Y, Okamura S, Hussain SP, Nagashima M, He P, Shiseki M, Miura K, Harris CC. Regulation of cyclooxygenase-2 expression by the Wnt and ras pathways. Cancer Res. 2003;63(3):728-734.

47. Cuthbert R, Wilson J, Scott N, Coletta P, Hull M. Differential CD74 (major histocompatibility complex Class II invariant chain) expression in mouse and human intestinal adenomas. Eur J Cancer. 2009;45(9):1654-1663.

48. Cheng R-j, Deng W-g, Niu C-b, Li Y-y, Fu Y. Expression of macrophage migration inhibitory factor and CD74 in cervical squamous cell carcinoma. Int J Gynecol Cancer. 2011;21(6).

49. Guo P, Wang J, Liu J, Xia M, Li W, He M. Macrophage immigration inhibitory factor promotes cell proliferation and inhibits apoptosis of cervical adenocarcinoma. Tumour Biol. 2015;36(7):5095-5102.

50. Wang Q, Wei Y, Zhang J. Combined Knockdown of D-dopachrome Tautomerase and Migration Inhibitory Factor Inhibits the Proliferation, Migration, and Invasion in Human Cervical Cancer. Int J Gynecol Cancer. 2017 May;27(4):634-642.

51. Cavalli E, Mazzon E, Mammana S, Basile MS, Lombardo SD, Mangano K, Bramanti P, Nicoletti F, Fagone P, Petralia MC. Overexpression of Macrophage Migration Inhibitory Factor and Its Homologue D-Dopachrome Tautomerase as Negative Prognostic Factor in Neuroblastoma. Brain Sci. 2019 Oct 19;9(10).

52. Tilstam PV, Schulte W, Holowka T, Kim BS, Nouws J, Sauler M, Piecychna M, Pantouris G, Lolis E, Leng L, Bernhagen J, Fingerle-Rowson G, Bucala R. MIF but not MIF-2 recruits inflammatory macrophages in an experimental polymicrobial sepsis model. J Clin Invest. 2021 Dec 1;131(23).

53. Rajasekaran D, Zierow S, Syed M, Bucala R, Bhandari V, Lolis EJ. Targeting distinct tautomerase sites of D-DT and MIF with a single molecule for inhibition of neutrophil lung recruitment. FASEB J. 2014;28(11):4961-4971.

54. Winner M, Meier J, Zierow S, Rendon BE, Crichlow GV, Riggs R, Bucala R, Leng L, Smith N, Lolis E, Trent JO, Mitchell RA. A novel, macrophage migration inhibitory factor suicide substrate inhibits motility and growth of lung cancer cells. Cancer Res. 2008;68(18):7253-7257.

55. Lolis E, Bucala R. Therapeutic approaches to innate immunity: severe sepsis and septic shock. Nat Rev Drug Discov. 2003;2(8):635-645.

56. Cournia Z, Leng L, Gandavadi S, Du X, Bucala R, Jorgensen WL. Discovery of human macrophage migration inhibitory factor (MIF)-CD74 antagonists via virtual screening. J Med Chem. 2009;52(2):416-424.

57. Fasshauer M, Blüher M. Adipokines in health and disease. Trends Pharmacol Sci. 2015;36(7):461-470.

58. Ishimoto K, Iwata T, Taniguchi H, Mizusawa N, Tanaka E, Yoshimoto K. D-dopachrome tautomerase promotes IL-6 expression and inhibits adipogenesis in

preadipocytes. Cytokine. 2012 Dec;60(3):772-7.

59.   Iwata T, Taniguchi H, Kuwajima M, Taniguchi T, Okuda Y, Sukeno A, Ishimoto K, Mizusawa N, Yoshimoto K. The action of D-dopachrome tautomerase as an adipokine in adipocyte lipid metabolism. PLoS One. 2012;7(3):e33402.

60.   Gr S, Be K. amPK in health and disease. Physiol Rev. 2009;89:1025-1078.

61.   GARTON AJ, YEAMAN SJ. Identification and role of the basal phosphorylation site on hormone-sensitive lipase. Eur J Biochem. 1990;191(1):245-250.

62.   Atsumi T, Cho Y-R, Leng L, McDonald C, Yu T, Danton C, Hong E-G, Mitchell RA, Metz C, Niwa H, Takeuchi J, Onodera S, Umino T, Yoshioka N, Koike T, Kim JK, Bucala R. The proinflammatory cytokine macrophage migration inhibitory factor regulates glucose metabolism during systemic inflammation. J Immunol. 2007;179(8):5399-5406.

63.   Verschuren L, Kooistra T, Bernhagen Jr, Voshol PJ, Ouwens DM, van Erk M, de Vries-van der Weij J, Leng L, van Bockel JH, van Dijk KW, Fingerle-Rowson G, Bucala R, Kleemann R. MIF deficiency reduces chronic inflammation in white adipose tissue and impairs the development of insulin resistance, glucose intolerance, and associated atherosclerotic disease. Circ Res. 2009;105(1):99-107.

64.   Iwata T, Kuribayashi K, Nakasono M, Saito-Tarashima N, Minakawa N, Mizusawa N, Kido R, Yoshimoto K. The AMPK/mTOR pathway is involved in D-dopachrome tautomerase gene transcription in adipocytes differentiated from SGBS cells, a human preadipocyte cell line. Cytokine. 2017 Aug;96:195-202.

65.   Kim BS, Tilstam PV, Arnke K, Leng L, Ruhl T, Piecychna M, Schulte W, Sauler M, Frueh FS, Storti G, Lindenblatt N, Giovanoli P, Pallua N, Bernhagen J, Bucala R. Differential regulation of macrophage activation by the MIF cytokine superfamily members MIF and MIF-2 in adipose tissue during endotoxemia. FASEB J. 2020.

66.   Qi D, Atsina K, Qu L, Hu X, Wu X, Xu B, Piecychna M, Leng L, Fingerle-Rowson G, Zhang J, Bucala R, Young LH. The vestigial enzyme D-dopachrome tautomerase protects the heart against ischemic injury. J Clin Invest. 2014;124(8):3540-3550.

67.   Miller EJ, Li J, Leng L, McDonald C, Atsumi T, Bucala R, Young LH. Macrophage migration inhibitory factor stimulates AMP-activated protein kinase in the ischaemic heart. Nature. 2008;451(7178):578-582.

68.   Gao X-M, Liu Y, White D, Su Y, Drew BG, Bruce CR, Kiriazis H, Xu Q, Jennings N, Bobik A, Febbraio MA, Kingwell BA, Bucala R, Fingerle-Rowson G, Dart AM, Morand EF, Du X-J. Deletion of macrophage migration inhibitory factor protects the heart from severe ischemia–reperfusion injury: a predominant role of anti-inflammation. J Mol Cell Cardiol. 2011;50(6):991-999.

69.   Garner LB, Willis MS, Carlson DL, DiMaio JM, White MD, White DJ, Adams IV GA, Horton JW, Giroir BP. Macrophage migration inhibitory factor is a cardiac-derived myocardial depressant factor. Am J Physiol Heart Circ Physiol. 2003;285(6):H2500-H2509.

70.   Ma Y, Su KN, Pfau D, Rao VS, Wu X, Hu X, Leng L, Du X, Piecychna M, Bedi K, Campbell SG, Eichmann A, Testani JM, Margulies KB, Bucala R, Young LH. Cardiomyocyte d-dopachrome tautomerase protects against heart failure. JCI Insight. 2019 Sep 5;4(17).

71.   Song S, Liu B, Habibie H, van den Bor J, Smit MJ, Gosens R, Wu X, Brandsma C-A, Cool RH, Haisma HJ, Poelarends GJ, Melgert BN. D-dopachrome tautomerase contributes to lung epithelial repair via atypical chemokine receptor 3-dependent Akt signaling. EBioMedicine. 2021;68:103412.

72.   Bernhagen J. A new cytokine target for chronic obstructive pulmonary disease? EBioMedicine. 2021;69.

73.   Sauler M, Leng L, Trentalange M, Haslip M, Shan P, Piecychna M, Zhang Y, Andrews N, Mannam P, Allore H, Fried T, Bucala R, Lee PJ. Macrophage migration inhibitory factor deficiency in chronic obstructive pulmonary disease. Am J Physiol Lung Cell Mol Physiol. 2014;306(6):L487-L496.

74.   Kim S-J, Wan F, Zhang X, Zhang Y, Ifedigbo E, Leng L, Bucala R, Sauler M, Lee P. MIF-CD74 Signaling Protects against Endothelial Senescence in Chronic Obstructive Pulmonary Disease. FASEB J. 2020;34(S1):1-1.

75.   Hiyoshi M, Konishi H, Uemura H, Matsuzaki H, Tsukamoto H, Sugimoto R, Takeda H, Dakeshita S, Kitayama A, Takami H, Sawachika F, Kido H, Arisawa K. D-Dopachrome tautomerase is a candidate for key proteins to protect the rat liver damaged by carbon tetrachloride. Toxicology. 2009 Jan 8;255(1-2):6-14.

76.   Strey CW, Winters MS, Markiewski MM, Lambris JD. Partial hepatectomy induced liver proteome changes in mice. Proteomics. 2005;5(1):318-325.

77.   Yang F, Yan S, He Y, Wang F, Song S, Guo Y, Zhou Q, Wang Y, Lin Z, Yang Y, Zhang W, Sun S. Expression of hepatitis B virus proteins in transgenic mice alters lipid metabolism and induces oxidative stress in the liver. J Hepatol. 2008;48(1):12-19.

78.   Sonesson B, Rosengren E, Hansson AS, Hansson C. UVB-induced inflammation gives increased d-dopachrome tautomerase activity in blister fluid which correlates with macrophage migration inhibitory factor. Exp Dermatol. 2003;12(3):278-282.

79.   Schwarz T, Luger T. New trends in photobiology: Effect of UV irradiation on epidermal cell cytokine production. J Photochem Photobiol B. 1989;4(1):1-13.

80.   Kim BS, Tilstam PV, Hwang SS, Simons D, Schulte W, Leng L, Sauler M, Ganse B, Averdunk L, Kopp R, Stoppe C, Bernhagen J, Pallua N, Bucala R. D-dopachrome tautomerase in adipose tissue inflammation and wound repair. J Cell Mol Med. 2017;21(1):35-45.

81.   Kim B-S, Stoppe C, Grieb G, Leng L, Sauler M, Assis D, Simons D, Boecker AH, Schulte W, Piecychna M, Hager S, Bernhagen J, Pallua N, Bucala R. The clinical significance of the MIF homolog d-dopachrome tautomerase (MIF-2) and its circulating receptor (sCD74) in burn. Burns. 2016;42(6):1265-1276.

82.   Grieb G, Simons D, Piatkowski A, Bernhagen J, Steffens G, Pallua N. Macrophage migration inhibitory factor—A potential diagnostic tool in severe burn injuries? Burns. 2010;36(3):335-342.

83.   Pohl J, Hendgen-Cotta UB, Stock P, Luedike P, Rassaf T. Elevated MIF-2 levels predict mortality in critically ill patients. J Crit Care. 2017;40:52-57.

84.   Bauer J, Huitinga I, Zhao W, Lassmann H, Hickey WF, Dijkstra CD. The role of macrophages, perivascular cells, and microglial cells in the pathogenesis of experimental autoimmune encephalomyelitis. Glia. 1995;15(4):437-446.

85.   Niino M, Ogata A, Kikuchi S, Tashiro K, Nishihira J. Macrophage migration inhibitory factor in the cerebrospinal fluid of patients with conventional and optic-spinal forms of multiple sclerosis and neuro-Behcet's disease. J Neurol Sci. 2000;179(1-2):127-131.

86.   Cox GM, Kithcart AP, Pitt D, Guan Z, Alexander J, Williams JL, Shawler T, Dagia NM, Popovich PG, Satoskar AR, Whitacre CC. Macrophage migration inhibitory factor potentiates autoimmune-mediated neuroinflammation. J Immunol. 2013;191(3):1043-1054.

87.   Benedek G, Meza-Romero R, Jordan K, Zhang Y, Nguyen H, Kent G, Li J, Siu E, Frazer J, Piecychna M, Du X, Sreih A, Leng L, Wiedrick J, Caillier SJ, Offner H, Oksenberg JR, Yadav V, Bourdette D, Bucala R, Vandenbark AA. MIF and D-DT are potential disease severity modifiers in male MS subjects. Proc Natl Acad Sci U S A. 2017;114(40):E8421-E8429.

88.   Akcali A, Pehlivan S, Pehlivan M, Sever T, Neyal M. Association of macrophage migration inhibitory factor gene promoter polymorphisms with multiple sclerosis in Turkish patients. J Int Med Res. 2010;38(1):69-77.

89.   Han Z, Qu J, Zhao J, Zou X. Genetic Variant rs755622 Regulates Expression of the Multiple Sclerosis Severity Modifier D-Dopachrome Tautomerase in a Sex-Specific Way. Biomed Res Int. 2018;2018:8285653.

90.   Cavalli E, Mazzon E, Basile MS, Mangano K, Di Marco R, Bramanti P, Nicoletti F, Fagone P, Petralia MC. Upregulated Expression of Macrophage Migration Inhibitory Factor, Its Analogue D-Dopachrome Tautomerase, and the CD44 Receptor in Peripheral CD4 T Cells from Clinically Isolated Syndrome Patients with Rapid Conversion to Clinical Defined Multiple Sclerosis. Medicina (Kaunas). 2019 Oct 1;55(10).

91.   Stefanantoni K, Sciarra I, Vasile M, Badagliacca R, Poscia R, Pendolino M, Alessandri C, Vizza C, Valesini G, Riccieri V. Elevated serum levels of macrophage migration inhibitory factor and stem cell growth factor β in patients with idiopathic and systemic sclerosis associated pulmonary arterial hypertension. Reumatismo. 2014:270-276.

92.   Corallo C, Paulesu L, Cutolo M, Ietta F, Carotenuto C, Mannelli C, Romagnoli R, Nuti R, Giordano N. Serum levels, tissue expression and cellular secretion of macrophage migration inhibitory factor in limited and diffuse systemic sclerosis. Clin Exp Rheumatol. 2015;33(4 Suppl 91):S98-S105.

93.   Vincent FB, Lin E, Sahhar J, Ngian GS, Kandane-Rathnayake R, Mende R, Hoi AY, Morand EF, Lang T, Harris J. Analysis of serum macrophage migration inhibitory factor and D-dopachrome tautomerase in systemic sclerosis. Clin Transl Immunology. 2018;7(12):e1042.

94.   Roger T, Schlapbach LJ, Schneider A, Weier M, Wellmann S, Marquis P, Vermijlen D, Sweep FC, Leng L, Bucala R, Calandra T, Giannoni E. Plasma Levels of Macrophage Migration Inhibitory Factor and d-Dopachrome Tautomerase Show a Highly Specific Profile in Early Life. Front Immunol. 2017;8:26.

95.   Baron-Stefaniak J, Schiefer J, Lichtenegger P, Miller EJ, Berlakovich GA, Faybik P, Baron DM. D-dopachrome tautomerase predicts outcome but not the development of acute kidney injury after orthotopic liver transplantation. HPB (Oxford). 2019 Apr;21(4):465-472.

96.   Murray CJ, Lopez AD. Global mortality, disability, and the contribution of risk factors: Global Burden of Disease Study. The Lancet. 1997;349(9063):1436-1442.

97.   Ross R. Atheroslcerosis-an inflammatory disease. N Engl J Med. 1999;340:115-126.

98.   Virchow R, CHANCE F. Cellular Pathology as based upon physiological and pathological histology. Twenty lectures delivered in... 1858. Translated from the second edition of the original by F. Chance. With notes and numerous emendations principally from MS. notes of the author, and illustrated by... engravings on wood. 1860.

99.   Libby P, Ridker PM, Maseri A. Inflammation and atherosclerosis. Circulation. 2002;105(9):1135-1143.

100.   Libby P, Ridker PM. Inflammation and atherothrombosis: from population biology and bench research to clinical practice. J Am Coll Cardiol. 2006;48(9 Supplement):A33-A46.

101.   Libby P, Okamoto Y, Rocha VZ, Folco E. Inflammation in atherosclerosis: transition from theory to practice. Circ J. 2010;74(2):213-220.

102.   Libby P, Lichtman AH, Hansson GK. Immune effector mechanisms implicated in atherosclerosis: from mice to humans. Immunity. 2013;38(6):1092-1104.

103.   Libby P, Hansson GK. From focal lipid storage to systemic inflammation: JACC

review topic of the week. J Am Coll Cardiol. 2019;74(12):1594-1607.

104. Ridker PM, Everett BM, Thuren T, MacFadyen JG, Chang WH, Ballantyne C, Fonseca F, Nicolau J, Koenig W, Anker SD, Kastelein JJP, Cornel JH, Pais P, Pella D, Genest J, Cifkova R, Lorenzatti A, Forster T, Kobalava Z, Vida-Simiti L, Flather M, Shimokawa H, Ogawa H, Dellborg M, Rossi PRF, Troquay RPT, Libby P, Glynn RJ, Group CT. Antiinflammatory therapy with canakinumab for atherosclerotic disease. N Engl J Med. 2017;377(12):1119-1131.

105. Libby P, Bornfeldt KE. How Far We Have Come, How Far We Have Yet to Go in Atherosclerosis Research. Circ Res. 2020;126(9):1107-1111.

106. Williams JW, Winkels H, Durant CP, Zaitsev K, Ghosheh Y, Ley K. Single cell RNA sequencing in atherosclerosis research. Circ Res. 2020;126(9):1112-1126.

107. Charo IF, Ransohoff RM. The many roles of chemokines and chemokine receptors in inflammation. N Engl J Med. 2006;354(6):610-621.

108. Bachelerie F, Ben-Baruch A, Burkhardt AM, Combadiere C, Farber JM, Graham GJ, Horuk R, Sparre-Ulrich AH, Locati M, Luster AD, Mantovani A, Matsushima K, Murphy PM, Nibbs R, Nomiyama H, Power CA, Proudfoot AEI, Rosenkilde MM, Rot A, Sozzani S, Thelen M, Yoshie O, Zlotnik A. International Union of Basic and Clinical Pharmacology. LXXXIX. Update on the extended family of chemokine receptors and introducing a new nomenclature for atypical chemokine receptors. Pharmacol Rev. 2014;66(1):1-79.

109. Luster AD. Chemokines—chemotactic cytokines that mediate inflammation. N Engl J Med. 1998;338(7):436-445.

110. Lukacs NW, Oliveira SH, Hogaboam CM. Chemokines and asthma: redundancy of function or a coordinated effort? J Clin Invest. 1999;104(8):995-999.

111. Inoue S, Egashira K, Ni W, Kitamoto S, Usui M, Otani K, Ishibashi M, Hiasa K-i, Nishida K-i, Takeshita A. Anti-monocyte chemoattractant protein-1 gene therapy limits progression and destabilization of established atherosclerosis in apolipoprotein E–knockout mice. Circulation. 2002;106(21):2700-2706.

112. de Jager SC, Bot I, Kraaijeveld AO, Korporaal SJ, Bot M, van Santbrink PJ, van Berkel TJ, Kuiper J, Biessen EA. Leukocyte-specific CCL3 deficiency inhibits atherosclerotic lesion development by affecting neutrophil accumulation. Arterioscler Thromb Vasc Biol. 2013;33(3):e75-e83.

113. Krohn R, Raffetseder U, Bot I, Zernecke A, Shagdarsuren E, Liehn E, Santbrink PVv, Nelson P, Biessen E, Mertens P, Weber C. Y-Box Binding Protein-1 Controls CC Chemokine Ligand-5 (CCL5) Expression in Smooth Muscle Cells and Contributes to Neointima Formation in Atherosclerosis-Prone Mice. Circulation. 2007;116:1812-1820.

114. Weber C, Meiler S, Döring Y, Koch M, Drechsler M, Megens RT, Rowinska Z, Bidzhekov K, Fecher C, Ribechini E, van Zandvoort MAMJ, Binder CJ, Jelinek I, Hristov M, Boon L, Jung S, Korn T, Lutz MB, Förster I, Zenke M, Hieronymus T, Junt T, Zernecke A. CCL17-expressing dendritic cells drive atherosclerosis by restraining regulatory T cell homeostasis in mice. J Clin Invest. 2011;121(7):2898-2910.

115. Akhavanpoor M, Gleissner CA, Gorbatsch S, Doesch AO, Akhavanpoor H, Wangler S, Jahn F, Lasitschka F, Katus HA, Erbel C. CCL19 and CCL21 modulate the inflammatory milieu in atherosclerotic lesions. Drug Des Devel Ther. 2014;8:2359.

116. Liehn EA, Schober A, Weber C. Blockade of keratinocyte-derived chemokine inhibits endothelial recovery and enhances plaque formation after arterial injury in ApoE-deficient mice. Arterioscler Thromb Vasc Biol. 2004;24(10):1891-1896.

117. Stachon P, Peikert A, Michel NA, Hergeth S, Marchini T, Wolf D, Dufner B, Hoppe

N, Ayata CK, Grimm M, Cicko S, Schulte L, Reinöhl J, von zur Muhlen C, Bode C, Idzko M, Zirlik A. P2Y6 deficiency limits vascular inflammation and atherosclerosis in mice. Arterioscler Thromb Vasc Biol. 2014;34(10):2237-2245.

118.   Sachais BS, Turrentine T, McKenna JMD, Rux AH, Rader D, Kowalska AM. Elimination of platelet factor 4 (PF4) from platelets reduces atherosclerosis in C57Bl/6 and apoE-/-mice. Thromb Haemost. 2007;98(11):1108-1113.

119.   Rousselle A, Qadri F, Leukel L, Yilmaz R, Fontaine J-F, Sihn G, Bader M, Ahluwalia A, Duchene J. CXCL5 limits macrophage foam cell formation in atherosclerosis. J Clin Invest. 2013;123(3):1343-1347.

120.   Heller EA, Liu E, Tager AM, Yuan Q, Lin AY, Ahluwalia N, Jones K, Koehn SL, Lok VM, Aikawa E, Moore KJ, Luster AD, Gerszten RE. Chemokine CXCL10 promotes atherogenesis by modulating the local balance of effector and regulatory T cells. Circulation. 2006;113(19):2301-2312.

121.   Zernecke A, Bot I, Djalali-Talab Y, Shagdarsuren E, Bidzhekov K, Meiler S, Krohn R, Schober A, Sperandio M, Soehnlein O, Bornemann J, Tacke F, Biessen EA, Weber C. Protective role of CXC receptor 4/CXC ligand 12 unveils the importance of neutrophils in atherosclerosis. Circ Res. 2008;102(2):209-217.

122.   Chatterjee M, von Ungern-Sternberg SN, Seizer P, Schlegel F, Büttcher M, Sindhu N, Müller S, Mack A, Gawaz M. Platelet-derived CXCL12 regulates monocyte function, survival, differentiation into macrophages and foam cells through differential involvement of CXCR4–CXCR7. Cell Death Dis. 2015;6(11):e1989-e1989.

123.   Merckelbach S, van der Vorst EP, Kallmayer M, Rischpler C, Burgkart R, Döring Y, de Borst G-J, Schwaiger M, Eckstein H-H, Weber C, Pelisek J. Expression and cellular localization of CXCR4 and CXCL12 in human carotid atherosclerotic plaques. Thromb Haemost. 2018;118(01):195-206.

124.   Aslanian AM, Charo IF. Targeted disruption of the scavenger receptor and chemokine CXCL16 accelerates atherosclerosis. Circulation. 2006;114(6):583-590.

125.   Riopel M, Vassallo M, Ehinger E, Pattison J, Bowden K, Winkels H, Wilson M, de Jong R, Patel S, Balakrishna D, Bilakovics J, Fanjul A, Plonowski A, Larson CJ, Ley K, Cabrales P, Witztum JL, Olefsky JM, Lee YS. CX3CL1-Fc treatment prevents atherosclerosis in Ldlr KO mice. Mol Metab. 2019;20:89-101.

126.   Schober A, Bernhagen J, Weber C. Chemokine-like functions of MIF in atherosclerosis. J Mol Med. 2008;86(7):761-770.

127.   Kapurniotu A, Gokce O, Bernhagen J. The multitasking potential of alarmins and atypical chemokines. Front Med (Lausanne). 2019;6:3.

128.   Kalinina N, Agrotis A, Antropova Y, DiVitto G, Kanellakis P, Kostolias G, Ilyinskaya O, Tararak E, Bobik A. Increased expression of the DNA-binding cytokine HMGB1 in human atherosclerotic lesions: role of activated macrophages and cytokines. Arterioscler Thromb Vasc Biol. 2004;24(12):2320-2325.

129.   Porto A, Palumbo R, Pieroni M, Aprigliano G, Chiesa R, Sanvito F, Maseri A, Bianchi ME. Smooth muscle cells in human atherosclerotic plaques secrete and proliferate in response to high mobility group box 1 protein. FASEB J. 2006;20(14):2565-2566.

130.   Fiuza C, Bustin M, Talwar S, Tropea M, Gerstenberger E, Shelhamer JH, Suffredini AF. Inflammation-promoting activity of HMGB1 on human microvascular endothelial cells. Blood. 2003;101(7):2652-2660.

131.   Ito T, Maruyama I. Thrombomodulin: protectorate God of the vasculature in thrombosis and inflammation. J Thromb Haemost. 2011;9:168-173.

132.   Inoue K, Kawahara K-i, Biswas KK, Ando K, Mitsudo K, Nobuyoshi M, Maruyama I. HMGB1 expression by activated vascular smooth muscle cells in advanced human atherosclerosis plaques. Cardiovasc Pathol. 2007;16(3):136-143.

133. Kake S, Kawaguchi H, Nagasato T, Yamada T, Ito T, Maruyama I, Miura N, Tanimoto A. Association between HMGB1 and thrombogenesis in a hyperlipaemia-induced microminipig model of atherosclerosis. In Vivo. 2020;34(4):1871-1874.

134. Kanellakis P, Agrotis A, Kyaw TS, Koulis C, Ahrens I, Mori S, Takahashi HK, Liu K, Peter K, Nishibori M, Bobik A. High-mobility group box protein 1 neutralization reduces development of diet-induced atherosclerosis in apolipoprotein E–deficient mice. Arterioscler Thromb Vasc Biol. 2011;31(2):313-319.

135. Schiraldi M, Raucci A, Muñoz LM, Livoti E, Celona B, Venereau E, Apuzzo T, De Marchis F, Pedotti M, Bachi A, Thelen M, Varani L, Mellado M, Proudfoot A, Bianchi ME, Uguccioni M. HMGB1 promotes recruitment of inflammatory cells to damaged tissues by forming a complex with CXCL12 and signaling via CXCR4. J Exp Med. 2012;209(3):551-563.

136. Cipollone F, Iezzi A, Fazia M, Zucchelli M, Pini B, Cuccurullo C, De Cesare D, De Blasis G, Muraro R, Bei R, Chiarelli F, Schmidt AM, Cuccurullo F, Mezzetti A. The receptor RAGE as a progression factor amplifying arachidonate-dependent inflammatory and proteolytic response in human atherosclerotic plaques: role of glycemic control. Circulation. 2003;108(9):1070-1077.

137. Harja E, Bu D-x, Hudson BI, Chang JS, Shen X, Hallam K, Kalea AZ, Lu Y, Rosario RH, Oruganti S, Nikolla Z, Belov D, Lalla E, Ramasamy R, Yan SF, Schmidt AM. Vascular and inflammatory stresses mediate atherosclerosis via RAGE and its ligands in apoE–/–mice. J Clin Invest. 2008;118(1):183-194.

138. Liu M, Yu Y, Jiang H, Zhang L, Zhang P-p, Yu P, Jia J-g, Chen R-z, Zou Y-z, Ge J-b. Simvastatin suppresses vascular inflammation and atherosclerosis in ApoE−/− mice by downregulating the HMGB1-RAGE axis. Acta Pharmacol Sin. 2013;34(6):830-836.

139. Wu CY, Zhou ZF, Wang B, Ke ZP, Ge ZC, Zhang XJ. MicroRNA-328 ameliorates oxidized low-density lipoprotein-induced endothelial cells injury through targeting HMGB1 in atherosclerosis. J Cell Biochem. 2019;120(2):1643-1650.

140. Taylor K, Clarke DJ, McCullough B, Chin W, Seo E, Yang D, Oppenheim J, Uhrin D, Govan JR, Campopiano DJ, MacMillan D, Barran P, Dorin JR. Analysis and separation of residues important for the chemoattractant and antimicrobial activities of β-defensin 3. J Biol Chem. 2008;283(11):6631-6639.

141. Röhrl J, Yang D, Oppenheim JJ, Hehlgans T. Human β-defensin 2 and 3 and their mouse orthologs induce chemotaxis through interaction with CCR2. J Immunol. 2010;184(12):6688-6694.

142. Li L, Bian T, Lyu J, Cui D, Lei L, Yan F. Human β-defensin-3 alleviates the progression of atherosclerosis accelerated by Porphyromonas gingivalis lipopolysaccharide. Int Immunopharmacol. 2016;38:204-213.

143. Bian T, Li L, Lyu J, Cui D, Lei L, Yan F. Human β-defensin 3 suppresses Porphyromonas gingivalis lipopolysaccharide-induced inflammation in RAW 264.7 cells and aortas of ApoE-deficient mice. Peptides. 2016;82:92-100.

144. Ann S-j, Chung JH, Park BH, Kim SH, Jang J, Park S, Kang S-M, Lee S-H. PPARα agonists inhibit inflammatory activation of macrophages through upregulation of β-defensin 1. Atherosclerosis. 2015;240(2):389-397.

145. Tiszlavicz Z, Endrész V, Németh B, Megyeri K, Orosz L, Seprényi G, Mándi Y. Inducible expression of human β-defensin 2 by Chlamydophila pneumoniae in brain capillary endothelial cells. Innate Immun. 2011;17(5):463-469.

146. Rhee SG, Kil IS. Multiple functions and regulation of mammalian peroxiredoxins. Annu Rev Biochem. 2017;86:749-775.

147. Moore KJ, Tabas I. Macrophages in the pathogenesis of atherosclerosis. Cell.

2011;145(3):341-355.

148. Hadri KE, Mahmood DFD, Couchie D, Jguirim-Souissi I, Genze F, Diderot V, Syrovets T, Lunov O, Simmet T, Rouis M. Thioredoxin-1 promotes anti-inflammatory macrophages of the M2 phenotype and antagonizes atherosclerosis. Arterioscler Thromb Vasc Biol. 2012;32(6):1445-1452.

149. Li W, Xu X, Dong D, Lei T, Ou H. Up-regulation of thioredoxin system by puerarin inhibits lipid uptake in macrophages. Free Radic Biol Med. 2020.

150. Wang Y, Ji N, Gong X, Ni S, Xu L, Zhang H. Thioredoxin-1 attenuates atherosclerosis development through inhibiting NLRP3 inflammasome. Endocrine. 2020;70(1):65-70.

151. Wang X, Zhao H, Yan W, Liu Y, Yin T, Wang S, Fan M, Li C, Zhang L, Tao L. Thioredoxin-1 promotes macrophage reverse cholesterol transport and protects liver from steatosis. Biochem Biophys Res Commun. 2019;516(4):1103-1109.

152. Burger-Kentischer A, Goebel H, Seiler Rd, Fraedrich G, Schaefer HE, Dimmeler S, Kleemann R, Bernhagen Jr, Ihling C. Expression of macrophage migration inhibitory factor in different stages of human atherosclerosis. Circulation. 2002;105(13):1561-1566.

153. Luedike P, Hendgen-Cotta UB, Sobierajski J, Totzeck M, Reeh M, Dewor M, Lue H, Krisp C, Wolters D, Kelm M, Bernhagen J, Rassaf T. Cardioprotection through S-nitros (yl) ation of macrophage migration inhibitory factor. Circulation. 2012;125(15):1880-1889.

154. Schmeisser A, Marquetant R, Illmer T, Graffy C, Garlichs CD, Böckler D, Menschikowski D, Braun-Dullaeus R, Daniel WG, Strasser RH. The expression of macrophage migration inhibitory factor 1α (MIF 1α) in human atherosclerotic plaques is induced by different proatherogenic stimuli and associated with plaque instability. Atherosclerosis. 2005;178(1):83-94.

155. Kontos C, El Bounkari O, Krammer C, Sinitski D, Hille K, Zan C, Yan G, Wang S, Gao Y, Brandhofer M, Megens RTA, Hoffmann A, Pauli J, Asare Y, Gerra S, Bourilhon P, Leng L, Eckstein H-H, Kempf WE, Pelisek J, Gokce O, Maegdefessel L, Bucala R, Dichgans M, Weber C, Kapurniotu A, Bernhagen J. Designed CXCR4 mimic acts as a soluble chemokine receptor that blocks atherogenic inflammation by agonist-specific targeting. Nat Commun. 2020;11(1):1-18.

156. Chen Z, Sakuma M, Zago AC, Zhang X, Shi C, Leng L, Mizue Y, Bucala R, Simon DI. Evidence for a role of macrophage migration inhibitory factor in vascular disease. Arterioscler Thromb Vasc Biol. 2004;24(4):709-714.

157. Burger-Kentischer A, Göbel H, Kleemann R, Zernecke A, Bucala R, Leng L, Finkelmeier D, Geiger G, Schaefer HE, Schober A, Weber C, Brunner H, Rütten H, Ihling C, Bernhagen J. Reduction of the aortic inflammatory response in spontaneous atherosclerosis by blockade of macrophage migration inhibitory factor (MIF). Atherosclerosis. 2006;184(1):28-38.

158. Lin S-G, Yu X-Y, Chen Y-X, Huang XR, Metz C, Bucala R, Lau C-P, Lan HY. De novo expression of macrophage migration inhibitory factor in atherogenesis in rabbits. Circ Res. 2000;87(12):1202-1208.

159. Schober A, Bernhagen J, Thiele M, Zeiffer U, Knarren S, Roller M, Bucala R, Weber C. Stabilization of atherosclerotic plaques by blockade of macrophage migration inhibitory factor after vascular injury in apolipoprotein E–deficient mice. Circulation. 2004;109(3):380-385.

160. Wirtz TH, Tillmann S, Strüßmann T, Kraemer S, Heemskerk JW, Grottke O, Gawaz M, von Hundelshausen P, Bernhagen J. Platelet-derived MIF: a novel platelet chemokine with distinct recruitment properties. Atherosclerosis. 2015;239(1):1-10.

161.   Klasen C, Ohl K, Sternkopf M, Shachar I, Schmitz C, Heussen N, Hobeika E, Levit-Zerdoun E, Tenbrock K, Reth M, Bernhagen J, El Bounkari O. MIF promotes B cell chemotaxis through the receptors CXCR4 and CD74 and ZAP-70 signaling. J Immunol. 2014;192(11):5273-5284.

162.   Asare Y, Schmitt M, Bernhagen J. The vascular biology of macrophage migration inhibitory factor (MIF). Thromb Haemost. 2013;109(3):391-398.

163.   Schwartz V, Lue H, Kraemer S, Korbiel J, Krohn R, Ohl K, Bucala R, Weber C, Bernhagen J. A functional heteromeric MIF receptor formed by CD74 and CXCR4. FEBS Lett. 2009;583(17):2749-2757.

164.   Sanz J, Fayad ZA. Imaging of atherosclerotic cardiovascular disease. Nature. 2008;451(7181):953-957.

165.   Pantouris G, Bucala R, Lolis EJ. Structural plasticity in the C-terminal region of macrophage migration inhibitory factor-2 is associated with an induced fit mechanism for a selective inhibitor. Biochemistry. 2018;57(26):3599-3605.

166.   Tilstam PV, Pantouris G, Corman M, Andreoli M, Mahboubi K, Davis G, Du X, Leng L, Lolis E, Bucala R. A selective small-molecule inhibitor of macrophage migration inhibitory factor-2 (MIF-2), a MIF cytokine superfamily member, inhibits MIF-2 biological activity. J Biol Chem. 2019;294(49):18522-18531.

167.   Sayiner M, Koenig A, Henry L, Younossi ZM. Epidemiology of nonalcoholic fatty liver disease and nonalcoholic steatohepatitis in the United States and the rest of the world. Clin Liver Dis. 2016;20(2):205-214.

168.   Tsochatzis EA, Bosch J, Burroughs AK. Liver cirrhosis. The Lancet. 2014;383(9930):1749-1761.

169.   Musso G, Gambino R, Cassader M. Recent insights into hepatic lipid metabolism in non-alcoholic fatty liver disease (NAFLD). Prog Lipid Res. 2009;48(1):1-26.

170.   Satapathy SK, Sanyal AJ. Epidemiology and natural history of nonalcoholic fatty liver disease. Semin Liver Dis. 2015;35(03):221-235.

171.   Hamabe A, Uto H, Imamura Y, Kusano K, Mawatari S, Kumagai K, Kure T, Tamai T, Moriuchi A, Sakiyama T, Oketani M, Ido A, Tsubouchi H. Impact of cigarette smoking on onset of nonalcoholic fatty liver disease over a 10-year period. J Gastroenterol. 2011;46(6):769-778.

172.   Carnethon MR, Fortmann SP, Palaniappan L, Duncan BB, Schmidt MI, Chambless LE. Risk factors for progression to incident hyperinsulinemia: the Atherosclerosis Risk in Communities Study, 1987–1998. Am J Epidemiol. 2003;158(11):1058-1067.

173.   Weitzman M, Cook S, Auinger P, Florin TA, Daniels S, Nguyen M, Winickoff JP. Tobacco smoke exposure is associated with the metabolic syndrome in adolescents. Circulation. 2005;112(6):862-869.

174.   Zelber-Sagi S, Godos J, Salomone F. Lifestyle changes for the treatment of nonalcoholic fatty liver disease: a review of observational studies and intervention trials. Therap Adv Gastroenterol. 2016;9(3):392-407.

175.   Kalia HS, Gaglio PJ. The Prevalence and Pathobiology of Nonalcoholic Fatty Liver Disease in Patients of Different Races or Ethnicities. Clin Liver Dis. 2016;20(2):215-224.

176.   Lonardo A, Bellentani S, Argo CK, Ballestri S, Byrne CD, Caldwell SH, Cortez-Pinto H, Grieco A, Machado MV, Miele L, Targher G. Epidemiological modifiers of non-alcoholic fatty liver disease: Focus on high-risk groups. Dig Liver Dis. 2015;47(12):997-1006.

177.   Kanwar P, Kowdley KV. The metabolic syndrome and its influence on nonalcoholic steatohepatitis. Clin Liver Dis. 2016;20(2):225-243.

178.   Macut D, Tziomalos K, Božić-Antić I, Bjekić-Macut J, Katsikis I, Papadakis E, Andrić

Z, Panidis D. Non-alcoholic fatty liver disease is associated with insulin resistance and lipid accumulation product in women with polycystic ovary syndrome. Hum Reprod. 2016;31(6):1347-1353.

179. Paschetta E, Belci P, Alisi A, Liccardo D, Cutrera R, Musso G, Nobili V. OSAS-related inflammatory mechanisms of liver injury in nonalcoholic fatty liver disease. Mediators Inflamm. 2015;2015.

180. Marra F, Tacke F. Roles for chemokines in liver disease. Gastroenterology. 2014;147(3):577-594. e1.

181. Berres M-L, Nellen A, Wasmuth HE. Chemokines as immune mediators of liver diseases related to the metabolic syndrome. Dig Dis. 2010;28(1):192-196.

182. Wehr A, Baeck C, Heymann F, Niemietz PM, Hammerich L, Martin C, Zimmermann HW, Pack O, Gassler N, Hittatiya K, Ludwig A, Luedde T, Trautwein C, Tacke F. Chemokine receptor CXCR6-dependent hepatic NK T Cell accumulation promotes inflammation and liver fibrosis. J Immunol. 2013;190(10):5226-5236.

183. Heinrichs D, Brandt EF, Fischer P, Köhncke J, Wirtz TH, Guldiken N, Djudjaj S, Boor P, Kroy D, Weiskirchen R, Bucala R, Wasmuth HE, Strnad P, Trautwein C, Bernhagen J, Berres M-L. Unexpected Pro-Fibrotic Effect of MIF in Non-Alcoholic Steatohepatitis Is Linked to a Shift in NKT Cell Populations. Cells. 2021;10(2):252.

184. Dambach DM, Watson LM, Gray KR, Durham SK, Laskin DL. Role of CCR2 in macrophage migration into the liver during acetaminophen-induced hepatotoxicity in the mouse. Hepatology. 2002;35(5):1093-1103.

185. Karlmark KR, Weiskirchen R, Zimmermann HW, Gassler N, Ginhoux F, Weber C, Merad M, Luedde T, Trautwein C, Tacke F. Hepatic recruitment of the inflammatory Gr1+ monocyte subset upon liver injury promotes hepatic fibrosis. Hepatology. 2009;50(1):261-274.

186. Ramm GA. Chemokine (C-C motif) receptors in fibrogenesis and hepatic regeneration following acute and chronic liver disease. Hepatology. 2009;50(5):1664-1668.

187. Marra F, Valente AJ, Pinzani M, Abboud HE. Cultured human liver fat-storing cells produce monocyte chemotactic protein-1. Regulation by proinflammatory cytokines. J Clin Invest. 1993;92(4):1674-1680.

188. Marra F, DeFranco R, Grappone C, Milani S, Pastacaldi S, Pinzani M, Romanelli RG, Laffi G, Gentilini P. Increased expression of monocyte chemotactic protein-1 during active hepatic fibrogenesis: correlation with monocyte infiltration. Am J Pathol. 1998;152(2):423.

189. Degré D, Lemmers A, Gustot T, Ouziel R, Trépo E, Demetter P, Verset L, Quertinmont E, Vercruysse V, Le Moine O, Devière J, Moreno C. Hepatic expression of CCL2 in alcoholic liver disease is associated with disease severity and neutrophil infiltrates. Clin Exp Immunol. 2012;169(3):302-310.

190. Kassel KM, Guo GL, Tawfik O, Luyendyk JP. Monocyte chemoattractant protein-1 deficiency does not affect steatosis or inflammation in livers of mice fed a methionine–choline-deficient diet. Lab Invest. 2010;90(12):1794-1804.

191. Galastri S, Zamara E, Milani S, Novo E, Provenzano A, Delogu W, Vizzutti F, Sutti S, Locatelli I, Navari N, Vivoli E, Caligiuri A, Pinzani M, Albano E, Parola M, Marra F. Lack of CC chemokine ligand 2 differentially affects inflammation and fibrosis according to the genetic background in a murine model of steatohepatitis. Clin Sci. 2012;123(7):459-471.

192. Baeck C, Wehr A, Karlmark KR, Heymann F, Vucur M, Gassler N, Huss S, Klussmann S, Eulberg D, Luedde T, Trautwein C, Tacke F. Pharmacological inhibition of the chemokine CCL2 (MCP-1) diminishes liver macrophage infiltration and steatohepatitis in chronic hepatic injury. Gut. 2012;61(3):416-426.

193.   Oo YH, Banz V, Kavanagh D, Liaskou E, Withers DR, Humphreys E, Reynolds GM, Lee-Turner L, Kalia N, Hubscher SG, Klenerman P, Eksteen B, Adams DH. CXCR3-dependent recruitment and CCR6-mediated positioning of Th-17 cells in the inflamed liver. J Hepatol. 2012;57(5):1044-1051.

194.   Hammerich L, Bangen JM, Govaere O, Zimmermann HW, Gassler N, Huss S, Liedtke C, Prinz I, Lira SA, Luedde T, Roskams T, Trautwein C, Heymann F, Tacke F. Chemokine receptor CCR6-dependent accumulation of γδ T cells in injured liver restricts hepatic inflammation and fibrosis. Hepatology. 2014;59(2):630-642.

195.   Medina-Santillán R, López-Velázquez JA, Chávez-Tapia N, Torres-Villalobos G, Uribe M, Méndez-Sánchez N. Hepatic manifestations of metabolic syndrome. Diabetes Metab Res Rev. 2013.

196.   Janssen A, Grobbee DE, Dendale P. Non-alcoholic fatty liver disease, a new and growing risk indicator for cardiovascular disease. Eur J Prev Cardiol 2020;27(10):1059-1063.

197.   Kim D, Kim WR, Kim HJ, Therneau TM. Association between noninvasive fibrosis markers and mortality among adults with nonalcoholic fatty liver disease in the United States. Hepatology. 2013;57(4):1357-1365.

198.   Adams LA, Anstee QM, Tilg H, Targher G. Non-alcoholic fatty liver disease and its relationship with cardiovascular disease and other extrahepatic diseases. Gut. 2017;66(6):1138-1153.

199.   Mishra S, Yadav D, Gupta M, Mishra H, Sharma P. A study of carotid atherosclerosis in patients with non-alcoholic fatty liver disease. Indian J Clin Biochem. 2013;28(1):79-83.

200.   Colak Y, Karabay CY, Tuncer I, Kocabay G, Kalayci A, Senates E, Ozturk O, Doganay HL, Enc FY, Ulasoglu C, Kiziltas S. Relation of epicardial adipose tissue and carotid intima-media thickness in patients with nonalcoholic fatty liver disease. Eur J Gastroenterol Hepatol. 2012;24(6):613-618.

201.   Sunbul M, Agirbasli M, Durmus E, Kivrak T, Akin H, Aydin Y, Ergelen R, Yilmaz Y. Arterial stiffness in patients with non-alcoholic fatty liver disease is related to fibrosis stage and epicardial adipose tissue thickness. Atherosclerosis. 2014;237(2):490-493.

202.   Ampuero J, Gallego-Durán R, Romero-Gómez M. Association of NAFLD with subclinical atherosclerosis and coronary-artery disease: meta-analysis. Rev Esp Enferm Dig. 2015;107(1):10-6.

203.   Pacifico L, Anania C, Martino F, Cantisani V, Pascone R, Marcantonio A, Chiesa C. Functional and morphological vascular changes in pediatric nonalcoholic fatty liver disease. Hepatology. 2010;52(5):1643-1651.

204.   Villanova N, Moscatiello S, Ramilli S, Bugianesi E, Magalotti D, Vanni E, Zoli M, Marchesini G. Endothelial dysfunction and cardiovascular risk profile in nonalcoholic fatty liver disease. Hepatology. 2005;42(2):473-480.

205.   Guleria A, Duseja A, Kalra N, Das A, Dhiman R, Chawla Y, Bhansali A. Patients with non-alcoholic fatty liver disease (NAFLD) have an increased risk of atherosclerosis and cardiovascular disease. Trop Gastroenterol. 2013;34(2):74-82.

206.   Yilmaz Y, Kurt R, Yonal O, Polat N, Celikel CA, Gurdal A, Oflaz H, Ozdogan O, Imeryuz N, Kalayci C, Avsar E. Coronary flow reserve is impaired in patients with nonalcoholic fatty liver disease: association with liver fibrosis. Atherosclerosis. 2010;211(1):182-186.

207.   Francque SM, van der Graaff D, Kwanten WJ. Non-alcoholic fatty liver disease and cardiovascular risk: Pathophysiological mechanisms and implications. J Hepatol. 2016 Aug;65(2):425-43.

208.   Siddiqui MS, Fuchs M, Idowu MO, Luketic VA, Boyett S, Sargeant C, Stravitz RT,

Puri P, Matherly S, Sterling RK, Contos M, Sanyal AJ. Severity of nonalcoholic fatty liver disease and progression to cirrhosis are associated with atherogenic lipoprotein profile. Clin Gastroenterol Hepatol. 2015;13(5):1000-1008. e3.

209.   Targher G, Bertolini L, Padovani R, Rodella S, Tessari R, Zenari L, Day C, Arcaro G. Prevalence of nonalcoholic fatty liver disease and its association with cardiovascular disease among type 2 diabetic patients. Diabetes Care. 2007;30(5):1212-1218.

210.   Patel SS, Siddiqui MS. The interplay between nonalcoholic fatty liver disease and atherosclerotic heart disease. Hepatology. 2019;69(4):1372-1374.

211.   Corey KE, Vuppalanchi R, Wilson LA, Cummings OW, Chalasani N, CRN N. NASH resolution is associated with improvements in HDL and triglyceride levels but not improvement in LDL or non-HDL-C levels. Aliment Pharmacol Ther. 2015;41(3):301-309.

212.   Laurin J, Lindor KD, Crippin JS, Gossard A, Gores GJ, Ludwig J, Rakela J, McGill DB. Ursodeoxycholic acid or clofibrate in the treatment of non-alcohol-induced steatohepatitis: a pilot study. Hepatology. 1996;23(6):1464-1467.

213.   Tang JJ, Li JG, Qi W, Qiu WW, Li PS, Li BL, Song BL. Inhibition of SREBP by a small molecule, betulin, improves hyperlipidemia and insulin resistance and reduces atherosclerotic plaques. Cell Metab. 2011 Jan 5;13(1):44-56.

214.   Li Y, Xu S, Mihaylova MM, Zheng B, Hou X, Jiang B, Park O, Luo Z, Lefai E, Shyy JY-J, Gao B, Wierzbicki M, Verbeuren TJ, Shaw RJ, Cohen RA, Zang M. AMPK phosphorylates and inhibits SREBP activity to attenuate hepatic steatosis and atherosclerosis in diet-induced insulin-resistant mice. Cell Metab. 2011;13(4):376-388.

215.   Eberle D, Hegarty B, Bossard P, Ferre P, Foufelle F. SREBP transcription factors: master regulators of lipid homeostasis. Biochimie. 2004 Nov;86(11):839-48.

216.   Horton JD, Goldstein JL, Brown MS. SREBPs: activators of the complete program of cholesterol and fatty acid synthesis in the liver. J Clin Invest. 2002;109(9):1125-1131.

217.   Eberlé D, Hegarty B, Bossard P, Ferré P, Foufelle F. SREBP transcription factors: master regulators of lipid homeostasis. Biochimie. 2004;86(11):839-848.

218.   Bengoechea-Alonso MT, Ericsson J. SREBP in signal transduction: cholesterol metabolism and beyond. Curr Opin Cell Biol. 2007;19(2):215-222.

219.   Bertolio R, Napoletano F, Mano M, Maurer-Stroh S, Fantuz M, Zannini A, Bicciato S, Sorrentino G, Del Sal G. Sterol regulatory element binding protein 1 couples mechanical cues and lipid metabolism. Nat Commun. 2019;10(1):1-11.

220.   Xiaoping Z, Fajun Y. Regulation of SREBP-mediated gene expression. Sheng Wu Wu Li Hsueh Bao. 2012;28(4):287.

221.   Osborne TF, Espenshade PJ. Evolutionary conservation and adaptation in the mechanism that regulates SREBP action: what a long, strange tRIP it's been. Genes Dev. 2009;23(22):2578-2591.

222.   Ferre P, Foufelle F. SREBP-1c transcription factor and lipid homeostasis: clinical perspective. Horm Res Paediatr. 2007;68(2):72-82.

223.   Shimomura I, Shimano H, Horton JD, Goldstein JL, Brown MS. Differential expression of exons 1a and 1c in mRNAs for sterol regulatory element binding protein-1 in human and mouse organs and cultured cells. J Clin Invest. 1997;99(5):838-845.

224.   Brown MS, Goldstein JL. The SREBP pathway: regulation of cholesterol metabolism by proteolysis of a membrane-bound transcription factor. Cell. 1997;89(3):331-340.

225.   Shimano H, Sato R. SREBP-regulated lipid metabolism: convergent physiology - divergent pathophysiology. Nat Rev Endocrinol. 2017 Dec;13(12):710-730.

226.   Lin Y-C, Wu M-S, Lin Y-F, Chen C-R, Chen C-Y, Chen C-J, Shen C-C, Chen K-C,

Peng C-C. Nifedipine modulates renal lipogenesis via the AMPK-SREBP transcriptional pathway. Int J Mol Sci. 2019;20(7):1570.

227. Moon Y-A, Liang G, Xie X, Frank-Kamenetsky M, Fitzgerald K, Koteliansky V, Brown MS, Goldstein JL, Horton JD. The Scap/SREBP pathway is essential for developing diabetic fatty liver and carbohydrate-induced hypertriglyceridemia in animals. Cell Metab. 2012;15(2):240-246.

228. Sekiya M, Yahagi N, Matsuzaka T, Takeuchi Y, Nakagawa Y, Takahashi H, Okazaki H, Iizuka Y, Ohashi K, Gotoda T, Ishibashi S, Nagai R, Yamazaki T, Kadowaki T, Yamada N, Osuga J-i, Shimano H. SREBP-1-independent regulation of lipogenic gene expression in adipocytes. J Lipid Res. 2007;48(7):1581-1591.

229. Sun W, Bi Y, Liang H, Cai M, Chen X, Zhu Y, Ye J, Weng J. Effects of early insulin therapy on sterol regulatory element binding protein 1 pathway and lipid accumulation in liver of type 2 diabetic rats. Zhonghua yi xue za zhi. 2011;91(26):1809-1812.

230. Liu J. Ethanol and liver: recent insights into the mechanisms of ethanol-induced fatty liver. World J Gastroenterol. 2014;20(40):14672.

231. Horton JD, Shimomura I, Ikemoto S, Bashmakov Y, Hammer RE. Overexpression of sterol regulatory element-binding protein-1a in mouse adipose tissue produces adipocyte hypertrophy, increased fatty acid secretion, and fatty liver. J Biol Chem. 2003;278(38):36652-36660.

232. Fujii N, Narita T, Okita N, Kobayashi M, Furuta Y, Chujo Y, Sakai M, Yamada A, Takeda K, Konishi T, Sudo Y, Shimokawa I, Higami Y. Sterol regulatory element-binding protein-1c orchestrates metabolic remodeling of white adipose tissue by caloric restriction. Aging Cell. 2017;16(3):508-517.

233. Amemiya-Kudo M, Oka J, Takeuchi Y, Okazaki H, Yamamoto T, Yahagi N, Matsuzaka K, Okazaki S, Osuga J-i, Yamada N, Murase T, Shimano H. Suppression of the pancreatic duodenal homeodomain transcription factor-1 (Pdx-1) promoter by sterol regulatory element-binding protein-1c (SREBP-1c). J Biol Chem. 2011;286(32):27902-27914.

234. Kato T, Shimano H, Yamamoto T, Yokoo T, Endo Y, Ishikawa M, Matsuzaka T, Nakagawa Y, Kumadaki S, Yahagi N, Takahashi A, Sone H, Suzuki H, Toyoshima H, Hasty AH, Takahashi S, Gomi H, Izumi T, Yamada N. Granuphilin is activated by SREBP-1c and involved in impaired insulin secretion in diabetic mice. Cell Metab. 2006;4(2):143-154.

235. Barbero-Camps E, Fernández A, Martínez L, Fernández-Checa JC, Colell A. APP/PS1 mice overexpressing SREBP-2 exhibit combined Aβ accumulation and tau pathology underlying Alzheimer's disease. Hum Mol Genet. 2013;22(17):3460-3476.

236. Gödel M, Hartleben B, Herbach N, Liu S, Zschiedrich S, Lu S, Debreczeni-Mór A, Lindenmeyer MT, Rastaldi M-P, Hartleben G, Wiech T, Fornoni A, Nelson RG, Kretzler M, Wanke R, Pavenstädt H, Kerjaschki D, Cohen CD, Hall MN, Rüegg MA, Inoki K, Walz G, Huber TB. Role of mTOR in podocyte function and diabetic nephropathy in humans and mice. J Clin Invest. 2011;121(6):2197-2209.

237. Porstmann T, Santos CR, Griffiths B, Cully M, Wu M, Leevers S, Griffiths JR, Chung Y-L, Schulze A. SREBP activity is regulated by mTORC1 and contributes to Akt-dependent cell growth. Cell Metab. 2008;8(3):224-236.

238. Krycer JR, Sharpe LJ, Luu W, Brown AJ. The Akt-SREBP nexus: cell signaling meets lipid metabolism. Trends Endocrinol Metab. 2010 May;21(5):268-76.

239. Du X, Kristiana I, Wong J, Brown AJ. Involvement of Akt in ER-to-Golgi transport of SCAP/SREBP: a link between a key cell proliferative pathway and membrane synthesis. Mol Biol Cell. 2006;17(6):2735-2745.

240. Yellaturu CR, Deng X, Cagen LM, Wilcox HG, Mansbach II CM, Siddiqi SA, Park

EA, Raghow R, Elam MB. Insulin enhances post-translational processing of nascent SREBP-1c by promoting its phosphorylation and association with COPII vesicles. J Biol Chem. 2009;284(12):7518-7532.

241.   Porstmann T, Santos CR, Lewis C, Griffiths B, Schulze A. A new player in the orchestra of cell growth: SREBP activity is regulated by mTORC1 and contributes to the regulation of cell and organ size. Biochem Soc Trans. 2009;37(1):278-283.

242.   Bengoechea-Alonso MT, Ericsson J. A phosphorylation cascade controls the degradation of active SREBP1. J Biol Chem. 2009;284(9):5885-5895.

243.   Horton JD, Shah NA, Warrington JA, Anderson NN, Park SW, Brown MS, Goldstein JL. Combined analysis of oligonucleotide microarray data from transgenic and knockout mice identifies direct SREBP target genes. Proc Natl Acad Sci U S A. 2003;100(21):12027-12032.

244.   Li X, Hu X, Pan T, Dong L, Ding L, Wang Z, Song R, Wang X, Wang N, Zhang Y, Wang J, Yang B. Kanglexin, a new anthraquinone compound, attenuates lipid accumulation by activating the AMPK/SREBP-2/PCSK9/LDLR signalling pathway. Biomed Pharmacother. 2021;133:110802.

245.   Horton JD, Cohen JC, Hobbs HH. Molecular biology of PCSK9: its role in LDL metabolism. Trends Biochem Sci. 2007;32(2):71-77.

246.   Maxwell KN, Breslow JL. Adenoviral-mediated expression of Pcsk9 in mice results in a low-density lipoprotein receptor knockout phenotype. Proc Natl Acad Sci U S A. 2004;101(18):7100-7105.

247.   Park SW, Moon Y-A, Horton JD. Post-transcriptional regulation of low density lipoprotein receptor protein by proprotein convertase subtilisin/kexin type 9a in mouse liver. J Biol Chem. 2004;279(48):50630-50638.

248.   Tavori H, Rashid S, Fazio S. On the function and homeostasis of PCSK9: reciprocal interaction with LDLR and additional lipid effects. Atherosclerosis. 2015;238(2):264-270.

249.   Horie T, Nishino T, Baba O, Kuwabara Y, Nakao T, Nishiga M, Usami S, Izuhara M, Sowa N, Yahagi N, Shimano H, Matsumura S, Inoue K, Marusawa H, Nakamura T, Hasegawa K, Kume N, Yokode M, Kita T, Kimura T, Ono K. MicroRNA-33 regulates sterol regulatory element-binding protein 1 expression in mice. Nat Commun. 2013;4(1):1-12.

250.   Horie T, Nishino T, Baba O, Kuwabara Y, Nakao T, Nishiga M, Usami S, Izuhara M, Nakazeki F, Ide Y, Koyama S, Sowa N, Yahagi N, Shimano H, Nakamura T, Hasegawa K, Kume N, Yokode M, Kita T, Kimura T, Ono K. MicroRNA-33b knock-in mice for an intron of sterol regulatory element-binding factor 1 (Srebf1) exhibit reduced HDL-C in vivo. Sci Rep. 2014;4(1):1-7.

251.   Karunakaran D, Richards L, Geoffrion M, Barrette D, Gotfrit RJ, Harper M-E, Rayner KJ. Therapeutic inhibition of miR-33 promotes fatty acid oxidation but does not ameliorate metabolic dysfunction in diet-induced obesity. Arterioscler Thromb Vasc Biol. 2015;35(12):2536-2543.

252.   Kamisuki S, Mao Q, Abu-Elheiga L, Gu Z, Kugimiya A, Kwon Y, Shinohara T, Kawazoe Y, Sato S-i, Asakura K, Choo H-YP, Sakai J, Wakil SJ, Uesugi M. A small molecule that blocks fat synthesis by inhibiting the activation of SREBP. Chem Biol. 2009;16(8):882-892.

253.   Teresi RE, Planchon SM, Waite KA, Eng C. Regulation of the PTEN promoter by statins and SREBP. Hum Mol Genet. 2008;17(7):919-928.

254.   Garg A, Grundy SM. Lovastatin for lowering cholesterol levels in non-insulin-dependent diabetes mellitus. N Engl J Med. 1988;318(2):81-86.

255.   Brody J. New type of drug for cholesterol approved and hailed as effective. New York

Times. 1987.

256. Group SSSS. Randomised trial of cholesterol lowering in 4444 patients with coronary heart disease: the Scandinavian Simvastatin Survival Study (4S). The Lancet. 1994;344(8934):1383-1389.

257. Group HPSC. MRC/BHF Heart Protection Study of cholesterol lowering with simvastatin in 20 536 high-risk individuals: a randomised placebocontrolled trial. The Lancet. 2002;360(9326):7-22.

258. Sahebkar A, Simental-Mendía L, Guerrero-Romero F, Golledge J, Watts G. Effect of statin therapy on plasma proprotein convertase subtilisin kexin 9 (PCSK9) concentrations: a systematic review and meta-analysis of clinical trials. Diabetes Obes Metab. 2015;17(11):1042-1055.

259. Everett BM, Smith RJ, Hiatt WR. Reducing LDL with PCSK9 inhibitors—the clinical benefit of lipid drugs. N Engl J Med. 2015;373(17):1588-91.

260. Sabatine MS, Giugliano RP, Wiviott SD, Raal FJ, Blom DJ, Robinson J, Ballantyne CM, Somaratne R, Legg J, Wasserman SM, Scott R, J Koren M, Stein EA, Investigators O-LSoL-TEaLCO. Efficacy and safety of evolocumab in reducing lipids and cardiovascular events. N Engl J Med. 2015;372(16):1500-1509.

261. Rami M, Guillamat-Prats R, Rinne P, Salvermoser M, Ring L, Bianchini M, Blanchet X, Megens RT, Döring Y, Walzog B, Soehnlein O, Weber C, Faussner A, Steffens S. Chronic intake of the selective serotonin reuptake inhibitor fluoxetine enhances atherosclerosis. Arterioscler Thromb Vasc Biol. 2018;38(5):1007-1019.

262. Domschke G, Linden F, Pawig L, Hafner A, Akhavanpoor M, Reymann J, Doesch AO, Erbel C, Weber C, Katus HA, Noels H, Erfle H, Gleissner CA, Runz H. Systematic RNA-interference in primary human monocyte-derived macrophages: A high-throughput platform to study foam cell formation. Sci Rep. 2018;8(1):1-11.

263. Asare Y, Campbell-James TA, Bokov Y, Yu LL, Prestel M, El Bounkari O, Roth S, Megens RT, Straub T, Thomas K, Yan G, Schneider M, Ziesch N, Tiedt S, Silvestre-Roig C, Braster Q, Huang Y, Schneider M, Malik R, Haffner C, Liesz A, Soehnlein O, Bernhagen J, Dichgans M. Histone deacetylase 9 activates IKK to regulate atherosclerotic plaque vulnerability. Circ Res. 2020;127(6):811-823.

264. Tsuru H, Osaka M, Hiraoka Y, Yoshida M. HFD-induced hepatic lipid accumulation and inflammation are decreased in Factor D deficient mouse. Sci Rep. 2020;10(1):1-10.

265. Müller II, Müller KA, Karathanos A, Schönleber H, Rath D, Vogel S, Chatterjee M, Schmid M, Haas M, Seizer P, Langer H, Schaeffeler E, Schwab M, Gawaz M, Geisler T. Impact of counterbalance between macrophage migration inhibitory factor and its inhibitor Gremlin-1 in patients with coronary artery disease. Atherosclerosis. 2014;237(2):426-432.

266. Pan J-H, Sukhova GK, Yang J-T, Wang B, Xie T, Fu H, Zhang Y, Satoskar AR, David JR, Metz CN, Bucala R, Fang K, Simon DI, Chapman HA, Libby P, Shi G-P. Macrophage migration inhibitory factor deficiency impairs atherosclerosis in low-density lipoprotein receptor-deficient mice. Circulation. 2004;109(25):3149-3153.

267. Dorado B. Methods in mouse atherosclerosis. Springer; 2015.

268. Chen Y-C, Bui AV, Diesch J, Manasseh R, Hausding C, Rivera J, Haviv I, Agrotis A, Htun NM, Jowett J, Hagemeyer CE, Hannan RD, Bobik A, Peter K. A novel mouse model of atherosclerotic plaque instability for drug testing and mechanistic/therapeutic discoveries using gene and microRNA expression profiling. Circ Res. 2013;113(3):252-265.

269. Kolte D, Libby P, Jang I-K. New insights into plaque erosion as a mechanism of acute coronary syndromes. JAMA. 2021;325(11):1043-1044.

270. Teupser D, Pavlides S, Tan M, Gutierrez-Ramos J-C, Kolbeck R, Breslow JL. Major reduction of atherosclerosis in fractalkine (CX3CL1)-deficient mice is at the brachiocephalic artery, not the aortic root. Proc Natl Acad Sci U S A. 2004;101(51):17795-17800.

271. Goel R, Schrank BR, Arora S, Boylan B, Fleming B, Miura H, Newman PJ, Molthen RC, Newman DK. Site-specific effects of PECAM-1 on atherosclerosis in LDL receptor–deficient mice. Arterioscler Thromb Vasc Biol. 2008;28(11):1996-2002.

272. Tilstam PV, Soppert J, Hemmers C, Harlacher E, Döring Y, van der Vorst EP, Schulte C, Alampour-Rajabi S, Theelen W, Asare Y, de Winther MPJ, Lawrence T, Bernhagen J, Schober A, Zernecke A, Jankowski J, Weber C, Noels H. Non-activatable mutant of inhibitor of kappa B kinase α (IKKα) exerts vascular site-specific effects on atherosclerosis in Apoe-deficient mice. Atherosclerosis. 2020;292:23-30.

273. Libby P, Hansson GK. Inflammation and immunity in diseases of the arterial tree: players and layers. Circ Res. 2015;116(2):307-311.

274. El Bounkari O, Zan C, Wagner J, Bugar E, Bourilhon P, Kontos C, Zarwel M, Sinitski D, Milic J, Jansen Y, Kempf WE, Mägdefessel L, Hoffmann A, Brandhofer M, Bucala R, Megens RTA, Weber C, Kapurniotu A, Bernhagen J. MIF-2/D-DT is an atypical atherogenic chemokine that promotes advanced atherosclerosis and hepatic lipogenesis. bioRxiv. 2021.

275. Gligorovska L, Bursać B, Kovačević S, Veličković N, Matić G, Djordjevic A. Mif deficiency promotes adiposity in fructose-fed mice. J Endocrinol. 2019;240(2):133-145.

276. Gligorovska L, Teofilović A, Vojnović Milutinović D, Miladinović N, Kovačević S, Veličković N, Djordjevic A. Macrophage migration inhibitory factor deficiency aggravates effects of fructose-enriched diet on lipid metabolism in the mouse liver. Biofactors. 2021.

277. Heinrichs D, Berres ML, Coeuru M, Knauel M, Nellen A, Fischer P, Philippeit C, Bucala R, Trautwein C, Wasmuth HE, Bernhagen J. Protective role of macrophage migration inhibitory factor in nonalcoholic steatohepatitis. FASEB J. 2014;28(12):5136-5147.

278. Hou J, Zhang J, Cui P, Zhou Y, Liu C, Wu X, Ji Y, Wang S, Cheng B, Ye H, Shu L, Zhang K, Wang D, Xu J, Shu Q, Colonna M, Fang X. TREM2 sustains macrophage-hepatocyte metabolic coordination in nonalcoholic fatty liver disease and sepsis. The Journal of Clinical Investigation. 2021;131(4).

279. Schuster GU, Parini P, Wang L, Alberti S, Steffensen KR, Hansson GrK, Angelin B, Gustafsson J-Ak. Accumulation of foam cells in liver X receptor-deficient mice. Circulation. 2002;106(9):1147-1153.

280. Tang K, Wang F, Zeng Y, Chen X, Xu X. Salusin-α attenuates hepatic steatosis and atherosclerosis in high fat diet-fed low density lipoprotein receptor deficient mice. Eur J Pharmacol. 2018;830:76-86.

281. Ma C, Zhang J, Yang S, Hua Y, Su J, Shang Y, Wang Z, Feng K, Zhang J, Yang X, Zhang H, Mao J, Fan G. Astragalus Flavone Ameliorates Atherosclerosis and Hepatic Steatosis Via Inhibiting Lipid-Disorder and Inflammation in apoE−/− Mice. Front Pharmacol. 2020;11.

282. Cui H, Lin Y, Xie L, Zhao J. Urantide decreases hepatic steatosis in rats with experimental atherosclerosis via the MAPK/Erk/JNK pathway. Mol Med Report. 2021;23(4):1-10.

283. Ma Y, Liang X, Li C, Li R, Tong X, Zhang R, Shan X, Yang J, Ma X, Lu W, Li R, Fu J. 5-HT2A Receptor and 5-HT Degradation Play a Crucial Role in Atherosclerosis by Modulating Macrophage Foam Cell Formation, Vascular Endothelial Cell

Inflammation, and Hepatic Steatosis. J Atheroscler Thromb. 2021:58305.

284.   Kim K, Yu J, Kang JK, Morrow JP, Pajvani UB. Liver-selective γ-secretase inhibition ameliorates diet-induced hepatic steatosis, dyslipidemia and atherosclerosis. Biochem Biophys Res Commun. 2020;527(4):979-984.

285.   Stachowicz A, Wiśniewska A, Kuś K, Kiepura A, Gębska A, Gajda M, Białas M, Totoń-Żurańska J, Stachyra K, Suski M, Jawień J, Korbut R, Olszanecki R. The influence of trehalose on atherosclerosis and hepatic steatosis in apolipoprotein E knockout mice. Int J Mol Sci. 2019;20(7):1552.

286.   Park SH, Sung Y-Y, Nho Kj, Kim DS, Kim HK. Effects of Viola mandshurica on Atherosclerosis and Hepatic Steatosis in ApoE−/− via the AMPK Pathway. Am J Chin Med. 2017;45(04):757-772.

287.   Xu Z-R, Li J-Y, Dong X-W, Tan Z-J, Wu W-Z, Xie Q-M, Yang Y-M. Apple polyphenols decrease atherosclerosis and hepatic steatosis in ApoE−/− mice through the ROS/MAPK/NF-κB pathway. Nutrients. 2015;7(8):7085-7105.

288.   Stachowicz A, Olszanecki R, Suski M, Wiśniewska A, Totoń-Żurańska J, Madej J, Jawień J, Białas M, Okoń K, Gajda M, Głombik K, Basta-Kaim A, Korbut R. Mitochondrial aldehyde dehydrogenase activation by Alda-1 inhibits atherosclerosis and attenuates hepatic steatosis in apolipoprotein E-knockout mice. J Am Heart Assoc. 2014;3(6):e001329.

289.   Bowes AJ, Khan MI, Shi Y, Robertson L, Werstuck GH. Valproate attenuates accelerated atherosclerosis in hyperglycemic apoE-deficient mice: evidence in support of a role for endoplasmic reticulum stress and glycogen synthase kinase-3 in lesion development and hepatic steatosis. Am J Pathol. 2009;174(1):330-342.

290.   Amersfoort J, Douna H, Schaftenaar FH, Foks AC, Kröner MJ, van Santbrink PJ, van Puijvelde GH, Bot I, Kuiper J. Defective autophagy in T cells impairs the development of diet-induced hepatic steatosis and atherosclerosis. Front Immunol. 2018;9:2937.

291.   Smith DD, Tan X, Raveendran VV, Tawfik O, Stechschulte DJ, Dileepan KN. Mast cell deficiency attenuates progression of atherosclerosis and hepatic steatosis in apolipoprotein E-null mice. Am J Physiol Heart Circ Physiol. 2012;302(12):H2612-H2621.

292.   Banko NS, McAlpine CS, Venegas-Pino DE, Raja P, Shi Y, Khan MI, Werstuck GH. Glycogen synthase kinase 3α deficiency attenuates atherosclerosis and hepatic steatosis in high fat diet–fed low density lipoprotein receptor–deficient mice. Am J Pathol. 2014;184(12):3394-3404.

293.   Kobayashi M, Uta S, Otsubo M, Deguchi Y, Tagawa R, Mizunoe Y, Nakagawa Y, Shimano H, Higami Y. Srebp-1c/Fgf21/Pgc-1α Axis Regulated by Leptin Signaling in Adipocytes—Possible Mechanism of Caloric Restriction-Associated Metabolic Remodeling of White Adipose Tissue. Nutrients. 2020;12(7):2054.

294.   Hardie DG. AMP-activated protein kinase: a master switch in glucose and lipid metabolism. Rev Endocr Metab Disord. 2004;5(2):119-125.

295.   Carlson CA, Kim K-H. Regulation of hepatic acetyl coenzyme A carboxylase by phosphorylation and dephosphorylation. J Biol Chem. 1973;248(1):378-380.

296.   Beg ZH, Allmann DW, Gibson DM. Modulation of 3-hydroxy-3-methylglutaryl coenzyme A reductase activity with cAMP and with protein fractions of rat liver cytosol. Biochem Biophys Res Commun. 1973;54(4):1362-1369.

297.   Kim YW, Kim YM, Yang YM, Kim TH, Hwang SJ, Lee JR, Kim SC, Kim SG. Inhibition of SREBP-1c-mediated hepatic steatosis and oxidative stress by sauchinone, an AMPK-activating lignan in Saururus chinensis. Free Radic Biol Med. 2010;48(4):567-578.

298.   Quan HY, Kim SJ, Jo HK, Kim GW, Chung SH. Betulinic acid alleviates non-

alcoholic fatty liver by inhibiting SREBP1 activity via the AMPK–mTOR–SREBP signaling pathway. Biochem Pharmacol. 2013;85(9):1330-1340.

299. Nammi S, Roufogalis BD. Light-to-moderate ethanol feeding augments AMPK-α phosphorylation and attenuates SREBP-1 expression in the liver of rats. J Pharm Pharm Sci. 2013;16(2):342-351.

300. Soetikno V, Sari FR, Sukumaran V, Lakshmanan AP, Harima M, Suzuki K, Kawachi H, Watanabe K. Curcumin decreases renal triglyceride accumulation through AMPK–SREBP signaling pathway in streptozotocin-induced type 1 diabetic rats. J Nutr Biochem. 2013;24(5):796-802.

301. Yang Y, Li W, Liu Y, Sun Y, Li Y, Yao Q, Li J, Zhang Q, Gao Y, Gao L, Zhao J. Alpha-lipoic acid improves high-fat diet-induced hepatic steatosis by modulating the transcription factors SREBP-1, FoxO1 and Nrf2 via the SIRT1/LKB1/AMPK pathway. J Nutr Biochem. 2014;25(11):1207-1217.

302. Liu S, Jing F, Yu C, Gao L, Qin Y, Zhao J. AICAR-induced activation of AMPK inhibits TSH/SREBP-2/HMGCR pathway in liver. PLoS One. 2015;10(5):e0124951.

303. Peng C-H, Yang M-Y, Yang Y-S, Yu C-C, Wang C-J. Antrodia cinnamomea prevents obesity, dyslipidemia, and the derived fatty liver via regulating AMPK and SREBP signaling. Am J Chin Med. 2017;45(01):67-83.

304. Yang R, Chu X, Sun L, Kang Z, Ji M, Yu Y, Liu Y, He Z, Gao N. Hypolipidemic activity and mechanisms of the total phenylpropanoid glycosides from Ligustrum robustum (Roxb.) Blume by AMPK-SREBP-1c pathway in hamsters fed a high-fat diet. Phytother Res. 2018;32(4):715-722.

305. Chen Q, Liu M, Yu H, Li J, Wang S, Zhang Y, Qiu F, Wang T. Scutellaria baicalensis regulates FFA metabolism to ameliorate NAFLD through the AMPK-mediated SREBP signaling pathway. J Nat Med. 2018;72(3):655-666.

306. Li J, Liu M, Yu H, Wang W, Han L, Chen Q, Ruan J, Wen S, Zhang Y, Wang T. Mangiferin improves hepatic lipid metabolism mainly through its metabolite-norathyriol by modulating SIRT-1/AMPK/SREBP-1c signaling. Front Pharmacol. 2018;9:201.

307. Chen J, Gong S, Wan X, Gao X, Wang C, Zeng F, Zhao C, Liu B, Huang Y. Hypolipidemic properties of Chlorella pyrenoidosa organic acids via AMPK/HMGCR/SREBP-1c pathway in vivo. Food Sci Nutr. 2021;9(1):459-468.

308. Zhang W, Li J-Y, Wei X-c, Wang Q, Yang J-y, Hou H, Du Z-W, Wu X-A. Effects of dibutyl phthalate on lipid metabolism in liver and hepatocytes based on PPARα/SREBP-1c/FAS/GPAT/AMPK signal pathway. Food Chem Toxicol. 2021;149:112029.

309. Lue H, Dewor M, Leng L, Bucala R, Bernhagen J. Activation of the JNK signalling pathway by macrophage migration inhibitory factor (MIF) and dependence on CXCR4 and CD74. Cell Signal. 2011;23(1):135-144.

310. Schwartz V, Krüttgen A, Weis J, Weber C, Ostendorf T, Lue H, Bernhagen J. Role for CD74 and CXCR4 in clathrin-dependent endocytosis of the cytokine MIF. Eur J Cell Biol. 2012;91(6-7):435-449.

311. Soppert J, Kraemer S, Beckers C, Averdunk L, Möllmann J, Denecke B, Goetzenich A, Marx G, Bernhagen J, Stoppe C. Soluble CD74 reroutes MIF/CXCR4/AKT-mediated survival of cardiac myofibroblasts to necroptosis. J Am Heart Assoc. 2018;7(17):e009384.

312. Knauel M, Bernhagen J. Molecular mechanisms underlying the protective effect of MIF in experimental liver fibrosis. Lehrstuhl für Biochemie und Molekulare Zellbiologie; 2014.

313. Dikovskaya D, Dinkova‐Kostova AT. Measuring Changes in Keap1-Nrf2 Protein

Complex Conformation in Individual Cells by FLIM-FRET. Curr Protoc Toxicol. 2020;85(1):e96.

314. Lerner E, Orevi T, Ishay EB, Amir D, Haas E. Kinetics of fast changing intramolecular distance distributions obtained by combined analysis of FRET efficiency kinetics and time-resolved FRET equilibrium measurements. Biophys J. 2014;106(3):667-676.

315. Clegg RM. Förster resonance energy transfer—FRET what is it, why do it, and how it's done. Laboratory techniques in biochemistry and molecular biology. 2009;33:1-57.

316. Roche-Molina M, Sanz-Rosa D, Cruz FM, Garcia-Prieto J, Lopez S, Abia R, Muriana FJ, Fuster V, Ibanez B, Bernal JA. Induction of sustained hypercholesterolemia by single adeno-associated virus-mediated gene transfer of mutant hPCSK9. Arterioscler Thromb Vasc Biol. 2015 Jan;35(1):50-9.

317. Zadelaar S, Kleemann R, Verschuren L, de Vries-Van der Weij J, van der Hoorn J, Princen HM, Kooistra T. Mouse models for atherosclerosis and pharmaceutical modifiers. Arterioscler Thromb Vasc Biol. 2007 Aug;27(8):1706-21.

318. Getz GS, Reardon CA. Do the Apoe−/− and Ldlr−/−mice yield the same insight on atherogenesis? Arterioscler Thromb Vasc Biol. 2016;36(9):1734-1741.

319. Decourt C, Janin A, Moindrot M, Chatron N, Nony S, Muntaner M, Dumont S, Divry E, Dauchet L, Meirhaeghe A. PCSK9 post-transcriptional regulation: Role of a 3′ UTR microRNA-binding site variant in linkage disequilibrium with c. 1420G. Atherosclerosis. 2020;314:63-70.

320. Caltabiano R, De Pasquale R, Piombino E, Campo G, Nicoletti F, Cavalli E, Mangano K, Fagone P. Macrophage Migration Inhibitory Factor (MIF) and Its Homologue d-Dopachrome Tautomerase (DDT) Inversely Correlate with Inflammation in Discoid Lupus Erythematosus. Molecules. 2021 Jan 1;26(1).

8. LIST OF FIGURES

9. LIST OF TABLES

10. LIST OF ABBREVIATIONS

AaRS: Aminoacyl-tRNA synthetases

ACC 1: Acetyl-CoA carboxylase 1

AICAR: 5-aminoimidazole-4-carboxyamide ribonucleoside

AMPK: AMP-activated protein kinase

AP-1: Activator protein-1

ApoE: Apolipoprotein E

AS: Atherosclerosis

ASCVD: Atherosclerotic cardiovascular disease

ATMs: Adipose tissue macrophages

BAFF-R: B cell-activating factor-receptor

BAT: Brown adipose tissue

BCA: Brachiocephalic artery

BM: Bone marrow

BMT: Bone marrow transplantation

CCL2/MCP-1: Monocyte chemoattractant protein-1

CCL3/MIP-1α: Macrophage inflammatory protein-1α

CCL5/RANTES: Regulated on activation, normal T cell expressed and secreted

CCL17/TARC: Thymusand activation regulated chemokine

CCL19/ECL/MIF-3β: EBl1 ligand chemokine/Macrophage inflammatory protein-3β

CCL21/SLC/Exodus-2/TCA4: Secondary lymphoid-tissue chemokine

CCl4: Carbon tetrachloride

ccRCCs: Clear cell renal cell carcinoma

CD44: Cluster of differentiation of 44

CD74: Cluster of differentiation of 74

CEA: Carotid endarterectomy

COPD: Chronic obstructive pulmonary disease

CR: Caloric restriction

CRC: Colorectal cancer

CRP: C-reactive protein

CVD: Cardiovascular disease

CXCL1/KC: Keratinocyte-derived chemokine

CXCL2/MIP-2α: Macrophage inflammatory protein-2α

CXCL4/PF4: Platelet factor 4

CXCL5/ENA-78: Epithelial-derived neutrophil-activating peptide 78

CXCL10/IP-10/SCY10: Interferon-γ-induced protein 10/Small inducible cytokine B10

CXCL12/SDF-1: Stromal cell-derived factor-1

CXCL16/Bonza/STRL33/TYMSTR: Thymocyte-expressed seven-transmembrane domain receptor

CX3CL1/Fc: Fractakine

CXCR4: C-X-C chemokine receptor type 4

CXCR7: C-X-C chemokine receptor type 7

CXCR2: C-X-C chemokine receptor type 2

D-dopachrome: 2-carboxy-2,3-dihydroindole-5,6quinone

D-DT/DOPD/MIF-2: Macrophage migration inhibitory factor-2/D-dopachrome tautomerase

DHICA: 5,6-dihydroxyindole-2-carboxylic acid

DKO: Double knockout

DLE: Discoid lupus erythematosus

ECs: Endothelial cells

EFT: Epicardial fat thickness

ELISA: Enzyme-linked immunosorbent assay

eQTL: expression Quantitative trait loci

ER: Endoplasmic reticulum

ERK: Extracellular signal-regulated kinase

EUSTAR: European scleroclerma trials

FACS: Fluorescence-activated cell sorting

FASN: Fatty acid synthase

FBS/FCS: Fetal bovine serum/Fetal calf serum

GLUT1/4: Glucose transporter 1/4

GR: Glucocorticoid receptor

GSK-3: Glycogen synthase kinase-3

HBDs: β-defensins

HBV: Hepatitis B virus

HE: Hematoxylin and eosin

HFD: High fat diet

HFHS: High fat, high sucrose

HIF-1/2: Hypoxia-inducible factor-1/2

HMGB1: High-mobility group box protein 1

HMGCR: 3-hydroxy-3-methyl-glutaryl-coenzyme A reductase/HMG-CoA reductase

HSCs: Hematopoietic stem cells

HSL: Hormone-sensitive lipase

IF: Immunofluorescence staining

IFN-γ: Interferon-γ

IL-12p70: Interlukin-12p70

IL-1β: Interlukin-1β

IL-6: Interlukin-6

IMT: Intima-media thickness

Jab1: c-Jun activation domain-binding protein-1

JNK: C-Jun N-terminal kinase

LDL: Low-density lipoprotein

LDLR: Low-density lipoprotein receptor

LPS: Lipopolysaccharides

LXR: Liver X receptor

MIF: Macrophage migration inhibitory factor

MIF-2-cKO: Cardiomyocytes-specific *Mif-2* knockout

MPM: Multiphoton laser-scanning microscopy

MS: Multiple sclerosis

mTOR: mammalian Target of rapamycin

MW: Molecular weight

NAFLD: Non-alcoholic fatty liver disease

NB: Neuroblastoma

NF-κB: Nuclear factor kappa-light-chain-enhancer of activated B cells

NLRP3: NLR Family Pyrin Domain Containing 3

NMR: Nuclear magnetic resonance

NSCLC: Non-small cell lung carcinoma

ORO: Oil red O

OSA: Obstructive sleep apnea

PCOS: Polycystic ovarian syndrome

PCSK9: Proprotein convertase subtilisin-like kexin type 9

PDAC: Pancreatic ductal adenocarcinoma

PECAM-1/CD31: Platelet/endothelial cell adhesion molecule-1

PI3K/AKT: Phosphatidylinositol 3'-kinase/Protein kinase B

PPARα: Peroxisome proliferator-activated receptor alpha

PPARG: Peroxisome proliferator-activated receptor gamma

RAGE: the receptor for advanced glycation end product

RCT: Reverse cholesterol transport

rD-DT: Recombinant D-DT

RT-qPCR: Reverse transcription polymerase chain reaction

SCAP: SREBP cleavage-activating protein

SCD 1: Stearoyl-CoA desaturase 1

SD: Sprague-Dawley

SMCs: Smooth muscle cells

SREBP-1/2: Sterol regulatory element-binding protein-1/2

SREs: sterol response elements

SS: Systemic sclerosis

SVF: Stromal vascular fraction

TCA: Transverse aortic constriction

TF: Transcriptional factor/sequence-specific DNA binding factor

TG: Triglyceride

TNF-α: Tumor necrosis factor-α

TPOR: Thiol-protein oxidoreductase

Trx: Thioredoxin

T2DM: Type 2 diabetes mellitus

UPR: Unfolded protein response

VLDL: Very low-density lipoprotein

WAT: White adipose tissue

WB: Western blot

ZAP-70: Zeta-chain-associated protein kinase 70

4-CPPC: 4-(3-carboxyphenyl)-2,5pyridinedicarboxylic acid

4-IPP: 4-iodo-6-phenylpyrimidine

6-PP: 6-phenylpyrimidine

11. ACKNOWLEDGEMENTS

Markus Brandhofer, Bishan Yang, Elena Siminkotitch and Elina Bugar for giving me many valuable suggestions for my thesis.

In addition to science, I also strongly appreciated great support from Dr. Dongmei Zhang from International office of LMU. She gave me a lot of directions and comforts at the beginning when I just came to Munich, took care of my situation, and provided many useful suggestions for my life. In the meantime, she also offered me some encouragements and chances to challenge myself, which made me notice my more potential.

Also, special acknowledgements are given to my beloved family members, especially my father Mr. Yunshan Zan and my mother Mrs. Tianxiang Lan, whose encouragements and great supports made my accomplishments possible. For so many years, they have always been supporting me and respecting me without conditions. Their love and care are the greatest fortune of my life. Especially, only with their selfless support, can I overcome those difficulties and pursue my study until now.

Specially, COVID-19 changed the world for its worst, and changed our work and life a lot since 2019. We faced with different difficulties even frustrations in everyday life. However, I would say we have more time to sit down to really think about what we want to do and which kind of person we want to be, at least for me. I have to make a decision for my career whatever happen. More importantly, I am thinking where I could give full play to my value. It is also a good and meaningful choice to go back to my hometown to join the local medical system. Honestly speaking, to be a doctor makes me feel a sense of achievement.

Here, also thanks to myself. Courage and belief kept me still moving on without hesitation. Persistence to science and enthusiasm on research work made it true for me to achieve a lot in my four-year PhD life. I have to mention here, it has been a great honor for me to invite Prof. Dr. Peter Libby to give a guest-speaker talk for the SFB seminar, which I am most proud of. In fact, I also felt frustrated and confused sometimes, whereas I held a strong faith that my dream would come true as long as you persevere. At least, I think I lived up to all my expectations here.

Finally, yet importantly, I would like to express the deepest appreciation to China Scholarship Council, who gives me an opportunity to achieve my doctor degree in LMU, Germany, and makes it true for me to peruse my research dream abroad. I indeed enjoy this period of oversea living, appreciate all the people I met with, and love the world I have never seen before.

12. AFFIDAVIT

Affidavit

Zan Chunfang

_____
Surname, first name

Leipartstraße 28-115

_____
Street

81369, Munich, Germany

_____
Zip code, town, country

I hereby declare, that the submitted thesis entitled:

The MIF homolog MIF-2/D-DT in atherosclerosis: Functional role and links to hepatic lipid metabolism

is my own work. I have only used the sources indicated and have not made unauthorized use of services of a third party. Where the work of others has been quoted or reproduced, the source is always given.

I further declare that the submitted thesis or parts thereof have not been presented as part of an examination degree to any other university.

_____Munich, 05.07.2022_____   _____Chunfang Zan_____
place, date   Signature doctoral candidate

13. CONFIRMATION OF CONGRUENCY

Confirmation of congruency between printed and electronic version of the doctoral thesis

Zan Chunfang

_____
Surname, first name

Leipartstraße 28-115

_____
Street

81369, Munich, Germany

_____
Zip code, town, country

I hereby declare, that the submitted thesis entitled:

The MIF homolog MIF-2/D-DT in atherosclerosis: Functional role and links to hepatic lipid metabolism
……………………………………………………………………………………………………

is congruent with the printed version both in content and format.

_____Munich, 05.07.2022_____   _____Chunfang Zan_____
place, date   Signature doctoral candidate

14. LIST OF PUBLICATIONS

Published manuscripts:

1. El Bounkari O[#], **<u>Zan C</u>**[#], Wagner J, Bugar E, Bourilhon P, Kontos C, Zarwel M, Sinitski D, Milic J, Jansen Y, Kempf W, Maegdefessel L, Hoffmann A, Brandhofer M, Bucala R, Megens RTA, Weber C, Kapurniotu A, Bernhagen J. MIF-2/D-DT is an atypical atherogenic chemokine that promotes advanced atherosclerosis and hepatic lipogenesis. bioRxiv. 2021. doi: https://doi.org/10.1101/2021.12.28.474328 (target journals Cell Metab, Circ Res)

2. Kontos C, El Bounkari O, Krammer C, Sinitski D, Hille K, **<u>Zan C</u>**, Yan G, Wang S, Gao Y, Brandhofer M, Megens RTA, Hoffmann A, Pauli J, Asare Y, Gerra S, Bourilhon P, Leng L, Eckstein HH, Kempf WE, Pelisek J, Gokce O, Maegdefessel L, Bucala R, Dichgans M, Weber C, Kapurniotu A, Bernhagen J. Designed CXCR4 mimic acts as a soluble chemokine receptor that blocks atherogenic inflammation by agonist-specific targeting. Nat Commun. 2020; 11(1): 5981.

3. Wang S, El Bounkari O, **<u>Zan C</u>**, Tian Y, Gao Y, Bernhagen J. Classical chemokines, atypical chemokines, and MIF proteins in ischemic stroke: effects, mechanisms and roles in conditioning. Cond Med. 2021; 4(1): 39-57.

4. **<u>Zan C</u>**, Wang S, Liu L, Gokce O, El Bounkari O, Bernhagen J. MIF proteins in neurological disorders: dichotomic role and perspectives for conditioning medicine. Cond Med. 2021; 4(5): 216-233.

Unpublished manuscripts/manuscripts in preparation:

1. Zan C, Kontos C, El Bounkari O, Kapurniotu A, Bernhagen J. Therapeutic effect of the CXCR4 ectodomain mimic ms4M-L1 in an *Apoe*$^{-/-}$ mouse model of atherosclerosis (in preparation; target journal Thromb Haemost)